Stochastic Resonance in Biological Systems

James Bernard Fallon

B.Sc., B.E. (Hons.)

Department of Electrical and Computer Systems Engineering

&

Department of Physiology

Monash University

June 2001

Table of Contents

Summary

Stochastic resonance is a mechanism whereby the addition of noise can aid in signal detection. Specifically, additional input noise can result in the detection of an otherwise sub-threshold periodic signal. A general description of stochastic resonance with an emphasis on the matching of time-scales, a resonance, and its relevance to biological systems is given. In the context of the narrower definition of stochastic resonance, one involving a matching of time-scales, a review of the biological systems that have been proposed to exhibit stochastic resonance is given. It is found that the majority of biological systems have not been examined thoroughly enough to determine if they are capable of exhibiting stochastic resonance.

A novel measure of the output signal-to-noise ratio of a series of action potentials, based on the cycle histogram, is developed. A comparison of the new measure with an existing measure based on the inter-spike interval histogram is made with the aid of the Hodgkin-Huxley model. It is found that the new measure is capable of being utilised to observe stochastic resonance, subject to specific constraints.

Several experimental observations of stochastic resonance, including a matching of time-scales, are then made. It is found that Golgi tendon organs, muscle spindle primary and secondary endings and slowly adapting Type I cutaneous mechanoreceptors are all capable of exhibiting stochastic resonance. The conditions under which these receptors are likely to exhibit stochastic resonance are discussed.

It is found that the sinusoidal detection threshold during psychophysical experiments is reduced by the addition of noise to the sinusoidal stimulus. It is proposed that this improved detection is a result of stochastic resonance. Interestingly, the detection of small sinusoidal movements of the elbow does not appear to be improved with the addition of noise.

Finally, the conditions under which stochastic resonance may have a functional benefit in a variety of biological systems is discussed with the aid of an example.

Declaration

I hereby declare that, to the best of my knowledge and belief, the work presented in this thesis is completely my own. It does not contain any material that has been previously published or written by any other person, except where due reference is made in the text, or any material that has been submitted for the award of any other degree or diploma in any university or other institution.

James Fallon

Acknowledgments

I am grateful for the guidance and support of Dr. David Morgan and Prof. Uwe Proske, and for giving me the opportunity to undertake the studies necessary for this thesis. The experience, advice and keen eye that was often provided by Dr. Ed Gregory was also invaluable.

Thanks to Andrew, Camilla, Nadia and Nick for many a long discussion in 'the lizard lounge', which helped make the days go by. Also thanks to Richard, for being there in body, if nothing else, during the late nights and early mornings.

A thank you to my family for their support, especially my Dad for proof reading.

Finally, but most importantly, Lyndal. Thank you for letting me stay at the lab all night, putting up with me getting home too tired to do anything, listening to endless stories 'from the lab', but most importantly, helping me keep it all in perspective.

Abbreviations

Abbreviation	Full Name	Page
γ_D	Dynamic fusimotor fibre	85
γ_S	Static fusimotor fibre	85
ASR	Aperiodic Stochastic Resonance	9
D	Noise intensity	3
D_{OPT}	Estimated optimal noise level	5
D_{PRE}	Predicted optimal noise level	6
EEG	Electroencephalogram	31
EMG	Electromyogram	28
FHN	Fitzhugh-Nagumo membrane model	45
ISIH	Inter-spike interval histogram	16
L_{MAX}	Maximum physiological length	89
PCA	Primary component analysis	74
SAI	Slowly adapting Type I cutaneous mechanoreceptor	122
SEM	Standard error of the mean	53
SNR	Signal-to-noise ratio	1
SNR_{AMP}	Output SNR measure based on EMG amplitude	29
SNR_{COR}	Output SNR measure based on the correlation of the input and output	8
SNR_{CYC}	Output SNR measure based on the cycle histogram	8
SNR_{CYCLE}	Output SNR measure based on the cycle histogram	55
SNR_{EXP}	Output SNR measure based on the cycle histogram	56
SNR_{ISIH}	Output SNR measure based on the inter-spike interval histogram, similar to SNR_{RES}	54
SNR_{PS}	Output SNR measure based on the output power spectrum	4
SNR_{RATE}	Output SNR measure based on the instantaneous rate	95
SNR_{RES}	Output SNR measure based on the residence time histogram, similar to SNR_{ISIH}	54
SNR_{SYNC}	Output SNR measure based on a synchronisation index	23
SNR_{THRES}	Output SNR measure based on an arbitrary threshold	58
SNR_{TINFO}	Output SNR measure based on Shannon's transinformation rate	25

Chapter One

Stochastic Resonance

In systems that are designed to detect small signals it is usual to attempt to reduce the level of ambient noise, as it is believed that an optimal output signal-to-noise ratio (SNR) is achieved when there is the largest input SNR. However, this is not always true and stochastic resonance is a theory that explains this.

Ice Ages

Stochastic resonance was first proposed as an explanation for a possible periodicity observed in earth's ice volume record (Benzi, Sutera & Vulpiani, 1981; Benzi, Parisi, Sutera & Vulpiani, 1982). There are two stable states for the earth's climate: ice ages (where there is a large proportion of the earth's surface covered in ice), and non-ice ages (such as the current climate). The two states are stable because of the reflective properties of ice. When the earth's surface is largely covered in ice, a large proportion of the sun's energy is reflected away from earth. Conversely, when only a small fraction of the surface is covered by ice, the oceans absorb the energy from the sun, re-enforcing the non-ice age.

The ice record shows a tendency to oscillate between these two stable states every 100,000 years (Figure 1.1). Day-to-day, or even year-to-year, fluctuations in the amount of energy delivered to the earth by the sun are too rapid to produce the apparent periodic changes in ice volume. On the time-scale of the proposed periodicity, the fluctuations appear as random changes around an essentially zero mean change. A rapid random change about a signal of interest is usually considered noise, so the fluctuations in the amount of energy from the sun are considered to be a 'noisy' input to the climate system. Terrestrial events, such as volcanoes, also affect the amount of energy the earth absorbs from the sun by altering the atmospheric conditions. The time-scales of these events are also rapid compared to the ice volume fluctuations, and therefore they would also be considered a 'noisy' input to the climate system.

The time course of the apparent periodicity in the ice volume record is similar to the time course of a slight eccentricity in the orbit of the earth. However, the eccentricity is
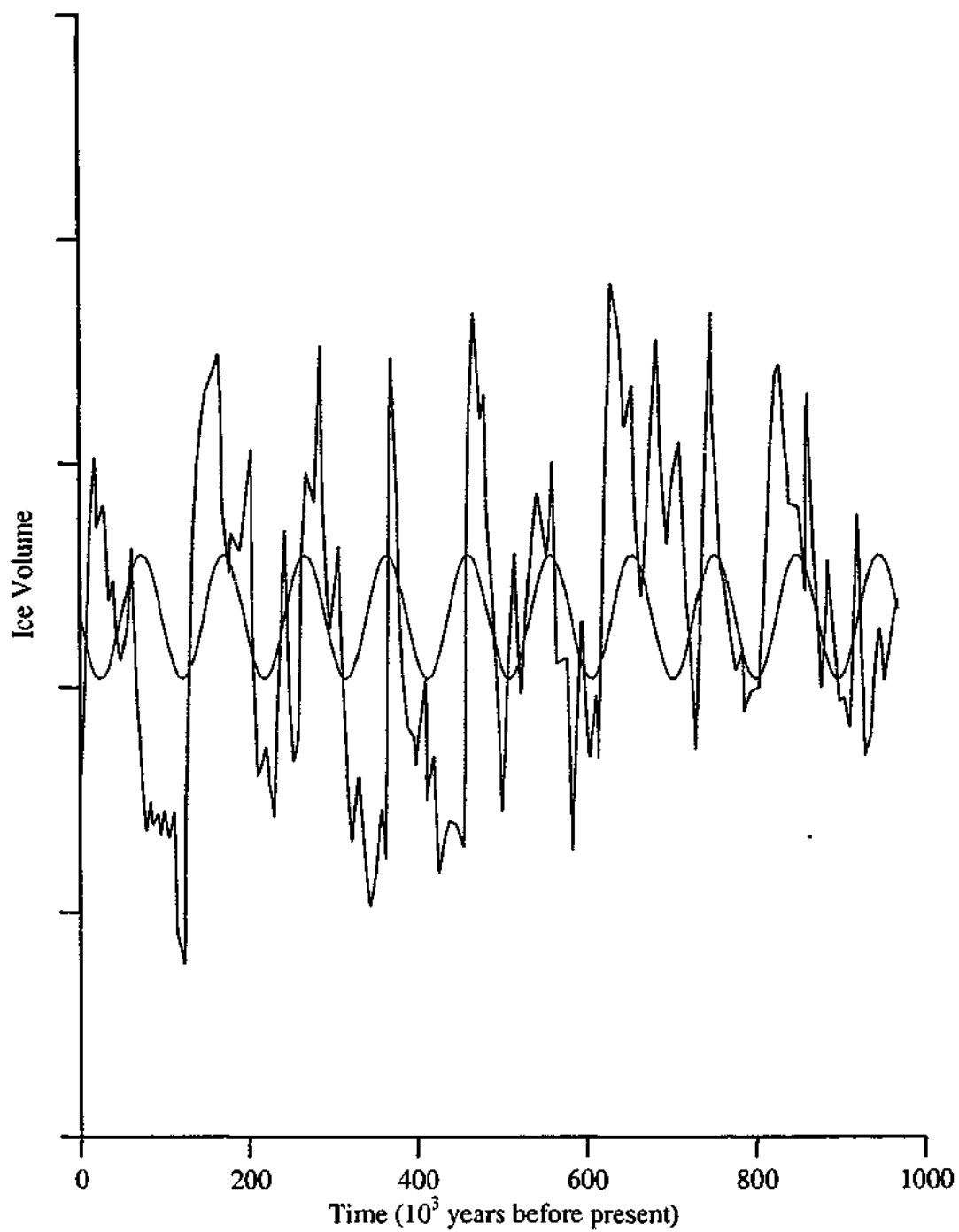
Figure 1.1 The apparent periodic fluctuations in the total volume of ice (blue line) have a period of approximately 100,000 years, indicated by the fitted sinusoid (black line). The ice volume data was taken from Figure 3 of Wiesenfeld & Jaramillo (1998). The sinusoid was fitted used a least-squares method and has a period of 97,000 years.

too small to cause a shift from an ice age to a non-ice age. Therefore, it was proposed that there is an interaction between the small periodic effects caused by the eccentricity of the orbit and the rapid fluctuations caused by changes in the sun and terrestrial events. The proposed mechanism is stochastic resonance, where a resonance (or matching of time-scales) occurs between the period of the eccentricity of the earth's orbit and the climate changes caused by the 'noisy' inputs.

One of the predictions of stochastic resonance is that with the addition of an appropriate noise signal at the input, a system can respond to an otherwise sub-threshold signal. This prediction was the basis of the link between the period of the eccentricity of the earth's orbit and the apparent periodicity in the ice ages. Another prediction of stochastic resonance is that a sub-threshold periodic stimulus with a higher frequency would require the addition of a larger noise signal. The ice volume record does not allow the testing of such a prediction, and therefore it is possible that the apparent periodicity in the ice volume record may not be a result of stochastic resonance.

Simple Model

It is not intuitively obvious how stochastic resonance occurs, so it is most convenient to discuss it with the aid of a simple model. The most commonly used model to demonstrate stochastic resonance is based on an over-damped particle in a symmetric bistable potential well, the double-well model. The potential well is given by Equation 1.1, and illustrated in the top-left panel of Figure 1.2. The output of the system is designated as the location of the particle within the well. If the particle is released from any position in the well, it will settle to the bottom of either the left half-well or the right half-well, depending on its initial position. These positions correspond to the stable states of the system, much as an ice age or non-ice age is a stable state for the earth.

$$U(x) = \frac{1}{4}x^4 - \frac{1}{2}x^2 \qquad\qquad\qquad \textbf{Equation 1.1}$$

If the particle is now subjected to zero-mean white Gaussian noise, $\xi(t)$, it will randomly move around the well. The particle will randomly change between the left half-well and the right half-well (Figure 1.2, middle-left panel). The rate of these
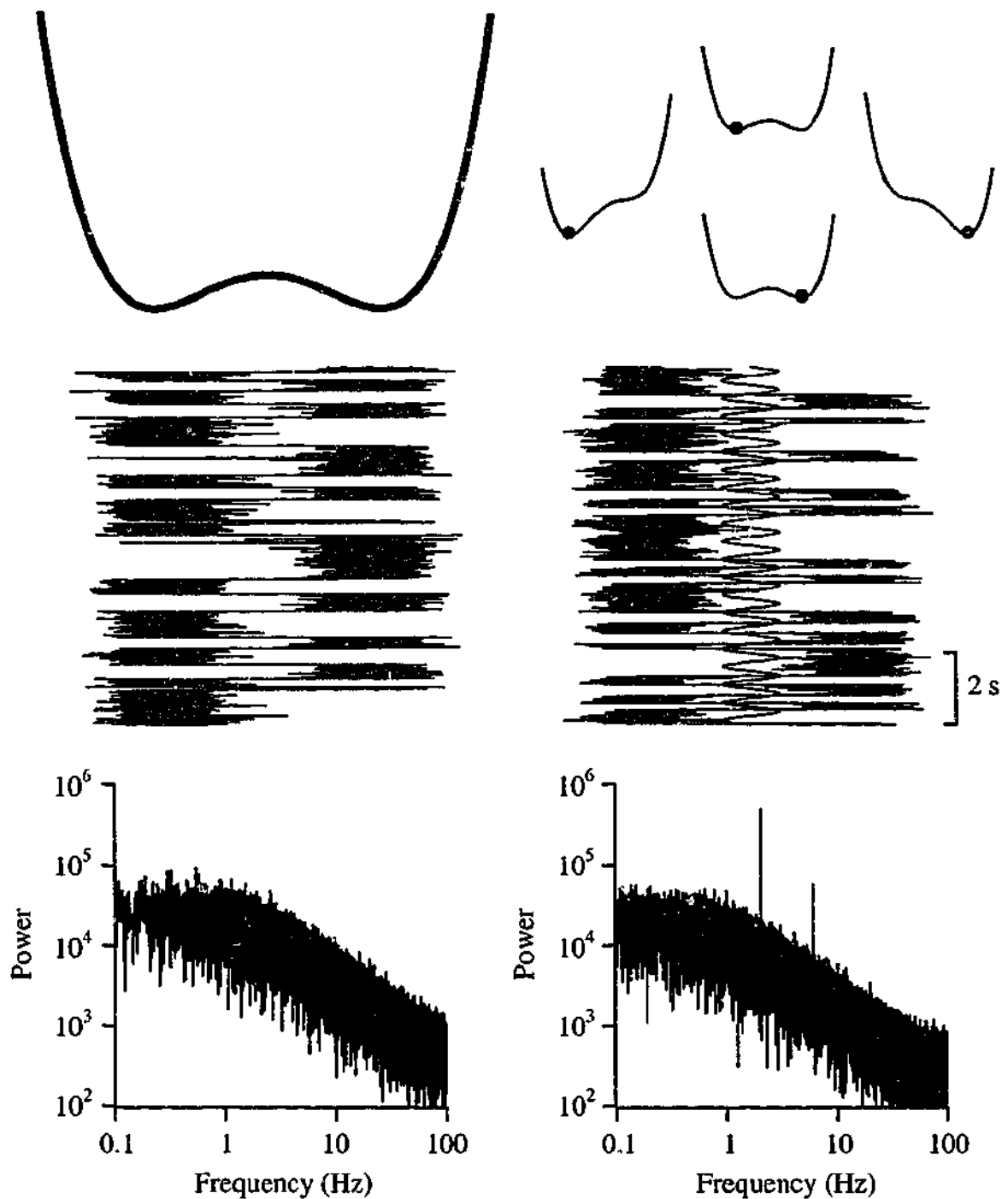
Figure 1.2   The unmodulated symmetric bistable potential (top-left panel) can be modulated by a periodic input (top-right panel). The particle randomly changes between half–wells under the influence of a Gaussian distributed random input (middle-left panel). The power spectrum (bottom-left panel) of the resulting output has a Lorentzian distribution, emphasising the random nature of the transitions. With a small periodic signal (2 Hz sinusoid, indicated by the red line in the middle-right panel) added to the input, the transitions between wells becomes phase locked to the stimulus and the power spectrum has peaks at 2 and 4 Hz (bottom-right panel).

transitions between wells (r_K) can be predicted using Kramers' rate (Kramers, 1940) and is given by Equation 1.2 (Gammaitoni, Hanggi, Jung & Marchesoni, 1998), where D is the input noise intensity given by Equation 1.3 and $\delta(t)$ is the unit impulse function.

$$r_K = \frac{1}{\sqrt{2\pi}} e^{-\frac{1}{4D}} \qquad\qquad \text{Equation 1.2}$$

$$\langle \xi(t)\xi(0) \rangle = 2 D \, \delta(t) \qquad\qquad \text{Equation 1.3}$$

It is worth emphasising that although there is an average rate of transitions, r_K, for a given input noise intensity, the actual transitions are randomly distributed in time. With the ice ages example, the transitions between ice ages and non-ice ages caused by the fluctuations in the sun and terrestrial events cause the rapid fluctuations in ice volume that are not linked to the 100,000 year oscillations illustrated Figure 1.1. The output power spectrum for the noise-alone response of the simple double-well is shown in Figure 1.2 (bottom-left panel), and follows a Lorentzian distribution, indicative of the random transitions (Moss, Pierson & O'Gorman, 1994).

In response to a periodic driving of the system, the motion of the particle is given by Equation 1.4, where A is the amplitude of the periodic driving and ω is the frequency of the periodic driving. This driving can either be interpreted as acting directly on the particle or by modulating the shape of the well, as illustrated in the top-right panel of Figure 1.2 and in Appendix A. The effect of the periodic driving depends on the amplitude of the driving relative to the height of the barrier between the two half-wells, ΔU, and also on the input noise intensity, D.

$$\dot{x} = -U'(x) + A\cos(\omega t) + \xi(t) \qquad\qquad \text{Equation 1.4}$$

The simplest situation is with no noise, $D = 0$. In this case if the amplitude of the periodic driving is below threshold, $A < \Delta U$, then the particle will not have enough energy to overcome the barrier and change between half-wells. This is similar to the eccentricity of the earth's orbit not being large enough to cause the transition from a non-ice age to an ice age. If, however, the periodic driving is large enough, $A > \Delta U$, then the particle will change between half-wells with each cycle of the periodic driving.

When noise is added to the system, $D > 0$, the particle will change half-wells due to the noise, but the timing of the transitions will be influenced by the periodic driving. The periodic driving can be imagined to change the probability of a transition occurring by modulating the height of the barrier (Figure 1.2, top-right panel). The modulation of the effective barrier height leads to a phase locking of the transitions between half-wells and the periodic driving (Figure 1.2, middle-right panel). The output power spectrum has peaks at the driving frequency (2 Hz) and at harmonics of the driving frequency, superimposed on the noise-alone Lorentzian background (Figure 1.2, bottom-right panel).

A common measure of the output SNR, is the ratio of the power at the signal frequency compared to the background power, SNR_{PS}. The SNR_{PS} for the double-well system driven by a periodic signal and a noise signal is a complex function of the input noise intensity (Figure 1.3, top panels). For a sub-threshold periodic input the SNR_{PS} has several distinct regions. One region is for small values of D that do not result in transitions between half-wells. Under these conditions the particle would oscillate within one of the half-wells. This oscillation would result in a large SNR_{PS}, as the power spectrum would be a spike at the periodic stimulus frequency on a very small noise background. In the limit of no noise the SNR_{PS} would be infinite, as the background noise level would be zero. If the particle does not change half-wells it is desirable for SNR_{PS} to be low, as the system has not changed from one stable state to another. Therefore, the output of the system is designated to be the state (or half-well) the particle is in, rather than the precise position of the ball within the well. The resulting two-state output can be used to calculate SNR_{PS}, resulting in an undefined SNR_{PS} if the particle never changes state.

As the intensity of noise increases the particle begins to make transitions between the half-wells. The SNR_{PS} increases with increasing noise intensity to a maximum. As the noise intensity is further increased the SNR_{PS} begins to decrease and resembles the SNR_{PS} for a supra-threshold periodic input and noise (Figure 1.3, top-right panel).

The SNR_{PS} of the double-well model, driven with a sub-threshold periodic input, has the characteristic shape of a stochastic resonance curve. The maximum output SNR is
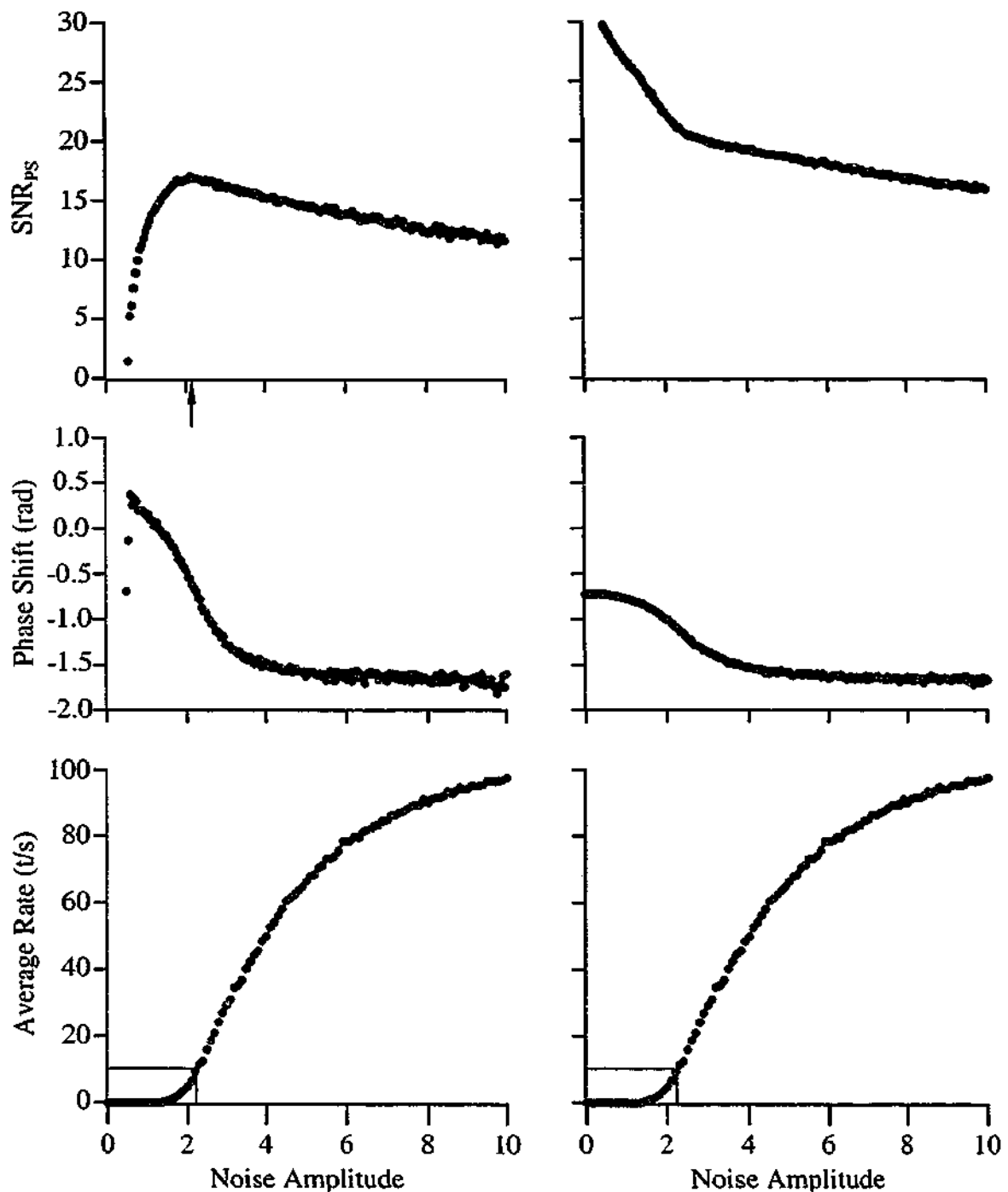
Figure 1.3   The classical shape of a stochastic resonance curve (top-left panel) is different from the curve produced with a supra-threshold periodic input (top-right panel). The phase shift of the output is also different for sub-threshold and supra-threshold periodic inputs (middle panels). The peak in the stochastic resonance curve occurs at a specific level of noise, D_{OPT} (indicated by the arrow). The predicted optimal noise level, D_{PRE}, (indicated by the grey lines in the bottom panels) is the noise level, that when applied alone, produces an average transition rate equal to the frequency of the periodic driving, in this case 10 Hz. The noise-alone response has been reproduced in both columns to aid in the comparison of features.

produced with the addition of some amount of input noise. This is not what would be intuitively expected, as the maximum output SNR does not coincide with the maximum input SNR. In fact the optimal output SNR occurs when the input SNR is less than one; that is, the signal of interest is smaller than the noise signal. The level of noise that results in the maximum output SNR is defined as the optimal noise, D_{OPT}.

The matching of time-scales (or resonance from which stochastic resonance derives its name) is illustrated with reference to the noise-alone response of the system (Figure 1.3, bottom panels). As the noise intensity increases, the average transitions rate, r_K, increases. The intensity of noise that produces the optimal output SNR produces an average transition rate that is equal to the periodic driving when applied alone (i.e. $r_K(D_{OPT}) = \frac{\omega}{2\pi}$).

Features of Stochastic Resonance

Any system that is designed to detect a small signal will typically have some finite input threshold. If an input signal is below this threshold it is not possible to detect it. Stochastic resonance can be used to effectively lower the threshold of a system, but stochastic resonance will not occur in every system. There are certain requirements for stochastic resonance to occur, and certain key features of stochastic resonance that distinguish it from other noise effects.

Non-linear System

A linear system is one in which the output is simply some portion of the input plus a constant. A simple linear system with an input, X, and an output, Y, is given by Equation 1.5. The output is simply the input multiplied by two plus a constant, five. If some noise, ξ, is added to the input then it will be transferred to the output, with the same ratio as the signal, X. Therefore, a linear system cannot exhibit stochastic resonance.

$$Y = 2 \times X + 5$$ **Equation 1.5**

5

There are many forms of non-linear systems, including the double-well system described above (p. 2). One of the simplest non-linear systems is a threshold of the type described by Equation 1.6. If the input is less than a half, the output is zero; while if the input is greater than or equal to a half, the output is one. Non-linear systems are usually far more complex than this simple system and do not always have such a sharp threshold.

$$y = \begin{cases} 0 \ \text{for } x < \frac{1}{2} \\ 1 \ \text{for } x \geq \frac{1}{2} \end{cases}$$

Equation 1.6

Most systems that exhibit stochastic resonance have a threshold, such that inputs less than a critical level produce no change in the output. This, however, is not a requirement of stochastic resonance, as stochastic resonance has been shown in systems with a smooth non-linearity. Provided the non-linearity has 'sufficient steepness' it is possible that the system will exhibit stochastic resonance (Chapeau-Blondeau & Godivier, 1997; Balazsi, Kiss & Moss, 1999). The 'steepness' of a non-linearity is a measure of how rapid the transition between the stable states is. For the simple threshold given in Equation 1.6 the non-linearity is inifinitely 'steep', as the transition of the output from zero to one occurs over an infinitely small interval.

Noise

A key feature of stochastic resonance is that the optimal output SNR does not occur with zero input noise; that is, some level of noise is required to optimise the response of the system. Unlike other noise effects such as dithering, discussed in more detail later in this chapter (p. 10), the level of noise that is required to produce the optimal output SNR is supra-threshold. The optimal noise level can in fact be predicted from the response of the system to noise alone (Figure 1.3, bottom panels). The predicted optimal noise level, D_{PRE}, is the level of input noise that, when applied alone, produces an average transition rate that is equal to the periodic stimulus frequency. The grey lines in the bottom panels of Figure 1.3 illustrate the method of predicting the optimal noise level. For a periodic stimulus of 10 Hz, the predicted optimal noise level is 2.2.

The mean transition rate between states is a monotonically increasing function of noise given by Kramers' rate (Equation 1.2). Therefore, higher periodic input signal frequencies require higher levels of input noise to optimise the output SNR; that is, D_{OPT} is dependent on the periodic input frequency. This is a key feature of stochastic resonance that does not occur with any other constructive noise effects. As a consequence of the matching of D_{OPT} and D_{PRE}, there is a limit to the range of frequencies over which a system will exhibit stochastic resonance. The maximum frequency is limited to the maximum noise-alone response of the system, which, for the system illustrated in Figure 1.3 is approximately 100 Hz.

In the majority of stochastic resonance studies the type of noise that is added to the input signal is an approximation to white noise with a normal distribution (Gaussian noise). However, the distribution of the noise is not critical to the stochastic resonance effect, with many different noise distributions facilitating signal transfer (Nozaki, Mar, Grigg & Collins, 1999). Different noise distributions will produce different values of peak output SNR and will also alter the shape of the output SNR vs noise curve, however the different noise distributions will not alter the basic stochastic resonance effect (Chapeau-Blondeau & Godivier, 1997).

Resonance

Deterministic or normal resonance occurs when the frequency of the input signal matches a characteristic frequency of the system. The frequency response curve of a resonant system shows the output SNR increasing up to a maximum value at a certain frequency ω_o, and then decreasing again. Resonance is said to occur at ω_o, as the output SNR is maximal at this frequency. Either the periodic input frequency or the characteristic system frequency can be altered in deterministic resonance. Similarly, in stochastic resonance, either the input frequency or the noise-induced rate can be altered. This means a system can be tuned to a particular frequency by altering the amount of input noise, or the input frequency can be selected to optimise the performance of a fixed level of noise.

The phase shift of the output can also be used to highlight resonance. The phase shift between input and output passes through $\pi/2$ at ω_o for deterministic resonance. A curve

7

with similar characteristics is produced when the phase shift is plotted against input noise for a system that exhibits stochastic resonance (Figure 1.3, middle panels).

True resonance can only occur with a periodic input to a system because a matching of two frequencies is required; the periodic input frequency and the characteristic system frequency. The most commonly used periodic input is a sinusoid, as it consists of a single frequency. Traditionally, stochastic resonance has also been shown with sinusoidal inputs, highlighting why the theory is called stochastic resonance; as there is an apparent resonance between the periodic input and the system under the influence of the noise (Gammaitoni, Marchesoni & Santucci, 1995; Giacomelli, Marin & Rabbiosi, 1999). There has been some discussion as to whether stochastic resonance can occur with a non-periodic input, 'aperiodic stochastic resonance' (ASR) (Collins, Chow & Imhoff, 1995a; Collins, Imhoff & Grigg, 1996a; Chialvo, Longtin & Muller-Gerking, 1997; Chow, Imhoff & Collins, 1998; Petracchi, 2000), which is disucssed later in this chapter (p. 9).

Output Signal Measurements

A difficulty in determining if 'aperiodic stochastic resonance' exists is that the standard definition of the SNR_{PS} measure is no longer relevant. The SNR_{PS} measure is typically defined as the ratio of output power in the signal frequency band, to the background level. If the signal is not of a narrow frequency range, ideally a single frequency, the SNR_{PS} measure is not applicable.

There are many possible ways of using the output of a system to calculate a SNR measure. The possible SNR measures include measurements based on: the residence time between transitions, SNR_{RES}; inter-spike interval histograms, SNR_{ISIH}; cycle histograms of the probability of a transition occurring, SNR_{CYC}; and the correlation between the input and output of the system, SNR_{COR}. All these measurements attempt to quantify the amount of signal present in the output compared to the amount of noise in the output. The different measurements have varied characteristics and therefore produce different shaped stochastic resonance curves (Shimokawa, Pakdaman & Sato, 1999a).

Although the SNR_{PS} measure is the most commonly used SNR measure, it has been proposed that if the SNR_{PS} measurement is used, it is not possible to observe stochastic resonance (Fox, 1989). Another common measurement that is used in many stochastic resonance investigations is based on residence time distribution, SNR_{RES}. A histogram of the times between transitions from one state to the other is shown in Figure 1.4 (top panel). The distribution is clearly multi-modal with peaks at integer multiples of the driving period. The standard measurement used to calculate SNR_{RES} is the probability of a transition occurring after a single period, the height of the first peak. The residence time measure produces results that are qualitatively similar to the SNR_{PS} measurement for this system, as can be seen by a comparison of the middle panels of Figure 1.4 with the top-left panel of Figure 1.3.

When both the SNR_{PS} and SNR_{RES} measurements are applied to other systems the results can be quantitatively quite different (Shimokawa et al., 1999a). The SNR_{PS} measurement produces results that have many of the features of stochastic resonance but also have some other fluctuations in the SNR_{PS} vs noise curve. These are thought not to arise from classical stochastic resonance effects, but to be the result of other influences of the additional input noise. This is in contrast to the SNR_{RES} measurement, which produces results that are consistent with all aspects of stochastic resonance.

The different results obtained from one system using different SNR measurements highlight some of the difficulties in determining if stochastic resonance occurs. To be certain that a system exhibits stochastic resonance the output measurement used must be considered part of the system, as the results can vary depending on the measurement used.

Aperiodic Stochastic Resonance

Collins et al. (1995a) proposed that 'aperiodic stochastic resonance' occurred in a simple excitable system, as the SNR_{COR} measure, the correlation between the input and the output, passed through a maximum as the level of input noise was increased. There is no doubt that the addition of noise enhanced the response of the system, but as there can be no matching of time-scales the effect cannot be stochastic resonance. By definition, stochastic resonance involves the matching of two time-scales (hence the
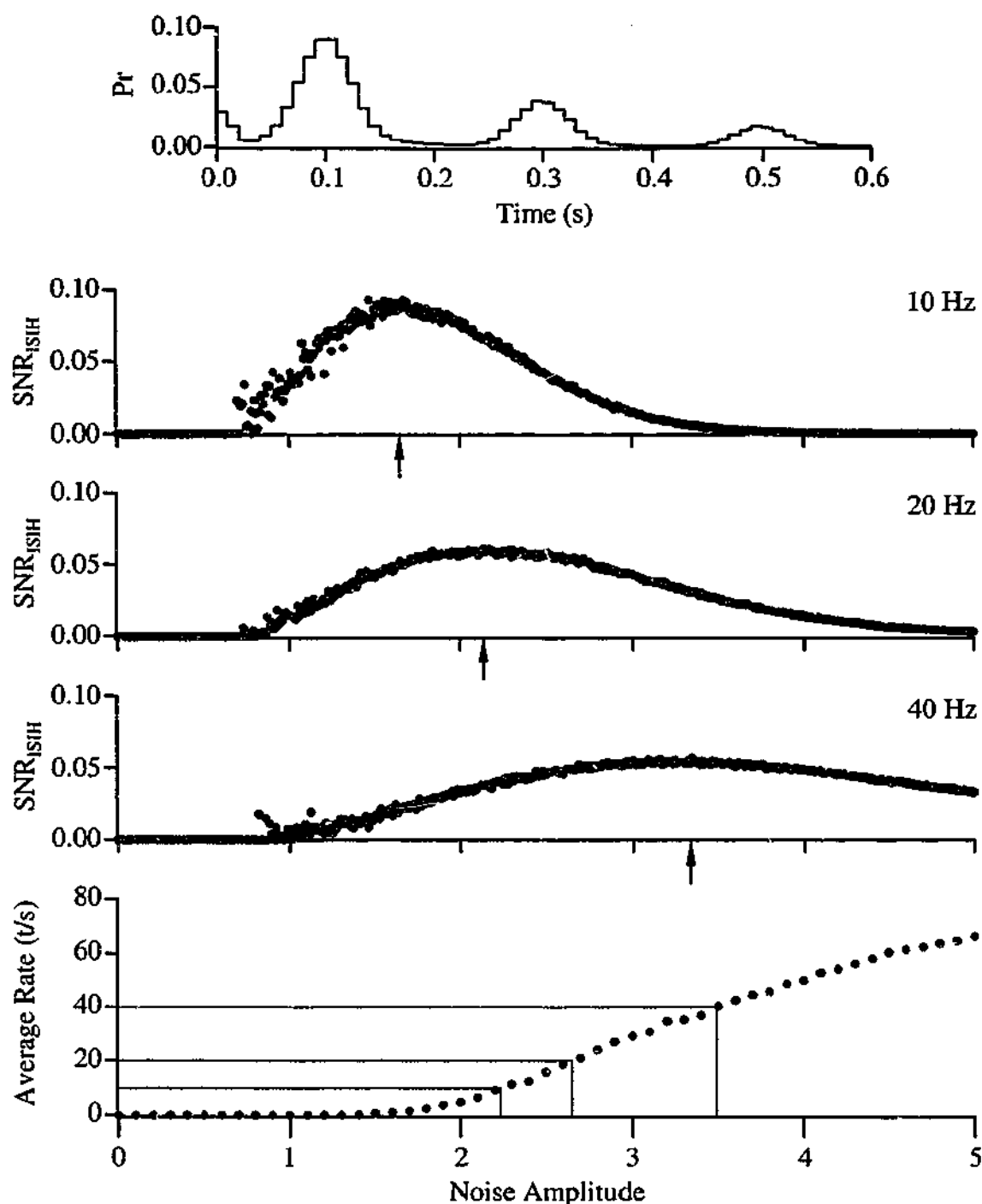
Figure 1.4   A probability histogram of the time between transitions from the left half–well to the right half–well has a multi-modal distribution (top panel). The height of the peak (or the area under the peak) at the period of stimulation (0.1 s) can be used as a measure of output SNR to produce a series of stochastic resonance curves (middle panels). These curves are similar in shape to the curve produced with the SNR_{PS} measurement (Figure 1.3, top-left panel). The noise-alone response is reproduced in the bottom panel. Note that the optimal noise levels (indicated by the arrows in the middle panels) increase with increased periodic stimulus frequency, as do the predicted optimal noise levels (indicated by the grey lines in the bottom panel). Ideally, the optimal noise levels would be equal to the predicted optimal noise levels (i.e. $D_{OPT} = D_{PRE}$).

resonance). One of the time-scales is a result of the sub-threshold periodic stimulus, while the other is a result of the noise-alone response of the system (hence the stochastic). Stochastic resonance occurs when there is a matching of a noise-induced time-scale and the sub-threshold periodic stimulus time-scale. Therefore 'aperiodic stochastic resonance' cannot occur.

A feature of the 'aperiodic stochastic resonance' described by Collins et al. (1995a), that is not characteristic of stochastic resonance, is that a single noise amplitude is optimal for all signals. Stochastic resonance predicts that each stimulus frequency will be optimised with a different level of noise, which is dependent on the noise-alone response of the system. As the input signals used to demonstrate 'aperiodic stochastic resonance' do not have a specific frequency, it is not possible to predict the level of noise that should optimise the system's response. 'Aperiodic stochastic resonance' has been considered as system linearisation or dithering, neither of which involve resonance (Gammaitoni, 1995; Chialvo et al., 1997). 'Aperiodic stohcastic resonance' highlights the fact that stochastic resonance is not the only phenomenon whereby noise can have a constructive effect to enhance the response of a system. Some other effects share many characteristics with stochastic resonance and it can be difficult to discriminate between them.

Dithering

The effect that is most commonly misinterpreted as stochastic resonance is dithering. Dithering may occur in any system with a threshold, but is most commonly discussed in terms of quantisation. The threshold described in Equation 1.6 can be considered as a quantising system for inputs between zero and one. The system effectively rounds the input to zero or one. This rounding of the input results in a loss of information, as there is no difference in the output of the system for inputs of 0.3 or 0.4, as in both cases the output will be zero. The difference between the input and the output can be considered an error, with the maximum error of this system being a half. The maximum error of a half occurs when the input is a half and the output is one.

The dithering effect is produced by adding noise to the input signal and averaging the output signal; this has the effect of reducing the error introduced by the quantisation.
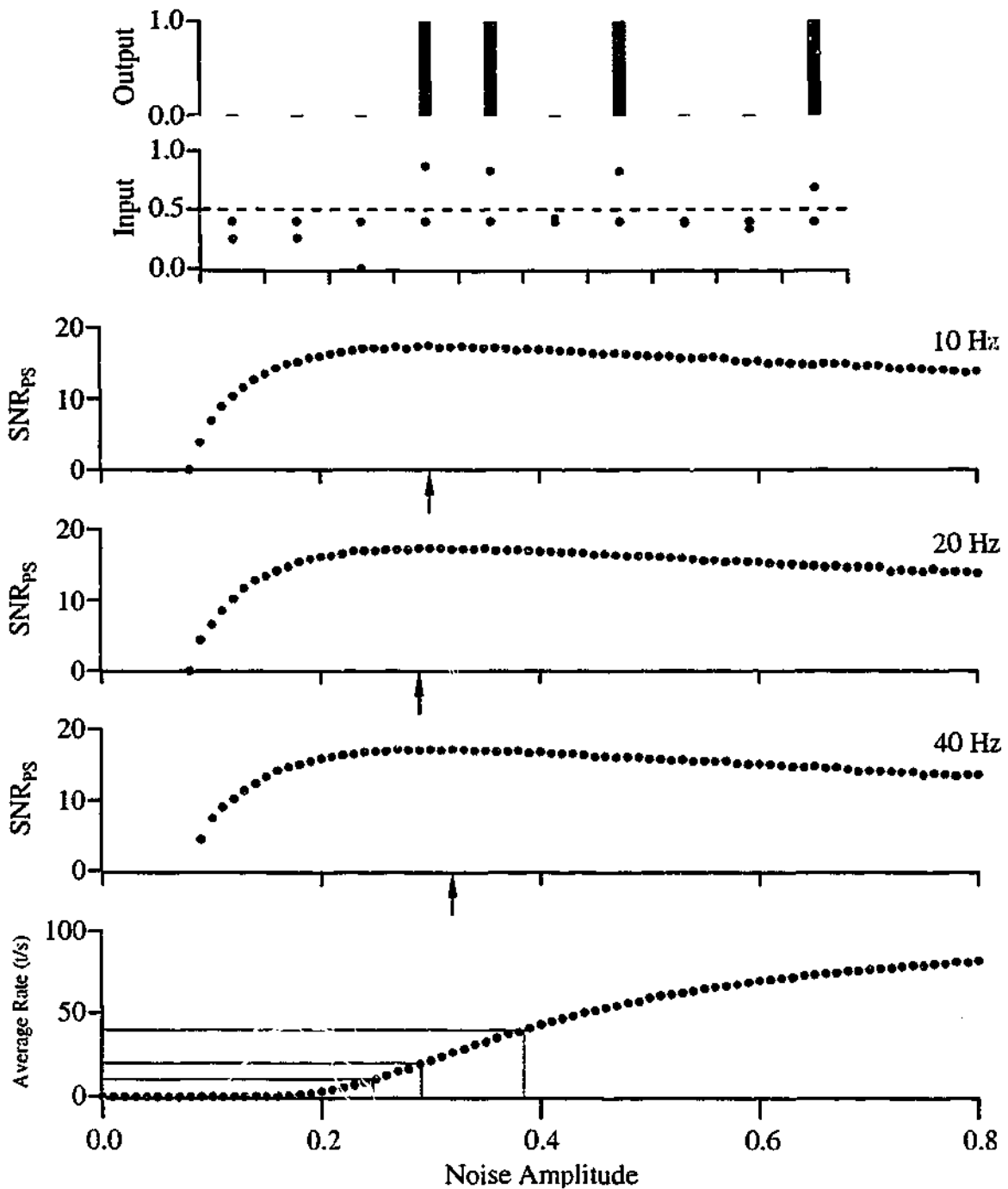
Figure 1.5 The top panel is an illustration of the dithering effect. For a system with a threshold of 0.5 an input of 0.4 will always produce an output of 0 (top panel, green symbols). However, with the addition of evenly distributed noise with amplitude 0.5 (top panel, pink symbols) four out of ten samples of the output will be one (top panel, solid bars), resulting in an average value of 0.4. The dithering effect can produce curves (middle panels) that are similar to stochastic resonance curves. The curves show an increase in SNR_{PS} for a non-zero level of input noise. However, the optimal noise levels (indicated by the arrows in middle panels) do not increase with increasing periodic stimulus frequency, unlike the predicted optimal noise levels (indicated by the grey lines in the bottom panel).

The optimal noise signal to add to the input of a quantising system is evenly distributed noise, with an amplitude equal to the quantisation level (Wannamaker, Lipshitz & Vanderkooy, 2000). Evenly distributed noise is a signal that has equal probability of being any value between two limits. For the system described in Equation 1.6 this results in a noise signal that is evenly distributed between -0.5 and +0.5; that is, any value between -0.5 and +0.5 is equally likely to occur.

An example of the dithering effect is illustrated in Figure 1.5 (top panel), with an input of 0.4 and an ideal noise signal. If no noise is added to the input, then the output is always zero, and the error produced by the system is 0.4. If the ideal noise distribution, evenly distributed noise between -0.5 and +0.5, is added to the input, then on average four out of ten inputs will be greater than 0.5 and the average output of the system will be 0.4. The addition of the optimal noise distribution effectively removes the error introduced by the system. The example illustrates that for this particular case dithering can reduce the error of the system to zero. If noise with a normal distribution is used, rather than an even distribution, it is impossible to reduce the error to zero, although significant reductions can still occur (Gammaitoni, 1995).

To compare dithering with stochastic resonance, a sinusoidal input can be used and the output SNR measured for various noise amplitudes. The resulting plot (Figure 1.5, lower panels), is qualitatively similar to those produced by stochastic resonance (Figure 1.4). The output SNR rises to a maximum with the addition of some level of input noise and then falls as larger amounts of noise are added. Unlike stochastic resonance, the maximum output SNR does not occur at a level of noise that can be predicted using the stimulus frequency and the system's response to noise alone.

An important difference between stochastic resonance and dithering is that the level of noise that produces an optimal output SNR for dithering is near the threshold level of noise, and is not dependent on the input signal frequency. In contrast the noise required to produce an optimal output SNR for stochastic resonance is supra-threshold and can be predicted from the sub-threshold stimulus frequency and the system's response to noise alone. Another difference between stochastic resonance and dithering is that dithering reduces the error between the average output and the input, while stochastic
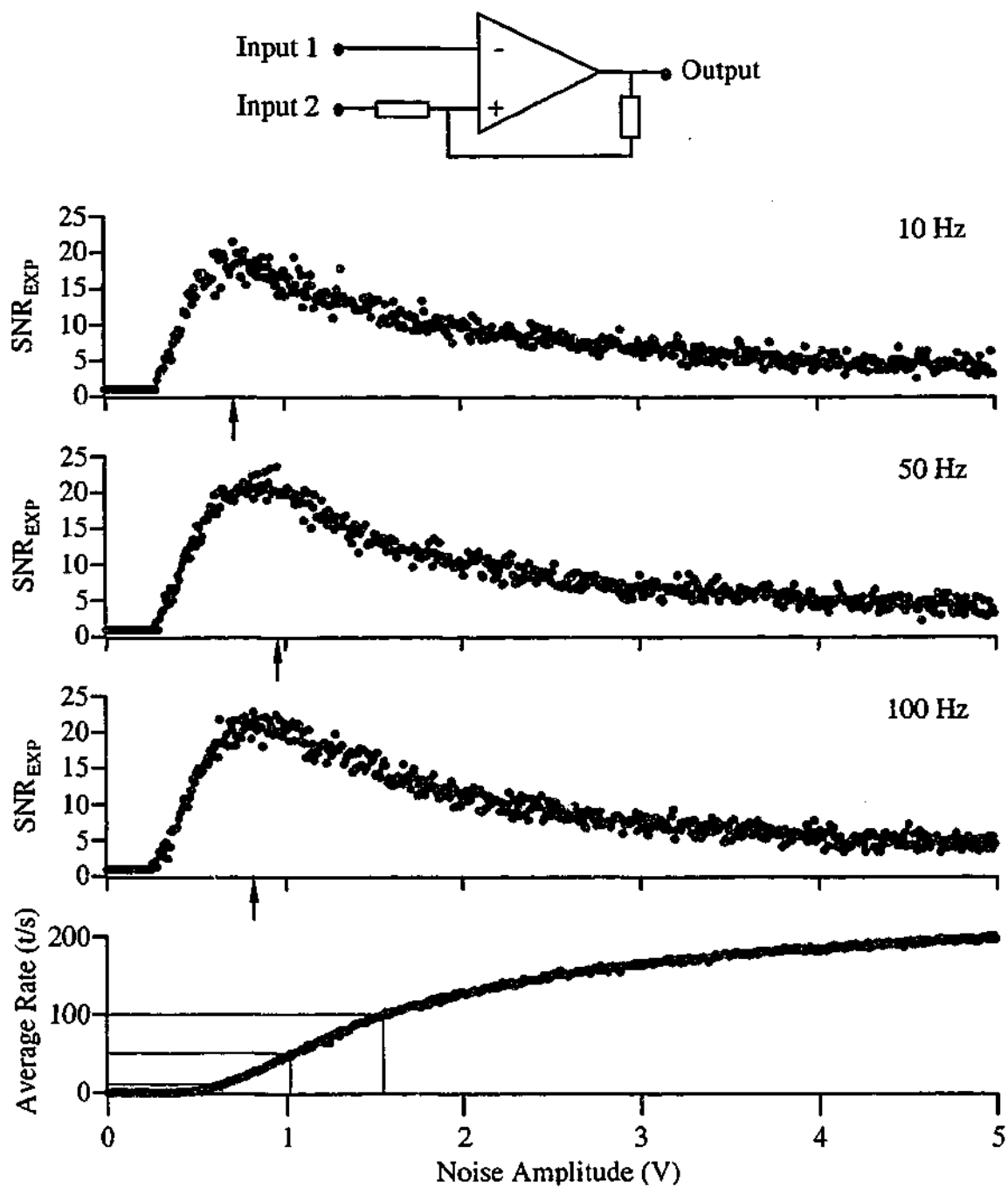
Figure 1.6 The Schmitt trigger (top panel) was the first experimental system proposed to exhibit stochastic resonance. Although there is an optimal SNR_{EXP} with the addition of noise (middle panels), the optimal noise levels (indicated by the arrows) do not increase with increasing stimulus frequency. An increase in optimal noise with increasing periodic stimulus frequency is a characteristic of stochastic resonance, therefore the Schmitt trigger does not appear to exhibit stochastic resonance. The optimal noise levels are close to the threshold level of noise, rather than the levels that are predicted from stochastic resonance (grey lines).

resonance produces an output with maximum signal content (Chapeau-Blondeau & Godivier, 1997).

Stochastic resonance may be considered as a special case of dithering, where the effective threshold of the system is determined by the frequency of the sub-threshold periodic input signal. Optimal dithering occurs at the minimum noise level that will produce a threshold crossing. For stochastic resonance to occur the noise must, on average, produce a threshold crossing within each period of the input signal, therefore the level of noise required increases with increasing periodic stimulus frequency. In this respect dithering is a more general effect that is likely to play a more significant role in practical systems than stochastic resonance.

Schmitt Trigger

The first experimental system proposed to exhibit stochastic resonance was the Schmitt trigger, a simple two-state electronic device (Fauve & Heslot, 1983). Since then stochastic resonance has been proposed to occur in a variety of systems including superconducting quantum interference devices (Rouse, Siyuan & Lukens, 1995); bistable ring lasers (McNamara, Wiesenfeld & Roy, 1988); and freestanding magnetoelastic beams (Spano, Wun-Fogle & Ditto, 1992).

Many of the systems that have been proposed to exhibit stochastic resonance may in fact be exhibiting dithering, not stochastic resonance. The Schmitt trigger, as illustrated in the top panel of Figure 1.6, is an example of such a system (Wannamaker et al., 2000). The system exhibits a maximum output SNR with the addition of noise (Figure 1.6, middle panels); however, the level of noise that produces this maximum output SNR does not increase with increasing periodic stimulus frequency, a key feature of stochastic resonance. Also, the level of noise that produces an optimal output SNR is near the threshold level of noise, rather than the level predicted from the sub-threshold periodic stimulus frequency and the noise-alone response of the system (grey lines in the bottom panel of Figure 1.6). Therefore, although many of the features of stochastic resonance are present in this system, the increase in output SNR is mostly likely due to dithering rather than stochastic resonance.

Biological Relevance of Stochastic Resonance

The central nervous system receives information about the environment from a wide variety of receptors. The signals that can be detected by the various receptors and interpreted by the central nervous system range from individual photons of light striking the retina, to the weight of an object held in the hands. Not only is there a vast range of different signals that may be detected, but each signal is subject to various environmental distortions and disruptions that make it more difficult to detect. As the receptors must operate in the presence of noise, it is possible that when small periodic signals are of interest the receptors may exhibit stochastic resonance.

Noise Sources

Each type of sensory receptor will be subjected to different kinds of noise, ranging from electromagnetic to chemical. The sources of noise are not limited to the external environment, as there are also many sources of noise within the body. To highlight some of the possible sources of noise it is convenient to look at a broad class of receptors, the mechanoreceptors.

Environmental

There are a wide variety of mechanoreceptors throughout the body that are used to detect various mechanical signals. Perhaps the most sensitive mechanoreceptors are those of the inner ear. Here, the cilia of the inner hair cells are capable of responding to vibrations of 0.1 nanometres (Jaramillo & Wiesenfeld, 2000). This sensitivity is even more amazing considering that the random (Brownian) motion of the cilia caused by thermal vibrations is three nanometres. In the case of the inner hair cells, the vibrations of their cilia, which is the final step in the mechanical transfer of sound waves, are the signals of interest. The Brownian motion of the cilia is not of interest and therefore can be considered a source of noise. The inner hair cells, therefore, can respond to stimuli that have a SNR of less than one, a situation that also occurs in systems that exhibit stochastic resonance.

Not all mechanoreceptors are as sensitive as the inner hair cells, and therefore are not affected by noise in the form of thermal vibrations. However, there are many sources of mechanical noise in the environment, ranging from seismic activity to ground-borne vibrations from passing traffic. Just as it is a rarity to experience true silence, it is also a rarity to experience an environment without mechanical stimulation. Therefore, many mechanoreceptors must operate in situations where the amplitude of noise can be equal to or greater than the amplitude of the signal of interest.

To overcome these situations some mechanoreceptors have a much greater sensitivity to stimuli delivered at certain frequencies, and are rather unresponsive to stimuli outside their preferred response range. The rapidly adapting cutaneous mechanoreceptors are good examples of such receptors. Meissner's corpuscles and hair basket endings are most sensitive to frequencies in the range of 20 to 150 Hz, while Pacinian corpuscles are most sensitive to even higher frequencies, greater than 200 Hz (Johansson, Landstrom & Lundstrom, 1982). The receptors' structures and locations result in effective high-pass mechanical filtering of the skin deformations that are their signals of interest. The selective sensitivity to such high frequencies reduces the influence of lower frequency sources of noise, thereby increasing the output SNR. Even so, it may be possible that stochastic resonance might also have a role to playing in detecting signals in noisy environments.

Intrinsic

As mentioned, noise sources are not limited to the external environment. The resting membrane potential is subject to thermal fluctuations, which may become a significant source of noise. The electrochemical gradients across a cell membrane that are a vital component of most receptors' transduction processes are influenced by thermal fluctuations in channel activity and membrane permeability. If the receptive systems are sufficiently sensitive then such thermal fluctuation can result in the generation of action potentials that are propagated into the central nervous system. Activity in adjacent nerve fibres can also act as a source of noise, especially within the central nervous system itself. The resulting changes in the composition of the extra-cellular fluid can constitute a source of noise, especially if they are not rapidly reversed. Synaptic transmission is

14

also an inherently noisy process, as the neurotransmitter process includes a sub-threshold spontaneous release and a finite diffusion time across the synaptic cleft. Finally, as a result of the interconnectivity that is a feature of the central nervous system, there is the potential for other parts of the central nervous system to act as a controllable source of noise. As a neural network can act as a noise source for stochastic resonance by producing an output consisting of a random train of action potentials (Mato, 1999).

Limited Sensitivity

Although there is a large range in sensitivity in the variety of receptors in the body, all receptors have a limit to their sensitivity. The signal received by the central nervous system from the receptor is a train of action potentials travelling along the afferent nerve fibre. There is a limit to the maximum rate at which action potentials can be generated, governed by the absolute refractory period of the axon. The limited dynamic range of the receptor imposes a limit on the amount of information that can be signalled. For example, the inner hair cell would not be suitable for detecting movements of greater than a few nanometres, because the output train of action potentials would saturate at the maximum rate.

The range of stimulus amplitudes signalled by each receptor therefore has an upper and lower limit. The lower limit constitutes a threshold, below which an input signal does not cause a change in the output. It may be possible to reduce the threshold of a receptor by making it more sensitive, although as the receptor has a fixed dynamic range this would not result in any increase in the amount of information that could be signalled by the receptor. The change in sensitivity would simply alter the range of stimuli that could be effectively signalled by the receptor. The reduction in threshold may result in an increase in input noise, as previously sub-threshold noise signals may now be supra-threshold. The may actually result in a reduction in the amount of information that can be signalled by the receptor.

It is possible to improve the SNR within the central nervous system by combining the responses from many receptors. Perhaps the simplest method is to average the responses from many receptors. If all the receptors receive a common signal of interest, but

different sources of noise, then the averaged signal will have a higher SNR than the individual receptors. As the number of receptors that are used to generate the average increases, the final SNR increases. There is evidence that the central nervous system is capable of using this type of averaging, as for some receptor types the signal from a single receptor does not produce a conscious sensation, but must be combined with signals from other receptors of the same type. An example of a receptor for which the signal from an individual receptor does not reach consciousness is the muscle spindle (Macefield, Gandevia & Burke, 1990).

Possibility of Stochastic Resonance

Sensory receptor systems may be capable of exhibiting stochastic resonance, as they fulfil all the requirements of systems that exhibit stochastic resonance. The receptors are non-linear systems with thresholds to small periodic signals. Therefore, it is possible that they may be stimulated with a sub-threshold periodic input, the first requirement of stochastic resonance. There are many sources of noise that could be combined with the sub-threshold periodic input. Often environmental sources of noise may result in the SNR of the signal being less than one, as is the case with the inner hair cells. These are the precise circumstances under which stochastic resonance is proposed to occur, and therefore we might be expected to observe stochastic resonance in biological systems.

There is a further similarity between biological receptors and systems that exhibit stochastic resonance and this is that residence time histograms of a bistable system are similar to inter-spike interval histograms (ISIH) that are commonly seen in neurophysiology. The ISIH is constructed by creating a histogram of the times between successive action potentials recorded from a nerve fibre. ISIH from auditory nerve fibres and the visual cortex have a similar shape to residence time histograms constructed from bistable systems, including exponentially decaying peaks at integer multiples of the stimulus frequency (Longtin, Bulsara & Moss, 1991). The similarities in the shapes arise because of the reset mechanism of neurones. After an action potential is initiated the neurone must undergo a recovery process before another action potential can be initiated. The neuronal reset can be interpreted as the transition back to the original half-well in the double-well model.

Biological Systems Proposed to Exhibit Stochastic Resonance

The similarities between biological receptors and systems that exhibit stochastic resonance have encouraged investigators to examine biological systems for stochastic resonance. It has been proposed that stochastic resonance occurs in many biological systems ranging from cell membranes (Bezrukov & Vodyanoy, 1995) to human tactile sensation (Collins, Imhoff & Grigg, 1996b). Some of these systems may exhibit stochastic resonance, and in others the observed increases in sensitivity are not a result of stochastic resonance, while for many examples it is not clear whether the effect is stochastic resonance or some other noise effect.

The wide variety of biological systems that have been claimed to exhibit stochastic resonance highlights some important issues about stochastic resonance. That such a variety of biological systems have been proposed to exhibit stochastic resonance illustrates that additional input noise can often increase the sensitivity of a system. Most of the systems studied have shown an increase in sensitivity with the addition of noise. Although the claims that the increases in sensitivity are the result of stochastic resonance are not justified for most of the systems, the increase in sensitivity is not in doubt.

Whether the increase in sensitivity is a result of stochastic resonance, dithering or some other constructive effect of the additional noise is of more than just academic interest. The stochastic resonance effect requires specific levels of additional noise to optimise particular frequencies of sub-threshold periodic stimulation. The level of noise required is different for each frequency, and to obtain optimal performance the level of noise must be adjusted depending on the frequency of the periodic stimulus. The detection of non-periodic signals cannot be optimised with stochastic resonance, but can be with dithering. Therefore, which effect is producing the increase in sensitivity is important if an increase in sensitivity by the addition of noise is to be of practical use.

Voltage Dependent Ion Channels

The basis of all neuronal signalling in animals is the electrically excitable cell membrane. The voltage-sensitive ion channels in the cell membrane predominantly determine its excitability. Many of the requirements for stochastic resonance are present even in such a simple system as the voltage sensitive ion channel. The ion channel can either be open or closed, leading to a bistable system. An ion channel may actually be a multi-stable system as there may be many stable 'closed' states, but the simplest models use a single closed state (Goychuk & Hanggi, 2000). The transition between states is voltage dependent and exhibits a threshold, which is a requirement for stochastic resonance.

Theoretical work has been done on simple two-state potassium channels and it was found that optimal information transfer required the addition of input noise (Goychuk & Hanggi, 2000). There were a few other requirements, such as the channel being predominantly in the closed state, and the effect was dependent on the initial voltage level. These extra requirements are similar to the standard biological conditions, and therefore raise the possibility that the effect may be experimentally observed in isolated voltage channels. The results were generalised to periodic and aperiodic input signals with no dependence of the optimal noise level on the frequency of periodic input. This generalisation suggests that the increase in information transmission is not due to stochastic resonance, but is the result of some other constructive noise effect, as a key feature of stochastic resonance is the dependence of the optimal noise level on the frequency of the periodic input.

Individual voltage-sensitive ion channels can be incorporated into lipid bilayers that can be conveniently used for experimentation. One such channel is the alamethicin channel, which has been used to experimentally study stochastic resonance (Bezrukov & Vodyanoy, 1995; Bezrukov & Vodyanoy, 1998). An optimum in SNR_{PS} was obtained with the addition of input noise, which is a key feature of stochastic resonance. However, the optimal noise level did not increase with an increase in frequency of the periodic stimulus (Bezrukov & Vodyanoy, 1997). The optimal noise level may in fact

decrease with an increase in stimulus frequency, which is the opposite of what is predicted from stochastic resonance theory.

This example of an experimental investigation of stochastic resonance highlights an important issue. Although the output SNR is optimised with the addition of some level of noise, as expected from stochastic resonance theory, the effect may not be stochastic resonance, but some other constructive noise effect. The other interesting feature is that the output signal power rises monotonically over all the ranges of noise used. This is deceptive; as although the signal output power continuously increases, the noise output power also continuously increases. The rise in the output SNR is the result of the signal output power initially rising more rapidly than the noise output power. The fall is due to the noise output power rising more rapidly than the signal output power at higher input noise levels.

Mechanoreceptors

The physical signal detected by a mechanoreceptor is a mechanical deformation of the receptor's receptive field. The deformation leads to a depolarisation of the receptor's membrane, which if sufficiently large, causes the initiation of an action potential. The action potential is then actively propagated into the central nervous system. Mechanoreceptors are suitable for stochastic resonance studies for a variety of reasons. One aspect is that the mechanical deformation can be precisely controlled, allowing for the combination of small periodic and noise signals. The receptors often have well defined thresholds, ensuring that the periodic stimuli can be kept sub-threshold while the noise is supra-threshold, the requirements for stochastic resonance to occur. Finally, the action potentials can be recorded from afferent nerve fibres and used to produce a variety of output measures.

Crayfish

One of the earliest studies of stochastic resonance in a biological system was a study of the mechanoreceptors in the tailfin of the crayfish *Procambarus clarkii* (Douglass, Wilkens, Pantazelou & Moss, 1993). The mechanoreceptors detect the motion of water over the crayfish tailfin. Many of the receptors have a maintained discharge without

external stimulation. For stochastic resonance experiments, receptors with a low maintained discharge were used, to allow a wider range of noise levels to be studied. This is because the maintained discharge can be modelled as the response to an internal source of noise. Therefore, a low maintained discharge should indicate a receptor with low internal noise. Stochastic resonance-like curves were produced using both the SNR_{PS} and the SNR_{ISIH} measures.

Both the curves had a maximum output SNR with the addition of some level of input noise, the first key feature of stochastic resonance. However, the other main feature of stochastic resonance, a frequency dependence of the optimal noise level, was not shown, as only a single frequency periodic stimulus was tested. A matching of the optimal noise level with the predicted optimal noise level, from the noise-alone response, another interpretation of the 'resonance' aspect of the stochastic resonance effect, also was not shown. It is therefore impossible to conclude whether the effect was stochastic resonance or some other constructive noise effect, such as dithering.

In a related study, Pantazelou, Dames, Moss, Douglass & Wilkens (1995) demonstrated that altering the temperature of the preparation could produce a similar effect. For receptors with a maintained discharge, an increase in temperature led to an increase in noise in the receptor output. The increase in noise led in turn to an increase in SNR_{PS}, which it was proposed, was due to stochastic resonance. However, again only a single stimulus frequency was tested and the SNR_{PS} monotonically increased with increasing noise level (i.e. did not have an optimal value), so it is impossible to exclude other constructive noise, or temperature, effects.

These studies of stochastic resonance are typical of many, in that although an increase in output SNR with the addition of noise was observed, it is not possible to determine if the increase in the output SNR was a result of stochastic resonance, or some other effect. As only a single frequency of sub-threshold periodic signal was used, it is not possible to observe the matching of time-scales (or resonance), that is characteristic of stochastic resonance. Either a frequency dependence of the optimal noise value, or a matching of the predicted optimal noise value and the measured optimal noise value, must be shown to distinguish stochastic resonance from other noise effects, such as

dithering. Therefore, it is not possible to conclude whether the increase in output SNR observed with the addition of input noise for the case of the crayfish tailfin mechanoreceptor is stochastic resonance, or some other noise effect.

Rat

'Aperiodic stochastic resonance' has been proposed to occur in the slowly adapting cutaneous mechanoreceptors of the rat using a correlation measure (Collins et al., 1996a). As discussed above (p. 9), 'aperiodic stochastic resonance' cannot be a true resonance as there is no matching of time-scales, and the effect seen is most likely to be dithering or system linearisation by noise (Chialvo et al., 1997).

Rapidly adapting mechanoreceptors of the rat have also been investigated for stochastic resonance (Nozaki et al., 1999). Stochastic resonance-like curves were produced when the receptors were stimulated with sub-threshold sinusoidal stimuli and various levels of noise. Different frequency spectra of noise were used with the same periodic input, with the expected result that the optimum noise level was dependent on the types of noise used. The resulting curves were also of different shapes as predicted by theoretical analysis of a simplified membrane model. The study did not involve different periodic frequencies, so it is difficult to determine if the effect observed was stochastic resonance (as claimed by the authors) or dithering.

Ivey, Apkarian & Chialvo (1998) studied both rapidly adapting and slowly adapting mechanoreceptors and concluded: 'the addition of noise enhances signal transmission.' The results are based on a correlation measure and the curves produced do not show a frequency dependence of the optimal noise level. This result may be due to the measure used, as closer examination of the cycle histograms suggests that if a SNR measure based on the cycle histogram is used, the optimal noise level may increase with increasing stimulus frequency. The results are further complicated by the use of supra-threshold periodic stimuli for some frequencies and sub-threshold periodic stimuli for others. Stochastic resonance requires that a sub-threshold periodic signal be used, and therefore the results with the supra-threshold periodic signal cannot be a result of stochastic resonance.

Auditory Encoding

Inner Hair Cells

Specialised mechanosensitive cells, hair cells, are used by the auditory systems in the transduction of sound. Most of the auditory information is encoded by the inner hair cells, which have free standing hair bundles that are deflected by movement of fluid within the cochlea. The deflection of the hair bundles leads to opening of Ca^{2+} channels, which in turn leads to the release of neurotransmitter onto a synapsing nerve fibre. The free ends of the hair bundles undergo Brownian motion with an amplitude of approximately 3 nm_{RMS} (Wiesenfeld & Jaramillo, 1998). As mentioned previously (p. 13), the Brownian motion is significantly larger than the threshold for signal detection by these cells, which is around 0.1 nm. The hair cells may be able to use the supra-threshold noise, via stochastic resonance, to aid in the detection of near-threshold stimuli (Jaramillo & Wiesenfeld, 2000).

Jaramillo & Wiesenfeld (1998) experimented on isolated inner hair cells and recorded SNR_{PS} curves that peaked with the addition of approximately 3 nm of noise, mimicking the level of noise found under normal conditions. Although the experiments were performed with two different frequencies of sinusoidal stimulation, data for both frequencies are not shown for a single cell. Therefore, it is difficult to determine if the effect is due to stochastic resonance (as claimed by the authors) or some other effect, as it is not possible to observe a frequency dependence of the optimal noise level. It is interesting to note that the optimal noise level is close to the level that is present under normal physiological conditions.

Gebeshuber (2000) performed simulations of the responses of inner hair cells to stimulation at various frequencies, keeping the noise level fixed at approximately the physiological noise level. Under these conditions the standard SNR_{ISIH} would be expected to pass through a maximum at a given stimulus frequency if stochastic resonance was occurring. The optimal frequency would be determined by the response of the system to the fixed noise level. The measure used by Gebeshuber (2000) is based on the number of spikes phase locked to the signal, defined as spikes that occur during

the first half of the period. The output SNR does appear to peak around 1 kHz, but this effect is apparent even at supra-threshold levels of stimulus. Therefore, this effect is most likely a result of the frequency response of the system and not stochastic resonance.

Cochlear Nerve

Henry (1999) recorded from the round window of the inner ear while presenting various supra-threshold sinusoidal and noise acoustic signals. In response to supra-threshold sinusoidal signals at 8 and 8.8 kHz a 'nerve ensemble response' to the 800 Hz 'acoustic stimulus envelope' could be detected in the power spectrum of the recorded signal. It was this 'nerve ensemble response' that was taken as the output signal of interest. With the addition of moderate levels of noise there was an initial increase in the power present at 800 Hz, but with the addition of larger noise levels the power at 800 Hz reduced to below no noise conditions, a situation reminiscent of stochastic resonance.

The observed increase in output signal power at 800 Hz with the addition of noise was claimed to be a result of stochastic resonance. As, only a single 'acoustic stimulus envelope' frequency was tested, it was not possible to observe a frequency dependent change in the optimal noise level. Most importantly however, the stimuli used were supra-threshold, and stochastic resonance will only occur if the input stimulus is a sub-threshold periodic signal. Therefore, the observed increase in output signal power at 800 Hz is unlikely to be a result of stochastic resonance.

Cochlear Implants

Cochlear implants attempt to restore hearing by directly stimulating the cochlear nerve, bypassing damaged sections of the ear, including the hair cells. The stimulation patterns produced by the implants attempt to reproduce the important features of a normal response to sounds such as speech. The sciatic nerve from the toad *(Xenopus laevis)* has been used to study the trains of action potentials produced when different levels of noise are added to the stimulus pattern produced by a cochlear implant (Morse & Meyer, 2000). A synchronisation index, SNR_{SYNC}, was calculated based on the Fourier transform of the peri-stimulus time histogram. The SNR_{SYNC} was optimised with the

addition of input noise, and it was proposed that the increase in SNR_{SYNC} was a result of stochastic resonance.

It is difficult to classify the type of signal used for stimulation by the cochlear implant as either periodic or aperiodic. The signal used was band-limited, covering frequencies from 200 to 671 Hz, but this is still a large frequency range and it is unlikely that a single noise level would optimise this broad a frequency range via stochastic resonance. Therefore, it is unlikely that the effect is stochastic resonance and it is probably a result of a dithering type effect.

Human Muscle Spindles

The responses of muscle spindles to changes in muscle length are non-linear. This has led to their use in stochastic resonance studies (Cordo, Inglis, Verschueren, Collins, Merfeld, Rosenblum, Buckley & Moss, 1996). Afferents from muscle spindles in the wrist and hand of human subjects were recorded using microelectrodes. The wrist of the subject was rotated, supplying a sinusoidal stimulus, while various levels of noise were applied via the tendon of the appropriate muscle. Plots of SNR_{PS} against noise for six out of eight subjects show an optimum SNR_{PS} with the addition of noise, which was proposed to be the result of stochastic resonance.

It is difficult to determine if the effect is stochastic resonance or some other noise effect, as some of the key features of stochastic resonance were not investigated. Only a single stimulus frequency was used, so it is not possible to determine if the optimal noise level was dependent on the stimulus frequency. It is also difficult to determine the noise threshold and whether the optimal noise level was above this threshold, a feature of stochastic resonance. Finally the effect was not seen in all subjects, and there was no explanation proposed for this.

Neural Networks

Once external signals have been converted into trains of action potentials by receptors, they are transmitted to the central nervous system where further processing takes place.

24

It is possible that neural networks may exhibit stochastic resonance, as they are non-linear systems and typically have a threshold.

The simplest networks consist of a one-to-one linkage of receptor afferents to interneurones that propagate the signal further into the central nervous system. Even these simple networks introduce noise into the signal, as synaptic transmission is a noisy event. The transmission across the synapse typically involves the release of chemical transmitters that then diffuse across the synaptic cleft and initiate a depolarisation in the post-synaptic cell. All these processes are inherently noisy and may combine to introduce a significant level of noise into the system.

More complex networks that consist of many receptor afferents terminating on a single interneurone or multiple layers of interneurones introduce further sources of noise. An increase in the number of receptors or interneurones leads to an increase in the noise, simply because there are more synapses. When multiple receptor afferents terminate on a single interneurone, timing jitter, the result of differences in propagation velocity, also becomes important, as temporal information between the receptors may be lost.

Cercal System of the Cricket

Small amplitude, low frequency air disturbances can be detected by the cricket *(Acheta domestica)* using a mechanosensory system, the cercal hair system (Levin & Miller, 1996). The system comprises mechanoreceptors that synapse onto interneurones in an abdominal ganglion. Recordings from the interneurones can be made while stimuli are applied to the mechanoreceptors in the form of air currents. A peaked SNR_{PS} curve was produced when various levels of noise were added to near-threshold sinusoidal signals in the form of air currents, indicative of stochastic resonance. Levin & Miller (1996) also used broadband stimulus signals and calculated the transinformation rate, SNR_{TINFO}, based on Shannon's transinformation rate (Shannon, 1949). SNR_{TINFO} was also optimised with the addition of noise, which was proposed to be the result of stochastic resonance.

SNR_{TINFO} is measured with a non-periodic input and therefore the effect cannot be stochastic resonance, as discussed above (p. 9). If the effect was dithering, the level of

optimal noise would be expected to be constant or to decrease with increasing stimulus intensity. The optimal noise level actually increases with increasing stimulus intensity, so the effect is unlikely to be dithering. The increase in SNR_{TINFO} may be due to a variety of reasons, including the measurement used or some form of facilitation within the neural network.

The amount of facilitation and inhibition by feedback and inter-connections within a neutral network can be significant. These effects can alter the output SNR of the system and must be accounted for in any studies of stochastic resonance. This study highlights a difficulty with stochastic resonance studies of neural networks, as it is not possible to determine the mechanism by which the noise has optimised the SNR_{TINFO}, due to the complexity of the system.

The level of noise that optimises SNR_{PS} is higher than that which optimises SNR_{TINFO}, but only a single frequency was studied, so again it is difficult to determine whether the effect is stochastic resonance. Given the peak in the SNR_{TINFO} curve, it is likely the effect observed with the SNR_{PS} measure is not stochastic resonance, although further investigations are required to clarify the effect.

Multi-modal Caudal Photoreceptor Interneurones of the Crayfish

The caudal photoreceptor interneurones of the crayfish *(Procambarus clarkii)* respond to light from direct illumination, and to hydrodynamic stimulation via mechanoreceptors in the tailfin (Pei, Wilkens & Moss, 1996b). The interneurones have a resting discharge with a flat power spectrum between 5 and 35 Hz. The ISIH of the resting discharge has a logNormal distribution, highlighting the random nature of the resting discharge. In response to an increase in the intensity of the light stimulus the mean discharge rate increases, but the ISIH still has a logNormal distribution. Therefore, the effective noise in the system can be adjusted by changing the intensity of light directed on the interneurones.

Hydrodynamic stimulation of the mechanoreceptors with a periodic stimulus leads to a peak in the power spectrum of the interneurones' firing at the stimulus frequency.

Therefore, it is possible to independently adjust the effective noise intensity and the periodic stimulus intensity, by adjusting the light intensity and the stimulus to the mechanoreceptors respectively. The SNR_{PS} of the interneurone can then be used to study stochastic resonance in the whole system.

The SNR_{PS} curves produced have the characteristic shape of stochastic resonance, if light intensity levels are taken to be equivalent to noise levels (Pei et al., 1996b). There is an optimum in SNR_{PS} with increasing light intensities, and the optimum appears to be at lower light intensities for the 3 Hz periodic stimulation than for the 10 Hz stimulation. The precise location of the peaks in the SNR_{PS} curves is difficult to determine, due to the sparse measurements, but the indication of lower optimal light intensities for lower stimulus frequencies is present. Therefore, all the key features of stochastic resonance are present in this system and the effect almost certainly is stochastic resonance, as no other noise effect would be expected to produce the dependence of the optimal noise (light) level on the periodic stimulus frequency.

Baroreflex

Changes in blood pressure in man are monitored by the arterial and cardiopulmonary baroreceptors. If either of the groups of baroreceptors detect a drop in blood pressure a reflex response, via the nucleus tractus solitarius in the brain stem, is initiated to increase the heart rate and vascular resistance in order to raise the blood pressure (Andresen & Kunze, 1994). The baroreflex provides a convenient system for stochastic resonance studies, as the two separate groups of baroreceptors can be individually stimulated and the responses integrated in the brain stem before there is a resulting change in heart rate.

Hidaka, Nozaki & Yamamoto (2000) used a computer controlled, sinusoidally oscillating tilt table to provide a sub-threshold sinusoidal signal to the cardiopulmonary baroreceptors. A pneumatic neck chamber was used to provide a noise signal to the arterial baroreceptors and the inter-beat interval was taken as the output signal of the baroreflex system. An increase in the variation of the inter-beat interval at the sinusoidal test frequency, an indication of an increase in sensitivity to the otherwise sub-threshold sinusoidal signal, was observed in all subjects.

Despite all subjects exhibiting an optimal sensitivity to the test sinusoidal stimulus with the addition of noise, it is not possible to determine if the increase in sensitivity was a result of stochastic resonance as proposed. As with many of the other studies, only a single sinusoidal frequency was used, so it is not possible to observe a dependence of the optimal noise level on the sub-threshold periodic signal frequency. This study is of interest though, as the increase in sensitivity must have occurred within the central nervous system, most likely within the brain stem, indicating that the noise-induced increases in sensitivity are not limited to the peripheral receptors, but may occur within the central nervous system.

Cardiac Neurones

As part of the neural network controlling the cardiac system there are densely interconnected populations of neurones. Both excitatory and inhibitory neurones are connected together in a system that exhibits hysteresis. Kember, Fenton, Collier & Armour (2000) have studied such a system and propose that it exhibits 'aperiodic stochastic resonance', as the switching between the two stable states can be optimised with the addition of input noise.

As discussed above (p. 9), 'aperiodic stochastic resonance' is not stochastic resonance but is probably the result of dithering or system linearisation. Any output SNR optimisation by noise, in a system that exhibits hysteresis, is also unlikely to be due to stochastic resonance, as the Schmitt trigger, a simple system that exhibits hysteresis, does not exhibit stochastic resonance.

Median Nerve

The response to electrical stimulation of the median nerve in humans during various levels of voluntary contraction has been proposed to exhibit stochastic resonance (Chiou-Tan, Magee, Robinson, Nelson, Tuel, Krouskop & Moss, 1996). The study used subliminal stimulation of the median nerve and electromyography (EMG) to record the electrical activity from the middle finger and abductor pollicis brevis. The surface activity recorded from the middle finger is proposed to represent activity in sensory

fibres in the median nerve, and the EMG from the abductor pollicis brevis is proposed to indicate the activity in the motor fibres in the median nerve.

The level of 'background noise' in the median nerve was controlled by voluntary contraction of the abductor pollicis brevis, with an increase in contraction strength leading to a significant increase in the root mean squared (RMS) value of both the sensory and motor activity. The output SNR measure used, SNR_{AMP}, was the amplitude of the stimulus-evoked response divided by the RMS of the record activity. The sensory SNR_{AMP} monotonically increased for increasing contraction strength, while the motor SNR_{AMP} appeared to be independent of the contraction strength.

The effect of increasing the strength of the voluntary contraction on SNR_{AMP} is clearly not stochastic resonance. The stimulus used is not periodic, so by definition the effect cannot be stochastic resonance. The increase in SNR_{AMP} may be due to some form of facilitation caused by the voluntary contraction increasing the excitability of the sensory neurones.

Mammalian Brain

The brain, with many millions of neurones interconnected in an extremely complex arrangement is a very noisy environment for individual neurones, for several reasons. A neurone will receive inputs from many other neurones, resulting in an increase in noise due to synaptic transmission and timing jitter. Another noise source present in the brain is the vast number of other neurones. The fluctuations of the extracellular fluid composition surrounding a neurone are affected by other neurones, as are the electrical fields around a neurone. The fluctuations in extracellular fluid and electric fields may be related to the signal that a neurone is processing, and therefore may aid in the processing. Conversely, the fluctuations may be unrelated to the signal of interest, and are therefore considered a source of noise.

Hippocampal Cells

Hippocampal CA1 cells receive inputs via many thousands of synapses that allow the integration of a vast amount of information. It is possible to stimulate slices of rat hippocampus with two separate signals and record the response of the CA1 cells. Stacey

& Durand (2000) stimulated rat *(Rattus norvegicus)* hippocampal slices with uniform current pulses. One electrode delivered a periodic train of pulses while the other delivered a train of random pulses. Adjusting the number of random pulses delivered varied the intensity of the noise. The SNR_{PS} measure calculated from the response of a single CA1 cell was optimised with the addition of a specific level of noise, via the train of random pulses. Interestingly the level of noise that corresponded to physiological conditions, as determined by the spontaneous activity, was on the rising edge of the SNR_{PS} plot.

It is difficult to determine if the increase in SNR_{PS} is a result of stochastic resonance, as claimed, for two reasons. Only a single frequency of periodic stimulation was used, so it is not possible to observe the frequency dependence of the optimal noise level that is a key feature of stochastic resonance. The other difficulty is the type of stimulus used, which consisted of a series of current pulses injected into the hippocampal slice. Stochastic resonance is only possible for a sub-threshold periodic stimulus and traditionally this is in the form of a sinusoidal input. However, it is still possible to observe stochastic resonance with a periodic train of pulses as the input, as illustrated in Chapter Two (p. 61). Therefore, it is quite possible that the effect observed was due to stochastic resonance, although experiments with several sub-threshold periodic signals at different frequencies would be required to confirm the increase in SNR_{PS} as being a result of stochastic resonance.

Hippocampal slices from rat brains can also be stimulated using an electric field, rather than current pulses through an electrode (Gluckman, Netoff, Neel, Ditto, Spano & Schiff, 1996). A stimulus can be applied by modulating the electric field, which results in activity in the CA1 cells. When noise alone is used to modulate the electric field the CA1 cells respond with random bursts of activity, while periodic modulation of the electric field results in periodic bursting. The SNR_{PS} of a designated output cell passes through an optimal value with increasing levels of additional noise, which was proposed to be the result of stochastic resonance (Gluckman, So, Netoff, Spano & Schiff, 1998).

Again, a key feature of stochastic resonance, the frequency dependence of the optimal noise level, was not seen as only a single test frequency was used. However, it is

possible to observe a related feature: the matching of the predicted optimal noise level, predicted from the noise-alone response, and the measured optimal noise level. The optimal noise level should, on average, produce one impulse per cycle when it is used to stimulate the hippocampal slices without any periodic signal. The optimal noise level measured by Gluckman et al. (1998) produced 0.4 impulses per stimulus period. This is not what is predicted from stochastic resonance theory, although it is still possible that the observed increase in SNR_{PS} is a result of stochastic resonance. This is because the optimal noise level is clearly above the threshold noise level, the level predicted for dithering, the another possible effect. Further investigation with different frequencies of periodic signal are required to confirm whether the increase in SNR_{PS} was a result of stochastic resonance, or some other noise effect.

Visually Evoked Potential

It is possible to observe periodic changes in the electroencephalogram (EEG) recorded from a subject viewing a periodically changing image. The stimulus-evoked periodic changes in the EEG are the result of current leakage from the pyramidal cells and are referred to as the visually evoked potential (VEP) (Mitzdorf, 1987).

Srebro & Malladi (1999) measured VEPs from subjects viewing a two-dimensional spatial grating which was periodically reversed. A peak in the power spectrum is apparent at twice the reversal frequency, which passes through an optimum for increasing levels of input noise. As with many of the stochastic resonance studies, as only a single grating reversal frequency was used, it is impossible to determine if the effect was stochastic resonance as claimed.

Auditory Evoked Responses

In a similar experiment to that performed by Srebro & Malladi (1999), Stufflebeam, Poeppel & Roberts (2000) measured the change in the magnetic field recorded from the left temporal area of the brain in response to an acoustic stimulus. They found that a measure based on the correlation of the response to a single presentation to the average response over a hundred presentations was significantly increased with the addition of noise to the acoustic stimuli.

A single test frequency was used, and there is no measure of the noise-alone response, therefore it is impossible to determine if the effect is stochastic resonance as claimed. As the correlation measure was optimised when the input SNR was near unity, it is likely that the effect may be a form of dithering, although further experiments using different test frequencies would be required to determine the cause of the increase in the correlation measure.

Perception

All the systems considered so far have relied on extensive computer processing of a recorded signal to determine the final output signal, in the form of an output SNR measurement. It is not known what type of processing is possible within the central nervous system, and therefore it is not known if it is possible for the central nervous system to utilise stochastic resonance.

The output SNR measurements used in stochastic resonance studies are typically calculated over a significant time period, with the processing usually involving some type of averaging across time. Time averaging is used because, if the noise is not correlated in time, then it will average to zero, while any periodic signal will be re-enforced if the averaging is done over an appropriate period. It is unlikely that the central nervous system averages responses over many seconds, as is often done in the stochastic resonance experiments, but the availability of many neurones in parallel can reduce the need to average in time. Spatial averaging, averaging the responses from many neurones or receptors, can replace time averaging provided that the noise signal for each neurone or receptor is not correlated. In this way it may be possible for the central nervous system to take advantage of stochastic resonance.

Paddlefish

The paddlefish *(Polyodon spathula)* can use electro-receptors in its rostrum to detect plankton *(Daphnia)* while feeding. The plankton produce a small electric field that can be considered a point dipole source (Greenwood, Ward, Russell, Neiman & Moss, 2000). The precise manner in which the paddlefish distinguish the plankton from environmental electric fields is not known, but is likely to involve some form of

processing within their central nervous system. The signal generated by the plankton decreases approximately as the inverse cube of the distance. Therefore, the strike rate of the paddlefish decreases with distance from their rostrum. That is, the plankton become more difficult to detect when they are further from the electro-receptors in the rostrum.

Russell, Wilkens & Moss (1999) studied the effect of noisy electric fields on the strike patterns of the paddlefish, and found that at intermediate noise levels there is a broadening of the spatial range (an increase in the distance from the rostrum that the paddlefish will strike). With high noise levels the spatial range is reduced to less than the control level, presumably because of the difficulty of detecting the plankton in the noisy electric field. They proposed that swarms of plankton might act as a natural source of noisy electric fields that are utilised by the paddlefish, via stochastic resonance, to detect specific plankton.

The increase in spatial range is proposed to result from a decrease in the threshold of detection of the plankton. It is proposed that the reduction in the threshold is the result of stochastic resonance, although the effect is more likely to be the result of dithering. The optimal noise level appears to be close to the threshold level of noise, as predicted for dithering but not stochastic resonance. The theoretical statistical analysis of the problem is also based on the dithering effect. Therefore, although the paddlefish appear to be capable of taking advantage of a noisy environment, it is unlikely that the advantage is gained by utilising stochastic resonance.

Tactile Sensation

Human tactile sensation is derived from the responses of mechanoreceptors located in the various layers of the dermis and subcutaneous tissue. Moderate levels of additional input noise have been shown to enhance the detection of small sinusoidal signals in various mechanoreceptors. Although, as discussed above (p. 19), none of these studies have conclusively proved that the effect is due to stochastic resonance.

Several research groups have investigated whether the central nervous system can take advantage of the extra information that is available when noise is added to a test stimulus. Ivey et al. (1998) measured the detection threshold for sinusoidal

33

displacements of the skin on the fingertip with various levels of noise added to the sinusoidal displacement. The results suggest that the addition of appropriate levels of noise can decrease the threshold of detection, although the result is not statistically significant. The reductions in detection threshold are frequency dependent, with a higher input frequency showing a smaller effect, but possibly at a larger noise variance (level) as predicted by stochastic resonance.

Although it is not possible to be certain the decrease in threshold is due to stochastic resonance, it is quite probable that it is. The optimal level of noise appears to be larger for higher stimulus frequencies, a key feature of stochastic resonance. Also, the level of noise that was used was above threshold, indicating that the effect was unlikely to be dithering, which has an optimal noise level around the noise threshold.

The detection of a ramp indentation of the skin on the fingertip has also been shown to be improved by the addition of an appropriate level of noise to the displacement (Collins et al., 1996b; Collins, Imhoff & Grigg, 1997). The percentage of correct responses to a randomised series of presentations was used as the output SNR measurement for these studies. With the addition of an optimal level of noise the percentage of correct answers was statistically significant, indicating that an otherwise sub-threshold ramp was detectable. Interestingly, noise applied by electrical stimulation of the finger, rather than mechanical noise, can also be used to enhance detection (Richardson, Imhoff, Grigg & Collins, 1998).

The improvement in detection is not due to stochastic resonance as the signal was not periodic, and therefore there can be no frequency dependence of the optimal noise level. The optimal level of noise appears to be near-threshold, rather than above threshold as is predicted by stochastic resonance, and therefore the effect is most probably a form of dithering.

Visual Perception

Visual perception typically involves complex processing in the brain, as indicated by the large amount of the brain devoted to the task. The type of processing involved is dependent on the particular visual stimuli. It is possible to recognise abstract

representations of objects, pinpoint small changes in intensity and discern details in patterns. Each of these tasks is subject to different types of noise from the visual environment, and therefore the brain may utilise stochastic resonance to enhance detection of specific features of an image.

Simonotto, Riani, Seife, Roberts, Twitty & Moss (1997) measured the minimum contrast that was required to discern a particular feature of an image that was constructed of black and white pixels. The image was constructed by converting a continuous grey scale image into black and white pixels using an arbitrary threshold. If the grey scale for a given pixel was above threshold, the pixel was set to black, while if it was below it was set to white. The minimum contrast that was required to discern a particular feature was reduced when an appropriate level of noise was added to the image. The minimum contrast level could be further reduced by introducing time varying noise.

The reduction in contrast threshold is probably due to dithering rather than stochastic resonance as proposed. The optimal level of noise appears to be approximately at a threshold level, as predicted by dithering. The further reduction of the threshold with a time varying noise can best be explained by considering the averaging effects of the visual system. As the rate of updating of the noise increased above the rate of averaging for the visual system, the contrast threshold began to decrease rapidly. Again this suggests the effect is a type of dithering effect, rather than stochastic resonance.

A similar effect was noted by Piana, Canfora & Riani (2000) using capital letters, rather than a particular pattern as the stimuli. They extended the study to include letter identification and found that the addition of noise increased the percentage of correct identifications for an otherwise unidentifiable letter. Again the results suggest that this improved identification was a result of dithering rather than stochastic resonance as claimed, as there was no periodic component to the test image.

A visual perception task using autostereograms, pictures that have a three-dimensional image encoded in two dimensions, was studied by Ditzinger, Stadler, Struber & Kelso (2000). The state of 'spatial perception' (a measure of the mode of observation of the subject) could be controlled by altering the 'period length' of the image. A peak in the

SNR$_{PS}$ of the 'spatial perception' state with the addition of noise to the image was observed for two subjects when an otherwise sub-threshold periodic modulation of the 'period length' of the image was presented. The peak in the SNR$_{PS}$ was claimed to be a result of stochastic resonance.

The changes between 'spatial perception' states had been shown to exhibit hysteresis. Therefore, as with the Schmitt trigger (p. 12), the improvement in the SNR$_{PS}$ with the addition of noise is likely to be a result of dithering, rather than stochastic resonance. However, as the 'period length' of the image was only modulated at a single frequency it is not possible to determine if the effect was stochastic resonance or not.

Haken's bistable visual perception drawings consist of a series of nineteen images that form a progression from a man's face to a woman's body. The images form a set that exhibits a perceptual hysteresis (Chialvo & Apkarian, 1993). If the series of images are randomly shown to a subject who is asked to rank them from one to nineteen, one being a face and nineteen being the woman, most of the responses will be either face or woman with few responses in between.

A periodic signal can be introduced into the perception task by using it to modulate which image is presented. In their stochastic resonance study, Chialvo & Apkarian (1993) chose the next image to present based on the subject's response to the current image, the sub-threshold sinusoidal modulation and a noise signal. Without any additional noise the image tended to be classified as either the face or woman, indicating that the sinusoidal modulation was sub-threshold. With the addition of noise to the signal, transitions between the stable states became phase locked to the sinusoidal modulation. A histogram of the time between transitions resembles the ISIH of a neurone or a histogram of the residence time of a particle in the double-well model. An increase in the SNR$_{RES}$ was found for increasing noise levels, and a peak in the SNR$_{RES}$ measurement for the second peak of the residence time histogram was also found.

The effect is likely to be stochastic resonance because the level of noise that produced optimal SNR$_{RES}$ for the peak at twice the period is close to that which produces an average transition rate of half the sinusoidal frequency. Therefore, there appears to be a matching with a sub-harmonic of the stimulus frequency, which is predicted by

stochastic resonance. The SNR_{RES} measure for the stimulus period continued to increase for increasing noise levels, implying that the optimal noise level was above the noise levels tested. This is also in agreement with stochastic resonance theory as the maximum average transition rate was below the stimulus frequency. A higher optimal noise level for SNR_{RES} at the stimulus frequency than SNR_{RES} at half the stimulus frequency is also predicted by stochastic resonance, as observed.

Audio Perception

Detection Thresholds

Acoustic detection threshold measurements are typically performed in specially constructed rooms designed to reduce ambient noise, as it is believed that any additional noise will result in an increase in the detection threshold. However, Zeng, Fu & Morse (2000) found the addition of subliminal levels of noise to the test signal actually reduced the detection thresholds in normal subjects. Similar results were also reported for subjects with impaired hearing who had been fitted with cochlear implants and also one who had been fitted with a brainstem implant.

The observed decreases in detection threshold are unlikely to be the result of stochastic resonance as claimed, for a variety of reasons. With the normal subject two different test frequencies were used, and although the optimal noise level was dependent on the test frequency, as occurs in stochastic resonance, the higher test frequency had a lower optimal noise level, the opposite shift to that expected if the effect was the result of stochastic resonance. All subjects with the cochlear implants or brainstem implants were tested with a fixed noise level, but with many test frequencies. Under these conditions stochastic resonance should be evident by different frequencies being optimised with different fixed noise levels. As only a single noise level was used, it is not possible to determine if the observed decrease in detection threshold was the result of stochastic resonance, or some other effect, such as dithering. It is likely the effect was a form of dithering, as the cochlear implant subjects also performed a frequency discrimination test, for which the addition of a near-threshold level of noise resulted in the most sensitive discrimination.

Response Times

The EEG of a person at rest is essentially a random signal, but may have a periodic modulation, such as an α wave. In response to an audio stimulus such as a brief burst of sound, an event-related potential is present in the EEG that can be seen by averaging the EEG over many presentations. Winterer, Ziller, Dorn, Frick, Mulert, Dahhan, Herrmann & Coppola (1999) studied the reaction time of subjects to an audio stimulus and found that there was a correlation with the noise level present in the EEG before the stimulus. A larger noise value was weakly correlated with a decrease in reaction time. The level of noise in the EEG was defined as 'the mean power of all single sweeps minus the power of the average signal.' The authors propose that this was evidence that the central nervous system was able to use stochastic resonance to decrease the reaction time.

The reduction in reaction time is weakly correlated with the noise level, with the correlation dependent on a few subjects who had high levels of noise. Any reduction in reaction time is unlikely to be stochastic resonance, as stochastic resonance would be expected to produce a minimum in the reaction time for a non-zero level of noise, not a monotonically decreasing reaction time. Although the reaction time may increase for higher levels of noise, there is no indication of this effect from the available data. Reaction time is not a periodic measurement, but the audio tones are periodic and therefore it is possible that their detection may be enhanced by stochastic resonance, as discussed above (p. 22). However, no difference in the reaction times for the two frequencies was reported, as would be expected if the effect was a result of stochastic resonance.

Memory Retrieval

Usher & Feingold (2000) measured the response time of subjects presented with a simple single-digit arithmetical multiplication. The simple task was designed to be a memory retrieval task, as the subjects were all well trained in the simple multiplications. It was found that the response time for a correct answer was significantly lower when the tests were performed in the presence of 60 dB of acoustic noise than when the tests were performed without the acoustic noise. More intense levels of acoustic noise resulted in an increase in response time, to near control levels. Usher & Feingold (2000)

	Stochastic Resonance	Dithering	'Aperiodic Stochastic Resonance'
Non-linear system	✓	✓	✓
Periodic input	✓	✓	X
Increase in output SNR with the addition of noise	✓	✓	✓
Optimal noise level is supra-threshold	✓	X	X
Optimal noise level is dependent on periodic stimulus frequency	✓	X	X
Optimal noise level can be predicted from the noise-alone response	✓	X	X

Table 1.1   Stochastic resonance can be distinguished from other noise effects, such as dithering, either by a system's noise-alone response or by the response at two different test frequencies. An increase in the output SNR is not enough to determine if a system is exhibiting stochastic resonance.

modelled the memory retrieval task as a competition between multiple leaky accumulators, with the first accumulators to exceed an arbitrary threshold being the memory recalled.

The presence of acoustic noise clearly reduced the response time of the subjects. However, it is unlikely that it was a result of stochastic resonance as claimed by Usher & Feingold (2000). The analysis and modelling were both done without reference to a periodic input, and the memory retrieval task is not periodic in nature; therefore a matching of time-scales, a key feature of stochastic resonance, cannot occur. The model is optimised with the addition of Gaussian noise with a standard deviation of approximately 0.4. This is the level of noise that would be expected to optimise a system exhibiting dithering (Gammaitoni, 1995), and therefore the observed decrease in response time is likely to be a result of dithering.

Summary

Stochastic Resonance

There are a few key features of stochastic resonance that are worth reiterating. These features separate the stochastic resonance effect from other noise enhancement mechanisms and are summarised in Table 1.1. Firstly, the system must be non-linear to exhibit stochastic resonance. Typically the non-linearity is in the form of a threshold, but it is not necessary that the system have a threshold, just that the non-linearity have 'sufficient steepness' (Chapeau-Blondeau & Godivier, 1997; Balazsi et al., 1999).

Secondly, the input signal of interest must be a sub-threshold periodic signal. Typically the signal is a sinusoidal one, although it is possible to observe stochastic resonance with a periodically modulated train of pulses (for details refer to Chapter Two, p. 61). Therefore, by this definition, 'aperiodic stochastic resonance' cannot occur, as the input signal is not periodic. Without a periodic signal, there can be no matching of time-scales or frequency, which is the 'resonance' part of stochastic resonance.

The stochastic resonance effect results in an increase in the output SNR with optimal levels of additional input noise. This effect is initially counter-intuitive, although on

closer inspection does not seem so strange. An optimal output SNR with the addition of input noise is not unique to stochastic resonance. In fact there are many other noise effects, such as dithering, that may also result in an optimal output SNR with the addition of noise, as illustrated in Figure 1.5. Therefore, simply because a system exhibits an increase in output SNR with the addition of input noise, it does not mean that the system is exhibiting stochastic resonance.

The feature that sets stochastic resonance apart from all other noise effects is the relation between the optimal noise level, D_{OPT}, and noise-alone response of the system. It is possible to predict the noise level that should optimise the output SNR, D_{PRE}, from the noise-alone response. It is the level of noise that, when applied alone, produces an average output rate from the system that is equal to the frequency of the sub-threshold periodic signal, illustrated by the grey lines in Figure 1.4 (bottom panel). As the noise-alone response is a monotonically increasing function of noise, larger noise levels are required to optimise higher frequency sub-threshold periodic stimuli. The matching of D_{PRE} and D_{OPT} and the resulting periodic stimulus frequency dependence of D_{OPT} are the key features of stochastic resonance that are not produced by any other noise effect.

A consequence of the matching of D_{OPT} and D_{PRE} is that D_{OPT} must be greater than the threshold noise value. With the threshold value of noise, the average noise-alone induced rate is just above zero. Therefore, this level of noise would only optimise a sub-threshold periodic stimulus with a near zero frequency. Another constraint imposed by the noise-alone response is that there is an upper limit to the noise-alone induced rate. This limits the maximum sub-threshold periodic signal frequency that can be optimised via stochastic resonance. For the bistable potential well system illustrated in Figure 1.3 and Figure 1.4, the maximum noise-alone induced rate is approximately 100 t/s. Therefore the maximum periodic signal frequency that can be optimised via stochastic resonance would be 100 Hz, although, it may be possible to optimise sub-harmonics of higher frequencies with the appropriate level of additional input noise.

To determine if a system exhibits stochastic resonance, two features must be present. Firstly, the output SNR must be optimised by some supra-threshold level of noise, D_{OPT}. Secondly, the optimal noise level must either be dependent on the periodic stimulus

frequency or match the predicted optimal noise level, D_{PRE}, which can be predicted from the noise-alone response of the system. Many noise effects can satisfy the first criteria, but only the stochastic resonance effect can satisfy both.

Stochastic Resonance in Biological Systems

Of all the biological systems that have been investigated for improved signal detection in the form of an increase in output SNR with additional input noise, very few have been proved to involve stochastic resonance as proposed (for a summary see Table 1.2). That the addition of noise had increased the sensitivity of most of the systems is not in doubt, but the mechanism by which the increase in sensitivity had occurred is. Of the biological systems studied, only the crayfish multi-modal interneurone (Pei et al., 1996b) convincingly exhibited stochastic resonance. Interestingly, in this study the noise and periodic stimuli were of different modalities, indicating that the stochastic resonance effect was occurring in the interneurone and not in the mechanoreceptor. This is important as it indicates that it may be possible for stochastic resonance to occur within the central nervous system, and that it is not limited to peripheral receptors. It is likely that many of the other systems studied could exhibit stochastic resonance, but the available results did not allow distinction between stochastic resonance and other noise effects, as the frequency dependence of the optimal noise level was not measured. Therefore, the majority of systems required further investigation to determine the effect of the increased output SNR. The further investigation must include the measurements of the response to several frequencies of sub-threshold periodic stimuli to be able to differentiate between stochastic resonance and other noise effects. The advantages of a system that exhibits stochastic resonance, over a system that exhibits other forms of noise enhanced sensitivity, such as dithering, will be discussed later in this thesis (p. 142).

Perhaps the most interesting results come from investigations into perception, where stochastic resonance has been observed with visual perception tasks (Chialvo & Apkarian, 1993) and perhaps in tactile detection tasks (Ivey et al., 1998). As the studies of tactile sensation emphasise, a system can exhibit stochastic resonance and also exhibit other constructive noise effects depending on the type of stimulation used and the analysis performed. Therefore, it is important that any investigations of stochastic resonance use carefully chosen stimuli and processing techniques to ensure the observed effects are truly stochastic resonance.

	Output signal to noise ratio is optimised by the addition of noise	Periodic stimulus	The optimal noise level increases with increasing periodic stimulus frequency	The optimal noise level matches that predicted from the noise-alone response	Stochastic Resonance	Page
Voltage dependent ion channels	✓	✓	X		X	18
Crayfish mechanoreceptors	✓	✓				19
Rat mechanoreceptors	✓	✓ / X	X		X	21
Inner hair cells	✓	✓				22
Cochlear nerve	✓	✓				23
Cochlear implants (sciatic nerve)	✓					23
Muscle spindles	✓	✓				24
Cricket cercal system	✓	✓ / X			X	25
Crayfish multi-modal caudal photoreceptor interneurones	✓	✓	✓		✓	26
Baroreflex	✓	✓				27
Cardiac neurones	✓	X			X	28
Median nerve	X	X			X	28
Hippocampal slices	✓	✓		X		29
Visually evoked potential	✓	✓				31
Acoustically evoked response	✓	✓				31
Paddlefish strike pattern	✓					32
Tactile sensation	✓	✓ / X	✓		✓ / X	33
Visual perception	✓	✓ / X		✓	✓ / X	34
Audio detection threshold	✓	✓	X		X	37
Response time to acoustic stimulus	X	✓	X		X	38
Memory retrieval	X	X			X	38

Table 1.2   Although many biological systems have been proposed to exhibit stochastic resonance, very few have been tested sufficiently to determine if the increase in output SNR is the result of stochastic resonance or some other effect. A '✓' indicates that the condition has been observed, while a X indicates that the condition did not occur, and a blank indicates that the condition was not tested.

Chapter Two

Modelling of Stochastic Resonance

Much of the work that has been done on stochastic resonance has been based on models. Theoretical analysis of the models is often difficult and simplifying approximations are often required. Therefore, simulations of the models are often used to gain insight into some of the more interesting features of stochastic resonance.

Bistable Potential Well

The bistable potential well model, described in Chapter One, is one of the simplest models for stochastic resonance that has been studied. Several variations of the potential well have been used but the results from different potentials are qualitatively similar (Benzi et al., 1981; Bulsara, Jacobs, Zhou, Moss & Kiss, 1991). Therefore, the model described in Chapter One has been taken as representative of all bistable potential well models.

All of the features of stochastic resonance are apparent in the bistable potential well model. These features include: an optimal output SNR with the addition of a supra-threshold level of input noise; an increase in the optimal noise level with an increase in sub-threshold periodic stimulus frequency; and a matching of the noise-alone induced transition rate to the sub-threshold periodic stimulus frequency at the optimal noise level. While many constructive noise effects may produce the first feature, only stochastic resonance will result in a frequency dependent optimal noise value, typified by the second two features. All these features were illustrated in Chapter One and were produced by numerical integration of Equation 1.1 and Equation 1.4 using a fixed step-size fourth-order Runge-Kutta method. The simulations were performed on a Macintosh Power PC (Macintosh, Cupertino, California, U.S.A.) using Igor Pro (WaveMetrics, Lake Oswego, Oregon, U.S.A.) with a custom written additional code module (Appendix A).

The bistable potential well model reproduces many of the statistical features of the discharge of neuronal systems subjected to sinusoidal stimulation of the appropriate modality (Longtin, Bulsara, Pierson & Moss, 1994). However, the bistable potential

well model cannot model some of the features of biological receptors, including a maintained discharge and the response to a non-periodic stimulus (e.g. a ramp-and-hold stimulus). Therefore, other more biologically relevant models have been used to investigate stochastic resonance in biological systems.

Biological Models

There have been many investigations of stochastic resonance in neurones using a variety of models. The models have various levels of complexity ranging from simple models such as the integrate-and-fire model, two-state models and the Fitzhugh-Nagumo model, to more complex models including the Hodgkin-Huxley model. The information contained in an action potential is transmitted either by propagating regeneratively or by causing the release of neurotransmitter, so the precise shape of the action potentials is not thought to be significant. Although, a reduction in size of the action potential, as a result of extremely high firing rates, can result in a reduction in the amount of neurotransmitter released. Therefore, the majority of the physiologically relevant information carried by a train of action potentials is the relative timing of the action potentials. The output of many of the simple models is a series of standard spikes that can be treated as a series of recorded action potentials, while the more complex models are capable of producing deterministic spikes.

Integrate-and-Fire Model

One of the simplest neurone models, the integrate-and-fire model, has been shown to exhibit all the features of stochastic resonance. The model is considered a first-order approximation of the full Hodgkin-Huxley model, which is the benchmark for excitable membrane models (Plesser & Geisel, 1999). The membrane voltage is modelled as a simple integrator of the input current with a threshold for spike generation. When the membrane voltage exceeds the threshold, a standard spike is generated and the membrane voltage is reset to a voltage below threshold. The depth of the reset voltage below threshold and the time constant of the membrane determine the refractory period of the model neurone. Although the model is quite simple it can reproduce many of the features of neurones.

The model exhibits resonance-like behaviour for a periodic stimulus at a set frequency with changing noise intensity, which is the classical stochastic resonance behaviour. Interestingly, the model can also show resonance-like behaviour for fixed noise intensity and changing stimulus frequency. This second tuning effect would also be expected from a system exhibiting stochastic resonance. However, the second tuning effect is dependent on the measure that is used. If the standard measure based on the output power spectrum, SNR_{PS} (p. 4), is used on the series of standard spikes then the effect is not seen (Plesser & Tanaka, 1997). However, if the measure based on the inter-spike interval histogram, SNR_{ISIH} (p. 54), is used then the resonance with changing frequency and constant noise is seen (Shimokawa et al., 1999a; Barbi, Chillemi & Di Garbo, 2000). This has led to the proposition that it is not possible for a system to exhibit stochastic resonance if the standard SNR_{PS} measure is used (Fox, 1989).

Ensembles of integrate-and-fire neurones have also been investigated for stochastic resonance (Shimokawa, Rogel, Pakdaman & Sato, 1999b). The neurones were modelled as being subject to a common input current signal, but with different noise sources. The output spike trains of the individual neurones were then summed at a higher order neurone, modelling synaptic transmission to an interneurone, to give the final output of the system. It was shown that the summing improved the signalling of the system, but the precise effect was dependent on the type of output measure that was used. The improvement in the output SNR is likely to be the result of a simple averaging across the population, as discussed in Chapter One (p. 10), and not stochastic resonance.

Mato (1999) used 1600 integrate-and-fire neurones in a network to produce a noise input, in the form of a random train of spikes, for another integrate-and-fire neurone. The result was a network of neurones that was able to produce many of the features of stochastic resonance without an external noise source. The network of neurones producing the noise input could be tuned to alter the noise distribution, with the result that the response of the system could equal a system with an ideal source of external noise (i.e. a noise source that produced a maximum increase in the output SNR). That a network of neurones can produce an adjustable random spike train that can be used, via stochastic resonance, to optimise the response of neurone has important ramifications

for signal detection throughout the central nervous system, as discussed in Chapter One (p. 14).

Simplified Spike Integrator

Godivier & Chapeau-Blondeau (1996) studied a simplified neurone model that numerically integrates changes in conductance initiated by input spikes. The model is based on the changes in conductance that occur in the membrane of a postsynaptic neurone in the region of the synaptic cleft. Each input spike initiates an increase in conductance, followed by a return to a resting level of conductance. The membrane voltage fluctuates as a result of the changing conductance. If the membrane voltage crosses a threshold level, it is reset to a resting level after a refractory period. The output of the neurone is a series of standard spikes at the times of the threshold crossings.

A periodic spike train and a series of random spike trains were used as inputs, with the power spectrum of the resulting series of standard spikes being used to calculate an output measure, SNR_{PS} (p. 4). The number of random spike trains was altered to change the effective level of noise in the system. An optimal SNR_{PS} was produced when more than one random spike train was used, as would be expected if the system was exhibiting stochastic resonance. As only a single periodic input frequency was used it is not possible to observe a dependence of the level of noise required to optimise the output SNR on the frequency of the periodic stimulus, a key feature of stochastic resonance.

Fitzhugh-Nagumo Model

The Fitzhugh-Nagumo (FHN) model is a two-state excitable membrane model described by Equation 2.1 (Fitzhugh, 1961). The two state variables have different dynamics and model different aspects of an excitable membrane. The 'fast' variable, v, models the membrane voltage, while the 'slow' variable, w, is a recovery variable. The input signal and noise are represented by S(t) and $\xi(t)$ respectively, while the remaining constants affect the dynamics of the model. The model is capable of producing many features of neuronal discharges including deterministic spikes that are reminiscent of
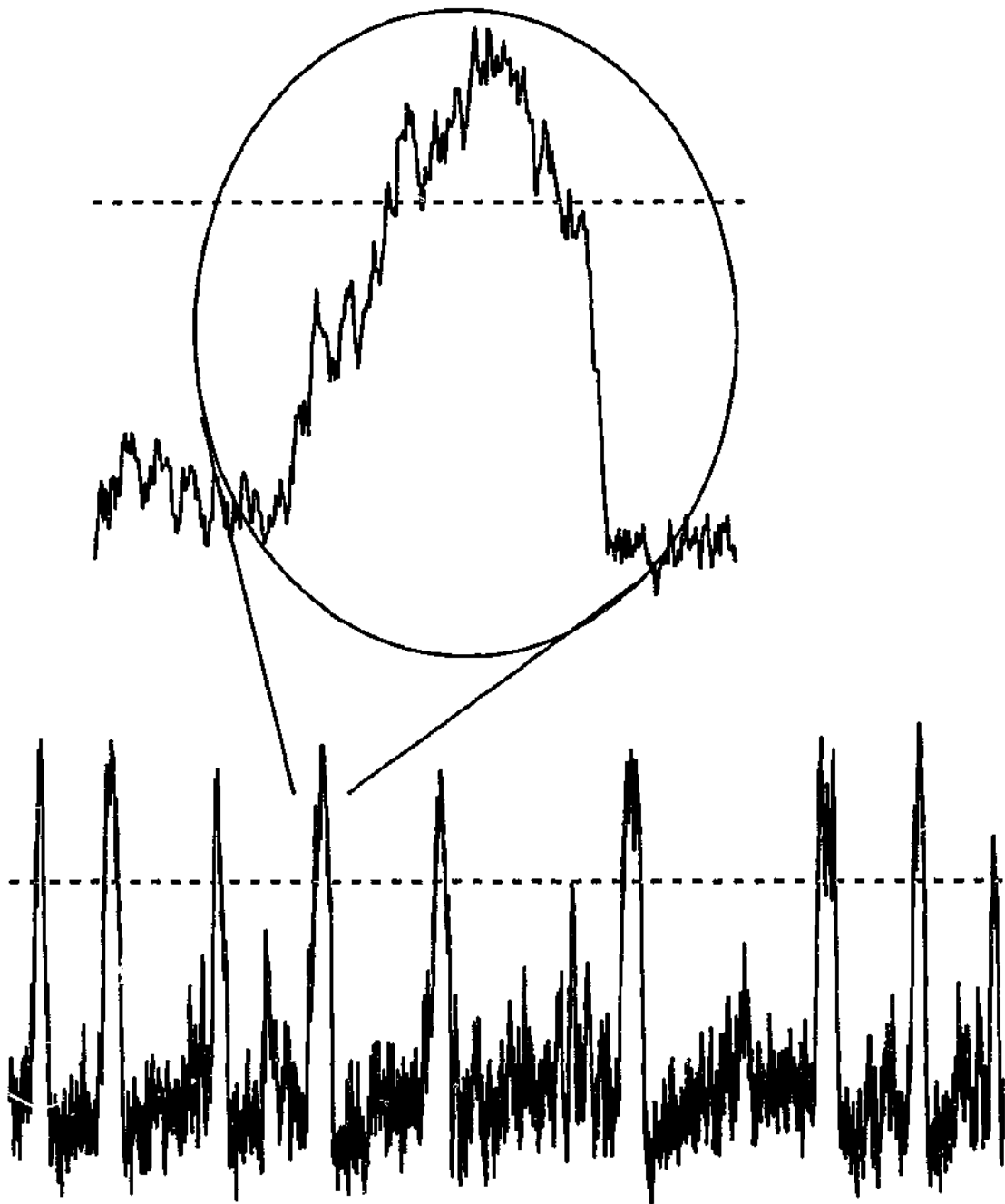
Figure 2.1   Fluctuations about an arbitrary threshold (grey dashed line) are present in the Fitzhugh-Nagumo model when large noise amplitudes are used, as illustrated by the magnified pulse. Although smaller noise amplitudes result in fewer fluctuations, the larger noise amplitudes are required to show the complete stochastic resonance effect. The simulation shown has arbitrary units for both the ordinate and abscissa that have not been shown.

action potentials, a maintained discharge and responses to non-periodic signals, such as ramp-and-hold stimuli.

$$\varepsilon \dot{v} = v(v-a)(1-v) - w + A + S(t) + \xi(t)$$
$$\dot{w} = v - w - b$$

Equation 2.1

The determination of the precise timing of the output spikes becomes difficult with increasing noise levels. If the noise is of sufficient amplitude the spikes may actually consist of several threshold crossings, as illustrated in Figure 2.1. The fluctuations about the threshold level are the result of the high frequency components of the noise. Although it would be possible to reduce the high frequency fluctuations of the output by reducing the amplitude of the input noise, the larger noise amplitudes are often required to show the full stochastic resonance effect. Some investigators therefore introduce an absolute refractory period into the model, which reduces the effect of these fluctuations. The absolute refractory period is implemented by ensuring the minimum time between threshold crossing is longer than the spike width, when converting the output 'v' into a series of standard spikes (Chialvo et al., 1997).

Stochastic resonance has been shown in the FHN model using both an output measure based on the cycle histogram, SNR_{CYC} (p. 8), with an absolute refractory period (Chialvo et al., 1997) and an output measure based on the inter-spike interval histogram, SNR_{ISIH} (p. 54), without an absolute refractory period (Longtin, 1993). Both investigations showed an increase in the optimal noise level for an increase in the periodic stimulus frequency, the key feature of stochastic resonance.

It has also been proposed that the FHN models exhibits 'aperiodic stochastic resonance' (Collins et al., 1995a). However, as discussed in Chapter One (p. 9), 'aperiodic stochastic resonance' is probably the result of dithering or system linearisation rather than a form of stochastic resonance (Chialvo et al., 1997). 'Stochastic resonance without tuning' has also been proposed to occur with the FHN model (Collins, Chow & Imhoff, 1995b). 'Stochastic resonance without tuning' is proposed to occur when the output from many FHN model neurones, that are subject to the same non-periodic input signal but different noise inputs, are combined. As the number of model neurones is increased the dependence of the output on the noise level changes. With only a few neurones the

output SNR varies with the level of input noise in a similar manner as it does for stochastic resonance. That is, the output SNR is optimised with the addition of a single level of noise. For large numbers of model neurones, approximately 1,000, there is not a single optimal noise level, simply a minimum noise level that is required for an optimal output SNR. Stochastic resonance without tuning is based on 'aperiodic stochastic resonance' and therefore is also proposed to be due to dithering or system linearisation (Chialvo et al., 1997).

Massanes & Vicente (1999) demonstrated a more traditional form of resonance in the FHN model. The model has a preferential firing rate at large noise intensities, with the rate being largely independent of the noise level used. That is, if stimulated with noise above a certain minimum level, the model fired at a near constant rate. Under these conditions, the model behaves as a deterministic resonant system, with a natural frequency, ω_0, set by the preferred firing rate. As the preferred rate is largely independent of the noise level used it is not possible to tune the model to different frequencies; therefore, this type of resonance is not stochastic resonance. The preferred firing rate is higher than the periodic frequencies used in many of the other studies. Therefore, it is unlikely that the effect observed in the other stochastic resonance studies is related to this resonance. However, this other type of resonance does highlight the difficult nature of stochastic resonance investigations.

An effect known as 'spatiotemporal stochastic resonance' has been observed in a two-dimensional network of FHN models (Balazsi et al., 1999). With the addition of appropriate levels of noise, waves of excitation can spread throughout the network. These waves of excitation cannot be propagated in the absence of additional input noise, as they are below threshold. The addition of too much noise leads to the break up of the waves, so the effective spread of the waves has a characteristic optimum with the addition of noise. The effect is similar to the dithering effect but spread throughout a two-dimensional network, therefore it is unlikely to be stochastic resonance.

Hodgkin-Huxley Model

One of the best known excitable membrane models is the four-dimensional Hodgkin-Huxley model (Hodgkin & Huxley, 1952). This model, first proposed in 1952, is based

on voltage clamp data from the squid *(Loligo)* giant axon. Although the equations were developed for the unmyelinated membrane in the giant axon, the model has been used to model a variety of excitable membranes.

Kanamaru, Horita & Okabe (1998) studied stochastic resonance using the Hodgkin-Huxley model. A sub-threshold periodic current and superimposed noise current was used as the input and the power spectrum of the resulting output voltage was used to calculate SNR_{PS} (p. 4). An optimal SNR_{PS} with the addition of noise was found. However, the simulations were performed with a single periodic stimulus frequency so it is not possible to determine if the effect was stochastic resonance, as claimed by the authors. The frequency dependence of SNR_{PS} with a constant noise level was shown to have an optimum at approximately 70 Hz, which could indicate stochastic resonance. However, the frequency dependence of SNR_{PS} with a fixed noise level is most likely to be a form of deterministic resonance that is related to the frequency dependence of the optimal noise level, D_{OPT}, shown by Lee & Kim (1999), also centred on 70 Hz.

The Hodgkin-Huxley model has a characteristic frequency of approximately 70 i/s, which is also approximately the lowest frequency at which the model will generate a maintained discharge. Therefore, the resonance effects are most likely to be a form of deterministic resonance, rather than stochastic resonance. The Hodgkin-Huxley model also exhibits dithering (Pei, Wilkens & Moss, 1996a), which further complicates interpretation of the effects of noise.

Non-membrane Models

Other biological models have been used in stochastic resonance studies, but none of them have convincingly shown stochastic resonance. Zhong & Xin (2000) modelled the dynamics of an oil-water interface that is proposed as a model of excitable bio-membranes, specifically the membranes of olfactory and gustatory cells. The oil-water interface exhibits periodic fluctuations in the amount of material transferred to a bulk organic phase under the influence of random variations in the concentrations of the constituents of the material to be transferred. A measure based on the power spectrum of the transfer rate, SNR_{PS} (p. 4), has an optimum for a non-zero level of noise, reminiscent of stochastic resonance. However, it is unclear how a noise-induced

periodic fluctuation can be considered a useful signal. Also, the induced periodic fluctuations are at a single frequency, determined by the system dynamics, so it is not possible to observe a change in the optimal noise level with frequency, a requirement of stochastic resonance.

Srebro & Malladi (1999) modelled part of the visual cortex with a neural network based on simple cells. The simple cells were modelled as having a fixed spatiotemporal response to the input. That is, the responses of the simple cells were modelled by convolving each test stimulus with a fixed spatiotemporal field that was characteristic of the simple cell. While the response of a cell was above a set threshold the cell was designated as firing at 200 i/s, otherwise it was silent. The responses from 100 such cells were summed and the power spectrum of the resulting signal used to calculate SNR_{PS} (p. 4). The results generated from the model matched measured visually evoked potential increases with additional noise. Unfortunately, both the model and experimental results used a single stimulus frequency so it is not possible to determine if the effect was stochastic resonance.

A model of simple cells in the visual cortex requiring a noise input to exhibit contrast invariant orientation tuning, a property observed under experimental conditions, was investigated by Anderson, Lampl, Gillespie & Ferster (2000). Contrast invariant orientation tuning refers to the observation that some neurones in the visual cortex respond only to stimuli of a particular orientation, and that this effect is independent of the contrast of the stimulus used. The effect was a system linearisation, not stochastic resonance as claimed, as the noise effectively removed the threshold.

Stemmler, Usher & Niebur (1995) also used a simplified model of the visual cortex to study the effect of noise. Their model was based on densely interconnected cells contributing excitatory or inhibitory influences with lateral connections. The effect of the noise on the model was to alter the ratio of excitatory and inhibitory inputs, which resulted in a linearisation of the response of the network and was not stochastic resonance as claimed.

Kashimori, Hoshino & Kambara (2000) used a simplified model of the torus semicircularis of the weakly electric fish *(Eigenmannia)* to investigate the effect of

noise on the fish's ability to adjust its electric organ discharge in response to the detection of another *Eigenmannia*. The small cells of the torus semicircularis were modelled as being part of a linear array of cells receiving time delayed inputs from two different receptive fields. The ability of the model network to discriminate small differences in the phase of the periodic signals presented to the two receptive fields was enhanced with the addition of noise. The optimal noise level was equal to the threshold level of detection, in the absence of noise. The threshold optimal noise level suggests that the enhanced detection was due to dithering rather than stochastic resonance as claimed.

Hodgkin-Huxley Model

Many different excitable membrane models have been proposed to exhibit stochastic resonance. However, the majority of the models, while exhibiting an optimal output SNR with the addition of noise, have not been examined thoroughly enough to prove that the increase in the output SNR is a result of stochastic resonance. A point of interest is that the same models appear to exhibit different behaviour based on the output SNR measure used. Therefore an evaluation of a variety of different output SNR measures using a common model, the Hodgkin-Huxley excitable membrane model, is of interest.

The Hodgkin-Huxley model, as previously mentioned, is one of the standard models for excitable membranes. The model is based on voltage sensitive ion channels that are present in the membrane. Only the sodium and potassium currents are specifically modelled, with the remaining ionic currents being modelled by a leakage current.

The model is capable of producing action potentials in response to injected current, which resemble those recorded from the giant axon of the squid *(Loligo)* under similar conditions. The previous studies into stochastic resonance using the Hodgkin-Huxley model have reported an optimum in a SNR measurement based on the output power spectrum, SNR_{PS} (p. 47), for a non-zero level of noise. However, the studies have failed to demonstrate all of the key features of stochastic resonance, particularly the frequency dependence of the optimal noise level.

Realisation of the Model

The set of equations used to implement the Hodgkin-Huxley model is given in Appendix B. The equations were solved using a fixed step-size fourth-order Runge-Kutta numerical integration technique. The simulations for the Hodgkin-Huxley model, and the remaining models discussed in this chapter, were performed on a Macintosh Power PC (Macintosh, Cupertino, California, U.S.A.) using Igor Pro (WaveMetrics, Lake Oswego, Oregon, U.S.A.) with custom written additional code modules (Appendix A). The simulations required an input current waveform and returned a voltage waveform consisting of a series of action potentials.

Response Curves

Figure 2.2 (top panel) is the threshold frequency response curve of the model when stimulated with a sinusoidal input current waveform. The stimulus was considered to be supra-threshold if it generated a one-to-one driving of the model, so that an action potential was produced once a cycle. There is a minimum at approximately 60 Hz, which corresponds to the characteristic frequency of the model as discussed previously (p. 47).

The response of the model to a noise-alone stimulus is shown in Figure 2.2 (bottom panel). The noise-alone stimulus consisted of a computer generated random input current waveform, which was normally distributed with a mean of zero and an adjustable standard deviation. The standard deviation of the noise-alone input current waveform was defined as the noise amplitude. The response is characterised by a threshold of approximately 5 mA, that is an input current waveform with a mean of zero and a standard deviation of 5 mA. The average rate then rises rapidly with increasing levels of noise up to a noise level of approximately 15 mA. The slope of the response then decreases and the average rate approaches an asymptotic value between 60 and 70 i/s. The noise-alone response can be fitted with a curve based on Kramers' rate for a bistable potential given by Equation 2.2. 'D' is the noise amplitude and α and β are arbitrary constants (Kramers, 1940).

51
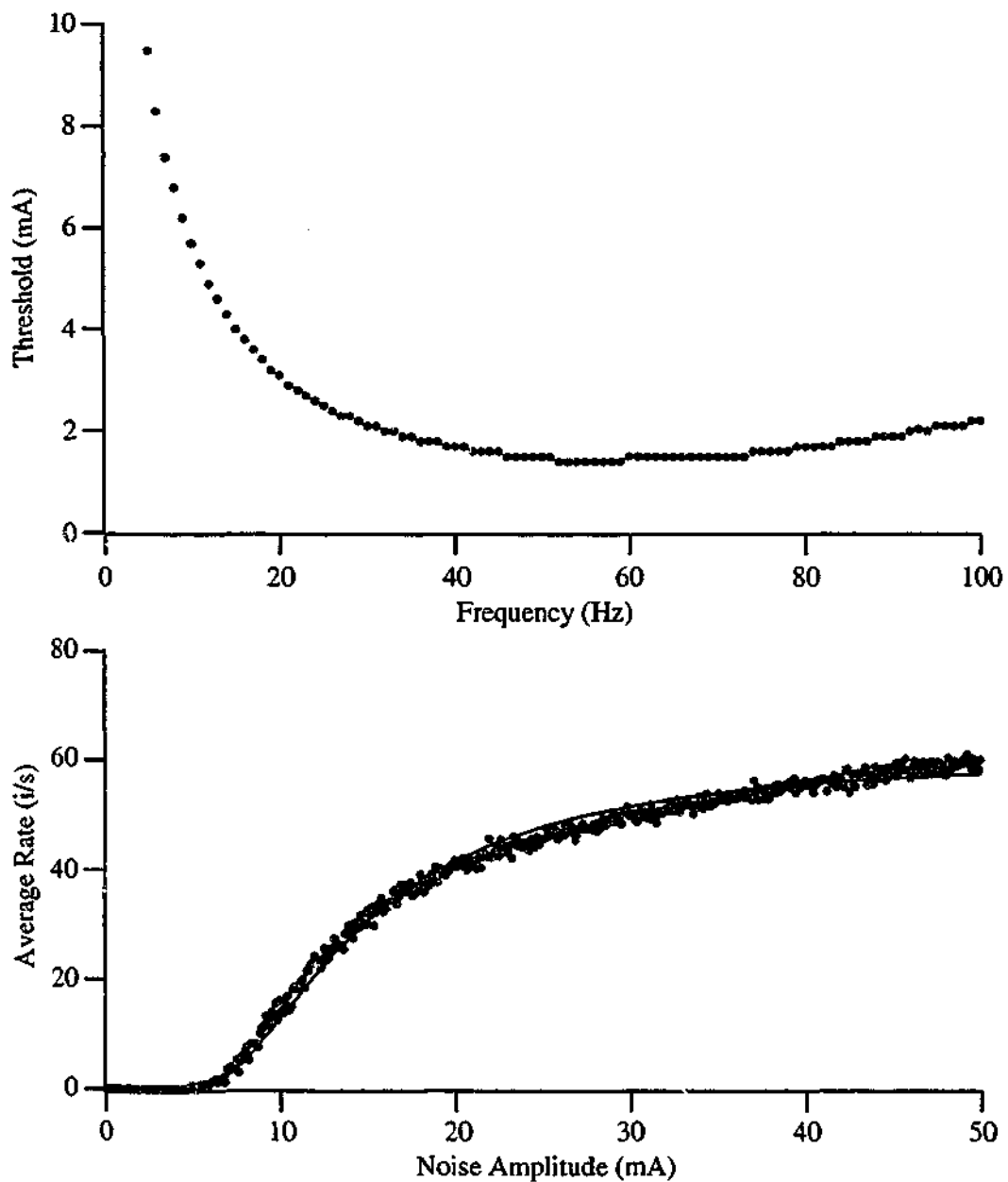
Figure 2.2 The frequency response of the Hodgkin-Huxley model (top panel) has a minimum around 60 Hz, near the characteristic frequency of the model. The threshold was defined as an input amplitude that produced one-to-one driving of the output spike train. The noise-alone response (bottom panel) exhibits a threshold of approximately 5 mA, after which the average rate increases monotonically with increasing noise amplitude. The noise-alone response has been fitted with a curve based on Kramers' rate (Equation 2.2, solid line). This and all subsequent simulations using the standard Hodgkin-Huxley model, described in Appendix B, were simulated using a fourth-order Runge-Kutta numerical integration technique with a fixed step size of 50 μs for a period of 100 s, unless otherwise specified.

$$\text{Rate} = \alpha e^{-\frac{\beta}{D^2}}$$ **Equation 2.2**

Different Output Measures

Whether a system exhibits stochastic resonance is dependent not only on the system being studied, but also the output measurement being used. The output of the Hodgkin-Huxley model is a voltage waveform containing a train of action potentials. Unlike the FHN model the action potentials do not exhibit high-frequency fluctuations about a threshold, even with large input noise amplitudes, so the conversion from a series of action potentials to a series of inter-spike intervals is simple.

Power Spectrum (SNR$_{PS}$)

The most commonly used output SNR measure is the SNR$_{PS}$ measure (p. 4), which is based on the power spectrum of the output signal from a system. To calculate SNR$_{PS}$ for the Hodgkin-Huxley model the series of action potential timings were converted into a train of unit spikes. A Fast-Fourier transform was then used to calculate the power spectrum of the spike train. The Fast-Fourier transform used resulted in a spectrum that was proportional to, but not equal to, the actual power spectrum. As a ratio of powers, rather than actual values, were used to calculate SNR$_{PS}$, the resulting SNR$_{PS}$ was equivalent to one calculated from the actual output power spectrum.

If the input current waveform to a standard Hodgkin-Huxley model is a sub-threshold periodic input and supra-threshold noise input, the power spectrum of the resulting spike train appears to be flat with peaks at odd harmonics of the stimulus frequency (Figure 2.3, top panel). The height of the peak at the sub-threshold periodic stimulus frequency divided by the background level near the periodic stimulus frequency is used to determine SNR$_{PS}$. For the power spectrum illustrated in the top panel of Figure 2.3 the periodic stimulus frequency was 30 Hz and the output 'power' at this frequency was approximately 64. The background level was approximately 6, resulting in an SNR$_{PS}$ of approximately 10.

The SNR$_{PS}$ measure for an otherwise sub-threshold periodic input passes through an optimum with the addition of noise, as reported by Kanamaru et al. (1998) and Lee &
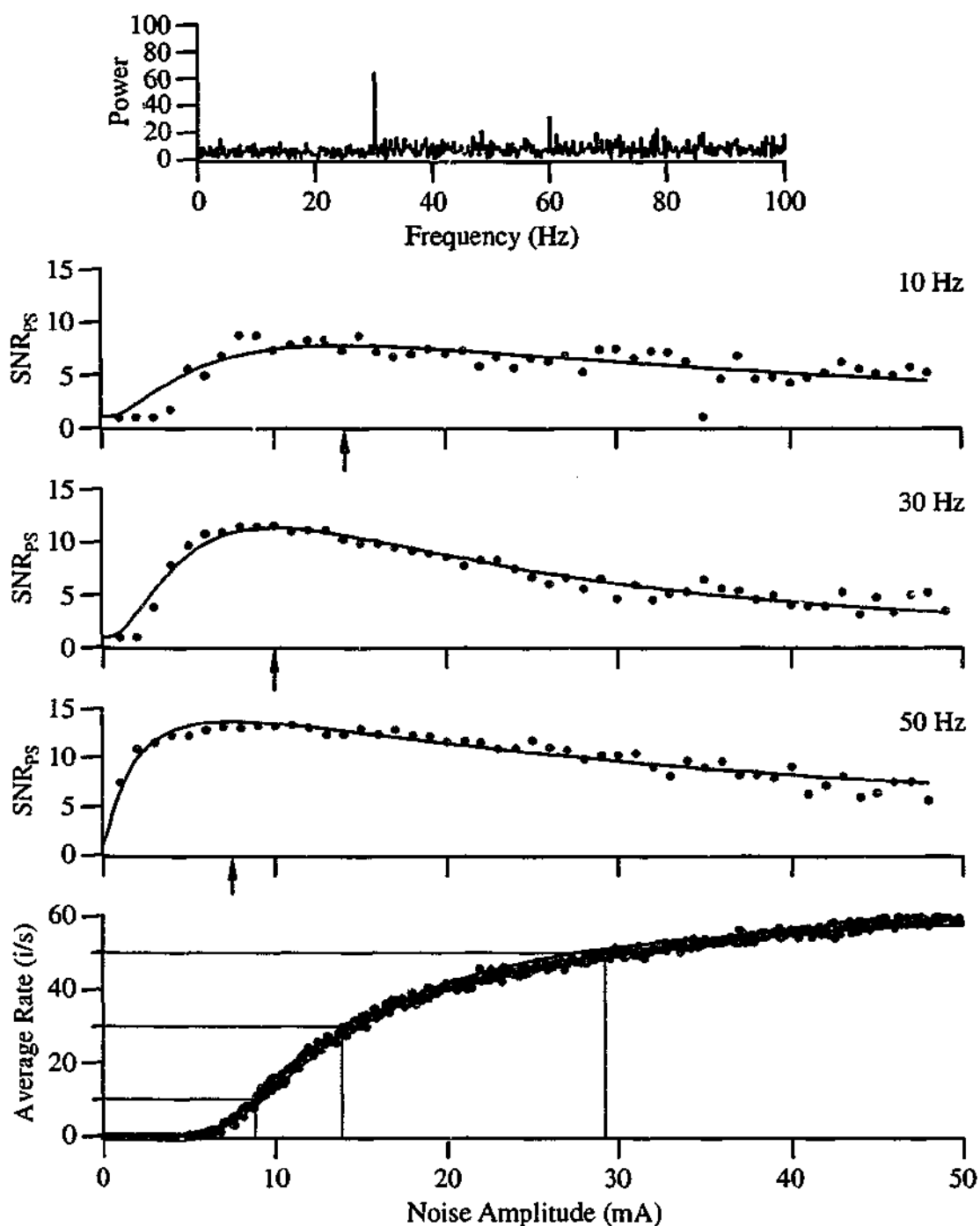
Figure 2.3   The Hodgkin-Huxley model does not appear to exhibit stochastic resonance when the SNR_{PS} measurement is used. The top panel is the power spectrum of a series of unit spikes calculated from a 100 s simulation of the model. The middle panels are the responses of the model to different frequencies of sub-threshold sinusoidal stimulation (the blue symbol represents the data shown in the top panel). Each point is calculated from 10 s of simulation with a sub-threshold sinusoid (1.4 mA). The fitted curves in the middle panels are logNormal curves used to estimate the optimal noise level, D_{OPT}, indicated by the arrows. The bottom panel is a reproduction of the noise-alone response from Figure 2.2, which has been fitted with a curve, based on Kramers' rate. The grey lines in the bottom panel indicate the predicted optimal noise value, D_{PRE}, for each test frequency.

Kim (1999). The SNR_{PS} vs noise curves for several frequencies of sub-threshold periodic input are illustrated in the middle panels of Figure 2.3. The measurements were well fitted by a logNormal curve, the formula for which is given by Equation 2.3, where 'a' is an arbitrary constant, 'D' is the noise level, 'D_{OPT}' is the optimal noise level, and 'Width' is a measure of the width of the curve. 'Z' is the SNR measure when the input is a sub-threshold periodic signal alone; for the SNR_{PS} this is defined as one (p. 4). This equation has the advantage that the optimal noise level, D_{OPT}, is a parameter and therefore it is possible to estimate the error in determining D_{OPT} (SEM) as well as D_{OPT} itself.

$$SNR = Z + a\,e^{-\left(\frac{\ln(D/D_{OPT})}{Width}\right)^2}$$

Equation 2.3

The dependence of the optimal noise level on the sub-threshold periodic stimulus frequency can be most clearly demonstrated if the test frequencies are chosen with the aid of the noise-alone response (Figure 2.3, bottom panel). The test frequencies can be chosen to lie within the approximately linear region of the noise-alone response curve, which should result in the optimal noise levels for each frequency being well separated. For the three test frequencies of 10, 30 and 50 Hz the predicted optimal noise levels, D_{PRE}, from the noise-alone response, are 9.2, 15 and 28 mA respectively. These predictions were made using the grey lines in the bottom panel of Figure 2.3.

The estimated optimal noise levels, as determined by the fitted logNormal curves, were 14 ± 1 mA, 10.0 ± 0.3 mA and 7.5 ± 0.3 mA for the 10, 30 and 50 Hz test frequencies respectively. These estimates of the optimal noise levels were independent of the amplitude of the sinusoid used, provided that it was sub-threshold. The estimated optimal noise levels do not agree with the predicted optimal noise levels. In fact the optimal noise levels exhibit the opposite trend to that expected from stochastic resonance; the optimal noise levels decrease with increasing periodic stimulus frequency. Therefore, the Hodgkin-Huxley model does not appear to exhibit stochastic resonance using the SNR_{PS} measure.

Residence Time (SNR$_{RES}$) and Inter-Spike Interval (SNR$_{ISIH}$)

The SNR$_{RES}$ measure is based on the residence time histogram of the transitions between stable states (p. 8). For the bistable potential well model, that corresponds to the time between transitions from one half-well to the other. The SNR$_{RES}$ measure is equivalent to the SNR$_{ISIH}$ measure, which is based on the inter-spike interval histogram (ISIH) which is often used in neurophysiology. The inter-spike interval histogram is constructed by calculating the interval between successive action potentials. An example of the resulting histogram is shown in Figure 2.4 (top panel). The distribution is clearly multi-modal with peaks at integer multiples of the stimulus period, which is 0.033 s for the simulation illustrated. The SNR$_{ISIH}$ measure is defined as the probability of an action potential occurring every period, which is given by the area of the peak at the period of stimulation. Alternatively, the height of the peak at the period of stimulation can be used if the inter-spike interval histogram is always constructed using the same bin width, as is done throughout this chapter.

The SNR$_{ISIH}$ measure for an otherwise sub-threshold periodic input passes through an optimum with the addition of noise, as illustrated in Figure 2.4 (middle panels). Values of the optimal noise level, D_{OPT}, were estimated by fitting the logNormal curve given by Equation 2.3 with $Z = 0$, as the SNR$_{ISIH}$ for a sub-threshold signal is zero. The estimated optimal noise levels follow a different trend using the SNR$_{ISIH}$ measure compared with the results using the SNR$_{PS}$ measure. For the three test frequencies of 10, 30 and 50 Hz, the estimated optimal noise levels were 8.53 ± 0.01, 9.8 ± 0.2 and 10.3 ± 0.5 mA respectively. Although these values are not precisely those predicted from the noise-alone response (9.2, 15 and 28 mA) they appear to follow the same trend of an increase in the optimal noise level with an increase in stimulus frequency, a key feature of stochastic resonance.

The estimated optimal noise level, D_{OPT}, is dependent on the amplitude of the sub-threshold sinusoid, as illustrated in Figure 2.5. As the amplitude of the sinusoid is reduced from near-threshold to zero, D_{OPT} approaches the predicted optimal noise level, D_{PRE}. For a zero amplitude periodic input (a noise-alone signal) the SNR$_{ISIH}$ measure was calculated as if an infinitely small amplitude periodic input had been used. So for
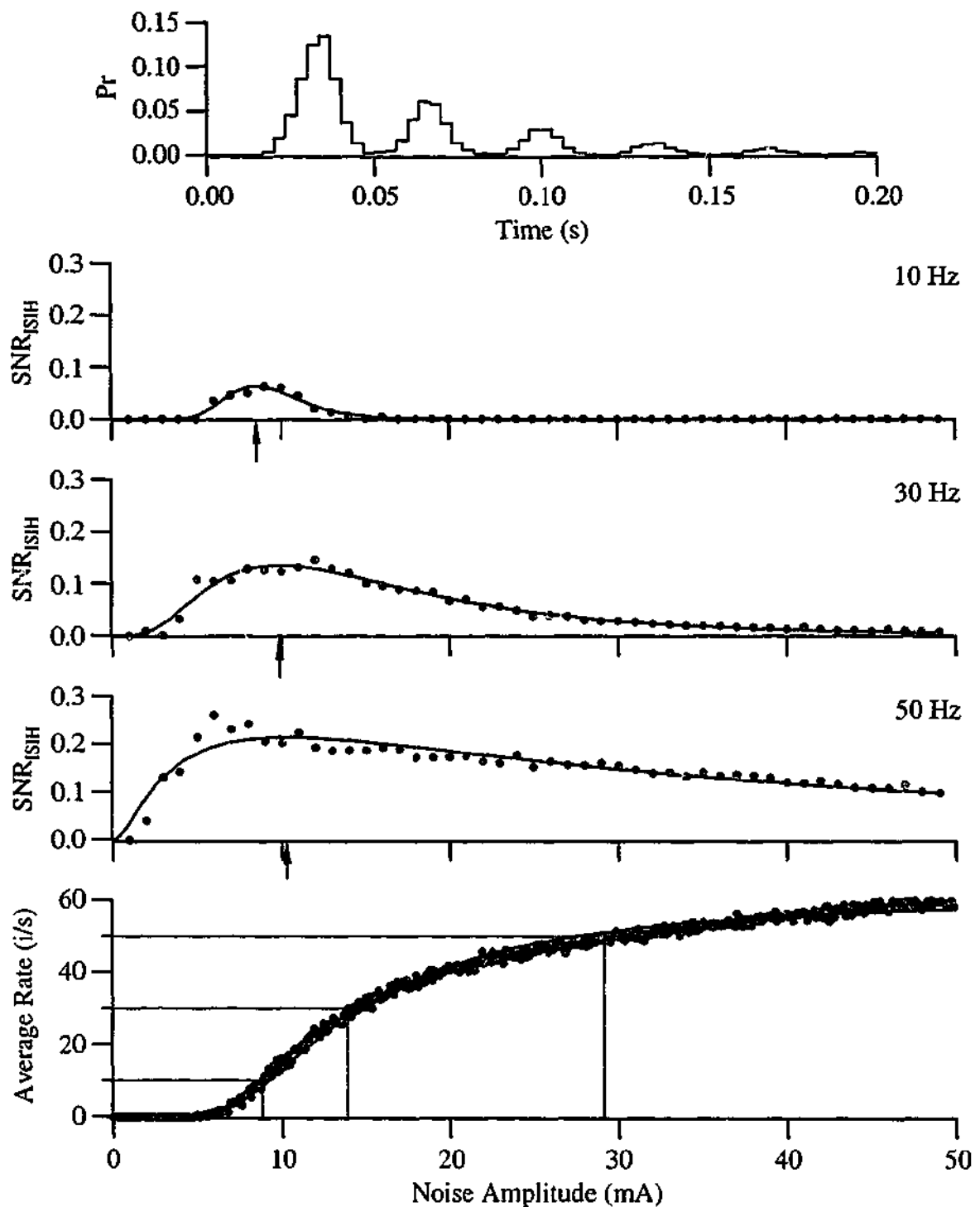
Figure 2.4 The inter-spike interval histogram (top panel) is multi-modal with peaks at integer multiples of the stimulus period (0.033 s). The Hodgkin-Huxley model appears to exhibit stochastic resonance when the SNR_{ISIH} measurement is used (lower panels). The blue symbol represents the data shown in the top panel. Each point is calculated from 100 s of simulation with a sinusoidal amplitude of 1.4 mA. The fitted curves in the middle panels are logNormal curves used to estimate the optimal noise level, D_{OPT}, indicated by the arrows. The bottom panel is a reproduction of the noise-alone response from Figure 2.2, which has been fitted with a curve based on Kramers' rate. The grey lines in the bottom panel indicate the predicted optimal noise value, D_{PRE}, for each test frequency.
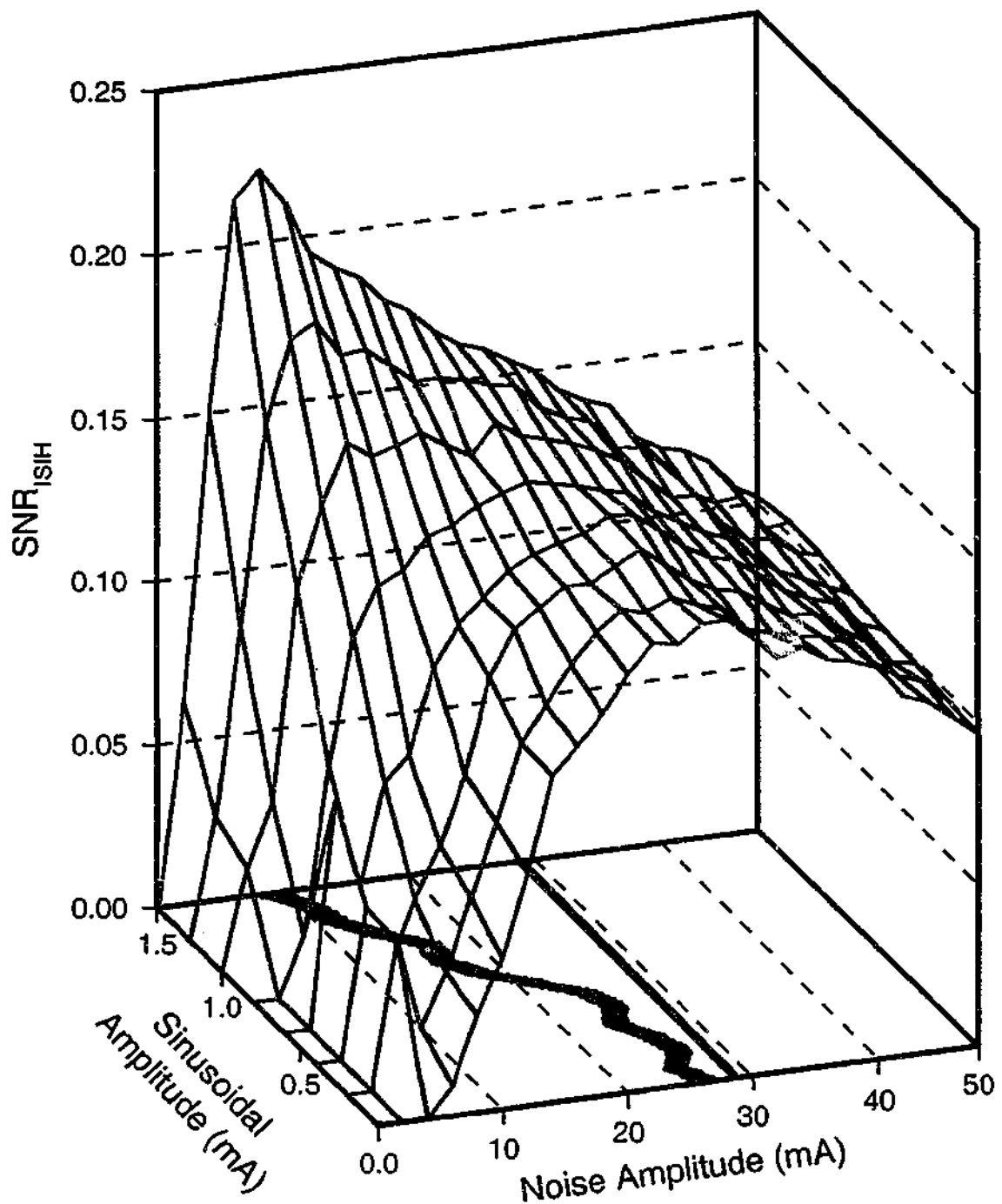
Figure 2.5 Simulations of the Hodgkin-Huxley model using a range of sinusoidal amplitudes and noise amplitudes result in a SNR_{ISIH} surface. The surface shown is for a 50 Hz sinusoid simulated for 100 s at each combination of sinusoid and noise amplitudes. The red line underneath indicates D_{OPT}, which corresponds to the ridgeline of the surface, while the grey line indicates the predicted optimal noise level, D_{PRE}. D_{OPT} decreases from the predicted noise level at small sinusoidal amplitudes to a value approaching the threshold for noise (approximately 5 mA) at larger sinusoidal amplitudes.

the example illustrated in Figure 2.5 the SNR_{ISIH} measure was calculated assuming that the input frequency for the zero amplitude periodic input was 50 Hz.

The sinusoidal amplitude dependence of estimated optimal noise, D_{OPT}, highlights a problem with the SNR_{ISIH} measure. In the case of no sinusoidal input, the SNR_{ISIH} measure can still exhibit a peak at the predicted optimal noise level, D_{PRE}, as illustrated in Figure 2.6. This problem was noted by Giacomelli et al. (1999) and led them to use only the area of the peak above the noise-alone distribution at the period of stimulation as their output SNR measure. Although this measure removes the problem with the noise-alone stimulus, it requires a large number of action potentials to accurately determine the noise-alone distribution (Marchesoni, Gammaitoni, Apostolico & Santucci, 2000). The number of action potentials required is in the order of several hundred thousand, and this measure is therefore not suitable for biological systems where the period of recording, and therefore the number of action potentials recorded, is limited.

Cycle Histogram

The probability of an action potential occurring during different phases of the periodic stimulus can be determined by constructing a cycle histogram (Figure 2.7). If the periodic stimulus is supra-threshold then the output train of action potentials is phase locked to the stimulus and the majority of action potentials occur in a narrow phase range (Figure 2.7, top panel). A noise-alone stimulus produces randomly distributed action potentials, so the cycle histogram is approximately flat (Figure 2.7, middle panel). A combination of sub-threshold periodic stimulus and supra-threshold noise result in a cycle histogram that has a peak (Figure 2.7, bottom panel).

Cycle Histogram Peak (SNR_{CYCLE})

The height of the peak, above the noise-alone response, is a measure of how much of the periodic signal is present in the output. Therefore, the SNR_{CYCLE} measure is defined as the height of the peak above the noise-alone response divided by the noise-alone response. This can be simplified to just the height of the peak, as the noise-alone response is a constant (Figure 2.7, middle panel). When the SNR_{CYCLE} measure is used
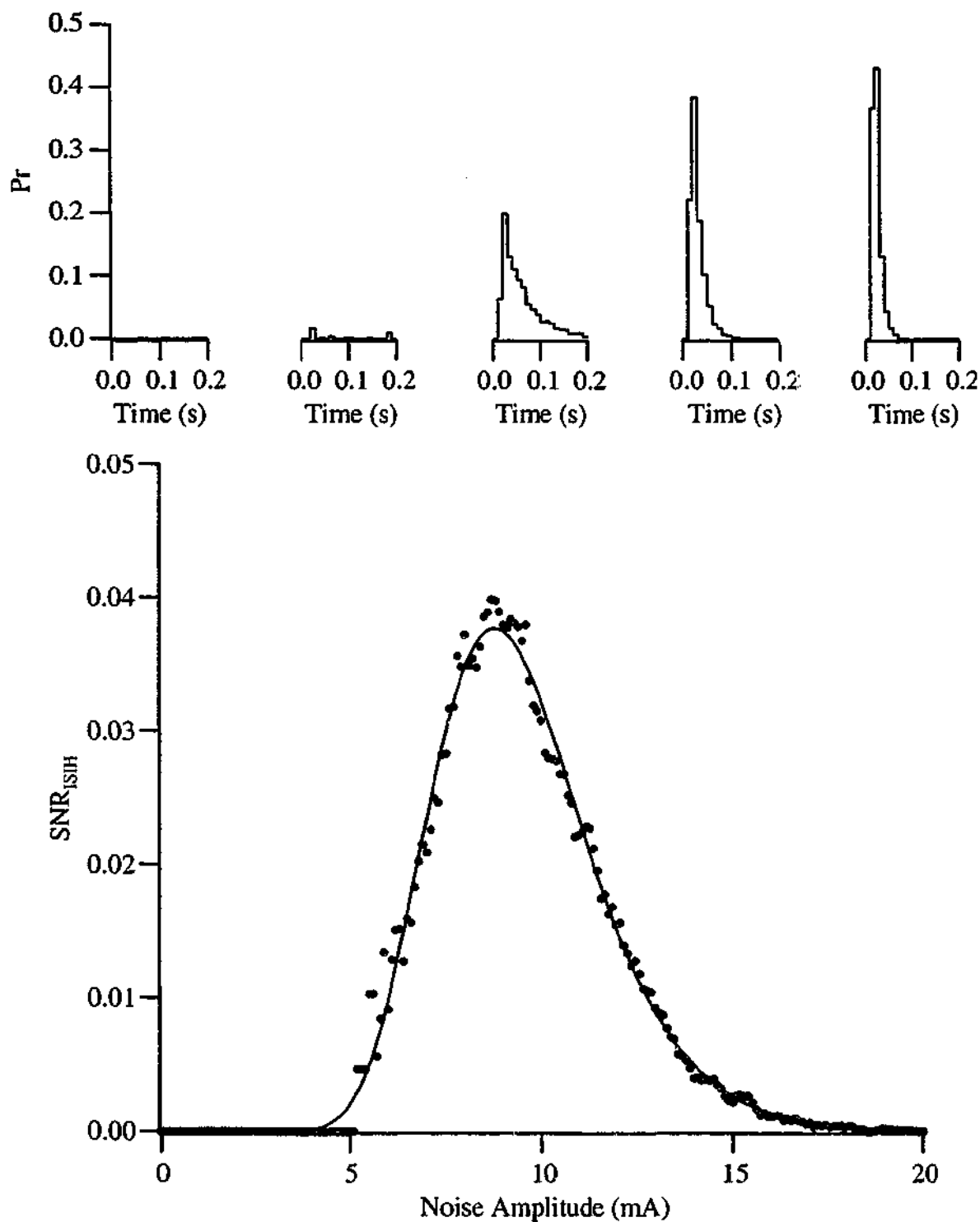
Figure 2.6   When using the SNR$_{ISIH}$ measure the Hodgkin-Huxley model exhibits an optimum with the addition of noise in the absence of a sinusoidal input (bottom panel). As the input noise level increases the inter-spike interval histogram becomes narrower and centred around shorter intervals (top panels). The inter-spike interval histograms for the different noise levels are positioned relative to the bottom noise axis and the values derived from them are shown in blue. Each point is calculated from 100 s of simulation with no sinusoidal input.
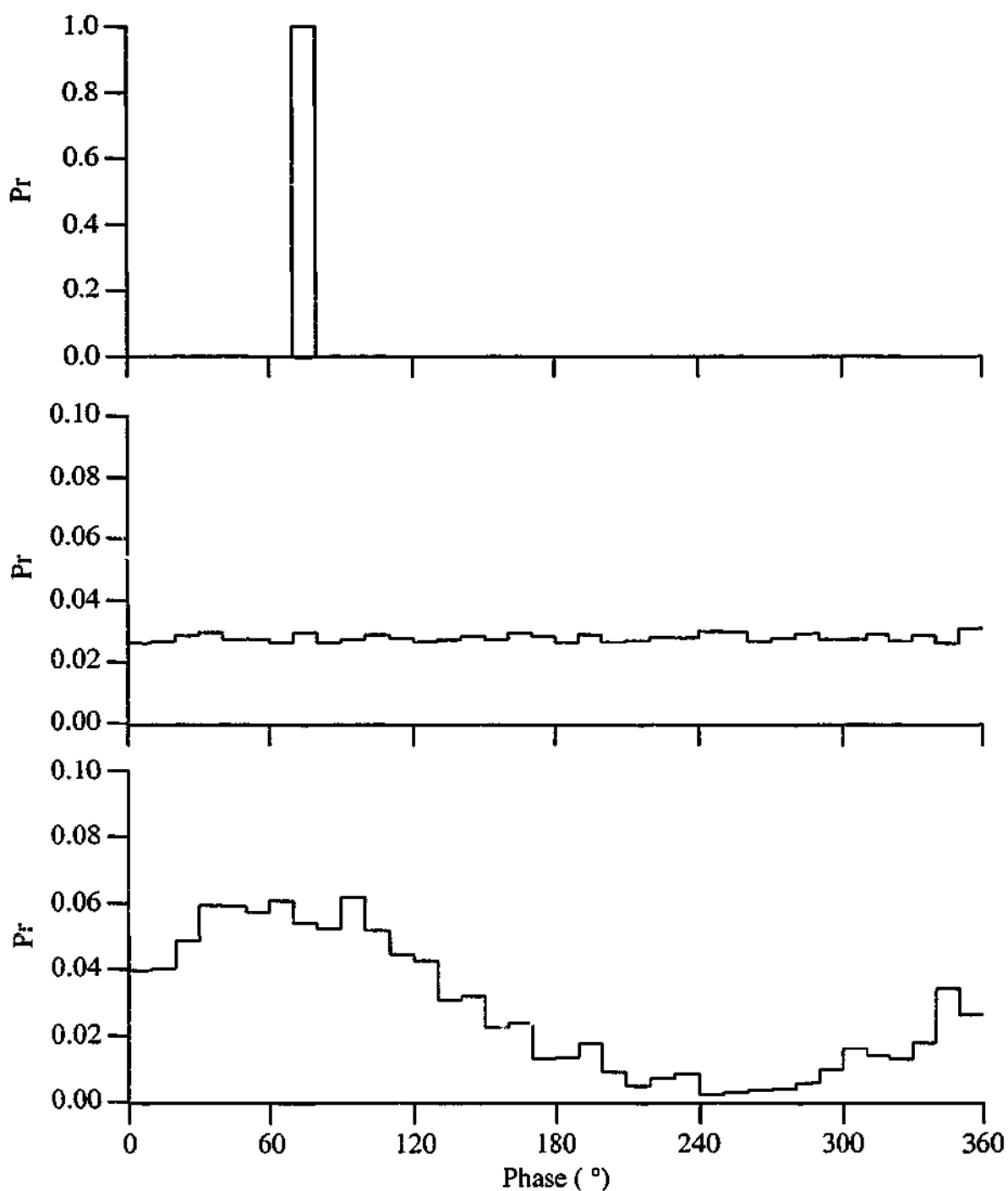
Figure 2.7 The cycle histogram of a supra-threshold periodic signal (5.7 mA, 10 Hz sinusoid) is a narrow peak at a single phase (top panel), while a noise-alone signal (30 mA) results in a flat cycle histogram (middle panel). The cycle histogram of a sub-threshold periodic signal (1.4 mA, 10 Hz sinusoid) and supra-threshold noise signal (8 mA) is a broad peak (bottom panel). The height of the peak above the noise-alone response can be used as an output measure, SNR_{CYCLE}. The cycle histograms were constructed from 100 s of simulations using 10° bins assuming a periodic stimulus frequency of 10 Hz.

the Hodgkin-Huxley model does not exhibit stochastic resonance (Figure 2.8). The smallest noise amplitude to result in a discharge has the largest SNR_{CYCLE} value. Values of noise below this level do not result in the initiation of any action potentials, and therefore it is impossible to construct a cycle histogram. The SNR_{CYCLE} measure is dependent on the sub-threshold periodic signal amplitude, as smaller sub-threshold periodic amplitudes require larger noise amplitudes before any action potentials can be produced. The estimated optimal noise level, D_{OPT}, is not relevant for the SNR_{CYCLE} measure, as the SNR_{CYCLE} measure is monotonically decreasing.

Cycle Histogram Modulation (SNR_{EXP})

It is possible to fit a sinusoid to the cycle histogram as illustrated in Figure 2.9. The amplitude of the fitted sinusoid has similar characteristics to the SNR_{CYCLE} measure, so would not be useful as an output SNR measure to investigate stochastic resonance. It is possible to estimate the error in the amplitude of the fitted sinusoid, as illustrated by the shaded area in Figure 2.9, which can then be used to calculate an output SNR measurement. The amplitude of the fitted sinusoid divided by the estimated error in the fit is used as the experimental output SNR measure SNR_{EXP}, as given by Equation 2.4. For the example illustrated in Figure 2.9, the fitted sinusoid has an amplitude of 0.027 ± 0.001, and therefore the calculated value of SNR_{EXP} is 27.

$$SNR_{EXP} = \frac{\text{Amplitude of Fitted Sinusoid}}{\text{Estimated Error of Fitted Sinusoid}}$$

Equation 2.4

For some cycle histograms the optimal fitted sinusoid would pass below the horizontal axis, which would correspond to negative probabilities. Therefore, constraints were imposed on the fitting procedures to ensure the fitted sinusoid did not pass below a probability of zero. It is not possible to calculate the SNR_{EXP} measure if no action potentials are produced, as is the case for sub-threshold stimulation. The SNR_{EXP} measure approaches one as the input approaches the threshold level, as the estimated error in the amplitude of the fitted sinusoid approaches the amplitude of the fitted sinusoid. Therefore, the SNR_{EXP} measure was defined as one if it was not possible to construct a cycle histogram.
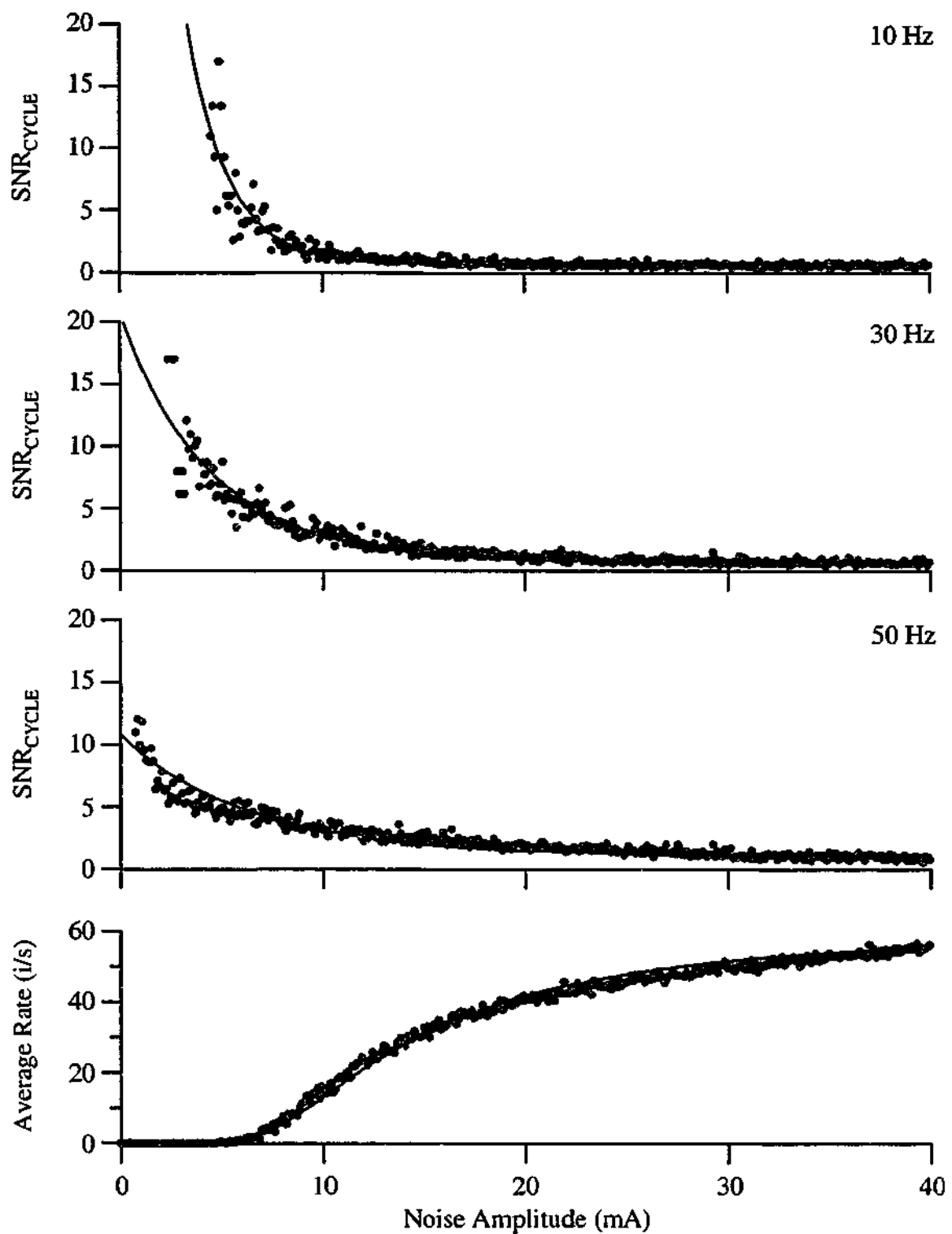
Figure 2.8 When using the SNR$_{CYCLE}$ measure the Hodgkin-Huxley model does not exhibit stochastic resonance, as SNR$_{CYCLE}$ monotonically decreases with increasing noise levels. Each point is calculated from 100 s of simulation with a sinusoidal input of 1.4 mA for the top three panels. The responses in the top three panels were fitted with exponentials, while the bottom panel was fitted with a curve based on Kramers' rate. The blue symbol represents the data shown in the bottom panel of Figure 2.7.
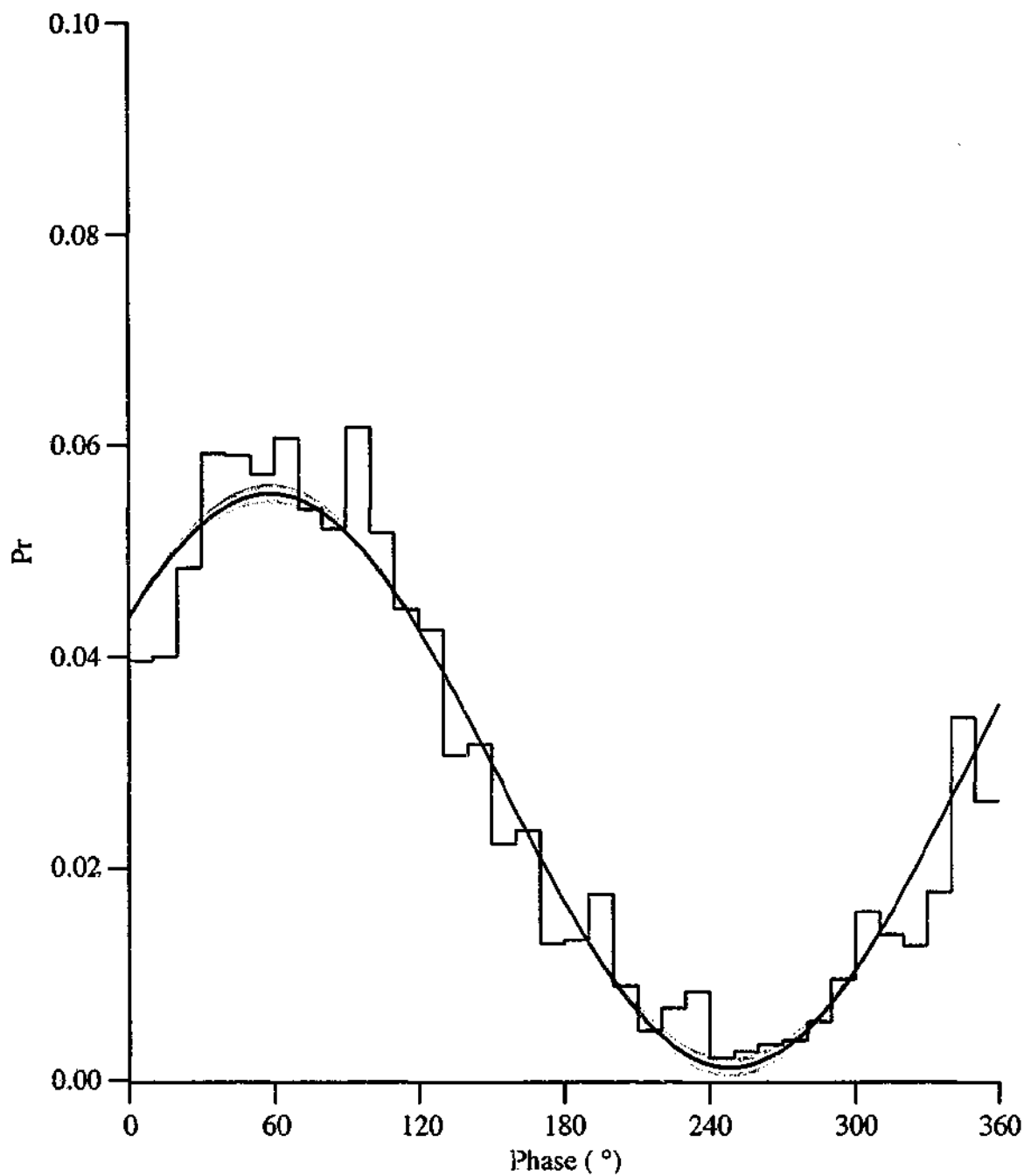
Figure 2.9   The cycle histogram of a sub-threshold periodic signal (1.4 mA, 10 Hz sinusoid) and supra-threshold noise signal (8 mA) is reproduced from the data shown in the bottom panel of Figure 2.7. The method of calculation SNR_{EXP} is shown. The fitted sinusoid (solid black line) has an amplitude of 0.027 with an error of 0.001 (grey shading). The resulting value of SNR_{EXP} is 27.

The SNR_{EXP} measure for an otherwise sub-threshold periodic input passes through an optimum with the addition of noise, as illustrated in Figure 2.10 (upper panels). The optimal noise levels were estimated by fitting the logNormal curve given by Equation 2.3, with $Z = 1$. The estimated optimal noise levels, D_{OPT}, follow a similar trend as for the SNR_{ISIH} measure. For the three test frequencies of 10, 30 and 50 Hz, the estimated optimal noise levels were 9.8 ± 0.1, 12.8 ± 0.1 and 20.3 ± 0.3 mA respectively. Although these values are not precisely those predicted from the noise-alone response (9.2, 15 and 28 mA) they do show the same trend of an increase in the optimal noise level with an increase in stimulus frequency, a key feature of stochastic resonance.

The estimated optimal noise level, D_{OPT}, is dependent on the amplitude of the sub-threshold sinusoid, as illustrated in Figure 2.11. As the amplitude of the sinusoid is increased from near zero to threshold, the estimated optimal noise level approaches the predicted optimal noise level. The sinusoidal amplitude dependence of D_{OPT} highlights a problem with the SNR_{EXP} measure. For input sinusoidal amplitudes that are significantly below threshold the estimated optimal noise level, D_{OPT}, is less than the predicted level, D_{PRE}.

The low estimated optimal noise levels, D_{OPT}, are the result of the interactions of sub-harmonics of the sinusoidal stimulation frequency. The cycle histograms for 5 mA of noise plus 1 mA sinusoids of 15 and 30 Hz are similar, as illustrated in Figure 2.12 (top and bottom panels). The middle panel of Figure 2.12 is the result of constructing a cycle histogram with a frequency of 30 Hz, from the results of the 15 Hz stimulus (i.e. a sub-harmonic stimulus). It is clear that there is a modulation of the cycle histogram that can be used to calculate an SNR_{EXP} value. Stochastic resonance should occur over a wide range of stimulus frequencies, including the sub-harmonic frequencies of the test frequencies. The low estimated optimal noise levels are a result of a sub-harmonic stochastic resonance, resulting in SNR_{EXP} at lower noise levels being elevated. The effect is most pronounced with low amplitude, high frequency sinusoidal inputs.

Despite the tendency for the SNR_{EXP} measure to underestimate the optimal noise level, D_{OPT}, compared to the predicted optimal noise level, D_{PRE}, the stochastic resonance effect can be seen over a large range of sinusoidal stimulus frequencies, as illustrated in
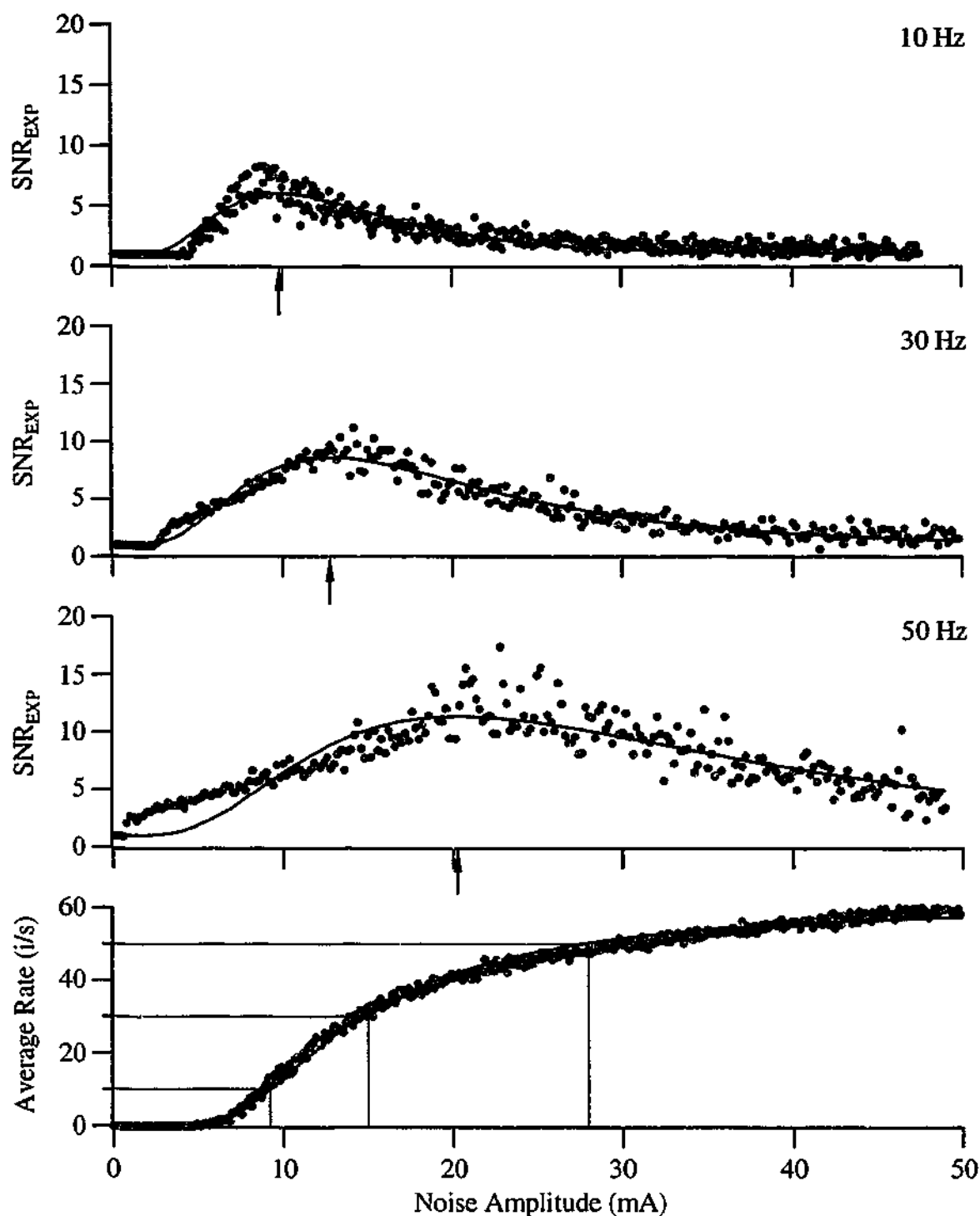
Figure 2.10 The Hodgkin-Huxley model exhibits stochastic resonance when the SNR_{EXP} measurement is used. Each point is calculated from 100 s of simulation with a sinusoidal amplitude of 1.4 mA. The fitted curves in the upper panels are logNormal curves used to estimate the optimal noise level, D_{OPT}, indicated by the arrows. The bottom panel is a reproduction of the noise-alone response from Figure 2.2, which has been fitted with a curve based on Kramers' rate. The grey lines in the bottom panel indicate the predicted optimal noise value, D_{PRE}, for each test frequency. The blue symbol represents the data shown in the bottom panel of Figure 2.7.
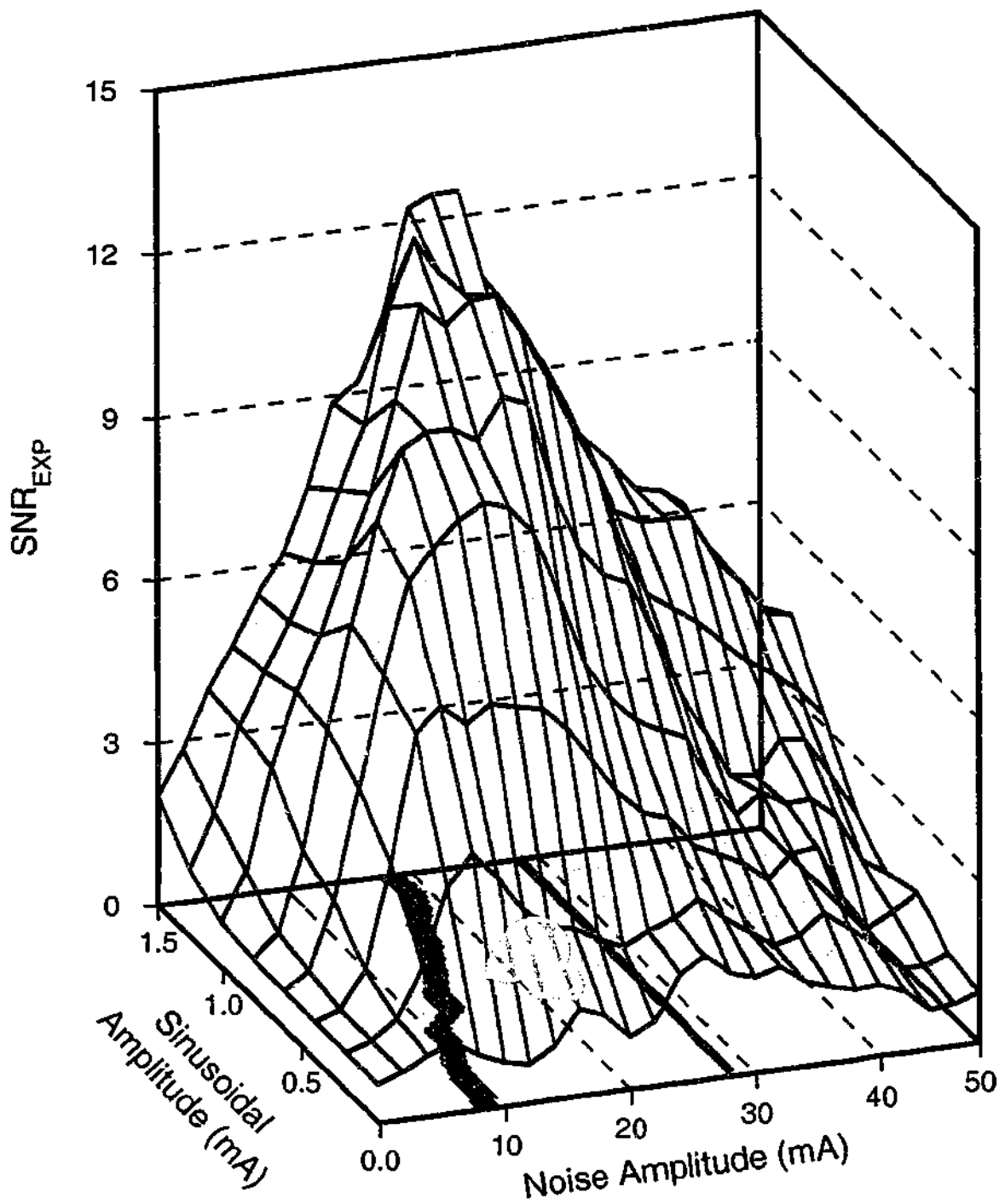
Figure 2.11 Simulations of the Hodgkin-Huxley model using a range of sinusoidal amplitudes and noise amplitudes result in a SNR_{EXP} surface. The surface shown is for a 50 Hz sinusoid simulated for 100 s at each combination of sinusoid and noise amplitudes. The red line underneath indicates D_{OPT}, which corresponds to the ridgeline of the surface, while the grey line indicates the predicted optimal noise level, D_{PRE}. D_{OPT} decreases from near the predicted noise level, D_{PRE}, at near-threshold sinusoidal amplitudes to a value approaching the threshold for noise (approximately 5 mA) for smaller sinusoidal amplitudes.
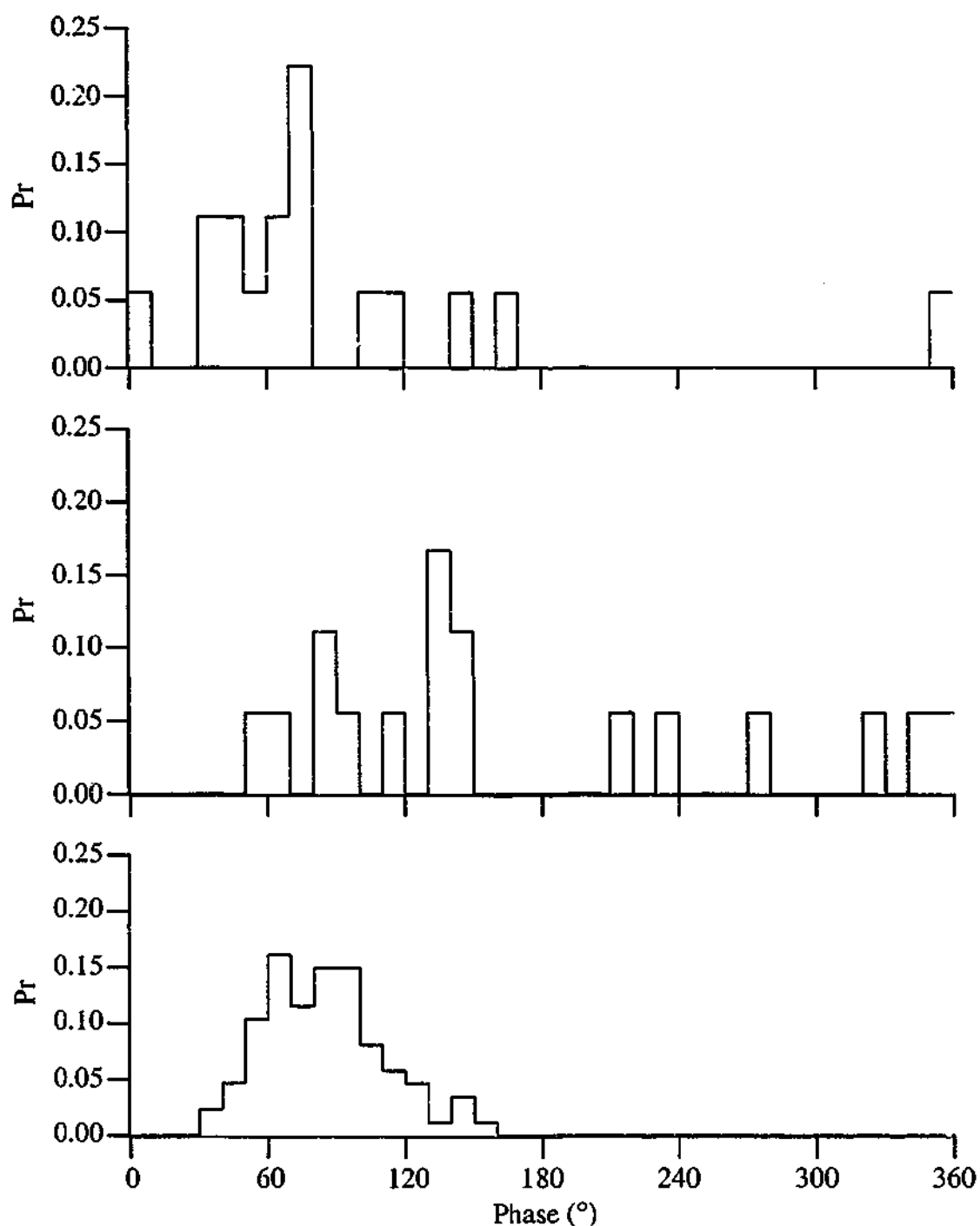
Figure 2.12 The top panel is a cycle histogram constructed from 100 s of simulation of the Hodgkin-Huxley model, stimulated with a 1mA, 15 Hz sinusoid with 5 mA of additional noise. The bottom panel is the cycle histogram constructed from a similar period of simulation, except the 15 Hz sinusoid was replaced with a 30 Hz sinusoid. The middle panel is a cycle histogram constructed from the same data as the top panel, but using the analysis for a 30 Hz sinusoid (i.e. the same analysis as the bottom panel). The sub-harmonic stimulation results in a modulated cycle histogram that is similar to that for the test frequency (i.e. the middle and bottom panels look similar). The cycle histograms were constructed using 10° bins and a period of 0.066 s for the top panel and 0.033 s for the middle and bottom panels.

Figure 2.13. At higher stimulus frequencies there is a trend for D_{OPT} to be less than D_{PRE}, which is a result of the sub-harmonic resonance that is more prominent at higher stimulus frequencies and also the flattening of the noise-alone response curve. The upper frequency limit is determined by the noise-alone response of the system, and therefore is dependent on the system being studied. The discrepancy at lower frequencies is due to the difficulty of estimating D_{OPT} when it is approximately equal to the noise threshold. Below the noise threshold few action potentials are produced, resulting in an ill-defined SNR_{EXP} measurement. The lower stimulus frequencies also result in far fewer action potentials during a set period of simulation. With fewer action potentials there is more error associated with the estimation of the optimal noise level.

Threshold (SNR_{THRES})

In some experimental situations, such as psychophysical experiments, it is not possible to construct cycle histograms from a series of action potentials as it is not possible to record directly from the afferents of interest. Often in such situations it is only possible to measure a threshold of detection to a stimulus, as determined by the response of a subject. It is possible to generate a measure based on the SNR_{EXP} measure that mimics such a situation by introducing an arbitrary threshold, SNR_{THRES}. An arbitrary level of SNR_{EXP} can be set as the threshold, provided that this level is above one, the minimum value of SNR_{EXP}, and below the maximum possible value for SNR_{EXP}.

Stochastic resonance using such a measure is evident in a minimum in the detection threshold with the addition of noise, an example of which is illustrated in Figure 2.14. The optimal noise levels were estimated by fitting a logNormal curve (Equation 2.3 with Z = no-noise threshold). For the test frequencies of 10, 30 and 50 Hz the estimated optimal noise levels, D_{OPT}, were 7 ± 1 mA, 11.9 ± 0.2 mA and 15.3 ± 0.4 mA respectively. Although these values are not precisely those predicted from the noise-alone response (9.2, 15 and 28 mA) they do show the same trend of an increase in the optimal noise level with an increase in stimulus frequency. The periodic frequency dependence of the estimated optimal noise levels indicates that the SNR_{THRES} measure, and related measures based on detection thresholds, can be used as a stochastic resonance measures.
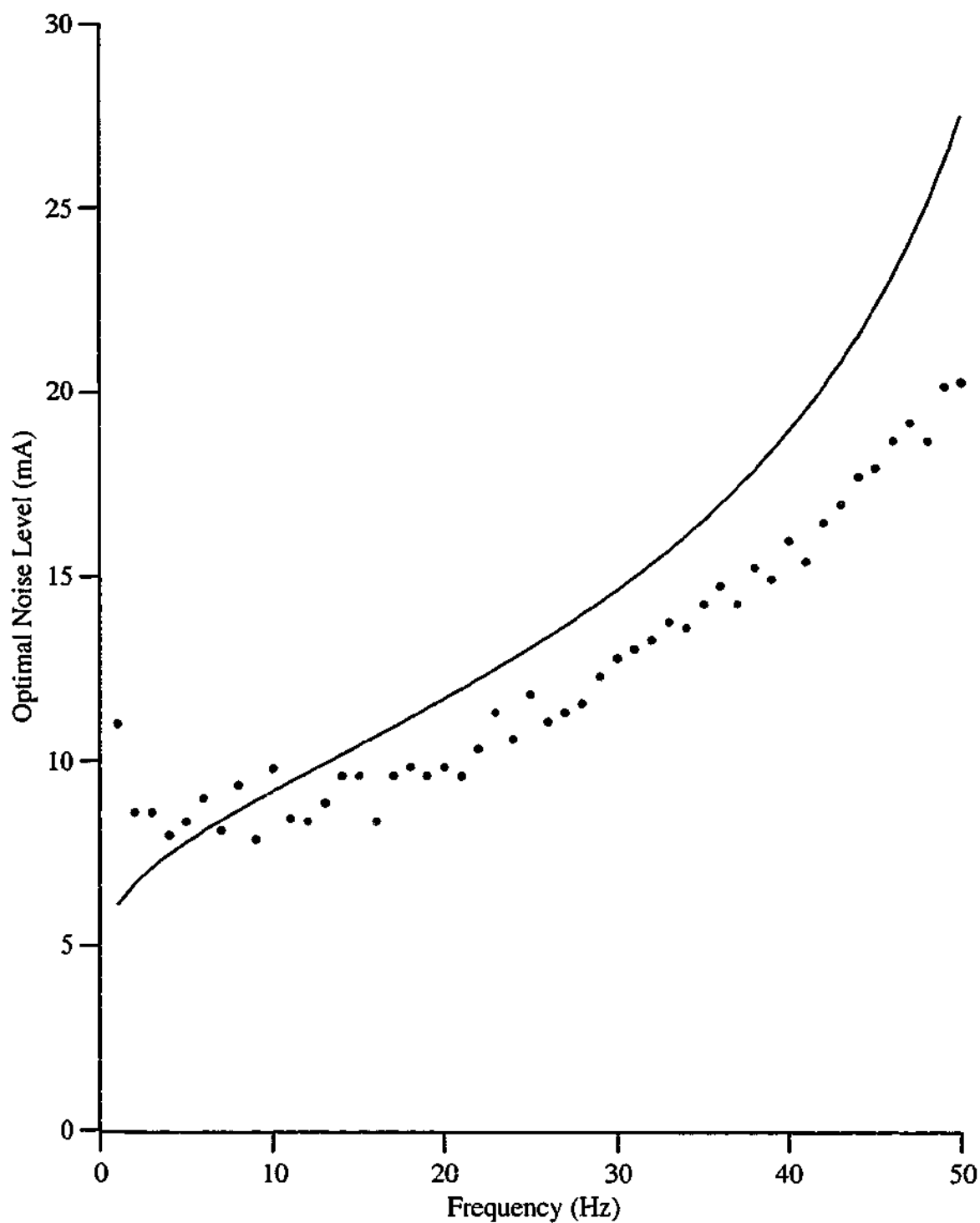
Figure 2.13   The predicted optimal noise levels (solid curve, D_{PRE}) and estimated optimal noise levels (points, D_{OPT}) are similar over a range of frequencies when a near threshold sinusoidal signal of 1.4 mA is used. This is as expected if the increase in the output SNR was a result of stochastic resonance. The points in blue are those corresponding to the data shown in Figure 2.10.

In many experimental circumstances it is not possible to measure a noise-alone response curve, as it is not possible to record directly from the afferent fibres. In these situations the frequency dependence of the optimal noise level can be determined by calculating the statistical significance of any increase in optimal noise level with increasing stimulus frequency. For the simulations illustrated in Figure 2.14 the estimated optimal noise is correlated with stimulus frequency (0.992 Pearson's Product), as would be expected of a system exhibiting stochastic resonance.

Effect of Different Output Signal-to-noise Ratio Measures

The output SNR measurement used affects the determination of the stochastic resonance effect. The basic Hodgkin-Huxley model can exhibit stochastic resonance if the SNR_{ISIH}, SNR_{EXP} or SNR_{THRES} measurements are used. However, the same model does not appear to exhibit stochastic resonance if the SNR_{PS} or SNR_{CYCLE} measurements are used. The dependence of stochastic resonance on the output measurement used highlights the complex nature of the effect. The processing done on the train of action potentials dramatically affects the information extracted from them. Therefore, any sensory system that is proposed to exhibit stochastic resonance must be capable of extracting the extra information that is available using measures such as SNR_{EXP}.

Noise Distribution

The stochastic resonance effect is not dependent on the noise distribution that is used (Nozaki et al., 1999). All the simulations presented have used zero-mean normally distributed noise. The disadvantage of normally distributed noise is that there is a small but finite probability of large noise values. This can be a problem in experimental situations. For example, if the input signal to a system is a length signal it may not be possible to produce large instantaneous changes in length, because of the response characteristics of the system. Also, large instantaneous changes in length may be damaging to the system being studied.

Rather than using zero-mean normally distributed noise, it is possible to use zero-mean evenly distributed noise, the distribution of which is illustrated in the top panel of Figure 2.15. If evenly distributed noise is used, every possible noise level between a
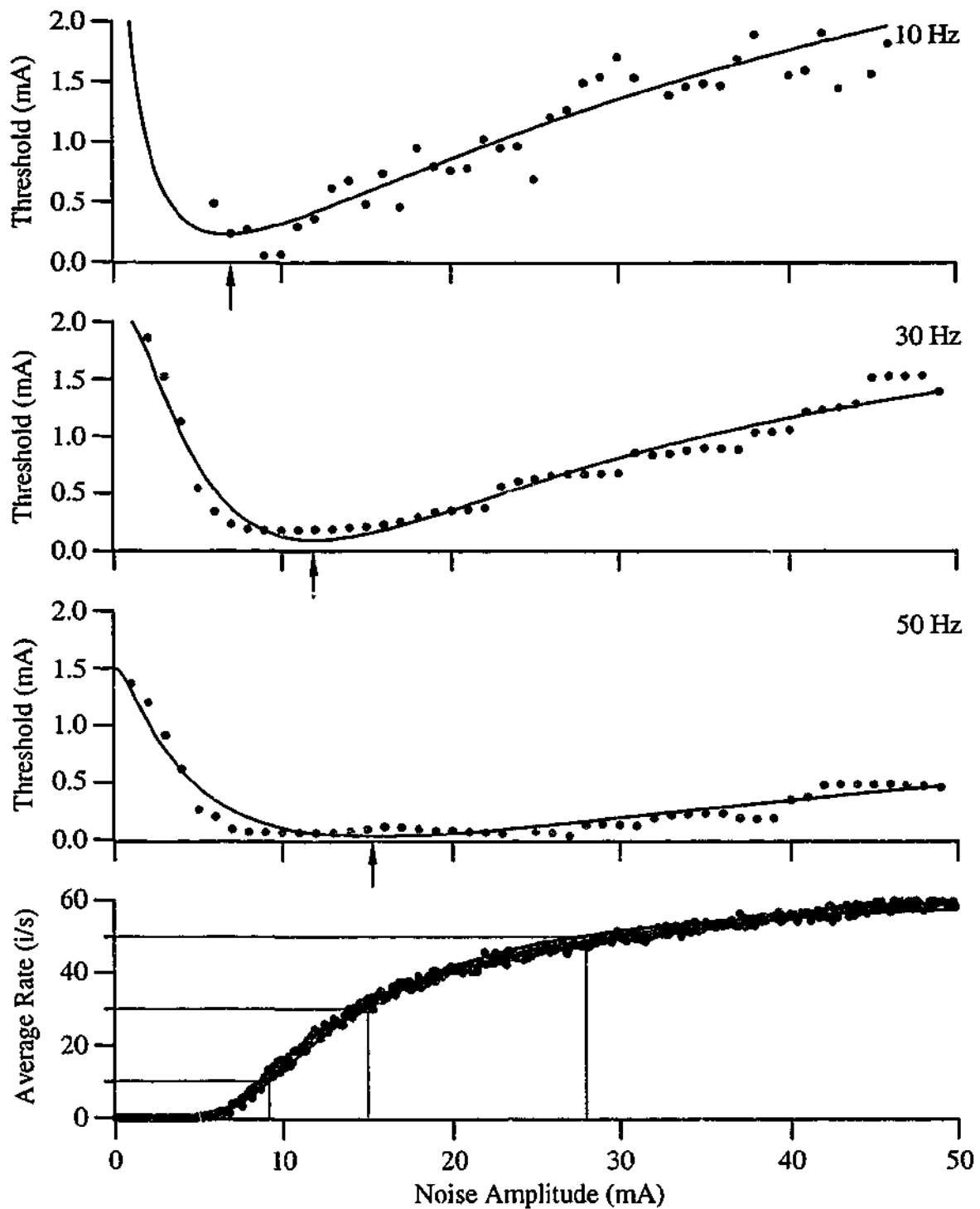
Figure 2.14 The Hodgkin-Huxley model exhibits stochastic resonance when the SNR$_{THRESH}$ measurement is used. Each point is calculated from 10 s of simulation. The threshold used in this case was SNR$_{EXP}$ ≥ 2. The fitted curves in the upper panels are logNormal curves used to estimate the optimal noise level, D$_{OPT}$, indicated by the arrows. The bottom panel is a reproduction of the noise-alone response from Figure 2.2, which has been fitted with a curve based on Kramers' rate. The grey lines in the bottom panel indicate the predicted optimal noise value, D$_{PRE}$, for each test frequency.
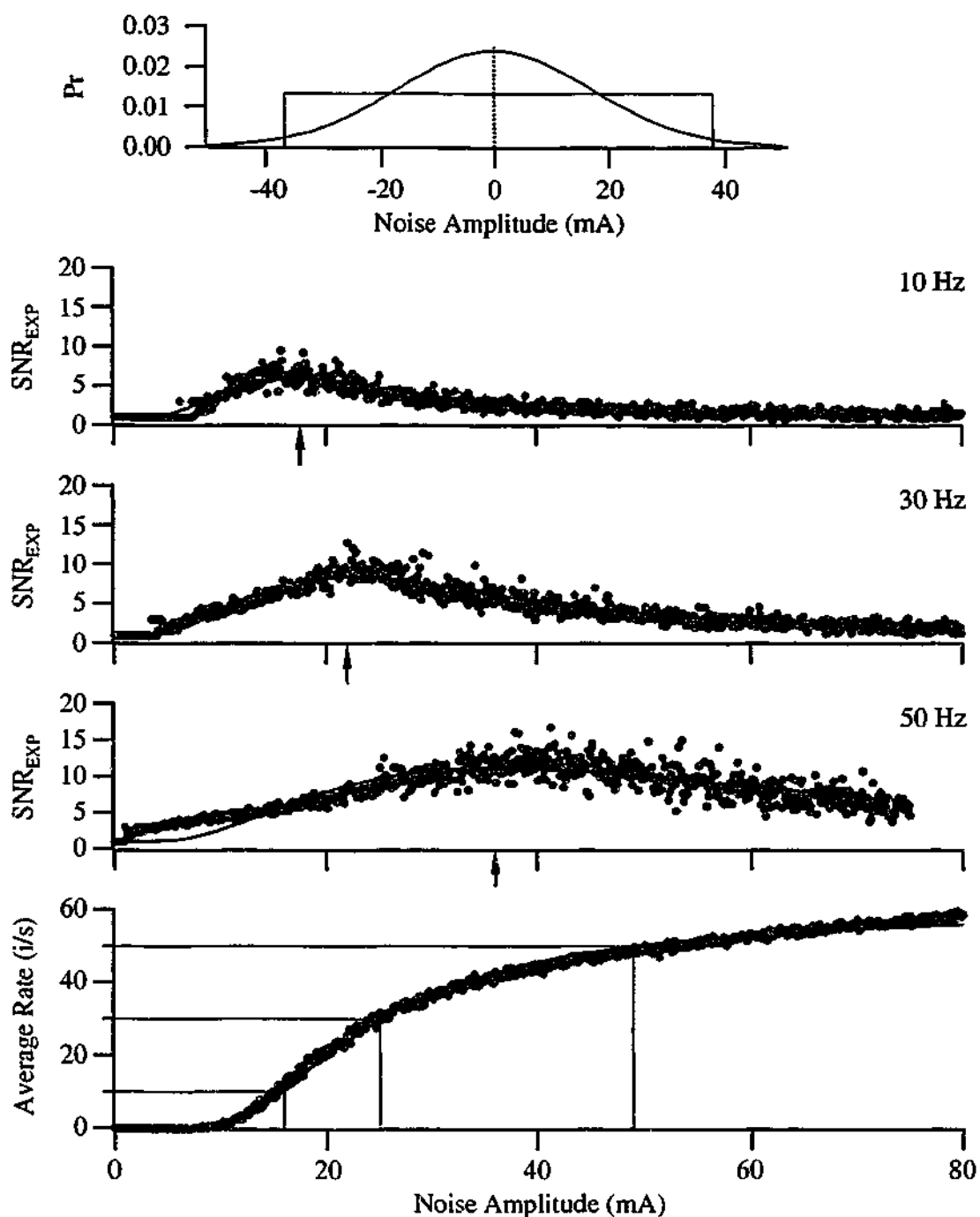
Figure 2.15 Evenly distributed noise (green) is strictly limited to values between a specified maximum and minimum, while normally distributed noise (purple) has a small but finite probability of producing noise values significantly outside a desired range (top panel). The effect of evenly distributed noise is to alter the values of D_{PRE} and D_{OPT}, but the stochastic resonance effect is still present (lower panels). Each point is calculated from 100 s of simulation with a sinusoidal amplitude of 1.4 mA. The fitted curves in the middle panels are logNormal curves used to estimate the optimal noise level, D_{OPT}, indicated by the arrows. The bottom panel is the noise-alone response, which has been fitted with a curve based on Kramers' rate. The grey lines in the bottom panel indicate the predicted optimal noise value, D_{PRE}, for each test frequency.

maximum and a minimum has an equal probability of occurring, but values above or below the extremes are not possible. Evenly distributed noise eliminates many of the problems of implementing the noise experimentally, as the absolute limits of the noise are known. Although evenly distributed noise affects the response of the system, stochastic resonance can still occur, as illustrated in Figure 2.15 (lower panels).

The predicted optimal noise values from the noise-alone response using evenly distributed noise are 16, 25 and 49 mA for the three test frequencies of 10, 30 and 50 Hz respectively. With evenly distributed noise the estimated optimal noise levels using the SNR_{EXP} measure are 17.6 ± 0.2 mA, 22.0 ± 0.2 mA and 36.0 ± 0.3 mA. The agreement between the estimated optimal noise level, D_{OPT}, and the predicted optimal noise level, D_{PRE}, for evenly distributed noise is similar to that for normally distributed noise.

Supra-threshold Stimuli

By definition, stochastic resonance will not occur for supra-threshold stimuli, because any increase in input noise will degrade the output SNR. However, the combination of the Hodgkin-Huxley model and the SNR_{EXP} measure cannot be used to illustrate this. The cycle histogram for a supra-threshold periodic signal, illustrated in the top panel of Figure 2.7, is identical to the cycle histogram for a single action potential; there is a probability of one of an action potential occurring for a single-phase value. An ideal output SNR measure would give a low value for the single action potential, and be maximal for the supra-threshold stimulus. The SNR_{EXP} measure does not achieve this; instead, the SNR_{EXP} measure is low for the single action potential and the supra-threshold stimulus. However, the SNR_{EXP} measurement is suitable for sub-threshold periodic and supra-threshold noise signals, the conditions under which stochastic resonance may occur. Under theses conditions, the output periodic signal is evident as a modulation in the otherwise random series of action potentials.

Multiple Input Averaging

All of the simulations shown so far have been done for at least 10 s, as many cycles of the periodic stimulus are required to clearly demonstrate stochastic resonance. The long simulation times allow for effective time averaging of the noise input. This reduces the

effect of any particular noise-induced action potential reducing the scatter in the SNR_{EXP} measurements.

Under physiological relevant conditions it is unlikely that 100 to 500 cycles of a periodic input will occur. Often only a few cycles of a periodic signal may occur before a response is required. Under these circumstances it is possible to effectively sample many more cycles of the periodic input by sampling across many receptors, all stimulated by the same periodic input, but with different noise inputs. The cycle histograms in Figure 2.16 illustrate that summing the output from many realisations of the Hodgkin-Huxley model, with different noise inputs, is equivalent to a much longer response from a single realisation of the model. This indicates that it would be possible to observe stochastic resonance in a system that integrated the response of many receptors with different sources of noise.

Periodic Pulsed Input

Only at the level of sensory receptors is the input signal to an excitable membrane a continuous function, typically in the form of a generator potential. From the first inter-neurone to deep within the central nervous system the signal from one neurone to the next is typically a chemical neuro-transmitter. The chemical neuro-transmitter causes a change in the membrane permeability of the post-synaptic neurone, which may result in excitatory post-synaptic currents (EPSCs). The ability of the Hodgkin-Huxley model to exhibit stochastic resonance with an input that consists of a periodic series of EPSCs has not previously been investigated.

The form of EPSCs recorded in the spinal motoneurones of anaesthetised cats is given by Equation 2.5 (Finkel & Redman, 1983). This basic form was used to model the EPSCs from a series of primary neurones terminating on a summing neurone, as illustrated in the top panel of Figure 2.17. Most of the primary neurones were driven with a supra-threshold noise-alone signal, while one was driven with a supra-threshold periodic signal. The EPSCs were scaled such that a single EPSC would not cause the summing neurone to fire, but a summation of two or more EPSCs would.

$$EPSC = T \exp^{-\alpha T}$$ **Equation 2.5**
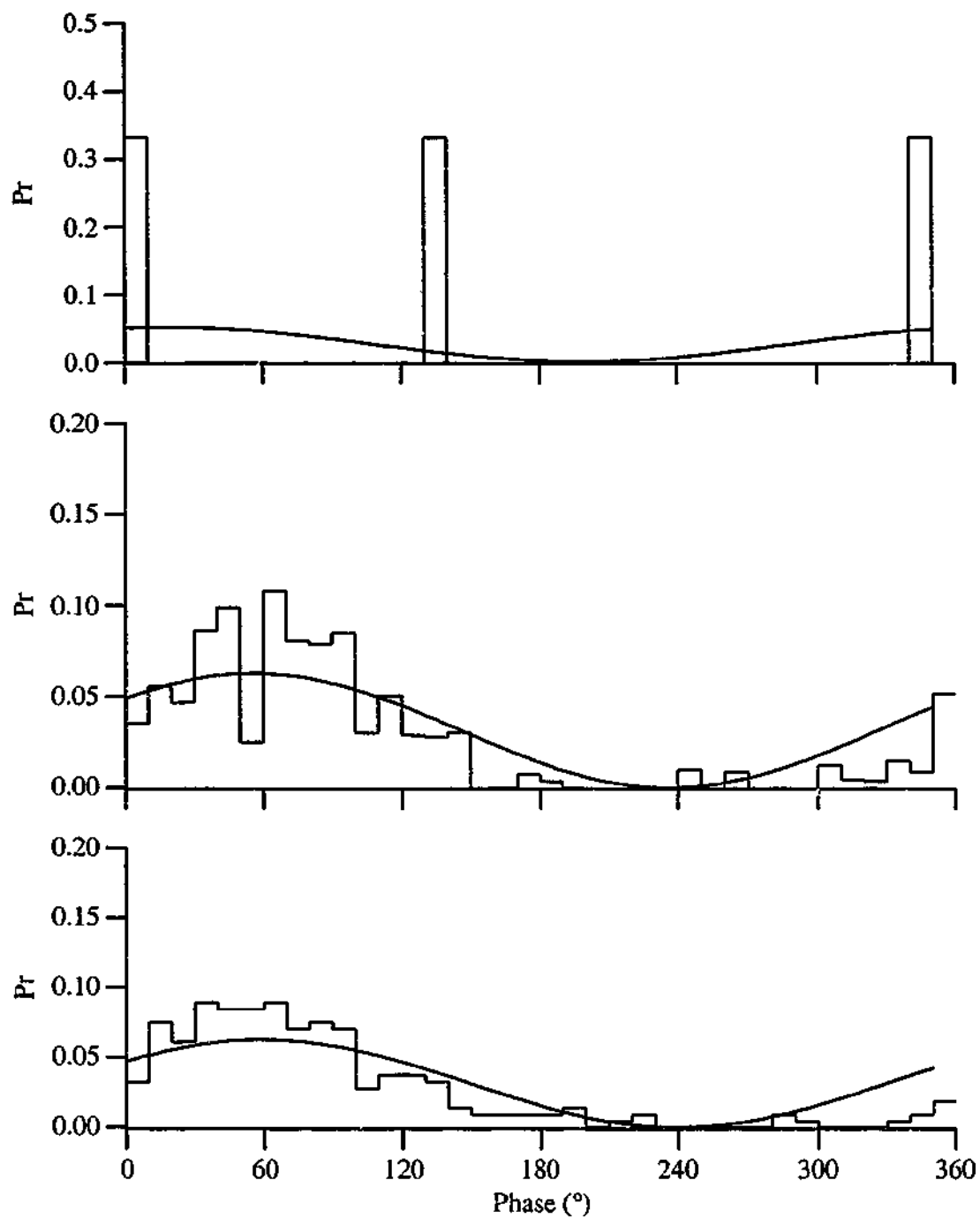
Figure 2.16 The cycle histogram of a 0.1 s simulation does not show significant modulation as only 3 spikes are produced resulting in a SNR_{EXP} of 1.13 (top panel). The middle panel is the summed cycle histogram of 100 such simulations and has a significant modulation ($SNR_{EXP} = 6.7$), and is similar to the cycle histogram for 10 s of simulation ($SNR_{EXP} = 7.6$) shown in the bottom panel. All simulations were done with a 1.4 mA, 30 Hz sinusoid and 10 mA of input noise. Note different vertical scale in the top panel. The cycle histograms were constructed using 10° bins and a period of 0.033 s.
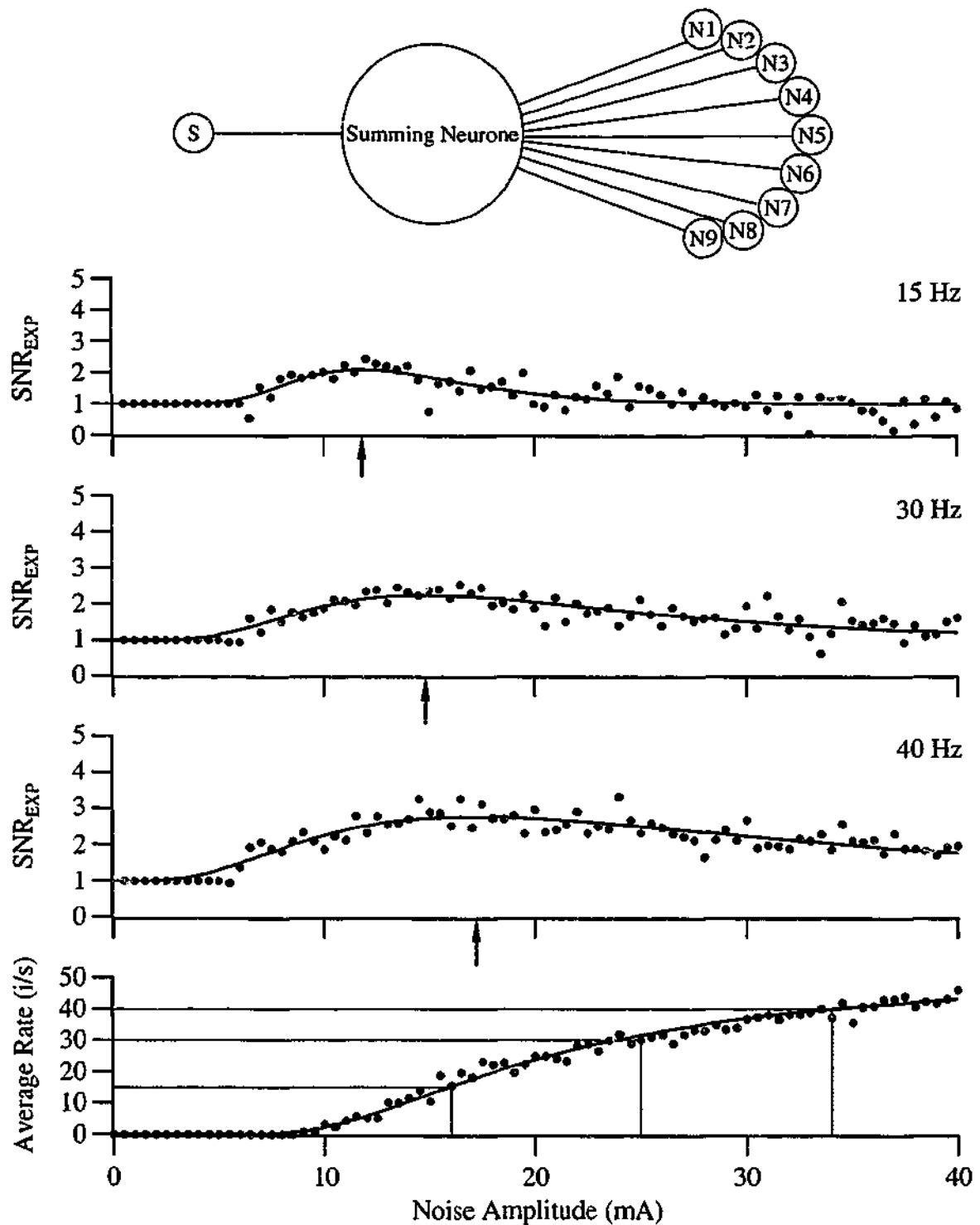
Figure 2.17 The network of Hodgkin-Huxley neurones consists of a single neurone driven by a supra-threshold periodic signal and nine neurones driven by supra-threshold noise-alone signals that are summed by a single second level neurone (top panel). This network exhibits the key features of stochastic resonance (lower panels). Each point is calculated from 10 s of simulation. The fitted curves in the middle panels are logNormal curves used to estimate the optimal noise level, D_{OPT}, indicated by the arrows. The bottom panel is the noise-alone response that has been fitted with a curve based on Kramers' rate. The grey lines in the bottom panel indicate the predicted optimal noise value, D_{PRE}, for each test frequency.

The network of Hodgkin-Huxley neurones exhibited many of the features of stochastic resonance, as illustrated in Figure 2.17 (lower panels). The agreement between the predicted optimal noise levels, D_{PRE}, (16, 25 and 34 mA) and the estimated optimal noise levels, D_{OPT}, (11.8 ± 0.5, 14.8 ± 0.5 and 17.2 ± 0.4 mA) for the three test frequencies (15, 30 and 40 Hz) is not as close as for the single neurone model. However, the essential feature of stochastic resonance, an increase in the optimal noise level with an increase in periodic stimulus frequency, is still present.

Maintained Discharge

A feature of some sensory receptors that is not modelled by the standard Hodgkin-Huxley model is a maintained discharge. 'Most axon membranes could not be used for graded rhythmic encoding because, in the face of steady stimulus current, they either fire only once and then remain refractory, or fire repetitively at a very high frequency that varies little with the stimulus intensity (Hille, 1992).' This is true of the Hodgkin-Huxley model as illustrated in the top panel of Figure 2.18. It is clear that above the threshold current of approximately 7 mA, the maintained discharge is already a significant fraction of the maximal rate.

The bottom panel of Figure 2.18 illustrates the effect of noise and a constant 9 mA of current. The average rate initially decreases from the maintained rate of 66 i/s to 59 i/s and then increases to 82 i/s. The response can be fitted with a modified form of Kramers' rate equation, given by Equation 2.6. 'D' is the noise amplitude, α and β are arbitrary constants and MD is the maintained discharge in the absence of noise. The modified Kramers' rate approximation does not include the initial decrease in average discharge, although it does fit the remaining data well. The response to noise in the presence of a maintained discharge is more complex than without a maintained discharge and there is also a smaller increase in average firing rate for a given noise amplitude: compare the two traces in the bottom panel of Figure 2.18.

$$\text{Rate} = \alpha\, e^{-\frac{\beta}{D^2}} + MD \qquad\qquad \textbf{Equation 2.6}$$
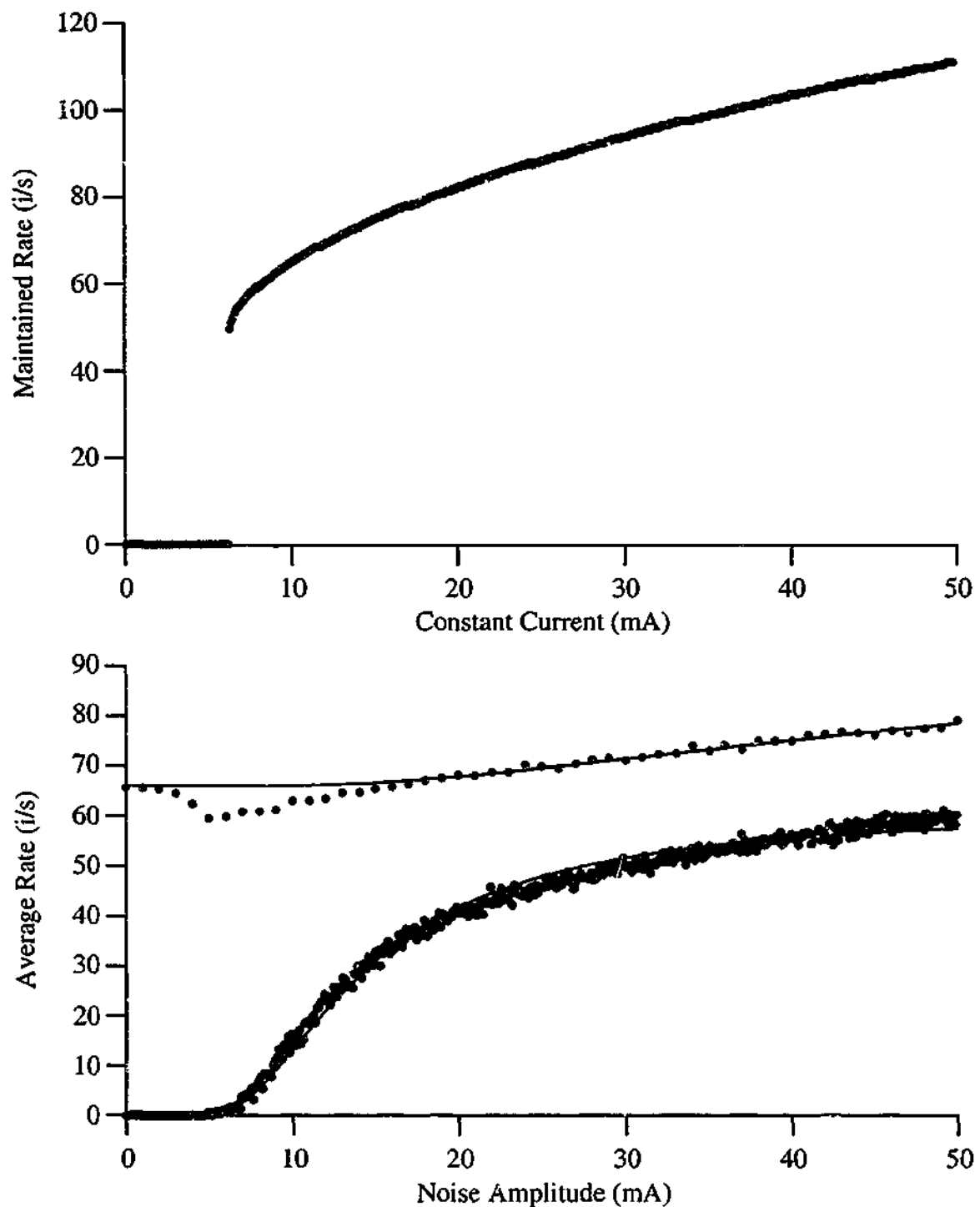
Figure 2.18 In response to a constant current the Hodgkin-Huxley model exhibits a slow increase in maintained firing rate with a threshold of approximately 7 mA (top panel). The addition of noise to a constant current stimulus of 9 mA, results in an initial decrease followed by an increase in the average firing rate (red points in the bottom panel). The response can be fitted with a modified Kramers' rate (solid line), although the fit does not follow the initial decrease in average rate. This is in contrast to the noise-alone response (i.e. no constant current, blue points), which is the same data as the bottom panel of Figure 2.2. All simulations were performed for 10 s using the standard Hodgkin-Huxley equations.

The smaller increase in average rate and the initial decrease in average rate with additional noise input is a result of the model being driven to near saturation by the constant current input. The maximum noise-alone induced rate is approximately 70 i/s (Figure 2.2, bottom panel), which is approximately the same as the minimum maintained rate that can be induced by a constant current. The small increase in average rate after the initial decrease in average rate would mean stochastic resonance could only occur over a very limited frequency range, if at all.

Stein Model

It is possible to lower the constant current threshold and also the minimum maintained discharge rate by reducing the inactivation of the sodium current and reducing the leakage conductance of the basic Hodgkin-Huxley model (Stein, 1967). The reduction in sodium inactivation is achieved by shifting the 'h' variable by -20 mV. Using a value of 0.007 mS / cm² rather than 0.3 mS / cm² reduces the leakage conductance. The model was implemented using the standard Hodgkin-Huxley equation (Appendix B) with the above modifications.

The constant current response of the resulting model is shown in the top panel of Figure 2.19. The minimum maintained discharge has been reduced to 15 i/s and occurs for a constant current of approximately 0.1 mA. The reduction in sodium inactivation and leakage conductance has removed the ability of this model to exhibit stochastic resonance, as indicated by the lower panels of Figure 2.19. For the three test frequencies of 2, 4 and 10 Hz, the predicted optimal noise levels, D_{PRE}, are 2.8, 3.5 and 6.5 mA respectively. The estimated optimal noise levels, D_{OPT}, of 4.2 ± 0.1 mA, 4.1 ± 0.1 mA and 4.2 ± 0.1 mA respectively, no longer exhibit a frequency dependence.

Connor-Stevens Model

Connor & Stevens (1971) proposed an excitable membrane model capable of a maintained discharge of as low as a single impulse per second. The model is based on a four-current model of the membrane. The currents are a leakage current, an inwards current and two outward currents. The model is able to produce a maintained discharge that is proportional to input current over a small range.
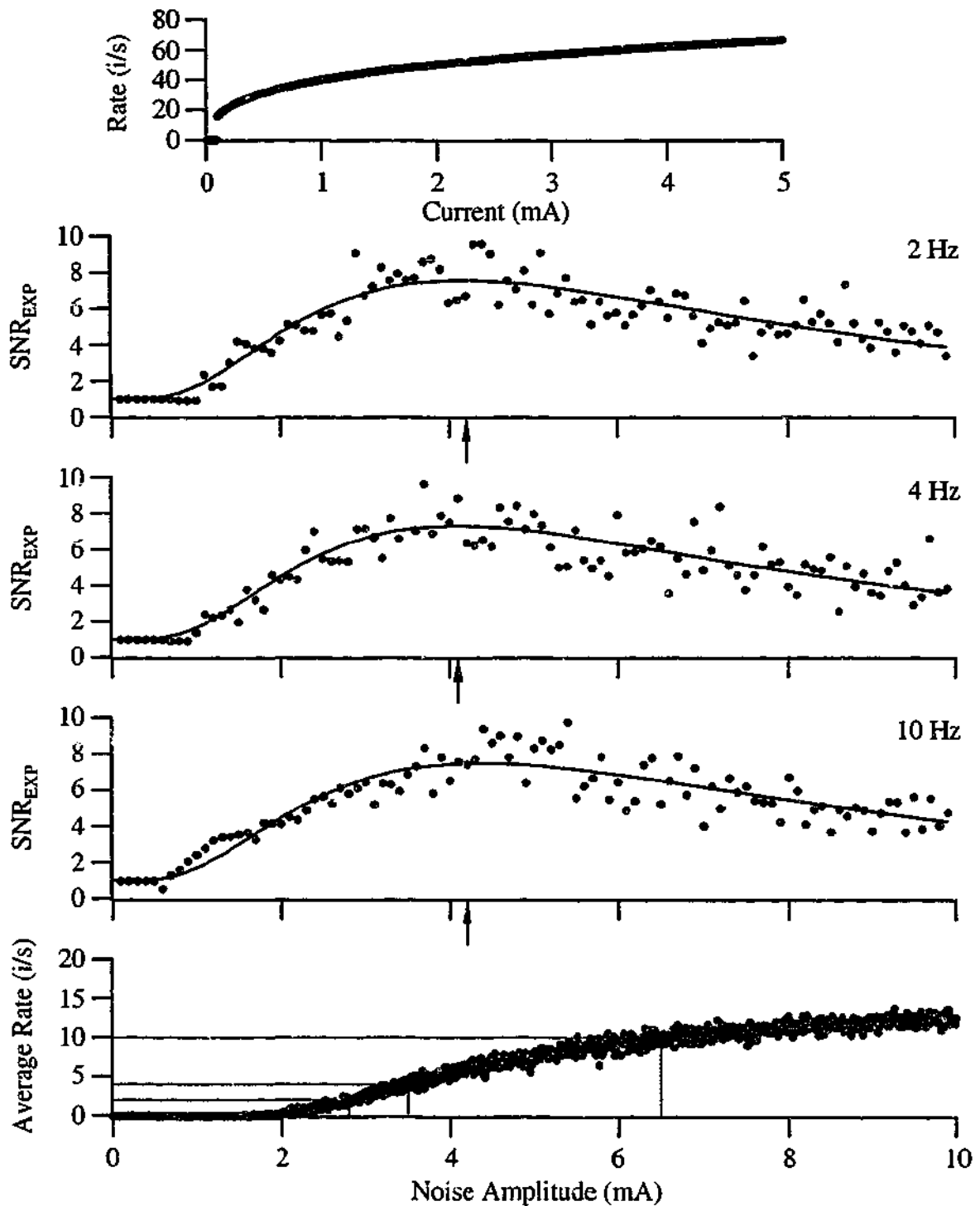
Figure 2.19 A reduction in sodium inactivation and a reduced leakage conductance reduces the threshold for maintained discharge of the basic Hodgkin-Huxley model (top panel). However, the modified model no longer exhibits stochastic resonance, as D_{OPT} is independent of frequency. The fitted curves in the middle panels are logNormal curves used to estimate the optimal noise level, D_{OPT}, indicated by the arrows. The bottom panel is the noise-alone response that has been fitted with a curve based on Kramers' rate. The grey lines in the bottom panel indicate the predicted optimal noise value, D_{PRE}, for each test frequency. Each point was calculated from 10 s of stimulation.

The model is based on a series of Hodgkin-Huxley-like equations, but with several variables specified by graphical means, rather than explicitly. The model was implemented using a fixed step-size fourth-order Runge-Kutta numerical integration technique with a step size of 1 millisecond.

The constant current response of the Connor-Stevens model is shown in the top panel of Figure 2.20. The maintained rate is an approximately linearly function of the constant current. The maximum rate induced by the noise-alone stimulus (Figure 2.20, bottom panel) is less than 1 i/s, which is approximately the minimum maintained rate. However, the noise-alone response is not a monotonically increasing function of noise amplitude. Therefore, it is not possible that the Connor-Stevens model could exhibit stochastic resonance.

Otten Model

Otten, Hulliger & Scheepstra (1995) proposed a series of changes to the myelinated nerve fibre model of Fankenhaeuser & Huxley (1964) to more closely model the response of a muscle spindle primary ending. The model consists of a sodium current, fast and slow potassium currents, a non-specific current and a leakage current. The model is capable of producing many of features of the response of a typical muscle spindle primary ending. These features include a sustained discharge down to near zero rates; a near linear relation between firing rate and receptor potential; a dynamic response to a step stimulus; a slow adaptation in response to a step stimulus; and 'band-pass filter properties' in response to sinusoidal stimuli. The model is described by the equations given in Appendix C, and was implemented using a fixed step-size fourth-order Runge-Kutta numerical integration technique.

The constant current response of the Otten model is shown in the top panel of Figure 2.21 and is approximately linear over the range of 20 i/s to 150 i/s. The model does not exhibit stochastic resonance, as illustrated by the lower panels of Figure 2.21. For the three test frequencies of 10, 50 and 100 Hz, the predicted optimal noise levels are 103, 202 and 344 nA respectively. The estimated optimal noise levels are not frequency dependent, and are all 120 ± 10 nA.
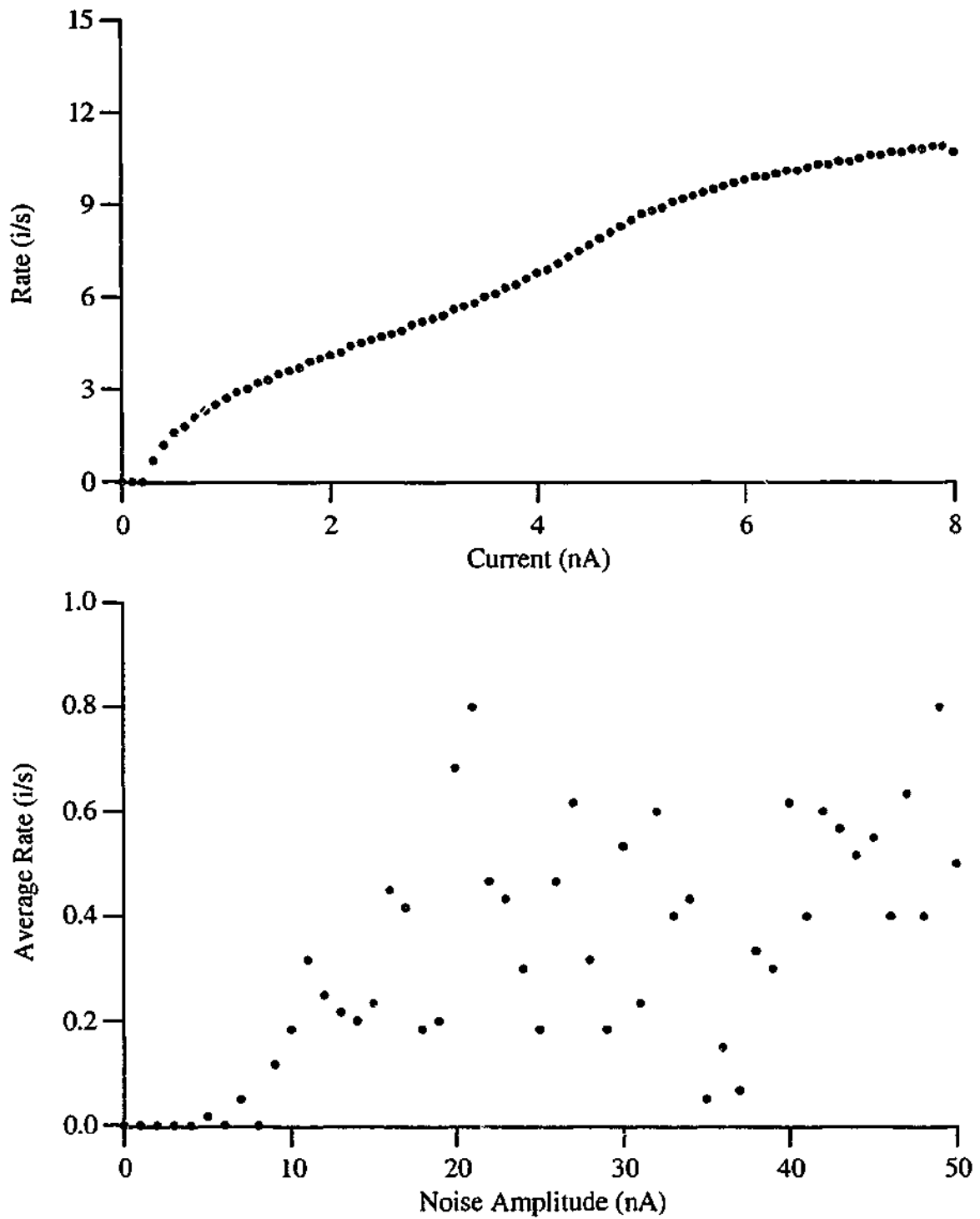
Figure 2.20 The excitable membrane model proposed by Connor & Stevens (1971), while capable of sustaining a low maintained discharge (top panel), does not respond to a noise-alone input in a consistent manner (bottom panel). For stochastic resonance to occur the noise-alone response must be a monotonically increasing function of noise. Each point was calculated from 10 s of stimulation.
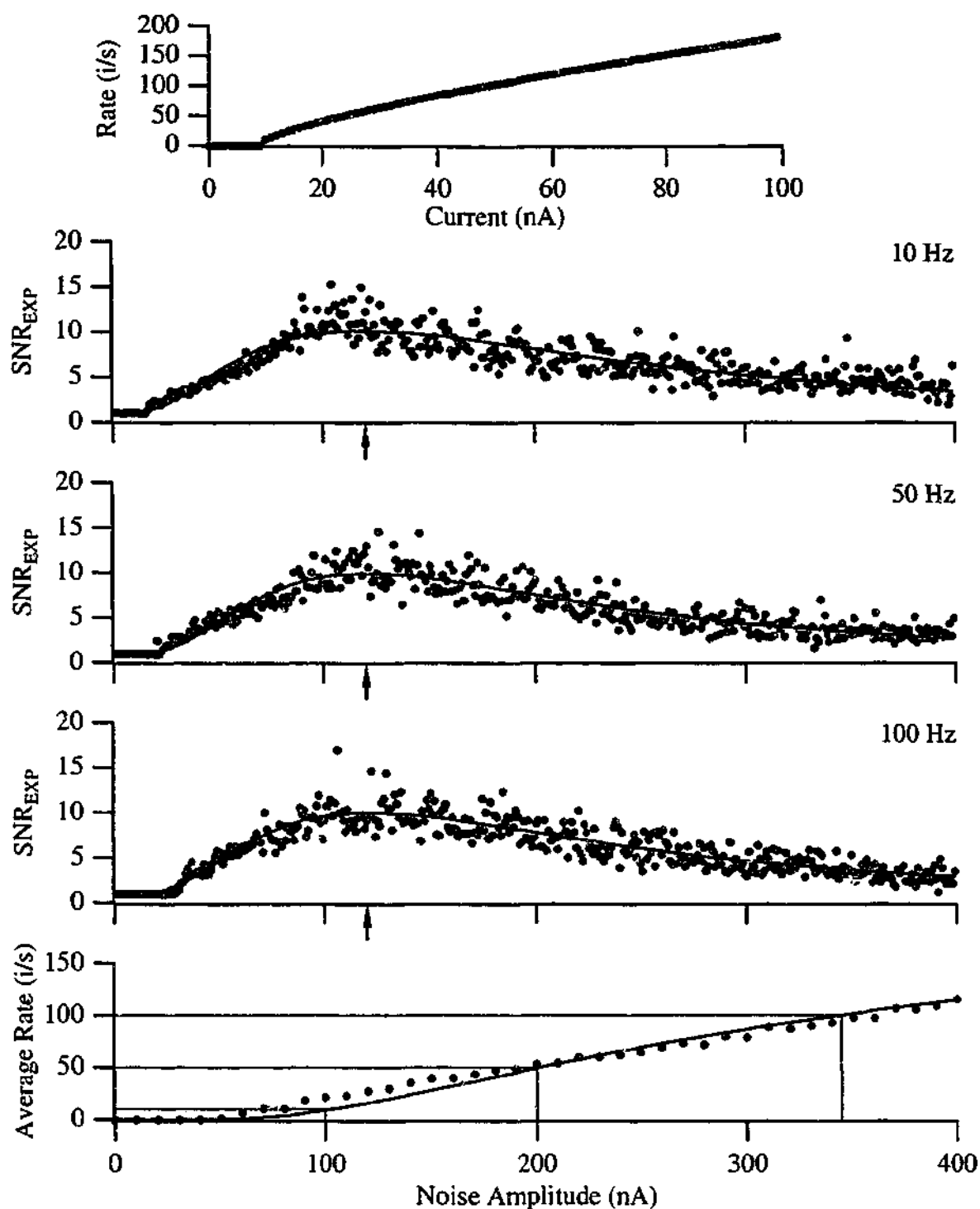
Figure 2.21 The model proposed by Otten, Hulliger & Scheepstra (1995) is capable of sustaining a low maintained discharge (top panel). The model does not exhibit stochastic resonance, as D_{OPT} is not dependent on the sinusoidal stimulus frequency. The fitted curves in the middle panels are logNormal curves used to estimate the optimal noise level, D_{OPT}, indicated by the arrows. The bottom panel is the noise-alone response that has been fitted with a curve based on Kramers' rate. The grey lines in the bottom panel indicate the predicted optimal noise value, D_{PRE}, for each test frequency. The simulations were done with a fixed step size of 10 μs and each point was calculated from 5 seconds of simulation.

It is interesting that none of the models capable of producing a maintained discharge at low rates exhibit stochastic resonance. Many of the models exhibit an optimum in output SNR with the addition of input noise and hence it is possible to calculate a D_{OPT} value. However, the estimated optimal noise levels are not dependent on the sinusoidal stimulus frequency for any of the models examined, and thus do not display a key feature of stochastic resonance. If the ability to generate low rates of maintained discharge does exclude a system from exhibiting stochastic resonance then many biological receptors are unlikely to exhibit stochastic resonance. Alternatively, if biological receptors exhibit stochastic resonance then none of the models examined that are capable of low rates of maintained discharge are accurate representations of the biological receptors.

Aperiodic Stochastic Resonance

Although 'aperiodic stochastic resonance' is not possible by definition (p. 9), it is possible to observe an 'aperiodic stochastic resonance' effect with the standard Hodgkin-Huxley model. Collins et al. (1996b) proposed that 'aperiodic stochastic resonance' occurred for the detection of small ramp-and-hold indentations of the skin on the tip of the middle index finger. The simplest method of detecting a ramp-and-hold indentation is based on comparing the average discharge rate during the hold phase with the average rate before the ramp phase.

The relevant output measure for the Hodgkin-Huxley model is the average rate produced with a constant current and noise, equivalent to the hold phase, relative to the noise-alone response, equivalent to the discharge before the ramp phase. If an arbitrary threshold of a doubling of the average discharge rate during the 'hold phase' is set, it is then possible to determine the minimum detectable stimulus, illustrated in the top panel of Figure 2.22. The minimum detection threshold occurs with the addition of approximately 6 mA of noise, which Collins et al. (1996b) would classify as 'aperiodic stochastic resonance'. However, the noise level that optimises the detection is approximately the threshold noise level, which is consistent with the effect probably being a form of system linearisation or dithering (Gammaitoni, 1995).
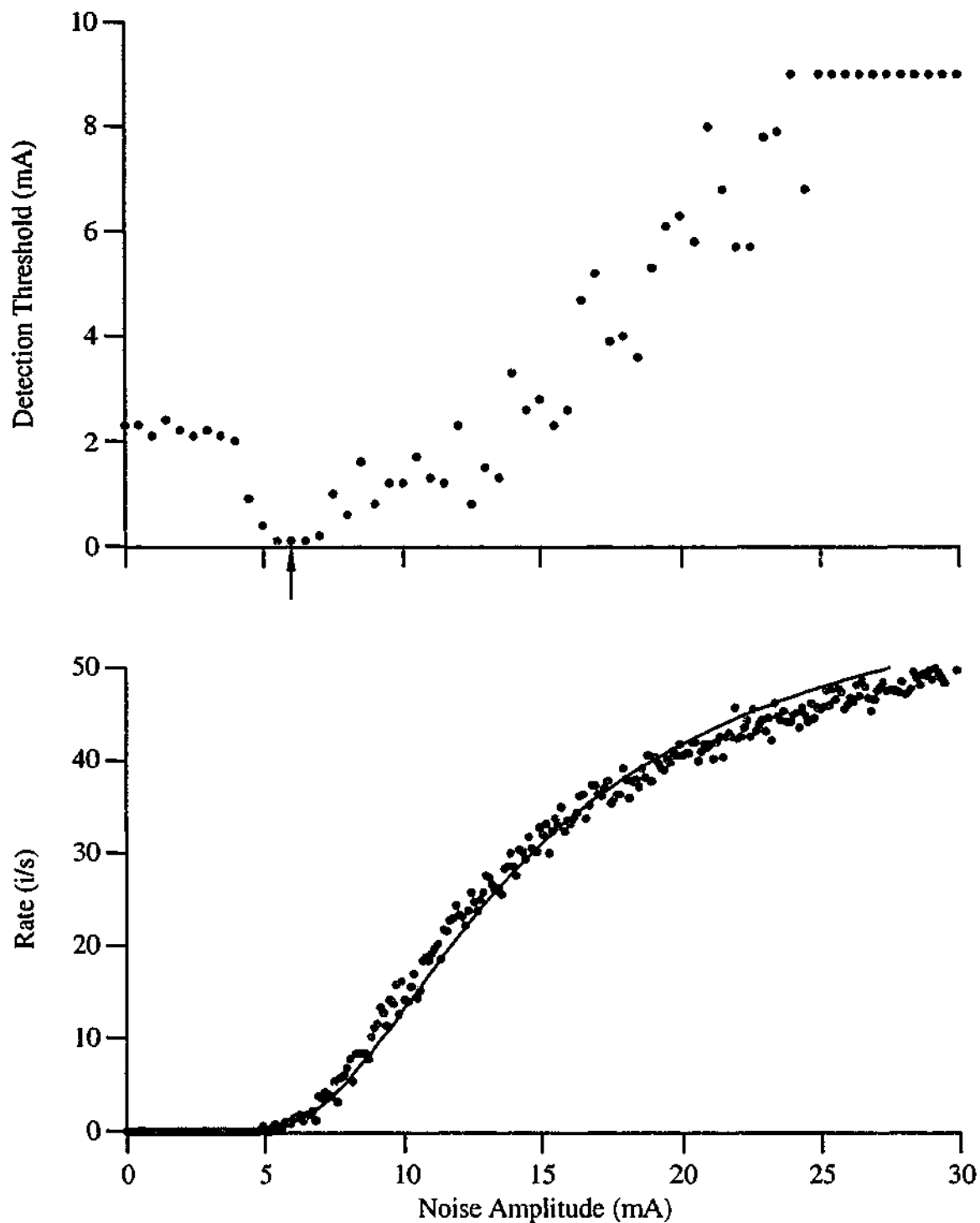
Figure 2.22 It is possible to observe 'aperiodic stochastic resonance' with the Hodgkin-Huxley model. The top panel indicates the constant current required to at least double the average firing rate over the noise-alone response. It is clear that the minimum detection threshold occurs with the addition of a near-threshold level of noise, indicated by the arrow. The optimal noise level is dependent on the time over which the simulation is performed; these simulations were performed for 2 s, using the standard Hodgkin-Huxley equations. The bottom panel is the noise-alone response, a reproduction of the bottom panel of Figure 2.2, to illustrate the noise level that produces the minimum threshold is near-threshold.

Discussion

The summary of models in Table 2.1 highlights several interesting features of the modelling done during stochastic resonance investigations. As previously mentioned (p. 59) the presence of stochastic resonance is dependent on the output SNR measure used. Although the majority of models exhibited an optimal output SNR with the addition of noise, this is not the only requirement of stochastic resonance. The optimal noise level must be dependent on the frequency of the periodic stimulation for the effect to be considered as stochastic resonance. The optimal noise level should also be able to be predicted from the noise-alone response.

The Hodgkin-Huxley excitable membrane model and the bistable potential well model both exhibit stochastic resonance when the SNR_{ISIH} (or the equivalent SNR_{RES}) measure is used, but not when the SNR_{PS} measure is used. As the majority of models tested were analysed using the SNR_{PS} measure it is not surprising that the majority of models, while exhibiting an optimum in SNR_{PS} with the addition of input noise, did not exhibit stochastic resonance. Also, some of the models were only tested with a single periodic stimulus frequency, so like many of the biological systems tested for stochastic resonance (discussed in Chapter One) it was not possible to determine if stochastic resonance had occurred.

Although stochastic resonance can be observed using the SNR_{ISIH} measure, the estimated optimal noise values are dependent on the amplitude of the sub-threshold periodic amplitude. In the extreme case of a zero amplitude periodic signal (a noise-alone signal) it is possible that the SNR_{ISIH} measure will still indicate the presence of stochastic resonance, but this would be a false positive detection of stochastic resonance. Therefore, the SNR_{EXP} measure was developed to study stochastic resonance. Although the estimated optimal noise levels using the SNR_{EXP} measure are also dependent on the sub-threshold periodic stimulus amplitude, the SNR_{EXP} measure will not give a false positive detection of stochastic resonance, but may in fact indicate the presence of dithering rather than stochastic resonance.

	Page	Studied by	Input Signal	Output Signal	Output measurement	Exhibits Optimal in SNR vs Noise	Frequency dependence of D_{opt}	Capable of low resting discharge
Bistable potential well	Ch1 & 42	Benzi, Sutera & Vulpiani Fox	Force acting on particle	Particle Position	SNR_{PS}	✓	✗	✗
		Gammaitoni, Hanggi, Jung & Marchesoni			SNR_{RES}	✓	✓	
Connor-Stevens	63	This chapter	Current	Voltage	SNR_{EXP}	NA	NA	NA
Fitzhugh-Nagumo	45	Longtin	"Current"	"Voltage"	SNR_{ISIH}	✓	✓	✗
		Kanamaru, Horita & Okabe This chapter			SNR_{PS}	✓	✗	
Hodgkin-Huxley	47 & 50-63		Current	Voltage	SNR_{CYCLE}	✓	✗	
		This chapter			SNR_{ISIH}	✓	✓	✗
					SNR_{EXP}	✓	✓	
					SNR_{THRESH}	✓	✓	
				Spike trains	SNR_{EXP}	✓	✓	
Integrate-&-Fire	43	Shimokawa, Pakdaman & Sato Barbi, Chillemi & Di Garbo Plesser & Geisel	Current	Series of standard spikes	SNR_{ISIH}	✓	✓	✓
					SNR_{PS}	✓	✓	
Oil-water membrane	48	Zhong & Xin	Concentration of material (noise-alone)	Transfer of material	SNR_{PS}	✓	✗	NA
Otten	64	This chapter	Current	Voltage	SNR_{EXP}	✓	✗	✓
Simple cells	49	Srebo & Malladi	Spike trains	Series of standard spikes	SNR_{PS}	✓	✗	✗
Spike integrator	45	Godivier & Chapeau-Blondeau	Spike trains	Series of standard spikes	SNR_{PS}	✓	Unsure	✓
Stein	63	This chapter	Current	Voltage	SNR_{EXP}	✓	✗	✓
Torus semicircularis	49	Kashimori, Hoshino & Kambara	Spike trains	Firing rate	Firing rate	✓	✗	✓
Visual cortex	49	Stemmler, Usher & Niebur	Spike trains	Firing rate	$P_{(correct)}$	✓	✗	✓

Table 2.1 Summary table of the models considered in this chapter, indicating their input and output signals, if they are capable of exhibiting an optimum in output signal to noise ratio with the addition of noise, if they exhibit stochastic resonance and if they are capable of producing a 'low' level of maintained discharge.

It is of interest that none of the models capable of generating relatively low rates of maintained discharge exhibit stochastic resonance. The implication is that systems that are capable of generating low rates of maintained discharge are not capable of exhibiting stochastic resonance. As many biological receptors are capable of producing maintained discharges, down to rates as low as a single action potential a second, the modelling to date indicates that these systems should not exhibit stochastic resonance. Alternatively, as suggested by stochastic resonance investigations of many biological receptors, if the receptors are capable of exhibiting stochastic resonance then the models are not correct and must be adjusted.

Summary of Stochastic Resonance

The presence and nature of the stochastic resonance effect is dependent on the output measure used. Therefore a summary of the features of stochastic resonance using the SNR_{EXP} measurement (the measurement to be used throughout the experimental chapters of this thesis) is useful. If stochastic resonance occurs in a system then there should be an optimal SNR_{EXP} with the addition of a supra-threshold level of input noise when the system is stimulated with an otherwise sub-threshold periodic signal. In other words, the addition of input noise makes an otherwise sub-threshold periodic signal detectable. However, the increase in the output SNR with the addition of noise is not unique to stochastic resonance.

The second feature of stochastic resonance, and one that sets it apart from other noise-induced effects, is the dependence of the optimal noise level, D_{OPT}, on the frequency of the sub-threshold periodic signal. The stochastic resonance involves the matching of two time-scales; the time-scale of the sub-threshold periodic signal and the noise-induced response of the system. The noise-induced response of the system is characterised by the noise-alone response of the system, which can be predicted using Kramers' rate (Kramers, 1940). The predicted optimal noise level, D_{PRE}, can then be predicted from the noise-alone response, as the optimal noise level should be the level of noise that, when applied alone, produces an average rate equal to the frequency of the sub-threshold periodic stimulus.

For the SNR_{EXP} measure, the correlation of estimated optimal noise level, D_{OPT}, and predicted optimal noise level, D_{PRE}, is dependent on the amplitude of the sub-threshold periodic signal. Figure 2.13 illustrates that when a near-threshold periodic signal is used the estimated optimal noise levels are well correlated with the predicted optimal noise levels over a wide range of frequencies. For sub-threshold periodic signal amplitudes that are far from threshold the estimated optimal noise level, D_{OPT}, approaches the threshold level for noise, as illustrated in Figure 2.11. Therefore, if a system exhibits a correlation between the estimated optimal noise level, D_{OPT}, and the predicted optimal noise level, D_{PRE}, with the SNR_{EXP} measure, it is probably exhibiting stochastic resonance.

Finally it is worth reiterating that the stochastic resonance effect is not dependent on the noise distribution used, as illustrated in Figure 2.15. Different noise distributions will result in modifications to both the noise-alone response of the system and the shape of the SNR vs noise curves. However, different noise distributions should not alter the presence or absence of the stochastic resonance effect.

Chapter Three

Multi-Channel Recorder

As part of this project a new multi-channel recording system, capable of recording from multiple afferent fibres simultaneously was designed and constructed. There are many advantages of a system that is capable of recording from multiple afferents simultaneously over a system that can only record from a single afferent at a time. There is useful information present in the response of a population of afferents that is not present in the repeated responses of a single afferent (Johansson, Bergenheim, Djupsjobacka & Sjolander, 1995; Owens, Denison, Versnel, Rebbert, Peckerar & Shamma, 1995). It is only possible to record this type of information if the response of multiple afferents can be simultaneously recorded. Simultaneous recording of the responses of multiple afferents can also elucidate whether variations in afferent responses are due to variations between individual afferents, differences between animals, or variations in recording conditions or experimental preparations.

Standard recording systems can be separated into two distinct sub-systems: hardware and software. Traditionally, much of the processing and analysis of recorded data was performed with purpose-built hardware. The role of computers and software was often confined to statistical analysis and storage of the data. Advances in desktop computers, including processing power and storage capacity, have allowed more processing and analysis of data to be performed in software rather than purpose built hardware. This allows for a more flexible recording system in which it is possible to rapidly implement different types of analysis. One of the design goals for the new multi-channel recorder was to move the software-hardware interface further towards the raw signals, allowing more of the analysis of the data to be performed with software, rather than custom built hardware.

The multi-channel recorder was specifically designed for recording afferent activity in dorsal root filaments of the anaesthetised cat. Therefore, certain constraints were placed on the recorder, including a restriction of the space available for electrodes, the need to interact with other equipment and the ability to operate in a relatively 'noisy' environment. Although some of the rationale involved in the design of the recorder may be specific to this particular experimental preparation, the general design rules will

apply to most experimental preparations involving extra-cellular recording of afferent activity.

As with traditional recording systems, the multi-channel recording system can be divided into two major sub-systems, hardware and software (Figure 3.1). The hardware consists of electrodes, amplifiers, filters and a computer with data acquisition capabilities that are designed to generate a digital representation of the afferent activity within the dorsal root filaments. The software was then developed to allow analysis and manipulation of the digital representation of the afferent activity.

Electrodes

Extra-cellular recording of afferent activity has traditionally been made with double platinum wire electrodes resulting in a bipolar recording (Bronzino, 1995). Alternatively, the afferent activity in a nerve filament can be recorded in a monopolar way as changes in the potential between the nerve filament and a reference potential. The reference potential is taken from either a 'dead' nerve filament, one without any activity, or another reference location on the experimental preparation, such as a needle placed into a passive muscle. With double wire electrode recording, the number of electrodes required is twice the number of active filaments being recorded. As the number of filaments being recorded increases, the number of electrodes required becomes a problem due to the limited space available for placing of the electrodes. A simple modification that can reduce the number of electrodes required is to have a single common reference electrode, so the number of electrodes required is equal to the number of active filaments being recorded, plus one.

Positioning of electrodes is influenced by several constraints, the most pressing of which is the limited space available for electrode placement. However, it is important that the electrode configuration used is mechanically stable as well as being compact. Another important consideration is separation of the active filaments. The active filaments must be kept separated from one another to reduce capacitive signal shunting that occurs if the filaments are allowed to come into close contact with each other.
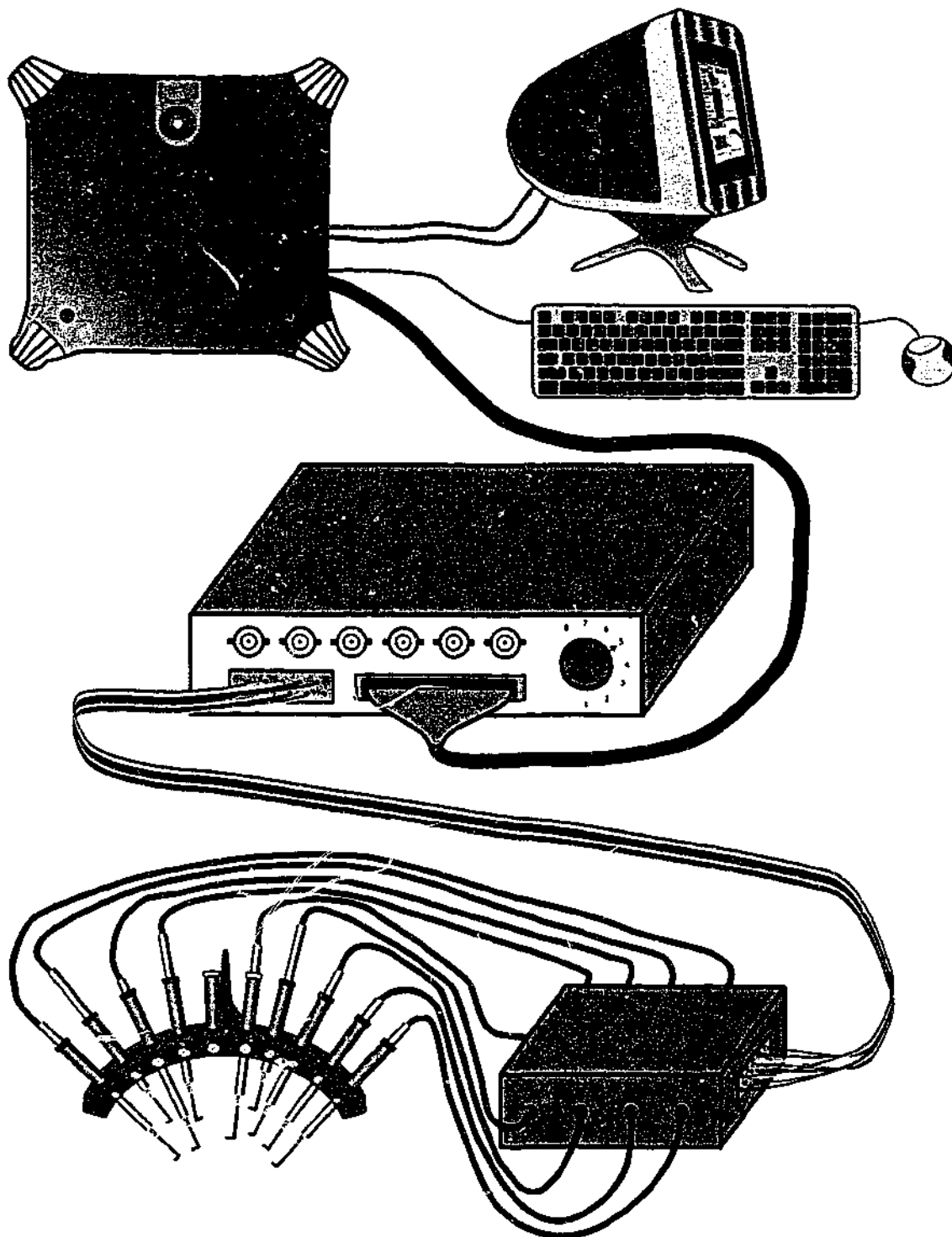
Figure 3.1   The multi-channel recorder hardware consists of a curved electrode array (bottom-left, also illustrated in Figure 3.2), the header stage amplifier (bottom-right), the second stage amplifier (middle), and the data acquisition card with the computer (top).

A hook electrode (Figure 3.2, top panel), has been used to record from twelve afferents simultaneously by Djupsjobacka, Johansson, Bergenheim & Sandstrom (1994). Although the hook electrode is mechanically strong and very compact, it is not very flexible. The fixed configuration of electrodes results in the same space being required whether one or twelve afferents are being recorded. The close spacing of the active filaments can also become a problem, leading to capacitive shunting of the afferent signals. Therefore, a curved electrode array consisting of ten single-wire platinum electrodes was constructed for this project in the mechanical workshop of the Department of Electrical and Computer Systems Engineering, Monash University (Figure 3.2, bottom panel). The curved array allows for placement of the electrode tips in a large three-dimensional volume. The placement of the electrode tips can be adjusted to give the greatest possible filament separation, reducing signal shunting. Unused electrodes can be removed to allow greater flexibility of electrode placement when recording from fewer afferent filaments.

Amplifiers and Filters

The extra-cellular potential changes caused by the activity in the dorsal root filaments are of the order of a few hundreds of microvolts. It is therefore necessary to amplify the potential changes, typically by a factor of around 1,000 before subsequent processing of the signal. In order to reduce the amount of noise introduced into the signals it is important to amplify the signals as close to their source as possible. Therefore, in traditional recording systems the amplification is often split into two stages, a header stage located near the experimental preparation and a second stage located further from the preparation. The header stage should provide as much amplification as possible, while retaining a small physical size, to reduce the effect of noise as the signal is transferred to the second stage.

Low frequency disturbances of the electrode potential, caused by the movement of the polarised fluids surrounding the electrodes, needs to be removed before the amplification is performed. Therefore the header stage also often contains high-pass filters to reduce the low frequency noise that can corrupt the signal. The second stage, located further from the experimental preparation, typically contains additional

71
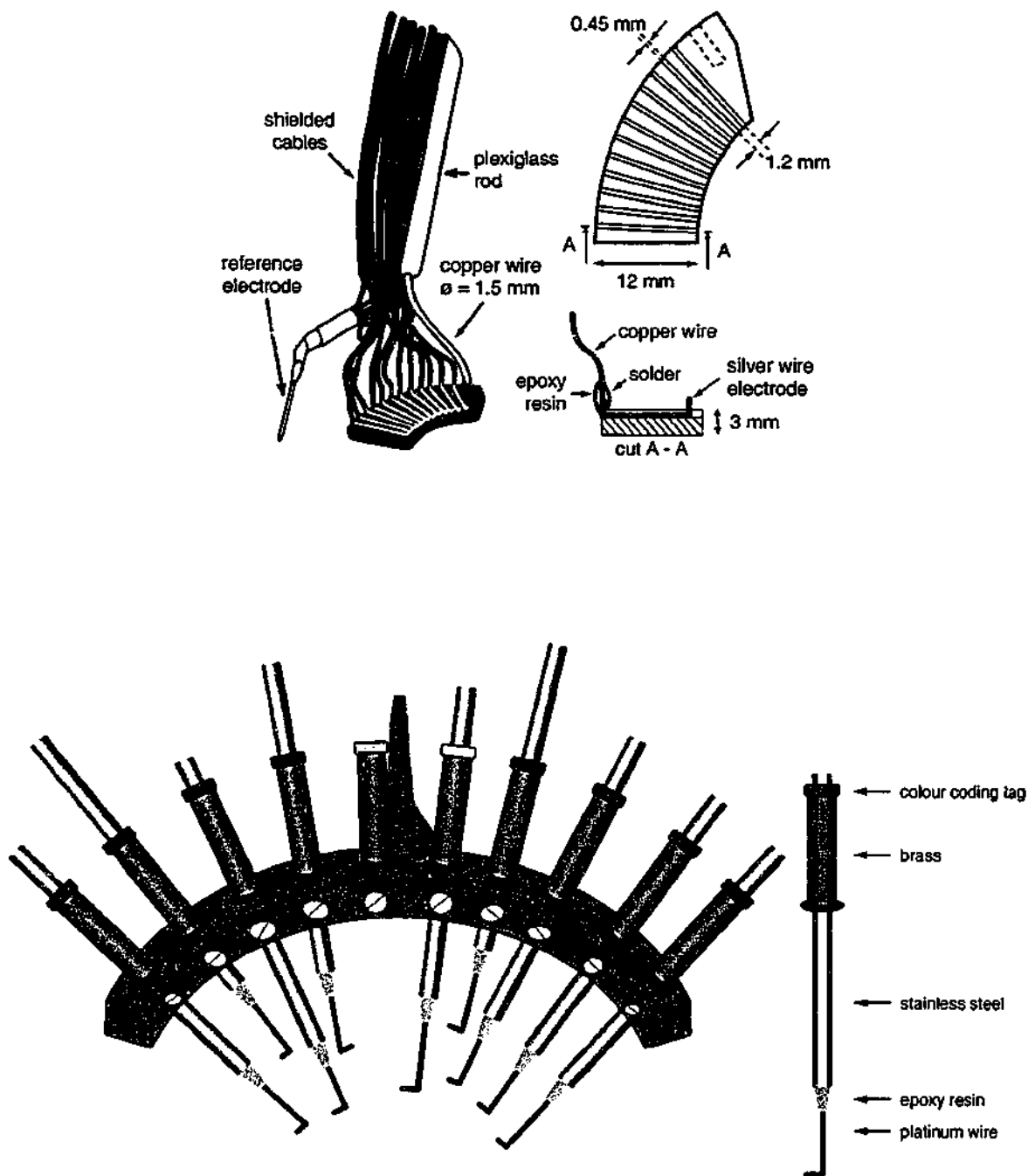
Figure 3.2 The hook electrode (top panel, adapted from Djupsjobacka et al. (1994)) is mechanically strong and very compact, although the rigidity of the design results in the same space being required if one or twelve filaments are being recorded. Also the close spacing of the active filaments may lead to capacitive shunting of the afferent signals. The curved electrode array (bottom panel) was used for the multi-channel recorder as it allows for placement of the electrode tips in a large three-dimensional volume and unused electrodes can be removed to save space.

amplification and filtering. A 50 Hz notch filter is often required to reduce the interference from the mains power supply.

The multi-channel recorder header stage, constructed using surface mount technology, consists of eight, 1,000 times, amplifiers with low-pass filtering with a corner frequency of 8 kHz and high-pass filtering with a corner frequency of 300 Hz. The circuit diagram for the header stage is shown in Appendix D. The low-pass filtering was required to reduce the high-frequency component of the signal before sampling by the data acquisition system. The header stage was constructed within a 108 x 148 x 75 mm metal box and is connected to the electrode array with miniature coaxial connectors and coaxial cable to provide shielding.

The header stage is connected to the second stage via ribbon cable, which carries both afferent signals and power for the header stage. As the afferent signals are of the order of hundreds of millivolts after amplification in the header stage, there is no need to provide shielding between the header stage and the second stage. The second stage, the circuit diagram of which is shown in Appendix E, provides a further amplification of 25 times. The frequency response of the complete amplification system is illustrated in Figure 3.3. The second stage also provides a single output signal of a selectable afferent channel that has a 50 Hz notch filter with an additional 1.5 times gain. The output signal can be used as the input for an audio speaker to allow experimenters to listen to the afferent discharge. The audio signal is used because it is often possible to discern changes in afferent output aurally before it is possible to observe the changes visually.

Impulse Discrimination

Most experiments require the isolation of a functionally single afferent unit. The initial isolation is performed by physically splitting a dorsal root filament containing many afferent fibres into smaller filaments. The splitting procedure is repeated until it is possible to identify a functionally single unit, which may involve around four divisions of the nerve filament. Each time a filament is divided, there is a risk that the unit of interest will be damaged or killed. Therefore, it is advantageous to reduce the amount of splitting required to identify functionally single units.
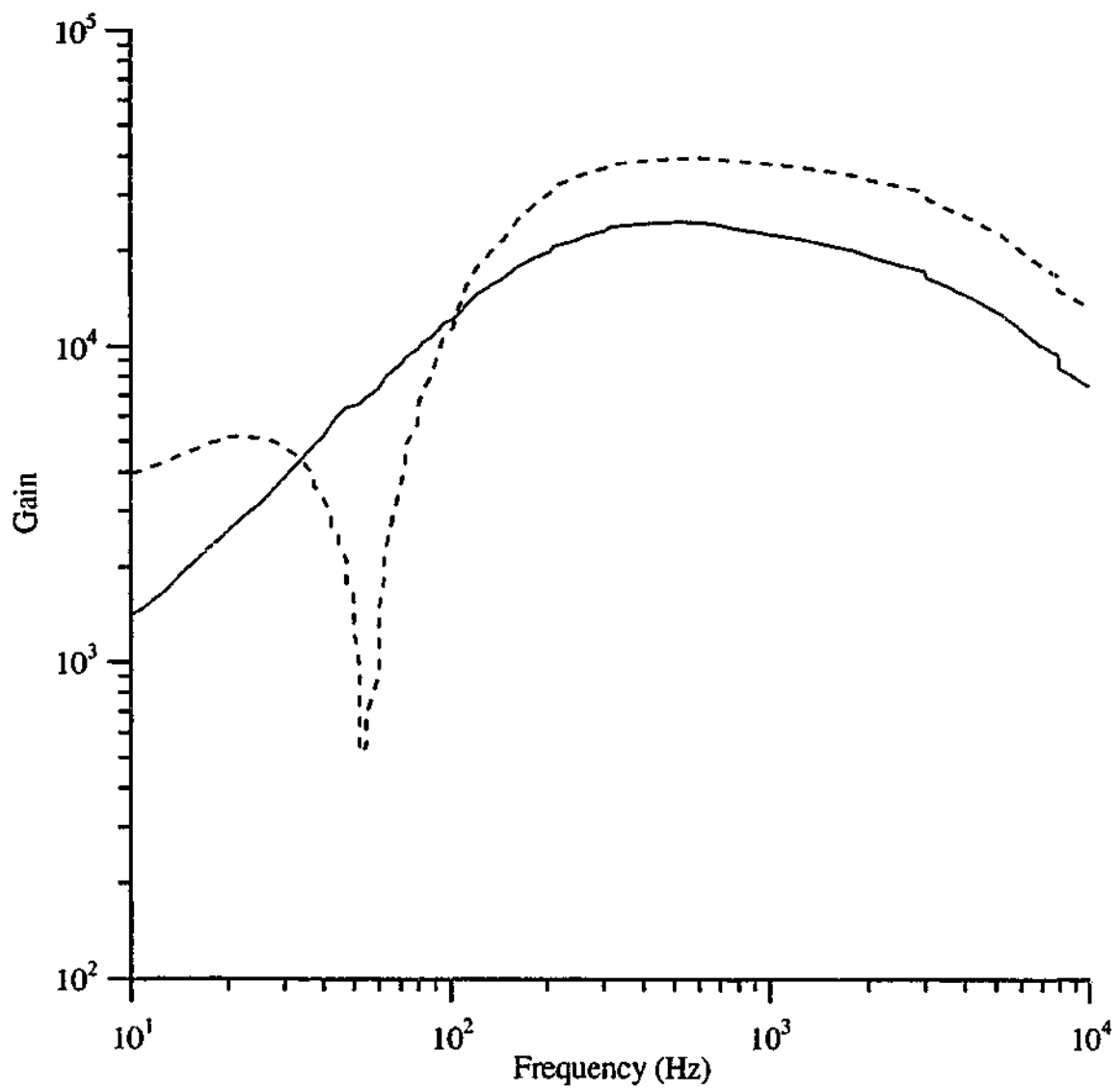
Figure 3.3 The multi-channel recorder has a gain of 25,000 with a high-pass filter with a corner frequency of 300 Hz, and a low-pass filter with a corner frequency of 8 kHz (red line). For audio and visual displays of the afferent signal a 50 Hz notch filter with an additional gain of 1.5 was used (dashed blue line).

The shape of the recorded impulse is dependent on many factors, including the location of the afferent fibre within the filament and the condition of the unit. Each unit will therefore produce an impulse with a slightly different shape from the others when recorded from the nerve filament, and this often allows it to be discriminated (Figure 3.4). Because single unite can be isolated in this way in multi-unit filaments, the amount of splitting required is reduced.

The physiologically relevant information carried by a series of action potentials is the timing of the action potentials, as the shape of the action potential is essentially fixed. It is therefore necessary to discriminate between action potentials from the unit of interest and other signal fluctuations, including action potentials in other afferent fibres. Other fluctuations may also be the result of external noise, such as interference from power supplies, other sources of electromagnetic interference, and movement artefacts.

Discrimination Techniques

Simple Threshold

The simplest technique for distinguishing an action potential from background noise is a threshold. A threshold voltage level can be set and any excursions above the threshold are ascribed to an action potential. This system can be easily implemented in hardware and can perform in 'real time' (i.e., a timing pulse can be delivered as soon as the voltage exceeds the threshold). Simple threshold discrimination can also be easily implemented in software, although the sampling process means that the analysis can never truly be performed in 'real time'.

The disadvantage of impulse discrimination based on a simple threshold is that only the largest impulses can be examined. In the case of the afferent signal shown in Figure 3.4, a simple threshold could distinguish between the large impulses (red and blue) and the small impulses (green) and the noise. However, a simple threshold would not be able to distinguish between the two large impulses as the largest of the red impulses are of an equivalent size to the smallest of the blue impulses. If the smaller (green) impulse is the one of interest, or one but not both of the large impulses, then it is necessary to physically divide the filament again, risking damaging the fibre of interest.
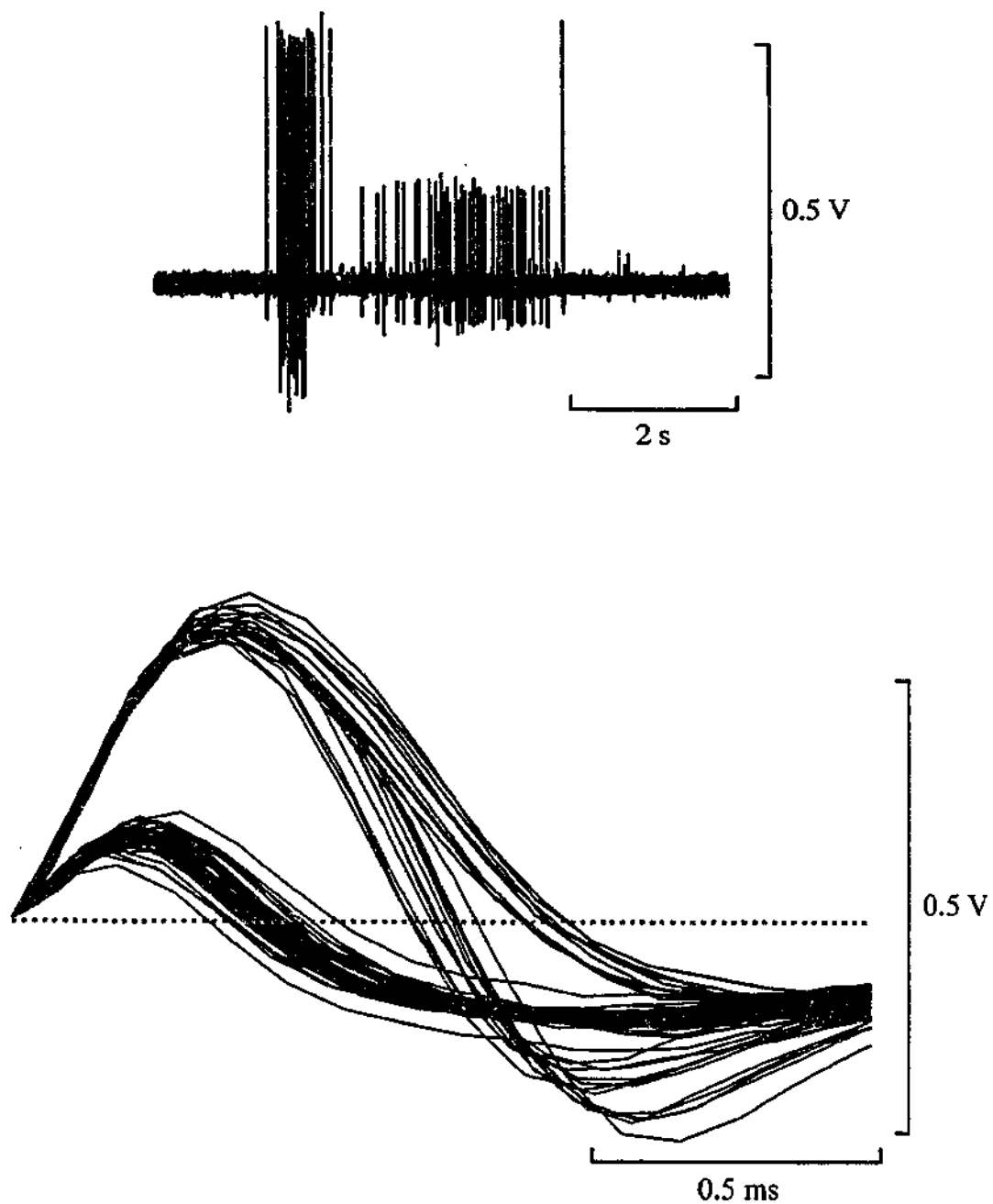
Figure 3.4 It is possible to isolate the impulses produced by one unit from another based on their shape. There are three different impulse shapes present in the signal shown in the top panel, recorded from afferent fibres from the cane toad. In the bottom panel the three different shaped impulses are shown in different colours (blue, green and red). All the impulses have been overlayed starting from the threshold crossing, indicated by the grey dashed line (bottom panel). The threshold has been set above the level of recorded background noise.

Voltage Window

Another commonly performed type of impulse discrimination uses a voltage 'window'. A threshold voltage level can be set and any excursions above the threshold, that also pass through a specified voltage 'window', are ascribed to an action potential (Figure 3.5, top panel). This type of impulse discrimination can be performed with purpose built hardware and will operate in 'real time'. The voltage 'window' can usually be adjusted by altering the maximum and minimum values of the 'window' and the delay after the threshold crossing at which the 'window' is applied. Voltage 'window' discrimination can also be performed with software techniques, although, as with the simple threshold technique, the sampling process means that the analysis can never truly be performed in 'real time'.

Multiple Voltage 'Windows'

A simple extension of the voltage 'window' technique is to increase the number of voltage 'windows' used. The extra voltage 'windows' can either be used to identify extra action potentials, or to identify impulses based on more features of the impulse shape. The extra impulse shape features that can be recognised are illustrated in Figure 3.5 (bottom panel). The red impulses could not be separated from the blue or green impulses using a single voltage 'window'. However, with the combination of two voltage 'windows', the pink and the brown voltage 'windows', it is possible to distinguish between them. Multiple voltage 'windows' can be implemented with hardware, although the number of individual voltage 'window' discriminators required would rapidly make it impractical. Software implementation of multiple voltage 'window' impulse discrimination does not suffer from such a problem, as the only penalty for increasing the number of voltage 'windows' is an increase in processing time.

Primary Component Analysis

Johansson et al. (1995) used primary component analysis (PCA) to discriminate between multiple afferent fibres recorded simultaneously. PCA determines the separation between different groups in a multi-dimensional space. The number of

74
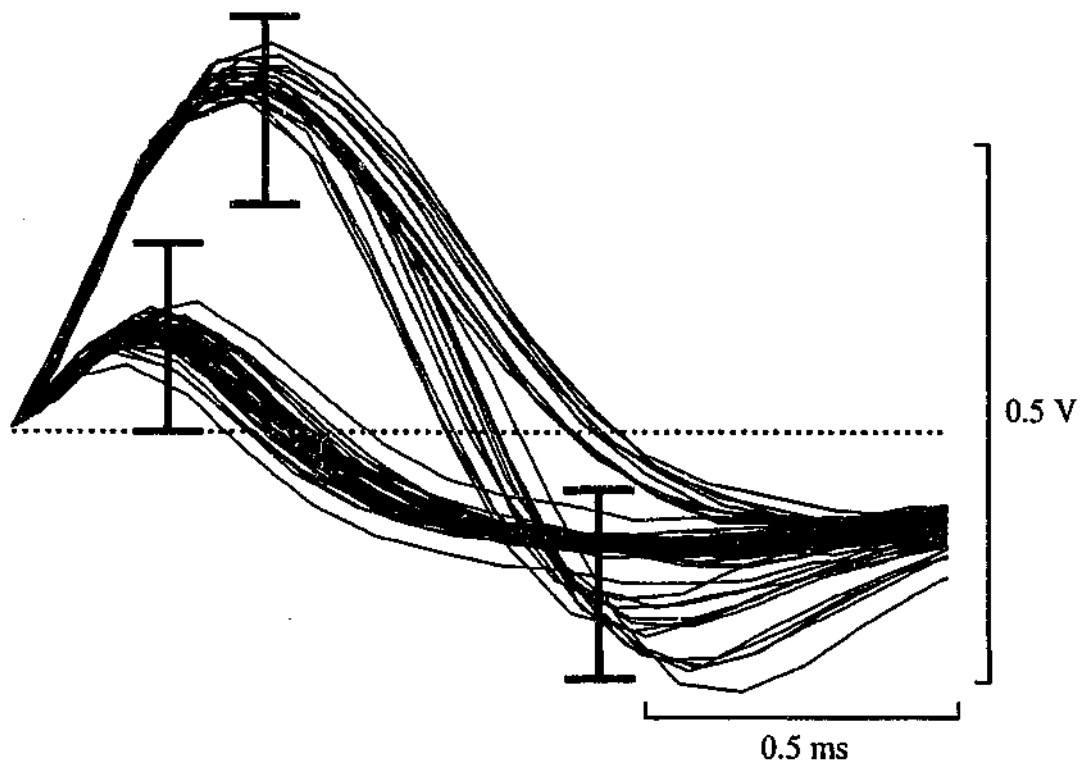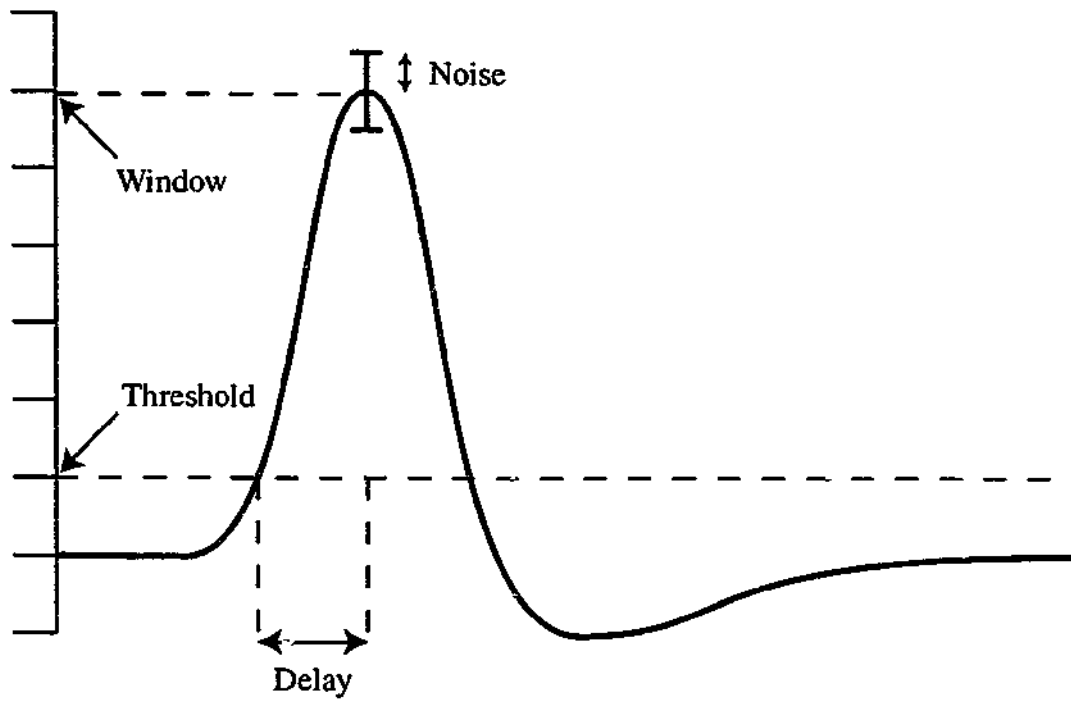
Figure 3.5   Threshold, window, delay and noise values define each voltage 'window' (top panel). It is only possible to extract the smaller impulses (green) with a voltage 'window' (draw in light green in the bottom panel). Using the two voltage 'windows' drawn in pink and brown it is possible to separate the red impulses from the blue and green impulses. Multiple voltage 'windows' are required to extract all three impulses simultaneously. The data shown in the bottom panel is the same data as the bottom panel of Figure 3.4.

dimensions used can be adjusted to account for different amounts of variation between the groups. PCA is effectively a method of mapping a high number of dimensions into fewer dimensions. The calculations involved in PCA are complex and could not be simply implemented using hardware techniques. Therefore, it is only possible to implement PCA using software based impulse discrimination.

Multi-channel Recorder

The simple voltage threshold and voltage 'window' impulse discrimination techniques can both be easily implemented in hardware because neither technique requires much information about the impulse shape to be stored. Hardware impulse discrimination has the advantage that it can be done in 'real time', and therefore if simple voltage threshold or single voltage 'window' impulse discrimination were sufficient, hardware impulse discrimination would be best. Other impulse discrimination techniques require more information about the impulse shape to be stored. Therefore, these techniques are typically implemented in software because they are too difficult to implement in hardware. The other advantage of using software to perform the impulse discrimination is that different forms of discrimination can be used in different circumstances. The multi-channel recorder system uses software impulse discrimination, as the advantages in reducing the number of nerve filament divisions and the flexibility of the software implementation was considered to outweigh the disadvantage of not being able to perform the discrimination in 'real time'.

Although PCA is a very powerful technique for discrimination between different impulse shapes, it is computationally very expensive and therefore is often found to be unwarranted. Consequently, the multi-channel recorder uses multiple voltage 'windows' to perform impulse discrimination. Even though in some circumstances, such as the one illustrated in Figure 3.6 (top panel), a simple threshold would be enough to discriminate the impulses from the background noise a minimum of a single voltage 'window' must be used for each afferent channel.

Threshold, window, delay and noise values define each voltage 'window' (Figure 3.5, top panel). To adjust the parameters of the voltage 'window' it is possible to 'draw the window on' by simply clicking in the 'Windowed' panel (Figure 3.6, top panel), and
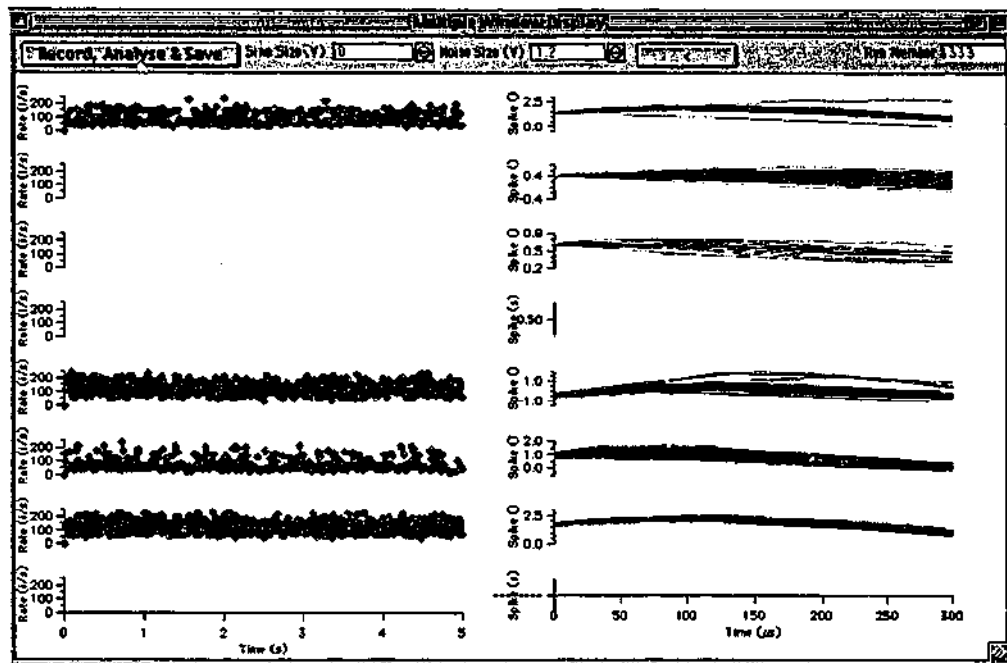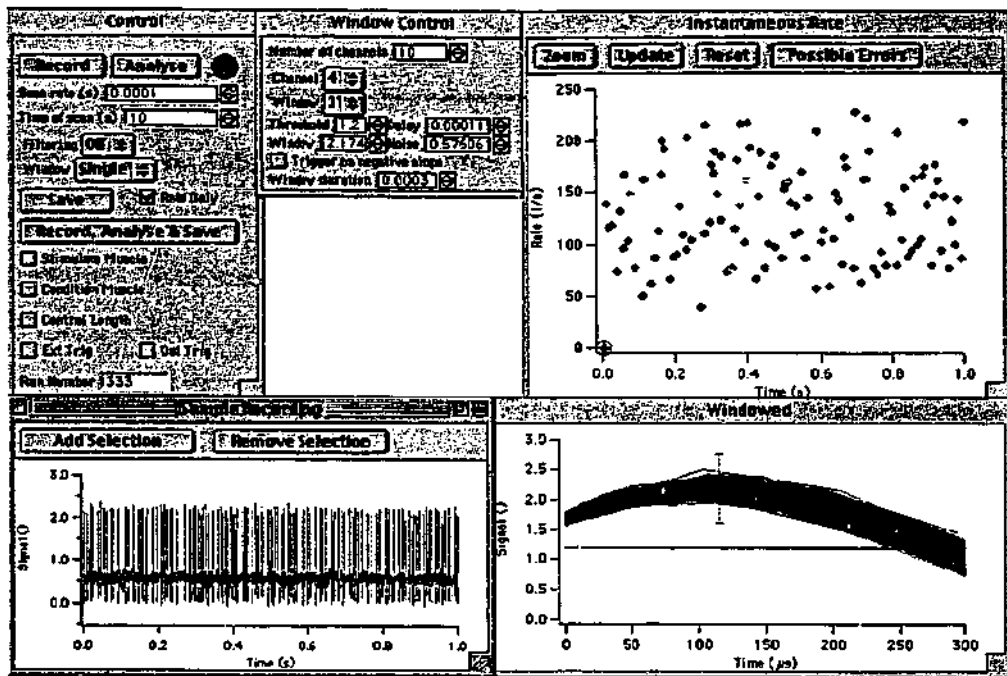
Figure 3.6 The basic recorder has two main interfaces. The channel set-up interface (top panel) is used to set the voltage 'windows' for each channel. In all examples of impulse discrimination shown, the blue impulses have been included while the green impulses did not pass through the voltage 'window'. Displays of a sample of the recorded data and the instantaneous rate display using the current voltage 'window' are provided to help in the positioning of the voltage 'window' (shown in purple). Once all the voltage 'windows' have been set the multi-channel inspection interface (bottom panel) can be used to monitor all the afferent records simultaneously, while controlling a limited number of stimulus conditions.

'dragging' over the range of the required voltage 'window'. The 'Window Control' panel can also be used to manually adjust the voltage 'window' parameters if required. For the voltage 'window' illustrated in Figure 3.7 the threshold was 1.4 V, the window was 1.65 V, the delay was 175 μs and the noise was 0.6 V.

An impulse will only be examined if it passes through the threshold level in the specified direction, either positive or negative going but not both. If the impulse then passes, after the specified delay, within the voltage 'window', defined as the window value $\pm$ the noise value, then it is included as a valid impulse, and is displayed in blue. If however, the impulse does not pass within the defined voltage 'window' it is excluded, and displayed in green. It is possible to use multiple voltage 'windows' on a single record of afferent data to aid in impulse discrimination, as illustrated in Figure 3.5 (bottom panel). If multiple voltage 'windows' are to be used to extract a single impulse (e.g. the red impulse in the bottom panel of Figure 3.5) then each voltage 'window' must have the same threshold value, so the specified delays are all relative to each other. If the multiple voltage 'windows' are to be used to extract different impulses (e.g. a voltage 'window' for the green impulse and another for the blue and red impulses in the bottom panel of Figure 3.5), then each voltage 'window' may have a different threshold value.

Sampling Rate

The type of impulse discrimination used affects the rate at which the voltage data must be sampled (Figure 3.8). Simple threshold discrimination requires the lowest sample rate, as a single sample per impulse is all that is required. Using a single voltage 'window' requires a higher sampling rate, as more information about the impulse shape is required. More complex impulse discrimination techniques require higher sampling rates, with PCA requiring the highest sampling rate possible.

A typical action potential recorded from dorsal root filaments of the cat has a duration of approximately 500 μs. The minimum required sampling rate is therefore approximately 2,000 samples per second for simple threshold impulse discrimination, to ensure at least one sample during the action potential. The multi-channel recorder uses a PCI-MIO-16E-4 data acquisition board (National Instruments Corporation, Austin,
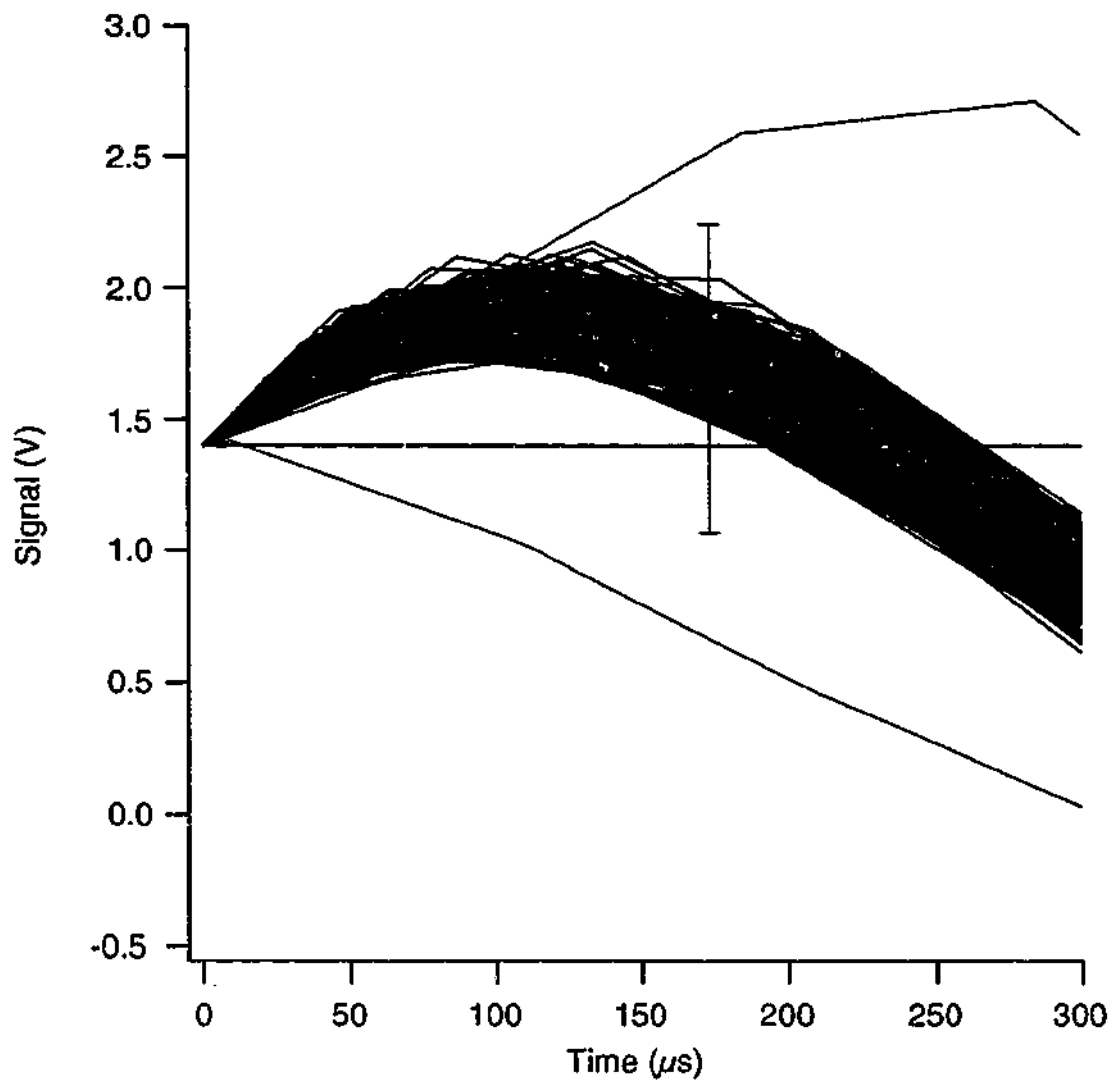
Figure 3.7   A voltage 'window' used for impulse discrimination is specified by a threshold value (horizontal black line) and window, delay and noise values that are used to construct the allowed voltage 'window' (purple bar). Impulses that cross the threshold and then pass within the specified voltage 'window' are recorded, and displayed in blue, while impulses that do not are excluded, and displayed in green.
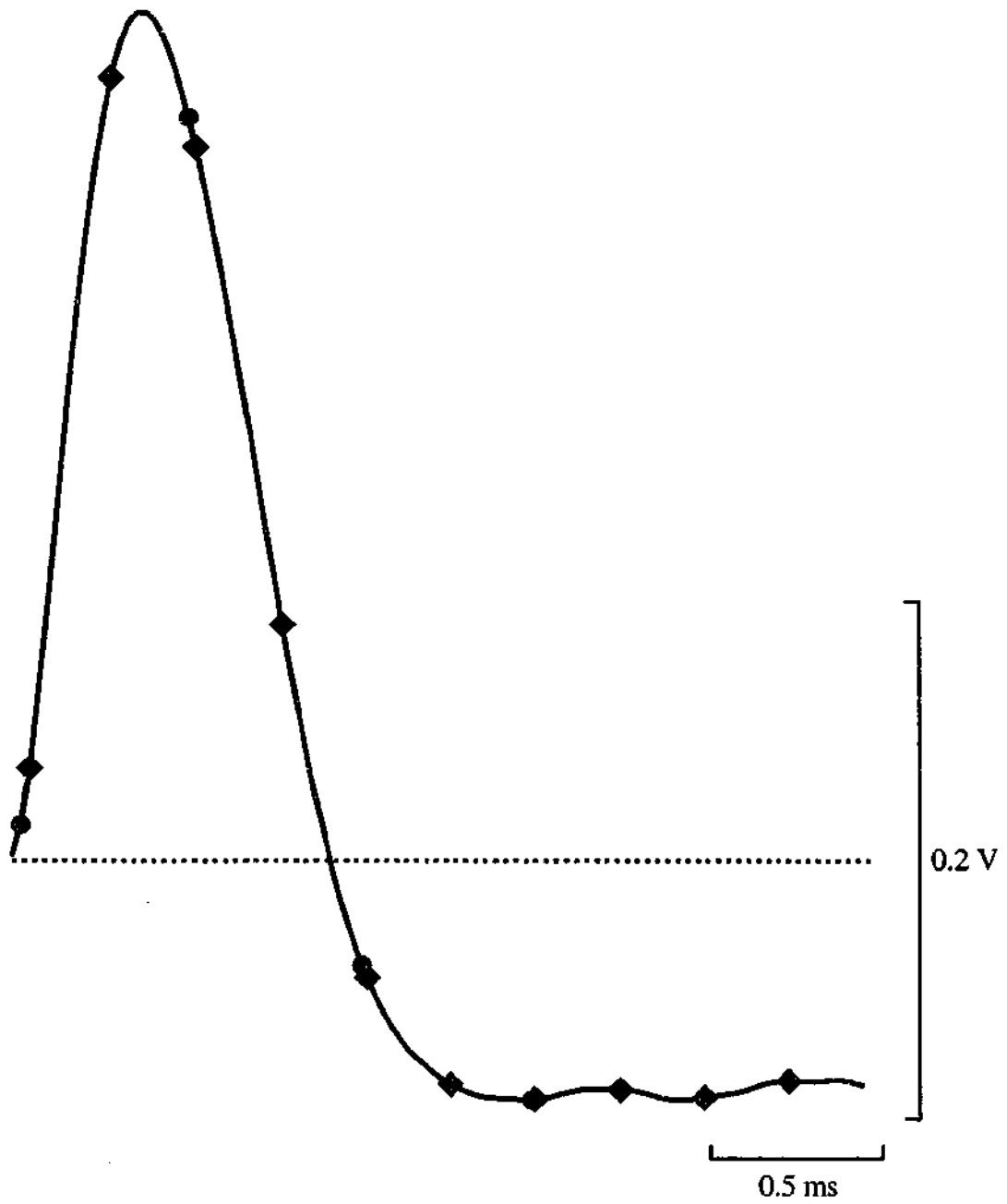
Figure 3.8 The sampling rate required is dependent on the impulse discrimination technique to be used. The simple threshold technique requires only a single sample per impulse (●) while multiple voltage 'windows' require a higher sampling rate (◆) to provide more information about the impulse shape. The data shown is the blue impulse from the data in Figure 3.4 (bottom panel). The dashed grey line indicates a possible threshold level that could be used.

Texas, U.S.A.) in a G3 desktop computer (Macintosh, Cupertino, California, U.S.A.) with a maximum sampling rate of 250,000 samples per second. The sample rate is shared across 16 channels, which results in a maximum sampling rate across all channels of 15,000 samples per second. The standard sample rate used is 10,000 samples per second, which is sufficient to allow multiple voltage 'window' discrimination techniques to be used.

Rate Conversion

The train of action potentials in an afferent fibre is converted into a series of event timings by impulse discrimination techniques, using either hardware or software techniques. The timing information can then be transformed into an instantaneous frequency before being displayed or further analysed. The instantaneous frequency is defined as the reciprocal of the time between the current impulse and the previous impulse (Equation 3.1).

$$Rate[p] = \frac{1}{Time[p] - Time[p-1]}$$ **Equation 3.1**

Hardware rate meters produce a voltage that is proportional to the instantaneous frequency, which can then be subsequently display or recorded for further analysis. Hardware determination of the instantaneous rate utilising hardware impulse discrimination is essentially error free, with the accuracy only limited by the precision of the hardware.

Determination of the instantaneous rate from sampled signals introduces two sources of error. Quantisation of the sampled rate signal from hardware rate meters introduces one error, as the analogue rate signal is quantised into discrete levels. However, the error introduced by sampling an otherwise hardware based rate determination is low. Larger errors are introduced when the rate conversion is performed in software rather than hardware.

If the impulse discrimination is done in hardware and the resulting timing pulses then sampled, large errors in the determination of the precise time of occurrence of the action potential can be introduced (Figure 3.9). The maximum error is equal to the reciprocal
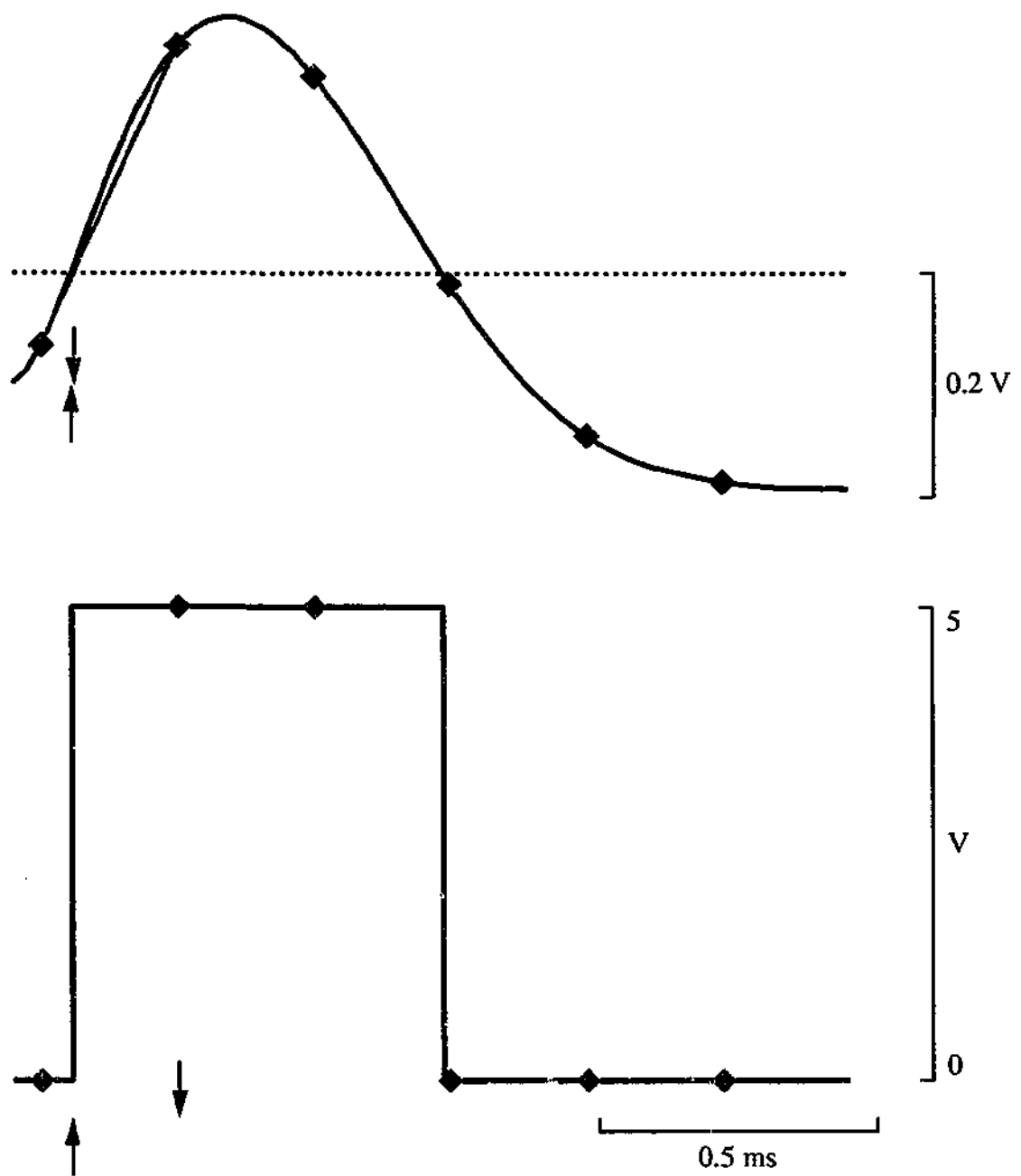
Figure 3.9 The timing of an impulse can be more accurately determined using software impulse discrimination (blue trace, top panel) than using hardware impulse discrimination and then digital sampling (black trace, bottom panel). The software impulse discrimination has a smaller error, indicated by the gap between the two arrows, because it is possible to interpolate between sampled data values to estimate the precise timing of the threshold crossing (green line). It is not possible to interpolate if the impulse has already been converted to a standard timing pulse with hardware impulse discriminators.

of the sampling rate. The errors introduced into the precise timing of the impulses will then result in errors in the instantaneous rate calculation. The errors will be most pronounced at high rates of firing, where the sampling interval will result in discrete high frequency quantisation levels.

Both impulse discrimination and calculation of the instantaneous rate in software will produce a more accurate result, for a given sampling rate, than will hardware impulse discrimination with software calculation of the instantaneous rate (Figure 3.9). By performing the impulse discrimination in software, it is possible to interpolate between sampled data values, to estimate the true impulse timing, thereby reducing the error in the timing. It is not possible to perform this interpolation if the impulse discrimination is done with hardware and then sampled. The interpolation can be simple linear interpolation, whereby the precise time the recorded action potential crosses the threshold voltage can be estimated by simply linearly interpolating between the two surrounding data values. The green line shows this in the top panel of Figure 3.9.

User Interface

The multi-channel recorder software can be divided into two functional sections, the basic recorder and a series of additional components. The basic recorder was developed within IGOR Pro (WaveMetrics, Lake Oswego, Oregon, U.S.A.) and is capable of recording muscle length, tension and eight channels of afferent data. The code for the recorder program consists of a series of procedure files that are used within IGOR Pro and compiled 'C' code in the form of XOPs that are used by IGOR Pro. All the code that constitutes the software of the multi-channel recorder is included as part of Appendix A. The basic recorder saves the afferent data to disk either as raw data, which allows impulse discrimination to be done off line, or as a series of impulse timings, after the impulse discrimination has been performed. The basic recorder is also capable of controlling muscle length, using simple length changes, and stimulation of the muscle, with simple stimulation patterns.

The two main recorder interfaces are illustrated in Figure 3.6. The top panel of Figure 3.6 illustrates the channel set-up interface, while the bottom panel illustrates the multi-

78

channel inspection interface. The set-up interface is used to set the properties of the voltage 'windows' that are to be used for the impulse discrimination, via the 'Windowed' and 'Window Control' panels. The 'Window Control' panel can also be used to alter the number of voltage 'windows' to be used on each channel of afferent data. A sample afferent record ('Sample Recording') and instantaneous rate plot ('Instantaneous Rate') are available and can be used to ensure that the impulse discrimination has been correctly set. Any false discriminations are often visible in the instantaneous rate plot as an extremely high rate, which results from an unusually short inter-impulse interval. Basic recording properties can also be altered using this interface via the 'Control' panel, including the duration of the recording period, the sampling rate and the number of channels of afferent data to record. Other properties of the recorder such as digital filtering and length or stimulation control can also be initiated from this interface.

The multi-channel inspection interface, 'Multiple Window Display', provides an overview of all the afferent data for the current record (Figure 3.6, bottom panel). The instantaneous firing rate of the afferents is presented on the left-hand side, while the impulse discrimination for each afferent is shown on the right. A limited number of control parameters (e.g. amplitude of the sinusoidal length change) are also included with this interface. The 'Multiple Window Display' was designed for use when recording from multiple afferents over a number of repetitions of similar conditions.

Other Signals

Recorded Signals

The response of afferent fibres is typically not the only signal of interest during experiments. Often the muscle's length and tension are simultaneously recorded to allow comparisons with the afferent response.

Length

The muscle's length can be controlled by an electro-magnetic position controller with feedback (Department of Physiology Electronics and Mechanical Workshops, Monash

University). The electro-magnetic controller also provides an output length signal. The response time of the position controller is of the order of a few milliseconds and it is capable of producing movements down to a few micrometers. The length signal is scaled to 200 mV/mm with a working range of 20 mm. The resulting length signal is of a similar magnitude to the amplified afferent signals and therefore can be directly recorded using the data acquisition card.

Tension

The force produced by the muscle can be monitored using a load-cell force transducer (Entran Devices, Fairfield, New Jersey, U.S.A.) which provides a signal of 1.95 mV/N. The response time of the force transducer is of the order of a few milliseconds and it is capable of measuring a maximum force of 100 N. For the typical forces produced by a fused contraction of the soleus muscle (approximately 20 N), the force signal is of a similar amplitude to the amplified afferent signals and therefore can be directly recorded using the data acquisition card.

Controlled Signals

It is often necessary to synchronise the actions of other equipment with specific phases of an afferent record. The PCI-MIO-16E-4 has a number of digital output lines and two analogue output channels that can be used for timing signals.

Length Control

The length of the muscle can be controlled by the electro-magnetic position controller, which in turn can be controlled be the multi-channel recorder. One of the analogue output channels can be used to produce an arbitrary waveform to be used as the length control signal. This allows for the generation of any length signal required with relative ease. While the multi-channel recorder is capable of producing any arbitrary voltage waveform that can be used as an input signal for the electro-magnetic length controller, only a few of the more common length stimuli have been included in the basic recorder software. The recorder is capable of producing any combination of a ramp-and-hold movement, a sinusoidal movement and a random movement (Figure 3.10, top panel). A
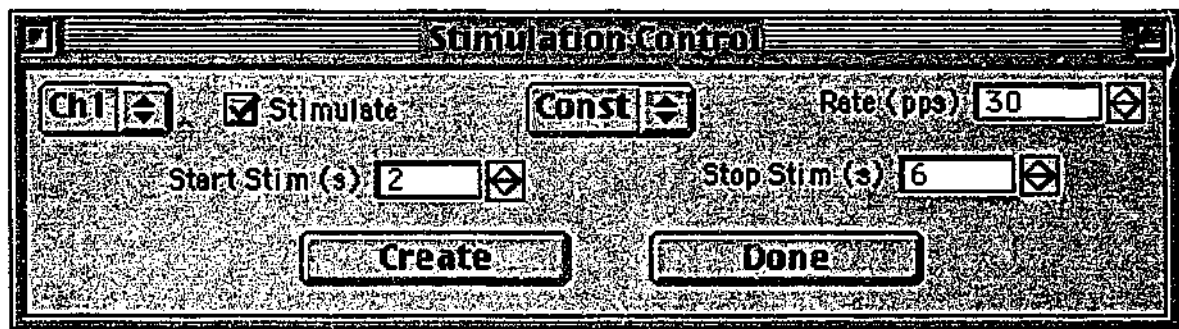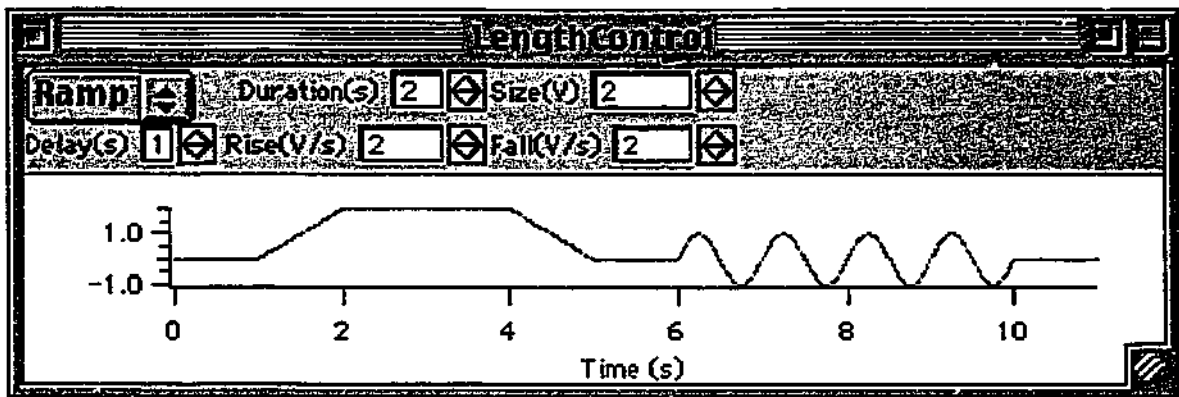
Figure 3.10 The basic recorder is capable of controlling muscle length, via the electro-magnetic position controller and the 'Length Control' panel, although only a few simple length changes, such as ramp-and-holds and sinusoids are available (top panel). Simple stimulation patterns are also available via the 'Stimulation Control' panel (bottom panel). Both the 'Length Control' and 'Stimulation Control' panels are activated from the main 'Control' panel illustrated in Figure 3.6.

record of the various attributes of the length-controlling signal is automatically stored to allow rapid reconstruction of an experiment.

Stimulation

The other analogue output channel can be used to deliver trigger pulses to a muscle stimulator. The stimulator is used to produce brief pulses (0.1 ms) that are too computationally heavy to be produced by the PCI-MIO-16E-4. To be able to produce short pulses the update rate of the analogue output must be less than the pulse width. For a 0.1 ms pulse the update rate must be greater than 10,000 samples each second. Both analogue output channels must be updated at the same rate, which results in an effective update rate of greater than 20,000 samples each second. Although it is possible to output signals at this rate using the PCI-MIO-16E-4, it is not a practical option because of the demands it places on the computer processor.

The multi-channel recorder is capable of providing stimulus pulses to trigger a commercially available stimulus pulse shaper, amplifier and isolator. It is possible to produce any arbitrary stimulus pattern that is required by constructing the appropriate output trigger wave. However, only a few of the more common stimulus patterns have been included in the basic recorder software. The recorder is capable of producing a single stimulus pulse, a short fixed frequency stimulus burst, ramping stimulus frequency bursts and a period of random (Poisson distributed) stimulation (Figure 3.10, bottom panel). Records of the various attributes of the stimulator-controlling signal are automatically stored to allow rapid reconstruction of an experiment.

Data Manipulation

Filtering

Although some filtering of the afferent signal is performed in the hardware of the multi-channel recorder, additional digital filtering may be required. The basic recorder has a digital filter that can be controlled with the 'Filter Control' panel (Figure 3.11, top panel). The high-pass and low-pass filters are infinite impulse response filter approximations to Butterworth filters made by using the bilinear transform. The
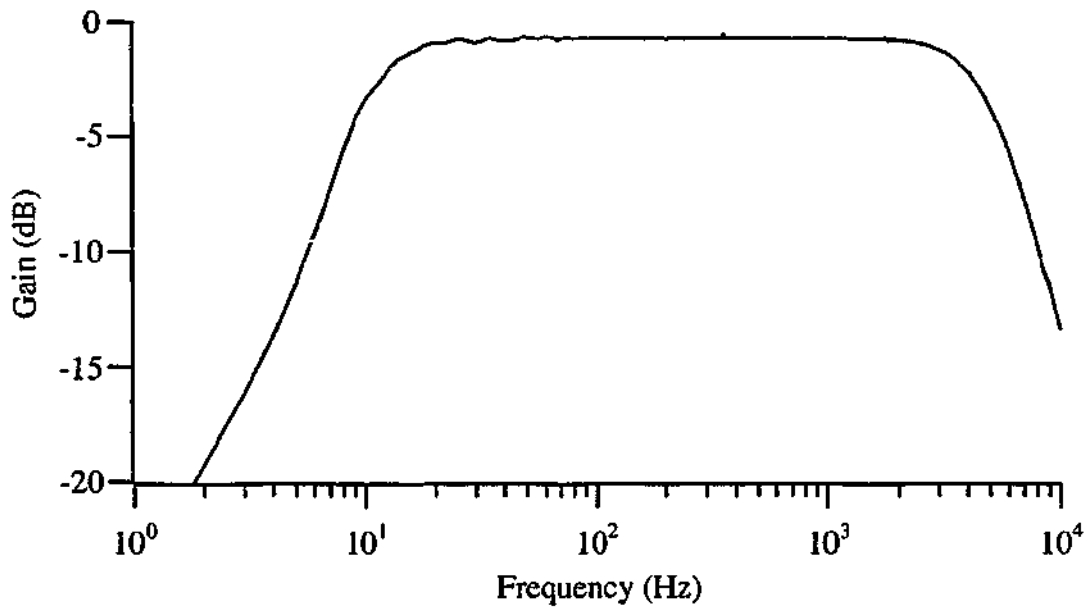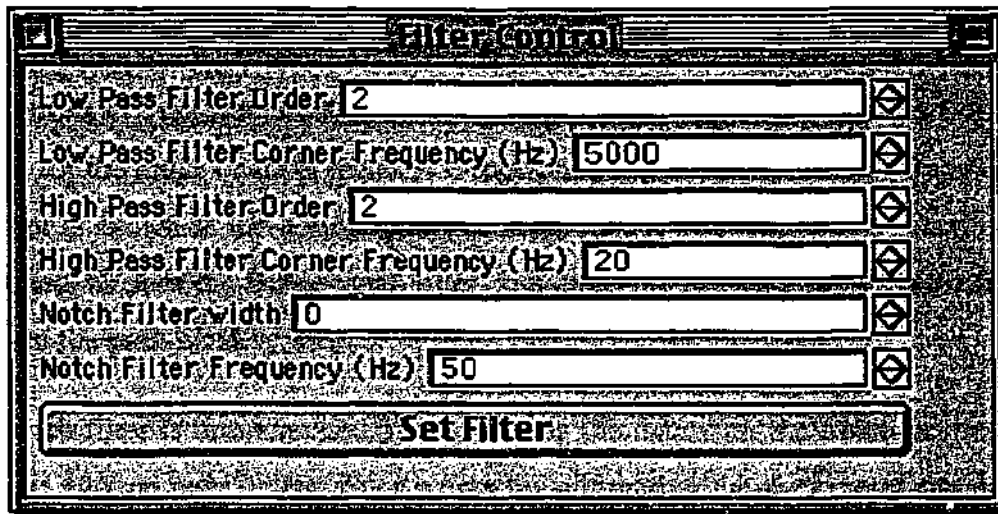
Figure 3.11 The 'Filter Control' panel (top panel) can be used to control the digital filter. The digital filter comprises low-pass, high-pass and notch filters that can all be independently adjusted. The bottom panel shows the filter response for the setting shown in the top panel.

calculations of the filter coefficients and the actual filtering are done as part of the XOP written for the multi-channel recorder (Appendix A). An example of the transfer ratio of the filter is shown in the bottom panel of Figure 3.11. The filter has a 'maximally flat' pass-band, as does the Butterworth filter, and therefore causes minimal distortion to the signal in the pass-band.

The notch filter is implemented by convolving the data with the function illustrated in Figure 3.12 (top panel). The filter works by subtracting the average of the data at the equivalent points in the cycle before and after each data value. The number of points and the number of cycles averaged are controlled by the width of the notch filter. Figure 3.12 (top panel) illustrates a 50 Hz notch filter with a width of 2. For this configuration each filtered value is calculated using Equation 3.2, where T is 1/ 'Notch filter Frequency' and Δt is 1/ 'Sample Rate'.

$$\text{Filtered}[p] = \text{Data}[p] - \frac{\text{Data}\left[p \pm \frac{T \pm \frac{1}{2}}{\Delta t}\right] + \text{Data}\left[p \pm \frac{2T \pm \frac{1}{2}}{\Delta t}\right]}{8} \qquad \textbf{Equation 3.2}$$

Although the filter is very effective at removing the specified frequency (Figure 3.12, middle panel), the method of averaging across cycles does introduce errors. The output of the filter is poorly defined at the ends of the data record, as multiple cycles of data are required. Therefore, the filter does not operate as well over the first few, and last few cycles. The notch filter also removes harmonics of the notch frequency, which can affect the shape of recorded impulses (Figure 3.12, bottom panel).

Data storage

The PCI-MIO-16E-4 must sample all channels at the same sampling rate. High sampling rates, in the order of 10,000 samples a second, are required to record the action potentials in afferent fibres, resulting in large quantities of data being recorded. To reduce the amount of data that is to be stored the length and tension data can be compressed before being saved. The simplest form of compression is to reduce the amount of data by effectively reducing the sampling rate. This is achieved by performing a box average of the data with the width of the box determined by the
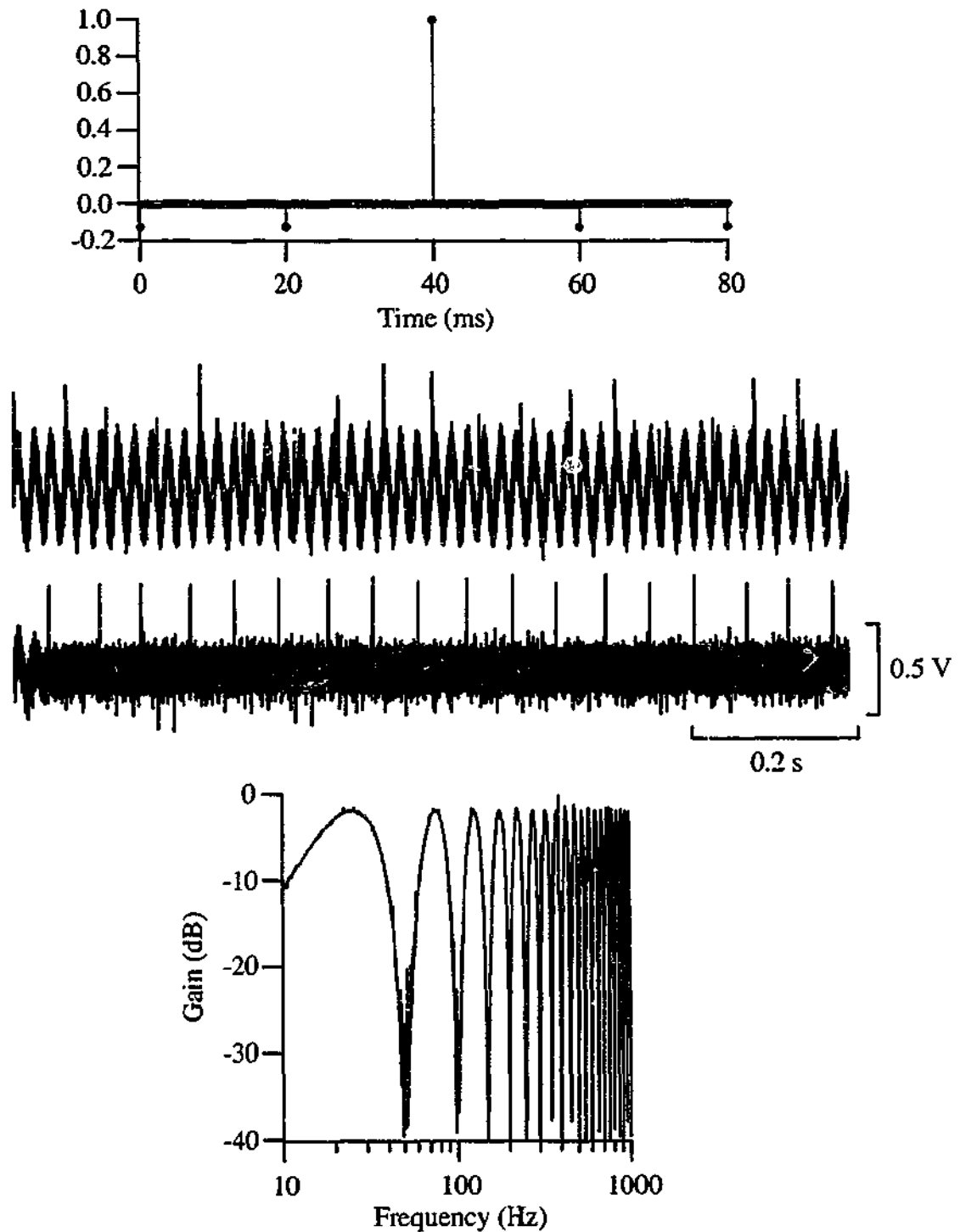
Figure 3.12 The digital notch filter was implemented by convolving the function shown in the top panel with the data. The function can be scaled to filter out different frequencies and widened to increase the width of the notch. An example of the filter is illustrated in the middle panel where it has been used to remove much of the 50 Hz mains interference from the raw signal (top trace), revealing the afferent impulses (bottom trace). The bottom panel is the filter's response using the function illustrated in the top panel, a 50 Hz notch filter with a width of 2.

appropriate sample period. Once reduced, the length and tension for each record is saved to disk with the corresponding record number.

Saving only the relevant information, which in most cases is the timing of the action potentials, can significantly reduce the amount of afferent data to be stored. The afferent timing data is retained within the main experimental file stored in a hierarchical structure within the file. If information about the shape of the action potentials is required, then the full afferent data can be saved to disk with a similar structure to that used for the length and tension records.

It is possible to save a comment with each record. The comments are saved with the individual records and also to a text file, where they are saved with time information.

Data Recall

It is often desirable during an experiment to compare the response of an afferent under several different experimental conditions. The simple hierarchical structure that has been used to store the afferent data allows for fast recall of previous records. The afferent responses from different records can be overlaid to allow visual comparisons of responses (Figure 3.13). For more detailed comparisons of the responses it may be necessary to perform some basic analysis, which is discussed in more detail in the Analysis Modules section (p. 86).

Specialised Additional Modules

A variety of specialised tasks are often performed in many experiments, and therefore a number of specialised additional software modules have been written for the multi-channel recorder to facilitate these tasks. All of the modules were written as procedure files that could be dynamically included into the main experimental file and are included in Appendix A.

Length-Tension Curves

A standard measurement performed in almost all studies involving muscles is to measure a length-tension curve. The method with which the length-tension curve is

Figure 3.13 The basic recorder is capable of overlaying different records using the 'Multiple Window Data Recall' display (top panel). The current record is displayed in red, while the previous records are displayed in pink.

recorded can alter the shape of the curve because of the thixotropic nature of muscle. Therefore, it is desirable to use a consistent, repeatable method to measure the length-tension curve.

An additional 'Length Tension' software module was written for the multi-channel recorder (Figure 3.14, top panel). The software module was designed to measure a length-tension curve over a specified muscle range. The length-tension curve is constructed dynamically starting from the shortest muscle length to be measured. After each point is recorded it is possible to move to the next length, repeat the measurement, or end the procedure. This extra user control is required to ensure that measurements are not taken at long muscle lengths that may cause damage. It is also possible to take a single additional measurement, which is taken after a brief conditioning contraction at the shortest muscle length previously tested.

Afferent Identification

When recording from afferent fibres in dorsal root filaments it may be desirable to identify the type of receptor afferent being recorded. Lloyd (1943) classified afferent fibres into four groups based on their condition velocities. Non-myelinated fibres with conduction velocities in the range of 0.5 – 2 m/s were classified as Group IV, also known as 'C fibres'. The smaller diameter myelinated fibres constitute Group II and Group III, and have conduction velocities in the ranges of 30 – 72 m/s and 6 – 30 m/s respectively. The afferent fibres from muscle spindle secondary endings are Group II fibres and respond to a whole muscle twitch with an 'in parallel' response (Fulton & Pi-Suñer, 1928). Large diameter myelinated fibres with conduction velocities in the range of 72 – 120 m/s constitute Group I. The Group I fibres associated with muscle afferents can be further subdivided into two groups based on their response to a whole muscle twitch. Afferent fibres from muscle spindle primary endings typically have a maintained discharge at all muscle lengths and respond to a twitch with an 'in parallel' response, which is a reduction in discharge, or silencing, during the rising phase of the twitch tension (Figure 3.14, middle-right panel). The 'in parallel' response of Group Ia afferents is contrasted by the 'in series' response of Group Ib afferents. Group Ib
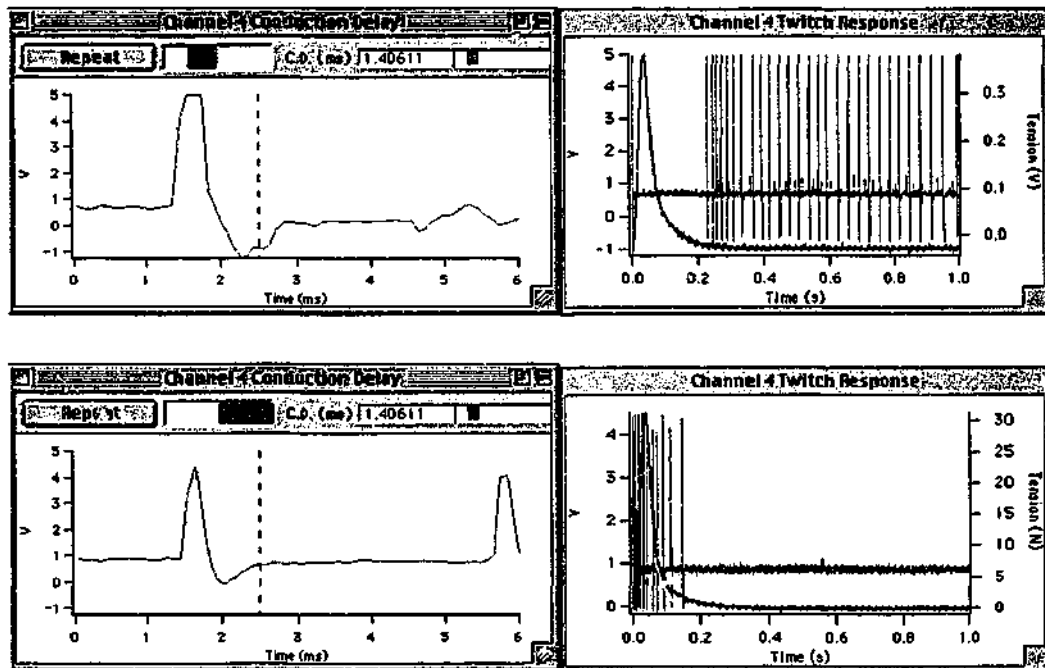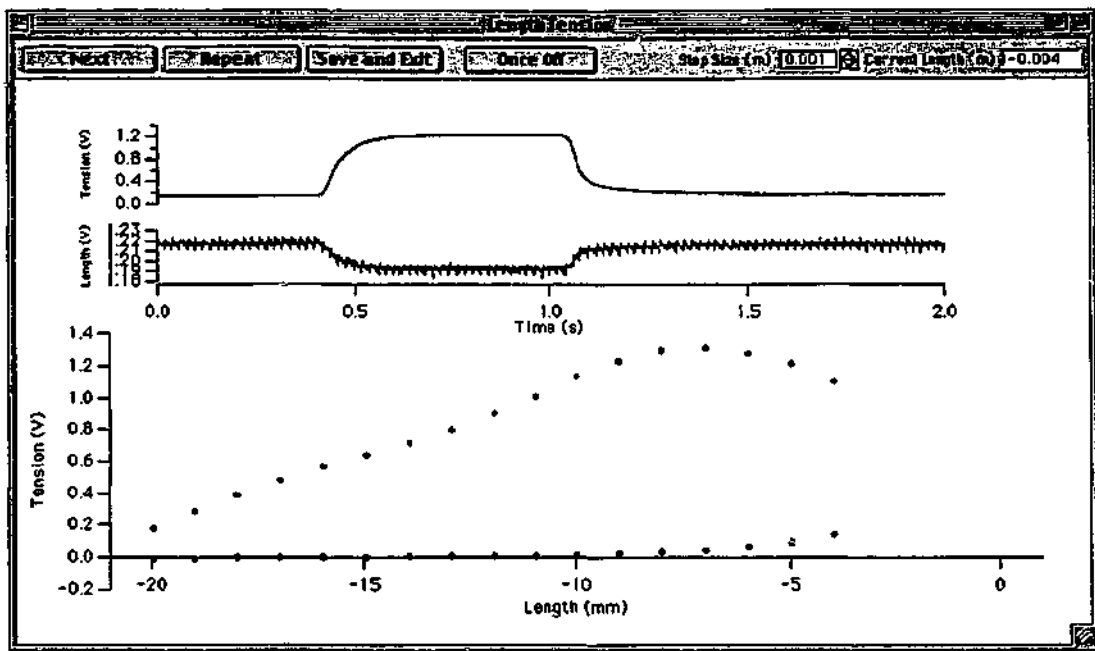
Figure 3.14 The interface for the 'Length Tension' module is shown in the top panel. The module allows rapid recording of a length-tension curve in a highly reproducible manner, with options to repeat measurements or to record 'once off' measurements at a specified length. The 'Afferent Identification' module (lower panels) can be used to differentiate between different types of afferent fibres, based on their conduction delay (left panels) and response to whole muscle twitch (right panels). The bottom row of panels is characteristic of an afferent innervating a Golgi tendon organ, Ib, while the middle row of panels is characteristic of an afferent innervating a muscle spindle primary ending, Ia.

afferents innervate Golgi tendon organs, which respond to the rising phase of the twitch tension with an increase in discharge (Figure 3.14, bottom-right panel).

An additional 'Afferent Identification' software module was written for the multi-channel recorder to aid in the identification of muscle afferents. The software module was designed to record the conduction delay and whole muscle twitch response of an afferent fibre, with one click of the mouse. The software module outputs a trigger pulse, used to trigger the muscle stimulator, and then records the afferent activity on the channel currently selected in the 'Window Control' panel (Figure 3.6, top panel). Two additional displays are created by the software module (Figure 3.14, lower panels) that display the electrically evoked response and the response to a whole muscle twitch. The electrically evoked response can be used to calculate the conduction delay, which is displayed at the top of the 'Conduction Delay' panel. For experiments using either the soleus or medial gastrocnemius muscle of the cat, Group I fibres have a delay of less than 2.5 ms, indicated by the dashed blue line. The electrically evoked response can also be used to determine if the nerve filament contains a functionally single afferent fibre. The twitch tension and afferent response are shown in the 'Twitch Response' panel and can be used to determine the 'in series' or 'in parallel' nature of the response. An estimate of the difference in the average discharge rate during the twitch and after the twitch is also displayed in the 'Conduction Delay' panel. A red bar indicates that the rate during the twitch is higher, while a blue bar indicates the rate after the twitch is higher. The length of the bar from the centre of the display area indicates the magnitude of the difference. Therefore, it is possible to identify quickly and easily the type of afferent, or afferents, present.

γ Identification

The response of a muscle spindle primary ending to the stimulation of a γ fibre can be used to classify the γ fibre as either a static γ fibre, γ_s, or a dynamic γ fibre, γ_D (Matthews, 1962; Emonet-Denand, Laporte, Matthews & Petit, 1977). The response of a muscle spindle primary afferent to stimulation of a γ_D fibre is an enhancement of the dynamic response to an imposed length change (Figure 3.15, top panel). The dynamic response can be quantified by calculating the dynamic index of the muscle spindle

85
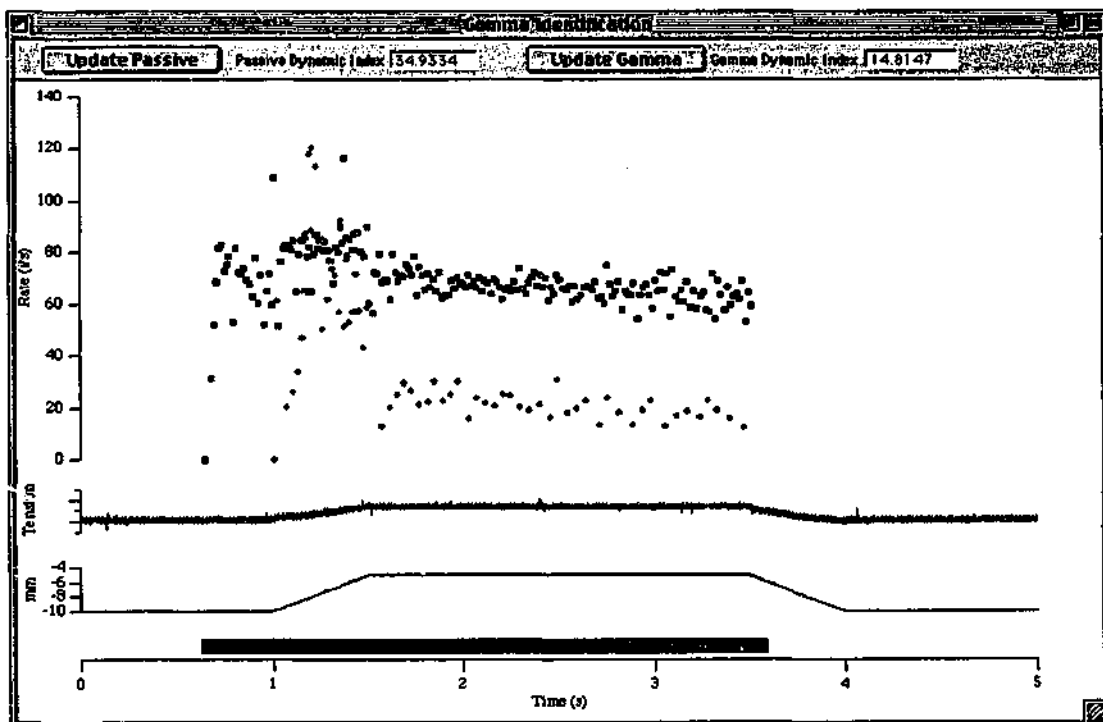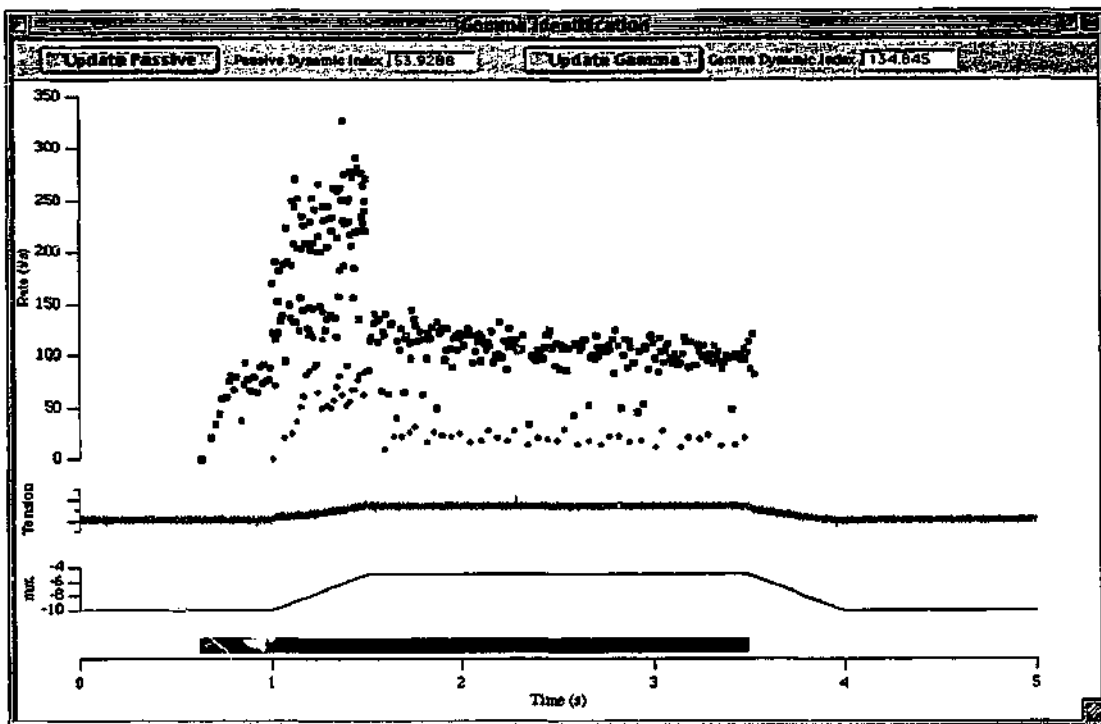
Figure 3.15 The interface for the 'γ Identification' software module consists of a single panel in which the responses of a muscle spindle primary ending to passive stretch (●) and a stretch during efferent stimulation (■) are superimposed to aid comparison. Stimulation of a γ_D efferent results in an enhanced dynamic response (top panel), while stimulation of a γ_S efferent increases the discharge during stimulation, without enhancing the dynamic response.

primary ending in response to a ramp-and-hold stretch (Crowe & Matthews, 1964). The dynamic index is calculated as the change in discharge rate during the first half-second of the hold phase (Equation 3.3). The response to stimulation of a γ_s fibre is an increase in afferent discharge rate during stimulation, without enhancement of the dynamic response (Figure 3.15, bottom panel).

Dynamic Index = Rate at end of ramp – Rate $\frac{1}{2}$ second later   **Equation 3.3**

An additional 'Gamma Identification' software module was written for the multi-channel recorder to aid in the identification of γ fibres. The software module was designed to record the response of a previously identified muscle spindle primary afferent to a ramp-and-hold stretch in a passive muscle. The stretch is then repeated during the stimulation of an efferent fibre and the resulting afferent response compared. The 'Gamma Identification' panel displays a passive control response, which can be used for visual comparisons with the test γ response. The dynamic index of the control and test γ responses are also displayed at the top of the panel to aid in γ identification.

Analysis Modules

The variety of different types of analysis that can be performed makes it impractical to write specified code modules capable of performing all types of analysis. The standard formatting of the saved data from the basic recorder allows for automation of many types of analysis, to be performed after experiments are complete. However, sometimes it is necessary to perform at least some amount of analysis during an experiment, and it is therefore possible to write software modules to perform the analysis on-line.

An example of an experiment that requires some level of on-line analysis is a stochastic resonance experiment. It is necessary to construct a noise-alone response curve to determine the appropriate sinusoidal frequencies to test. It is then necessary to measure stimulus-response curves for each of the test frequencies, before stochastic resonance measurements can be taken. The range of noise amplitudes used for stochastic resonance measurements can also be selected to cover the most appropriate range by performing preliminary analysis on-line.

Summary

The multi-channel recorder is capable of recording eight channels of afferent activity, along with several other channels (up to eight) of relevant information (e.g. muscle length and tension). Multiple voltage 'windows' can be used on each channel of afferent data to extract multiple functionally single afferents. Theoretically, the resolution of the sampling, and the number of 'windows' available are the only limits to the number of afferents that can be isolated from a single channel of afferent data. In practice, it has been found that with the current sampling rate (10,000 samples per second) and voltage resolution (2.5 mV) it is practical to isolate up to three afferents from each channel of afferent data. Thus, the total number of functionally single afferents that can be recorded with the current equipment is about twenty.

The basic recorder is capable of recording the afferent data, along with other associated information and storing the data on disk. The basic recorder can also output signals that can be used to control stimulators and the muscle length. A comment can be included with each record, and a complete list of comments is available, which in addition to the stored information from the length and stimulation control waves, can be used to quickly reconstruct an experiment.

The additional code modules that have been written for the recorder allow various common experimental tasks, such as recording length-tension curves and identifying afferents and γ efferents, to be performed simply and reliably. The ability to integrate new code modules for experimental recording or analysis also allows the multi-channel recorder to be extended to meet a large variety of experimental conditions.

The multi-channel recorder has moved the software-hardware interface further towards the raw data signals, allowing for more complex forms of analysis to be performed with ease. As the technology used in the data acquisition systems develops further it is envisaged that the software-hardware boundary will move ever closer towards the raw signals, allowing for even more flexible recording systems. For example, an increase in processing power would allow computer derived stimulus pulses to be used. This in turn would allow for the more integrated control of stimulus parameters. This type of control is necessary for experiments designed to use afferent information to control the efferent stimulation in order to mimic some of the natural control of muscle contractions (e.g., closing the muscle control loop).

Chapter Four

Golgi Tendon Organs

Golgi tendon organs are stretch-sensitive mechanoreceptors that are predominantly situated at musculo-tendinous junctions 'in series' with skeletal muscle fibres (Matthews, 1933). The following description is of mammalian Golgi tendon organs as the Golgi tendon organs of the cat were utilised in the stochastic resonance experiments. The afferents from Golgi tendon organs are large myelinated afferents with conduction velocities in the range of 72-120 m/s (Lloyd, 1943) and are classed as Ib afferents (Hunt, 1954). The 'in series' location of Golgi tendon organs lead to the view that they are monitors of muscle tension, as first suggested by Fulton & Pi-Suñer (1928).

Structure

Golgi tendon organs are encapsulated receptors. The capsule is divided into several compartments by transverse septa (Bridgeman, 1968). Small bundles of collagen fibres leave the main tendon or aponeurosis and enter the tendon organ capsule. As the collagen strands penetrate deeper into the capsule they split into fine strands that are separated by transverse septa. The collagen fibres then continue out of the capsule to form tendinous attachments with muscle fibres. Each Golgi tendon organ has attachments to between about 10 and 20 muscle fibres, each typically from a different motor unit (Figure 4.1).

The afferent axon, after entering the capsule, divides into numerous small unmyelinated branches that finally terminate on the fine collagen strands. It is supposed that under tension the collagen strands, on which the nerve branches terminate, cause mechanical deformation of the nerve terminal membrane (Bridgeman, 1968). The mechanical deformation leads to the generation of the receptor potential, which in turn generates action potentials. Therefore, the effective stimulus for Golgi tendon organs is strain, resulting in deformation of the sensory ending, rather than force (Fukami & Wilkinson, 1977).

The Golgi tendon organ is commonly considered to be mechanically 'in series' with its parent muscle (Matthews, 1933). Although the receptor is 'in series' with the muscle
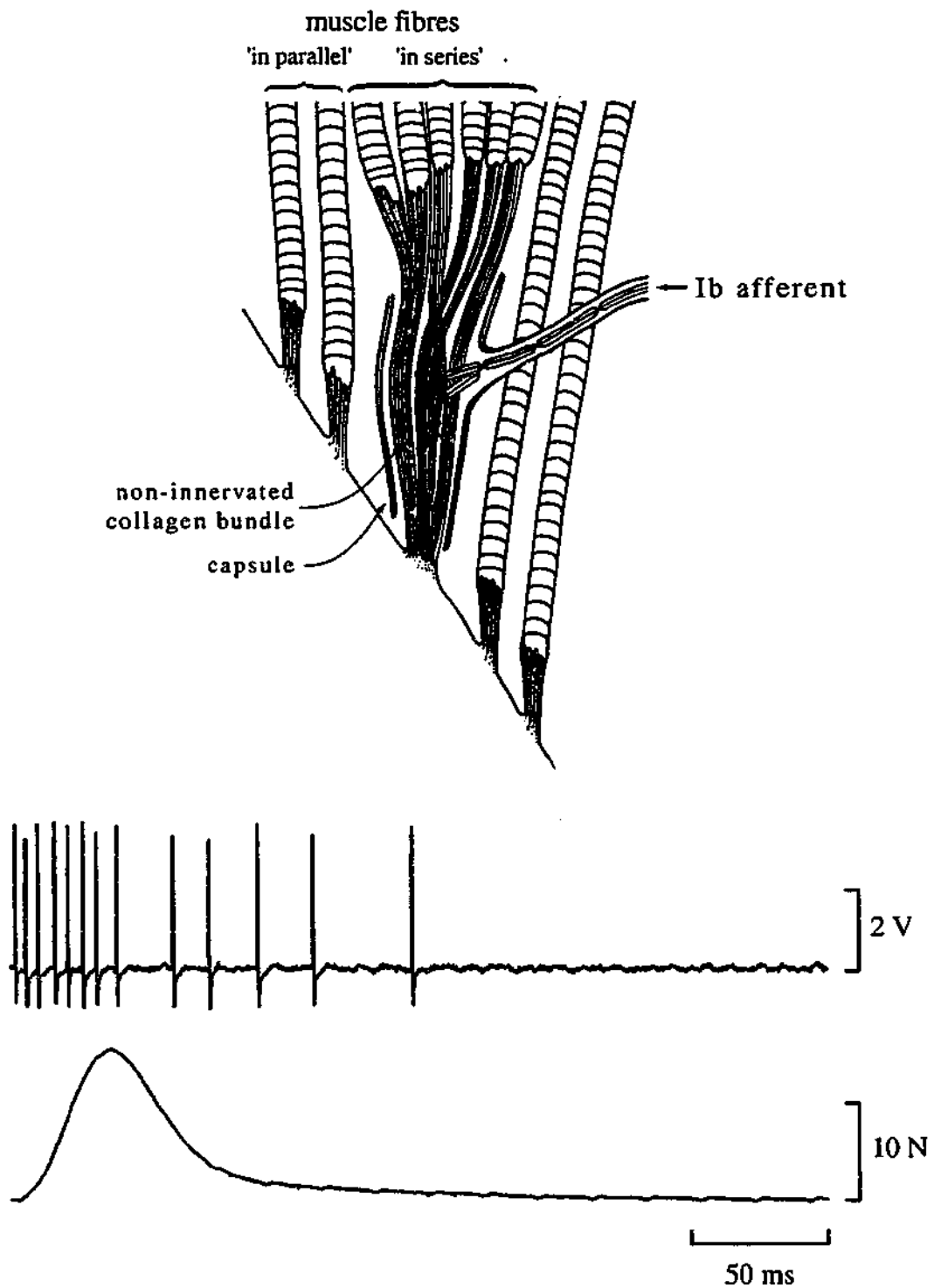
Figure 4.1 Schematic representations of a Golgi tendon organ, top panel, illustrating the 'in series' location of the receptor as well as the muscle fibres that are 'in parallel' (adapted from Figure 1 of Jami (1992)). The 'in series' nature of the Golgi tendon organ response is illustrated by the response to a whole muscle twitch, bottom panel.

fibres that attach to it, there are numerous other muscle fibres that attach directly to the tendon or to the outside of the receptor's capsule. These other fibres are 'in parallel' with the Golgi tendon organ. Therefore, the arrangement is more complex than that of a simple 'in series' receptor.

Response

Passive Muscle

Golgi tendon organs have an approximately linear response to constant passive tension above a certain threshold, with an increase in static passive tension resulting in a proportional increase in the static discharge rate (Jansen & Rudjord, 1964). To reach threshold the muscle must typically be stretched to near its maximum physiological length (L_{MAX}). Although there is some variation in the precise threshold, as a rule most Golgi tendon organs will respond to passive tension at L_{MAX}.

Some Golgi tendon organs will respond at muscle lengths significantly below L_{MAX}. The visco-elastic properties of muscle can result in a large transient tension in response to a rapid length changing. The transient tension may be large enough to elicit a response even at lengths significantly below L_{MAX}. The response to stretches below L_{MAX} is also a result of the dynamic sensitivity of the Golgi tendon organ. The receptor responds to changes in tension as well as the absolute tension (Jansen & Rudjord, 1964). The combination of the visco-elastic properties of muscle and the dynamic sensitivity of the Golgi tendon organ result in a precise, frequency dependent threshold for small sinusoidal changes in muscle length (Anderson, 1974). The threshold falls as the frequency of the sinusoidal length change is increased, since the maximum velocity of the movement is dependent on the frequency. The absolute muscle length also affects the threshold, with longer muscle lengths resulting in lower thresholds to small sinusoidal length changes.

Active Muscle

Golgi tendon organs are selectively sensitive to the tension in the few muscle fibres that directly insert into the receptor's capsule. Each muscle fibre may belong to a different

motor unit; therefore, the response to active tension is more complex than the response to passive tension. If the 'in series' muscle fibres, those that directly insert into the Golgi tendon organ, contract the receptor will be subjected to an increase in tension, since each contracting muscle fibre stretches the tendon strand to which it is attached and on which sensory endings lie. If however, 'in parallel' muscle fibres, those that surround the Golgi tendon organ, contract it is possible that, at short muscle lengths, the receptor will be unloaded. If both the 'in series' muscle fibres and the 'in parallel' muscle fibres contract then the resulting tension on the receptor will depend on the relative strength and velocity of contraction of the 'in series' and 'in parallel' muscle fibres (Gregory, Morgan & Proske, 1985).

The general impression that Golgi tendon organs are more sensitive to active tension than passive tension has been wildly accepted (see review by Jami, 1992). The sensitivity of the Golgi tendon organ, calculated as i/s/N, is a power function with a smooth transition from passive to active tension, produced by whole muscle contractions (Alnes, 1967). Under these circumstance the passive sensitivity will in fact be greater than active sensitivity. Alnes (1967) also found that the threshold for passive tension and tension produced by whole muscle twitch was similar for Golgi tendon organs located in the distal part of the muscle. Anderson (1974) used isometric contractions, passive stretches and a combination of contraction and length changes to alter whole muscle tension and also did not observe a difference in the dynamic characteristics.

The perceived increased sensitivity for active tension may be the result of the Golgi tendon organ responding to the changes in tension during an isometric twitch. The parameter measured by Jansen & Rudjord (1964) was the tension threshold of firing for both a twitch and a passive stretch. A twitch will typically result in a more rapidly changing tension than a passive stretch. The dynamic sensitivity of the Golgi tendon organ will therefore result in a lower threshold for the twitch contraction than the static passive tension. It is known that a Golgi tendon organ can respond to the activation of a single motor unit that inserts directly into the receptor (Houk & Henneman, 1967). Therefore, in the extreme case the threshold tension produced by an isometric muscle twitch may be the tension produced by a single motor unit.

Altering the rate of stimulation of the relevant muscle fibres modulates the response of a Golgi tendon organ by altering the level of active tension produced. Changing the length of relevant muscle fibres will also modulate the Golgi tendon organ's response via the active length-tension properties of the muscle fibres and the change in passive tension. It is therefore possible to stimulate a Golgi tendon organ with two different signals, stimulation rate and muscle length, which act via different mechanisms on the muscle tension.

The response of a Golgi tendon organ to a fused contraction is quite regular. The response to an unfused contraction is less regular, or more 'noisy', as the response follows the changes in tension. Therefore, it is possible to effectively modulate the amount of 'noise', or irregularity, present in the discharge by altering the stimulus frequency. Distributed stimulation can be used to reduce the overall stimulation frequency required to achieve a smooth contraction (Brown, Huang, Morgan, Proske & Wise, 1999). Distributed stimulation increases the range of tension over which the contraction remains fused. The different motor units that insert directly into the Golgi tendon organ can be sequentially stimulated to produce a constant discharge, which is below that possible with whole muscle stimulation or synchronous stimulation of the same motor units. The distributed stimulation also allows more control over the 'noise' in the Golgi tendon organ response, because it is possible to alter the precise timings of the distributed stimulation pulses.

Suitability for Stochastic Resonance

The Golgi tendon organ has many of the features that are required for stochastic resonance, and therefore it is a good candidate to test for behaviour consistent with stochastic resonance. The Golgi tendon organ response is non-linear in at least two respects. Most importantly for stochastic resonance investigations, the response has a clearly defined threshold for passive muscle stretches, a requirement of stochastic resonance. The Golgi tendon organ response is also non-linear above threshold, as an increase in muscle length results in an approximately exponential increase in response, due to the passive length-tension properties of muscle.

In passive muscle the Golgi tendon organ has a threshold for small sinusoidal length changes. The threshold is adjustable, via a change in absolute length, so it is possible to apply a near-threshold periodic signal, which is another requirement of stochastic resonance. Finally, it is possible to add noise to the system via an imposed length change or a change in the electrical stimulation of the muscle. The change in electrical stimulation can be via a change in rate or a change in the timing of the stimuli during distributed stimulation.

Cat Golgi Tendon Organs

A total of eight cats *(Felis domesticus)* of both sexes were used for the experiments to seek evidence for stochastic resonance in Golgi tendon organs in mammalian muscle. All experiments were performed with approval from the Monash University Physiology Animal Ethics Committee.

Materials and Methods

Anaesthesia

A single intraperitoneal injection of barbiturate anaesthetic (40 mg/kg pentobarbitone sodium, Nembutal®, Rhone Merieux Australia, Australia) was used to induce anaesthesia. An occlusive cannula was inserted into the right cephalic vein and advanced to the level of the shoulder for delivery of supplemental anaesthetic as required (6 mg pentobarbitone). Anaesthetic depth was regularly evaluated via the skin pinch withdrawal, pinna flick and eye blink reflexes and end tidal carbon dioxide levels (Normocap® CD-102, Datex, Finland). Animals were considered to emerge from deep anaesthesia when CO_2 levels began to fall significantly below 5%. Core temperature was monitored with a rectal probe and maintained with a heat blanket.

Dissection

Bi-lateral pins in the iliac crests and a head clamp were used to fix the animal in position over a metal base plate. The left hind limb was fixed via pins in the head of the fibula and the medial condyle of the tibia, and small cups over the lateral and medial

malleoli. Removal of the popliteal fat and overlying muscles (plantaris, lateral gastrocnemius and medial gastrocnemius) exposed the soleus muscle. The maximum physiological length of the soleus muscle, L_{MAX}, was marked for reference. To determine L_{MAX} the ankle was maximally dorsiflexed and the distance noted between a small marker on the tendon and a similar marker on the adjacent fibula.

The soleus muscle and its tendon were dissected free from surrounding tissue. A small hole was drilled in the calcaneum for connection to an electro-magnetic position controller (Department of Physiology Electronics and Mechanical Workshops, Monash University). The calcaneum was then cut and the position of the controller referenced to L_{MAX}. The calcaneum and tendon were wrapped lightly in Ringer-soaked gauze to prevent drying out of the tendon.

The nerve to soleus was separated from the nerve to lateral gastrocnemius, which was then cut. The nerve to medial gastrocnemius and the common peroneal, sural and tibial nerves were also cut. The left hind limb was denervated at the level of the hip, which included cutting the nerves to gluteus maximus, pyriformis, caudofemoralis and the pudendal nerve as well as branches supplying biceps femoris and tenuissimus.

Removal of the muscles dorsi communis, longissimus dorsi medialis and multifidus spinæ exposed the dorsal aspect of the vertebral column. The dura was exposed by removal of the dorsal portions of the L4 to L7 vertebrae and the rostro-dorsal portion of the sacrum. The L6 to S1 spinal roots were freed along their length, after sectioning of the dura, and cut at their point of entry into the cord. A clamp on the third lumbar vertebra was then used to fix the lumbar spine.

Pools were fashioned from both the lower limb and lumbar skin flaps. The pools were filled with mineral paraffin oil to prevent dehydration and also provided a high impedance medium for nerve stimulation. The paraffin oil was kept warm with radiant heat and bubbled with carbogen (5% CO_2 in O_2).

Equipment

The multi-channel recorder as illustrated in Figure 3.1 and Figure 3.6 and described in Chapter Three was used.

Experimental Protocol

Afferent Identification

Functionally single afferents recorded in filaments of dorsal root were identified based on their conduction velocity and their response during a muscle twitch. A unit was identified as a Golgi tendon organ (Ib afferent) if the conduction velocity was 72-120 m/s (Lloyd, 1943) and the unit discharged impulses during the rising phase of a whole muscle twitch, indicating an 'in series' response (Figure 4.1).

Passive Muscle

Discharges from several Golgi tendon organs were recorded simultaneously to increase the sample size from each experiment. Muscle length was adjusted so that the majority of Golgi tendon organs did not maintain a background discharge, and therefore a clear threshold to small sinusoidal movements could be established.

A response curve to noise-alone length changes was measured covering a wide range of noise amplitudes. The noise signal used was computer generated as part of the multi-channel recorder and consisted of zero-mean evenly distributed noise (p. 59), for details of the applied noise see Appendix F. The average rate in response to a noise-alone stimulus exhibited a plateau as can be seen in Figure 4.5. The maximum noise amplitude regularly used was chosen to fall below the amplitude required to reach the plateau response. The noise-alone response curve was then fitted with a curve based on Kramers' rate (Equation 2.2).

A stimulus-response curve to small sinusoidal length changes was measured at each of the three test frequencies to ensure that a sub-threshold periodic stimulus could be employed in the study. The test frequencies were chosen to lie within the approximately linear region of the noise-alone response of the Golgi tendon organ, as this would allow for optimal separation of the predicted optimal noise levels, D_{PRE}. A stimulus-response curve was constructed, rather than using an arbitrarily small stimulus, because, as

discussed in the Chapter Two (p. 56), it is desirable to have a near-threshold periodic stimulus for the SNR_{EXP} measure. The responses of the Golgi tendon organs were quite variable; therefore it was not always possible to achieve a near-threshold condition for all units. For some units a supra-threshold periodic stimulus was used, which provided a convenient control measurement.

Stochastic resonance curves at the three test frequencies were measured using various noise amplitudes. The precise noise amplitudes used were dependent on preliminary analysis that was performed during the experiment. Measurements were clustered around the peaks, if they existed, of the SNR_{EXP} vs Noise curves. The SNR_{EXP} vs Noise curves were fitted with a logNormal curve (Equation 2.3, with $Z = 1$). From the fitted curve it was possible to estimate the level of noise that resulted in an optimal SNR_{EXP}, D_{OPT}. The fitting procedure also produced an estimate of the error in D_{OPT}. The measured values of D_{OPT} were then compared with the predicted optimal noise values, D_{PRE}.

Active Muscle

Similar measurements were to be made on the Golgi tendon organs during muscle contractions. However, there was no discernible threshold to sinusoidal length changes for movements down to a few micrometres, the minimum reliable movement available with the current equipment, that were imposed on a fused contraction, as discussed below (p. 98). The procedure for recording the stimulus-response curves for the actively contracting muscle is illustrated in Figure 4.2 (top panel). The muscle was stimulated, at a rate sufficient to achieve a smooth isometric contraction (50 pps for synchronous and 11 pps for distributed stimulation), for 4 seconds. During the contraction, small sinusoidal length changes were imposed that resulted in a modulation of the response from the Golgi tendon organs.

During the smooth isometric contractions used, the Golgi tendon organs produced an average discharge rate of approximately 100 i/s. With this level of maintained activity the SNR_{EXP} measure becomes insensitive and a different measure was required. The measure used was based on the instantaneous rate response of the Golgi tendon organ. The instantaneous rate is the reciprocal of the inter-spike interval: an example of an instantaneous rate plot for a Golgi tendon organ is given in Figure 4.2 (bottom panel).
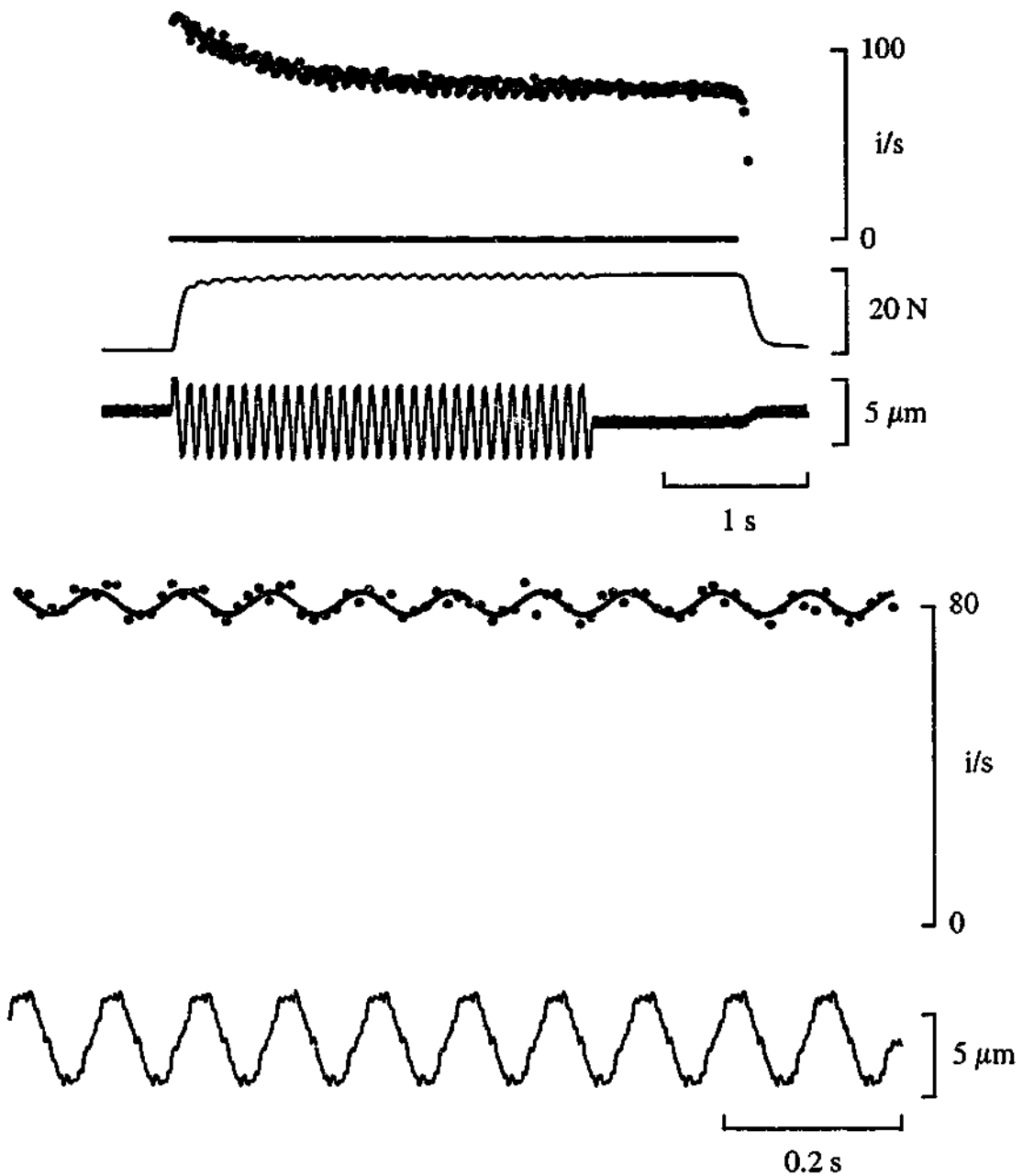
Figure 4.2   The procedure for recording a stimulus-response curve of a Golgi tendon organ in an actively contracting muscle is illustrated in the top panel. The top trace is the instantaneous frequency response of the Golgi tendon organ. The solid line under the Golgi tendon organ response indicates the 50 pps stimulus and also indicates the zero for the instantaneous rate. The imposed movement and resulting tension change are in the remaining traces in the top panel. The bottom panel illustrate the calculation of SNR_{RATE} and is taken from the last second of the imposed sinusoidal length change illustrated in the top panel: note the different time scale. On this scale the sinusoidal modulation of the Golgi tendon organ response is visible and has been fitted with a sinusoid to calculate SNR_{RATE}. The resulting value of SNR_{RATE} was 8.9.

The rate was modulated by the applied sinusoidal length change, and it was this modulation that was used to calculate SNR_{RATE}. A sinusoid was fitted to the last second of imposed movement and SNR_{RATE} was defined as the amplitude of the fitted sinusoid, divided by an estimate of the error in the amplitude of the fitted sinusoid. This is similar to the definition of SNR_{EXP} except it is based on the instantaneous rate and not the cycle histogram.

Results

Twenty-three Golgi tendon organs were examined for stochastic resonance behaviour. All Golgi tendons organs that were stimulated by movement under the appropriate conditions, sub-threshold periodic input and supra-threshold noise input, exhibited stochastic resonance.

Stimulus-Response Curve

A stimulus-response curve for small sinusoidal length changes is shown in Figure 4.3. For this Golgi tendon organ there was a threshold of approximately 500 μm for sinusoidal length changes (Figure 4.3, bottom panel). Below this amplitude the receptor did not respond at all. Figure 4.3 (top panel) illustrates the response of the same receptor at a longer test length, $L_{MAX} - 2.5$ mm compared to $L_{MAX} - 5.5$ mm. At this length the Golgi tendon organ had a maintained discharge of approximately 20 i/s. With a maintained discharge, this Golgi tendon organ responded to sinusoidal movements of 5 μm and therefore did not have a threshold within the range of length changes that were available with the current equipment.

Stochastic Resonance

The response of a Golgi tendon organ to three different types of stimuli is illustrated in Figure 4.4. The instantaneous rate and resulting cycle histograms that were used to calculate SNR_{EXP} are shown for each response. A supra-threshold sinusoidal stimulus (Figure 4.4, left panel) resulted in a cycle histogram where the majority of action potentials occurred at about the same phase of the stimulus cycle and yielded a moderate SNR_{EXP} (2.5). A supra-threshold noise-alone stimulus (Figure 4.4, right panel)
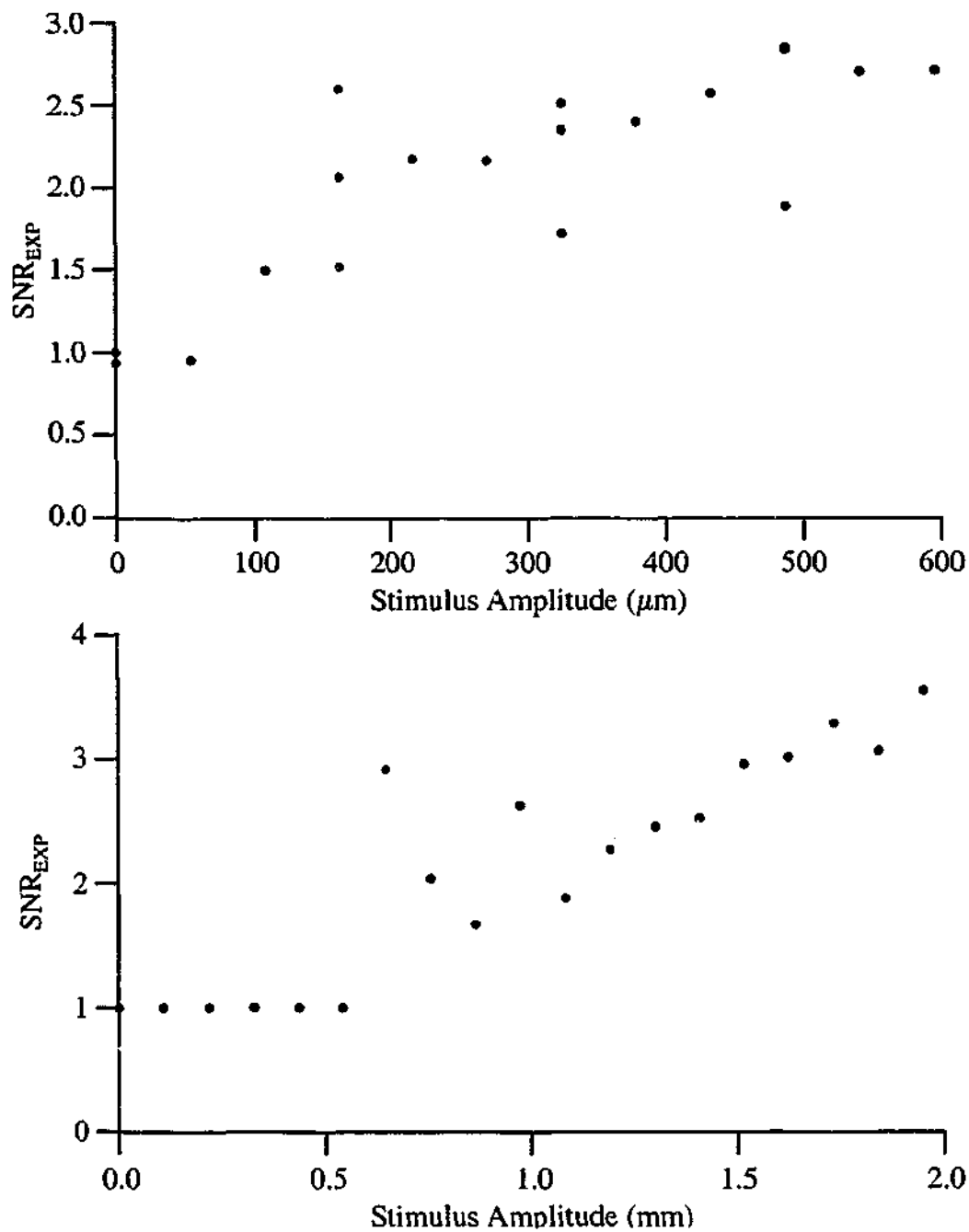
Figure 4.3 The response of a Golgi tendon organ to sinusoidal length changes in a passive muscle is dependent on the presence or absence of a maintained discharge at the test length. At a test length of $L_{MAX} - 2.5$ mm (top panel) the Golgi tendon organ had a maintained discharge of approximately 20 i/s, which resulted in the threshold to sinusoidal length changes being below the minimum amplitude that could be generated by the electro-magnetic length controller (5 μm). At a test length of $L_{MAX} - 5.5$ mm (bottom panel) the same Golgi tendon organ did not have a maintained discharge. Under these conditions the Golgi tendon organ did not respond to sinusoidal length changes of up to 500 μm. Each point was calculated from 20 s of recording, and all measurements were taken in a pseudo-random order.
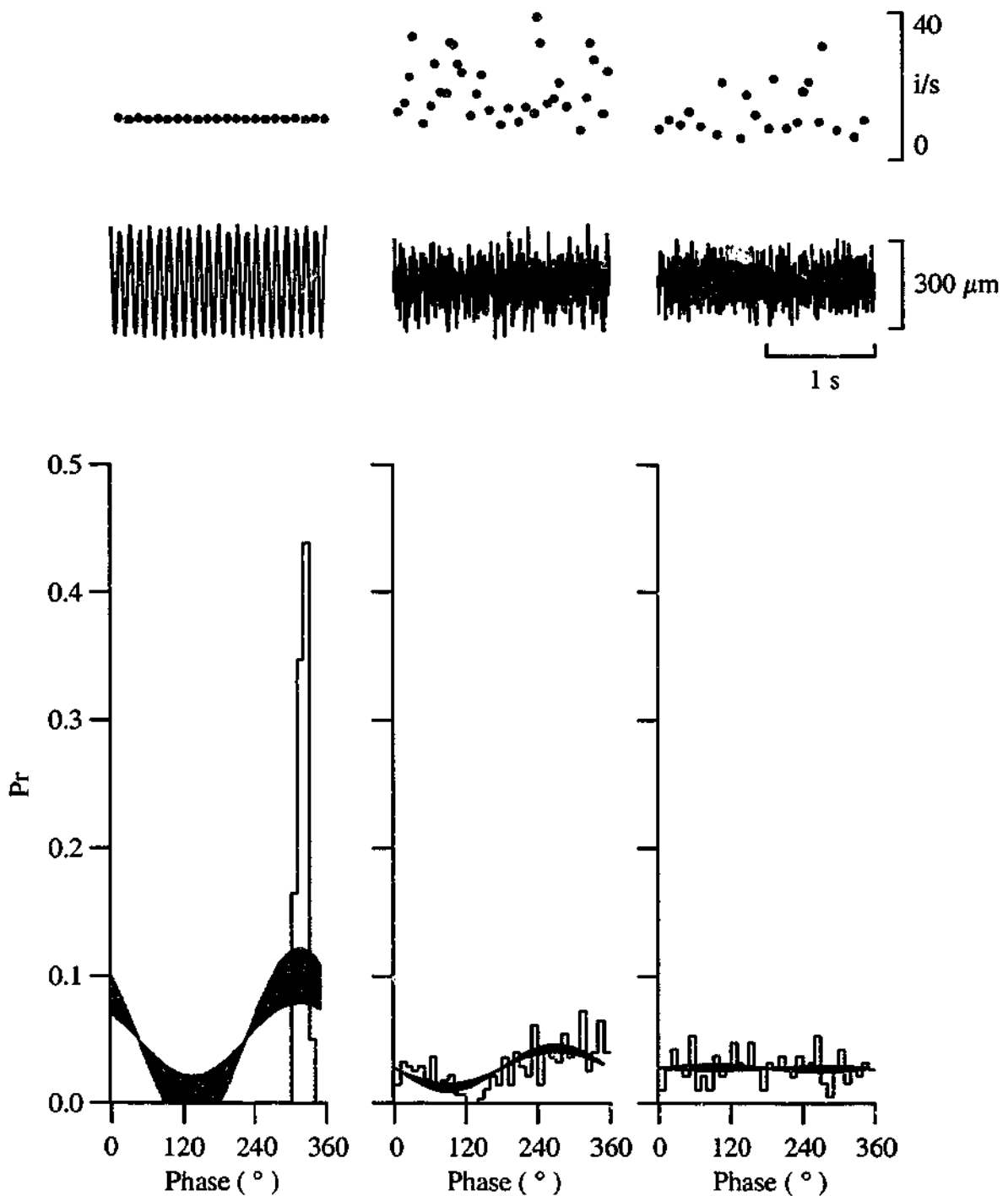
Figure 4.4 The response of a Golgi tendon organ to a supra-threshold sinusoidal stimulus (320 μm at 11 Hz, left panel), a sub-threshold sinusoidal stimulus and supra-threshold noise stimulus (60 μm at 11 Hz with 150 μm of noise, middle panel), and to a noise-alone stimulus (150 μm of noise, right panel). In each panel the top trace is the instantaneous discharge rate of the receptor and the trace underneath is the imposed change in muscle length about a test length of $L_{MAX} - 1.5$ mm. The graph at the bottom of each panel is a cycle histogram that has been fitted with a sinusoid to determine SNR_{EXP}. The values of SNR_{EXP} for the three stimuli are 2.50 (supra-threshold sinusoidal stimulus), 4.68 (sub-threshold sinusoidal stimulus and supra-threshold noise stimulus) and 0.86 (noise-alone stimulus).

resulted in a cycle histogram where the action potentials are evenly distributed across all phases of the stimulus and yielded a low SNR_{EXP} (0.86). A sub-threshold sinusoidal stimulus and supra-threshold noise stimulus (Figure 4.4, middle panel) resulted in a cycle histogram with a significant modulation of the distribution of the action potentials across the different phases of the stimulus and yielded a high SNR_{EXP} (4.68).

An example of the response of a Golgi tendon organ that exhibited an optimal SNR_{EXP} with the addition of input noise is shown in Figure 4.5. The noise-alone response is shown in the bottom panel and is the average discharge rate during the 20 s of imposed noise-alone movement. The noise-alone threshold was approximately 100 μm, above which the average rate increased with increasing noise amplitude to reach a plateau of about 65 i/s. The noise-alone response was well fitted by the curve based on Kramers' rate (Equation 2.2), allowing for accurate predictions of D_{PRE}. For the three test frequencies used in the stochastic resonance protocol of 5, 11 and 23 Hz the predicted optimal noise amplitudes were 121, 165 and 250 μm respectively, indicated by the grey lines in the bottom panel of Figure 4.5.

There is a clear peak in SNR_{EXP} for each of the test frequencies used. Each point was calculated from 20 s of response. The responses are well fitted by logNormal curves and the optimal noise values were 46.9±0.3 μm, 103±1 μm and 184±1 μm respectively (D_{OPT} ± SEM), indicated by the arrows in the upper panels of Figure 4.5. The increase of D_{OPT} with increasing sub-threshold periodic stimulus frequency is a key feature of stochastic resonance. The values of D_{OPT} are not precisely those predicted from the noise-alone response. However, there is a strong correlation between D_{OPT} and D_{PRE} (Pearson Product = 0.997).

The pooled results from fifteen Golgi tendon organs are presented in Figure 4.6. The data is shown on log-log axes as it extends over several orders of magnitude. Also, the errors associated with each measure are approximately proportional to the measurement, and therefore are best displayed on a log-log plot. Each point is the measured optimal noise level (± SEM) plotted against the corresponding predicted optimal noise level. Fourteen Golgi tendon organs were tested at three different frequencies, while one was tested at two, resulting in a total of 44 measurements. The data for each Golgi tendon
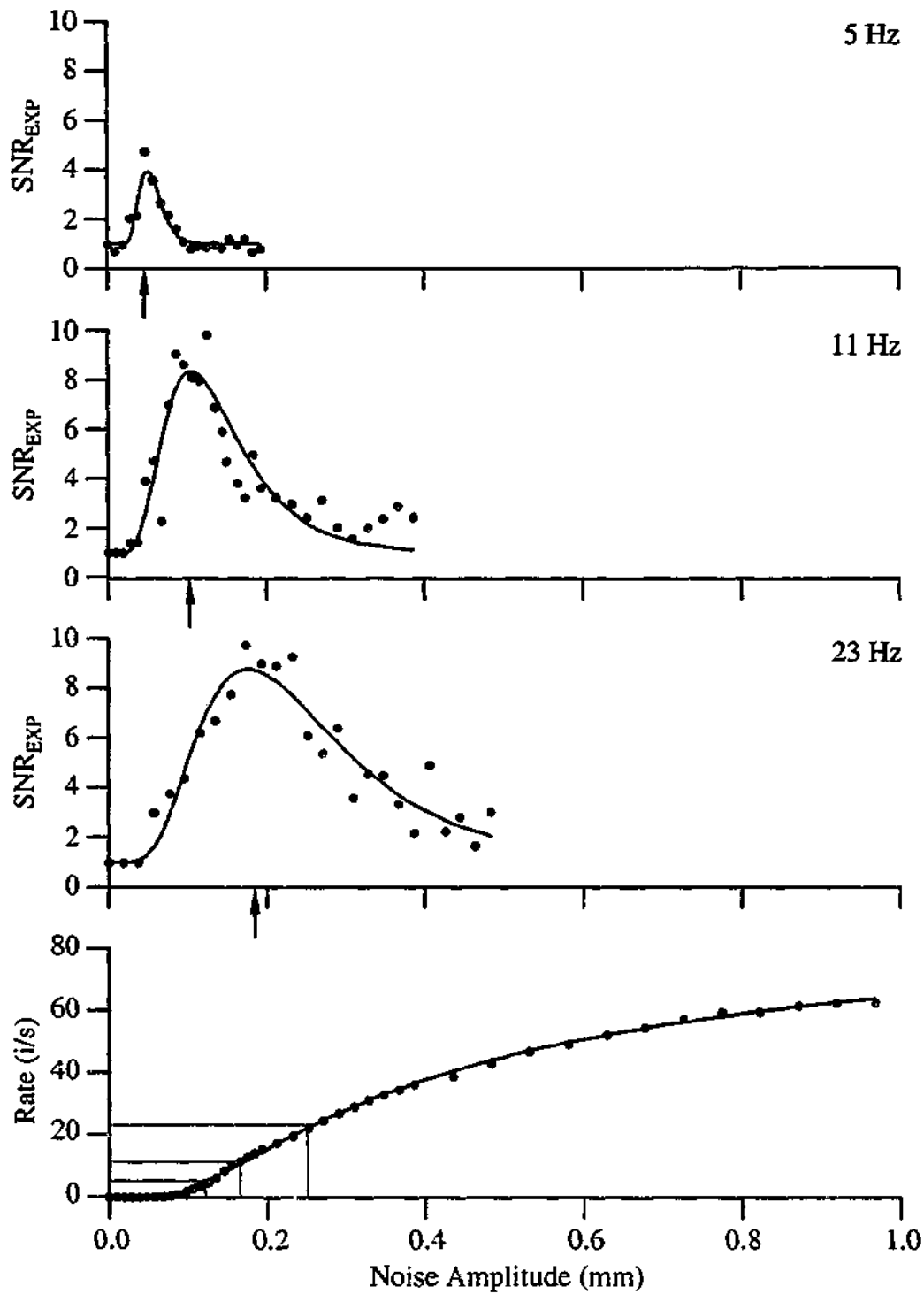
Figure 4.5   The response of a single Golgi tendon organ to passive stretches shows many of the characteristics of stochastic resonance. Each point is calculated from 20 s of response and the measurements were taken in a pseudo-random order (the blue symbol represents the data shown in Figure 4.4). The fitted curves in the upper panels are logNormal curves used to estimate D_{OPT}, indicated by the arrows, while the fitted curve in the bottom panel is based on Kramers' rate and is used to determine D_{PRE}. The grey lines in the bottom panel indicate the predicted optimal noise value, D_{PRE}, for each test frequency.
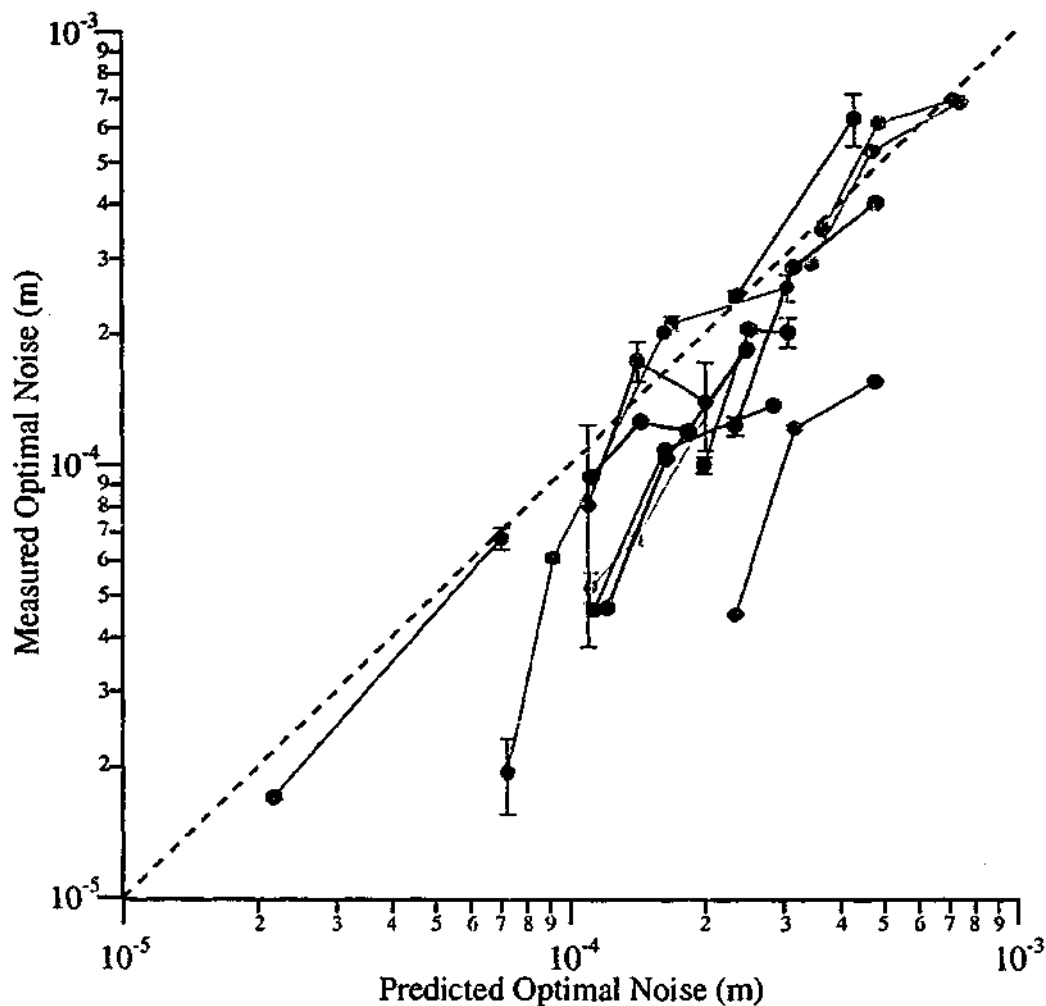
Figure 4.6   The pooled data from the 15 Golgi tendon organs that showed an optimal SNR$_{EXP}$ with the addition of noise, in passively stretched muscle, are scattered about the line of proportionality (dashed line) as predicted by stochastic resonance theory. However, there is a trend for D$_{OPT}$ to be lower than D$_{PRE}$. Values show D$_{OPT}$ and an estimate of the error in D$_{OPT}$ plotted against D$_{PRE}$. (For details refer to Chapter Two.) The results for each Golgi tendon organ are displayed in a different colour and are joined to highlight the correlation between D$_{OPT}$ and D$_{PRE}$ for individual Golgi tendon organs. The blue symbols represent the data from the Golgi tendon organ shown in Figure 4.5.

organ are joined to illustrate the correlation between D_{OPT} and D_{PRE} for each unit. The correlation between D_{OPT} and D_{PRE} for the pooled data was 0.889 (Pearson Product). The correlation between D_{OPT} and D_{PRE}, and therefore the sub-threshold periodic frequency dependence of the optimal noise level, is consistent with the hypothesis that the increase in SNR_{EXP} with additional noise is a result of stochastic resonance.

Maintained Discharge

Figure 4.7 illustrates the results of a stochastic resonance experiment on a Golgi tendon organ that had a maintained discharge of approximately 20 i/s at the test length. The noise-alone response has a similar shape to a Golgi tendon organ without a maintained discharge, but with the addition of a constant representing the maintained discharge. The response was fitted with a curve based on Kramers' rate, but with an additional constant to account for the maintained discharge (Equation 2.6).

The periodic stimulus used was supra-threshold for this Golgi tendon organ, as illustrated by the SNR_{EXP} values for zero noise (Figure 4.7, upper panels). SNR_{EXP} was a monotonically decreasing function of noise amplitude that was fitted by a single exponential. The monotonic decrease in SNR_{EXP} is expected, as stochastic resonance is not expected to operate for a supra-threshold periodic stimulus (as discussed in Chapter Two, p. 60).

Active Muscle

Golgi tendon organs in actively contracting muscle did not have a threshold for small periodic length changes within the range of movements that could be produced with the available equipment. As illustrated in Figure 4.8, for both whole muscle stimulation and distributed stimulation, the stimulus-response curve appears to pass through the origin. The smallest reliable movement of the electro-magnetic position controller was 5 μm. A 5 μm, 10 Hz sinusoidal movement produced a detectable modulation of the Golgi tendon organ response, as measured with SNR_{RATE}. Stochastic resonance requires a sub-threshold periodic input; therefore, with the available equipment it is not possible to observe stochastic resonance in a Golgi tendon organ of an actively contracting muscle.
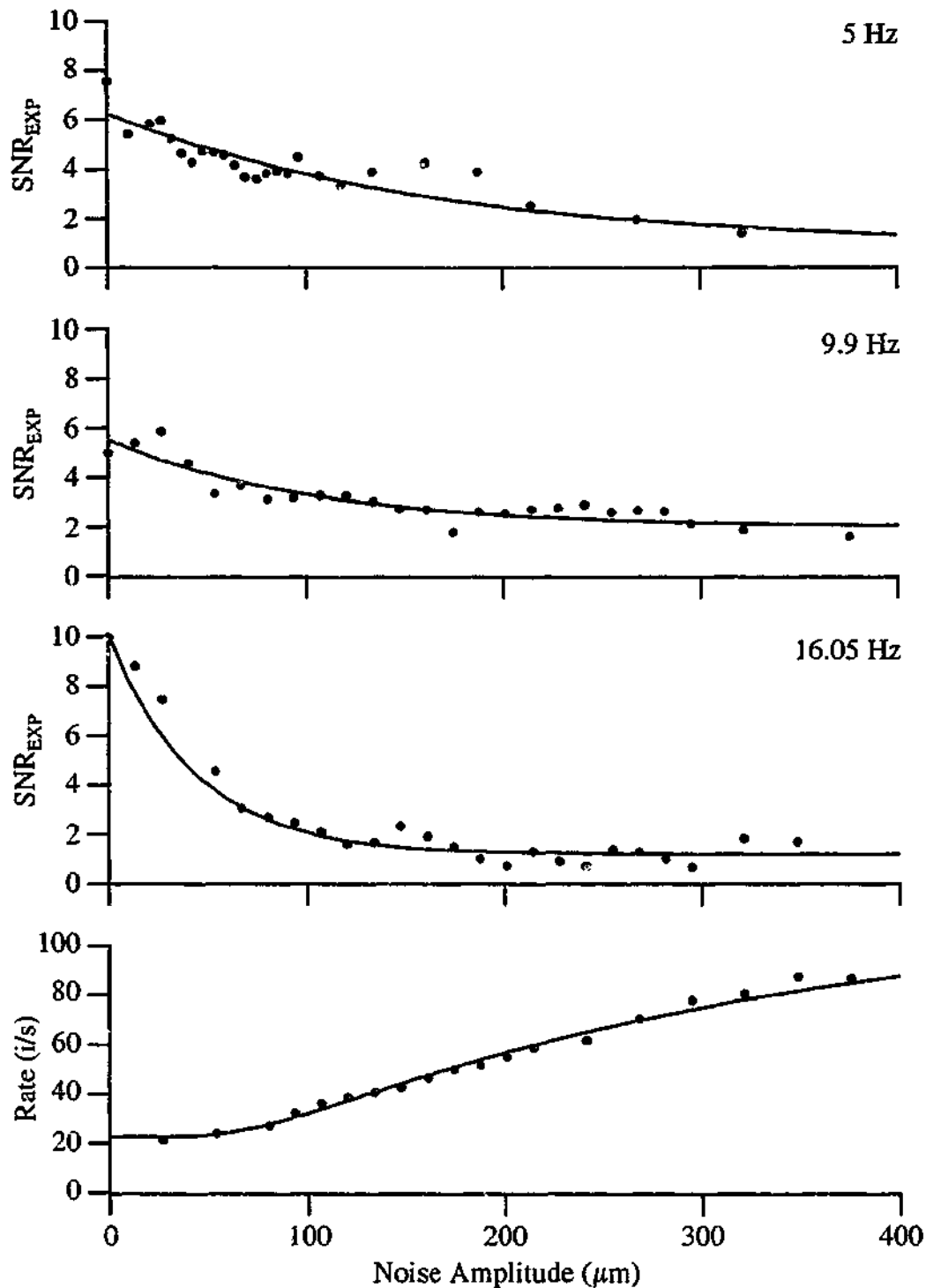
Figure 4.7 The response of a single Golgi tendon organ to a supra-threshold periodic input and noise input shows none of the characteristics of stochastic resonance. The SNR_{EXP} measure is a monotonically decreasing function of the input noise. Each point is calculated from 20 s of response and the measurements were taken in a pseudo-random order. The solid curves in the top three panels are exponential curves that have been fitted to the data. The bottom panel is the noise-alone response, which has been fitted with a curve based on Kramers' rate.
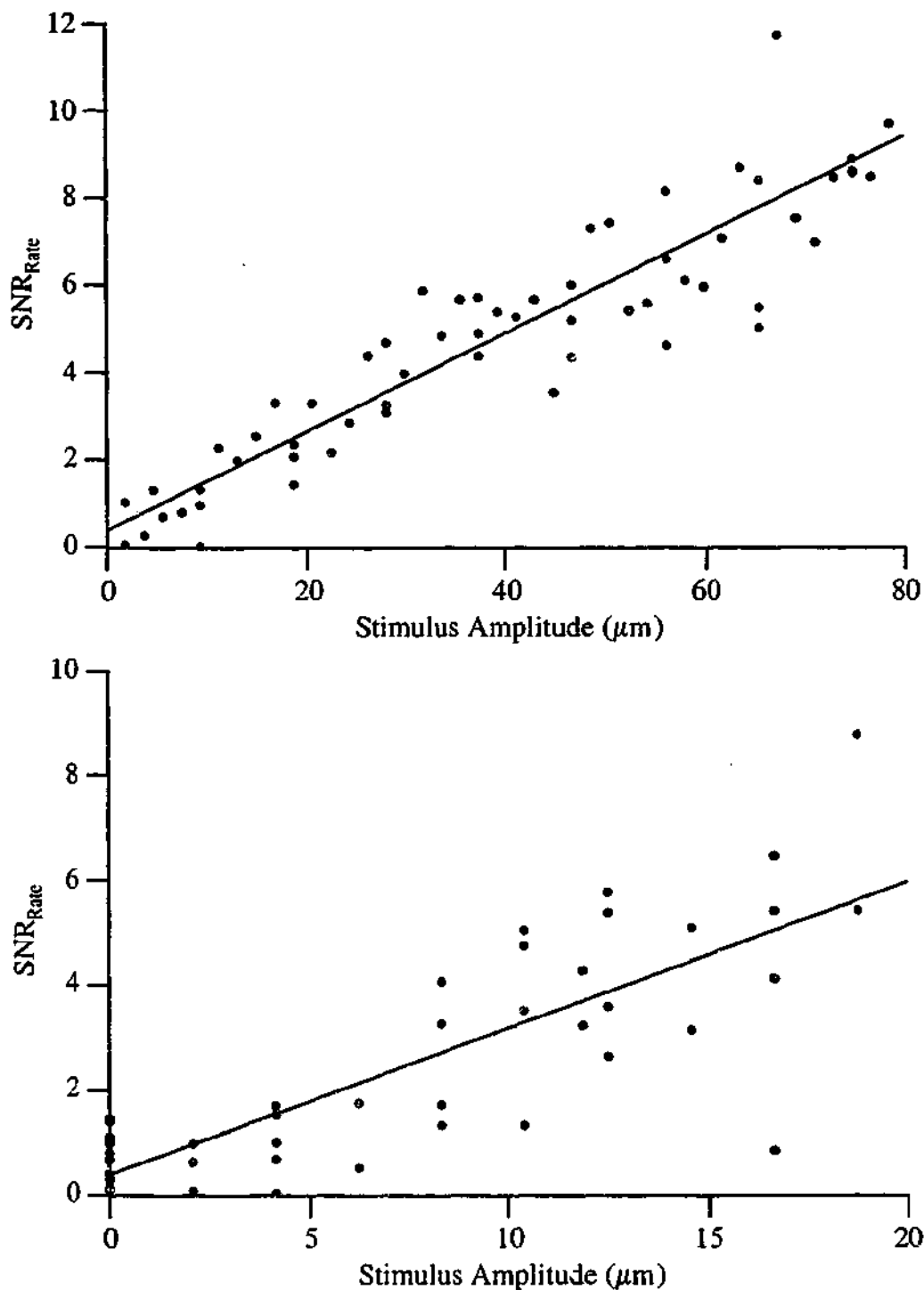
Figure 4.8 The threshold for small sinusoidal length change is below 5 μm (the limit of the equipment) for Golgi tendon organs in actively contracting muscles. Both synchronous (top panel) and distributed (bottom panel) stimulation result in a threshold to sinusoidal length changes of 10 Hz below the minimum amplitude which could be generated by the electro-magnetic length controller. Each point was calculated from the last second of imposed movement with a 30 s rest period between each measurement. All measurements were taken in a pseudo-random order and regression lines have been fitted to the data (solid lines).

Discussion

All of the key features of stochastic resonance are present in the responses of Golgi tendon organs in passive muscle. An optimal output SNR with the addition of noise was observed in all Golgi tendon organs examined under the appropriate conditions, a sub-threshold periodic signal and supra-threshold noise signal. Similar results have been observed in other biological systems but many of these systems are unlikely to exhibit stochastic resonance (see the discussion of systems that exhibit stochastic resonance in Chapter One, p. 17). Most systems either exhibited dithering, or they had not been tested sufficiently to distinguish between stochastic resonance and other kinds of behaviour.

The key feature of stochastic resonance that has been observed is the shifting of optimal noise level, D_{OPT}, with stimulus frequency. Each Golgi tendon organ was tested with several stimulus frequencies and D_{OPT} always increased with increasing stimulus frequency. This feature is unique to stochastic resonance as discussed in Chapter One (p. 7). The most remarkable result was the general agreement between predicted optimal noise amplitudes, predicted from the noise-alone response of the Golgi tendon organ, and the measured optimal noise amplitudes. Although this is predicted from stochastic resonance theory, it is only valid for the SNR_{EXP} measure with near-threshold periodic stimuli (p. 57). The periodic stimuli used in the Golgi tendon organ experiments were typically significantly sub-threshold to ensure that they remained sub-threshold for the duration of the experiment. Therefore, the agreement is quite surprising.

The trend for the measured optimal noise level to be less than the predicted value (Figure 4.6) is probably a result of the SNR_{EXP} measure. If the periodic stimulus amplitude is far from threshold then D_{OPT} is less than D_{PRE}, as discussed in Chapter Two (p. 57). There is also a trend for the optimal noise level for higher stimulus frequencies to be further from the predicted optimal noise level than at lower stimulus frequencies. This is because SNR_{EXP} can be distorted by the influence of sub-harmonics of the stimulus frequency.

The monotonically decreasing SNR_{EXP} with the addition of noise for a Golgi tendon organ with a supra-threshold periodic stimulus is as expected from stochastic resonance theory. It indicates that the increase in SNR_{EXP} for the other Golgi tendon organs was unlikely to be the result of some other noise influence, which may be expected to effect all Golgi tendon organs in a similar manner.

The threshold of a Golgi tendon organ to a sinusoidal length change imposed on an actively contracting muscle is less than 5 μm, which was the limit of the reliable movements that could be produced with the available equipment. Therefore, it is not possible to demonstrate stochastic resonance in Golgi tendon organ of actively contracting muscles using the current equipment. The addition of noise to the supra-threshold periodic input signal would result in a decrease in the output SNR, similar to that seen for the passive Golgi tendon organ with a supra-threshold periodic stimulus. Although it was not possible to observe stochastic resonance behaviour in Golgi tendon organs in actively contracting muscle, it does not exclude the possibility that stochastic resonance may occur in situations where a sub-threshold sinusoidal length change is present.

Whether the central nervous system has developed the capabilities to use to stochastic resonance remains uncertain. However, it is highly probably that the Golgi tendon organs in passive muscle can, and do, exhibit stochastic resonance given the evidence presented above. This is only the second conclusive observation of stochastic resonance in a biological system.

Chapter Five

Muscle Spindles

Muscle spindles are 2-4 mm long, encapsulated, stretch-sensitive mechanoreceptors that are situated within skeletal muscles in mammals, birds, reptiles and amphibians (Barker, 1974). The following description is of mammalian muscle spindles as the muscle spindles of the cat were utilised in the stochastic resonance experiments. Within each muscle spindle there are two morphologically distinct afferent endings that Ruffini (1898) named the primary and secondary endings. Primary endings respond to stretch with a prominent dynamic response, while secondary endings appear to signal only muscle length (Cooper, 1961). The afferents from muscle spindles can be divided into two groups based on their conduction velocities that are in the range of 72-120 m/s and 36-72 m/s and are classed as Ia and II afferents respectively (Lloyd, 1943; Hunt, 1954). The 'in parallel' location of muscle spindles has lead to the suggestion that they are monitors of muscle length (Fulton & Pi-Suñer, 1928).

Structure

Between two and twelve intrafusal muscle fibres are encapsulated within each muscle spindle (Sherrington, 1894), as illustrated in Figure 5.1. The intrafusal muscle fibres can be divided into two groups based on their size and the arrangement of nuclei within the equatorial region (Barker, 1948; Boyd, 1962). Nuclear chain fibres are thinner than the nuclear bag fibres and have a single chain-like arrangement of nuclei, while the nuclear bag fibres typically have more than three nuclei packed side-by-side in a bag-like swelling at their equator. The nuclear bag fibres can be further divided, based on the pH sensitivity of ATPase staining and other criteria, into nuclear bag_1 and nuclear bag_2 fibres (Ovalle & Smith, 1972).

There are typically between one and ten chain fibres in each muscle spindle, but only a single one of each type of nuclear bag fibre; although many variations of arrangements do exist, including muscle spindles without a nuclear bag_1 fibre (Richmond & Abrahams, 1975). The nuclear chain fibres typically do not extend beyond the limits of the capsule, while the nuclear bag fibres may extend for up to 8 mm. The polar segments of the intrafusal muscle fibres contain sarcomeres and are capable of
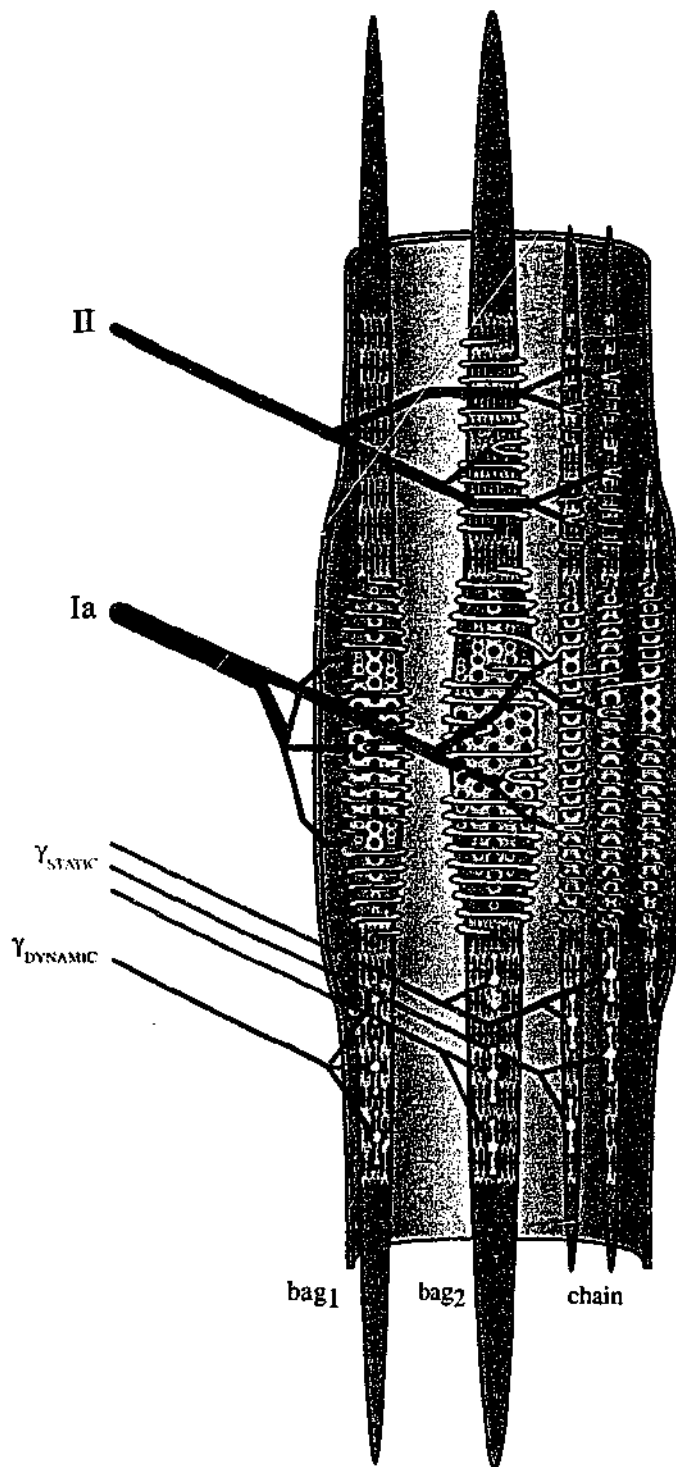
Figure 5.1 A muscle spindle encapsulates between two and twelve intrafusal muscle fibres that can be divided into nuclear chain and nuclear bag fibres. The muscle spindle illustrated has five intrafusal fibres. The Ia afferent innervates the muscle spindle primary endings, consisting of spiral endings around the equatorial regions on nuclear bag$_1$, nuclear bag$_2$ and nuclear chain fibres. The II afferent innervates the muscle spindle secondary endings that are found on the polar regions of the nuclear bag$_2$ and nuclear chain fibres. The γ_D efferent (shown in blue) innervates only the nuclear bag$_1$ fibre, while the γ_S efferent (shown in red) innervates both the nuclear bag$_2$ and nuclear chain fibres. Figure adapted from Figure 1.1 of Carr (1999).

contracting when activated; with the contraction of the polar segments leading to extension of the equatorial region (Bessou & Pagés, 1975). The nuclear chain fibres contract more rapidly than the nuclear bags fibres and also have a higher resistance to passive shortening than the nuclear bag fibres, which may result in 'kinking' of the intrafusal fibres as a result of passive shortening (Boyd & Ward, 1975).

The polar regions of the intrafusal muscle fibres are innervated by small myelinated fusimotor or gamma (γ) motoneurones. A single γ motoneurone typically innervates about six muscle spindles, while each muscle spindle is usually innervated by more than one γ motoneurone (Hunt & Kuffler, 1951). The fusimotor system can be divided into two groups, γ_S and γ_D, based on their functional characteristics (Matthews, 1962; Emonet-Denand et al., 1977). The γ_D axons innervate the nuclear bag$_1$ muscle fibres (Banks, 1981), and enhance the velocity sensitivity of the Ia afferent response but rarely affect the response of the II afferents. The γ_S axons innervate the nuclear bag$_2$ and nuclear chain fibres and may enhance the static position sensitivity of both the Ia and II afferent responses (Jansen & Matthews, 1962a).

Muscle spindle primary endings spiral about the equatorial regions of individual intrafusal fibres (Banks, Barker & Stacey, 1982). It is proposed that lengthening of the equatorial region results in lengthening of the terminal helices, which leads to stretch deformation of the terminal membrane. The mechanical deformation results in the generation of the receptor potential, which in turn results in the generation of action potentials. The muscle spindle primary ending is innervated by the Ia afferent, with a near unity ratio of Ia afferent to muscle spindle innervation (Barker, 1962). The Ia afferent branches to innervate endings on all three types of intrafusal fibres. The first order branch separates the endings on nuclear bag$_1$ fibres from those on the nuclear bag$_2$ and nuclear chain fibres (Banks, Barker & Stacey, 1977). It has been proposed that there are two separate sites of action potential initiation, one associated with the endings on the nuclear bag$_1$ fibre and another associated with the endings on the nuclear bag$_2$ and nuclear chain fibres (Proske, 1997).

Muscle spindle secondary endings are predominantly found on nuclear chain and nuclear bag$_2$ fibres lying to one side, but within 400 μm, of the primary ending, often on

striated portions of intrafusal fibres (Banks et al., 1982). The secondary endings form short helixes and flower spray endings on the nuclear chain and nuclear bag_2 fibres respectively (Barker, 1948; Boyd, 1962). There are also secondary endings on the nuclear bag_1 fibres of the flower spray type, but these are less common. The muscle spindle secondary ending is innervated by a Group II afferent, with as many as five Group II afferents innervating a single muscle spindle, although some muscle spindles are completely without Group II afferents (Boyd, 1962).

Response

The response of muscle spindles to imposed length changes in passive muscle can be largely explained by the mechanical properties of the intrafusal muscle fibres, as illustrated in the model by Schaafsma, Otten & van Willigen (1991). The response during combined fusimotor stimulation and imposed length changes is complex because of the interactions of the applied stretch, with the rate and duration of fusimotor stimulation (Kuffler, Hunt & Quilliam, 1951). As the stochastic resonance experiments were all performed with passive muscles the response during fusimotor activity will not be discussed in any detail.

Maintained Discharge

The majority of both primary and secondary endings exhibit a maintained or resting discharge in the passive muscle, with the discharge from the secondary ending being more regular (Stein & Matthews, 1965). The average rate of the maintained discharge is dependent on muscle length (Adrian, 1926; Bessou & Laporte, 1962; Gregory, Harvey & Proske, 1977), fusimotor activity (Hunt, 1951) and contraction history of the muscle; and may persist in the absence of whole muscle tension (Gregory, Morgan & Proske, 1991).

Ramp-and-Hold Stretches

The response of a muscle spindle primary ending to a ramp-and-hold stretch is composed of a dynamic phase and a static phase (Figure 5.2, bottom panels). The dynamic response shows an 'initial burst' that is attributed to stable cross-bridges within
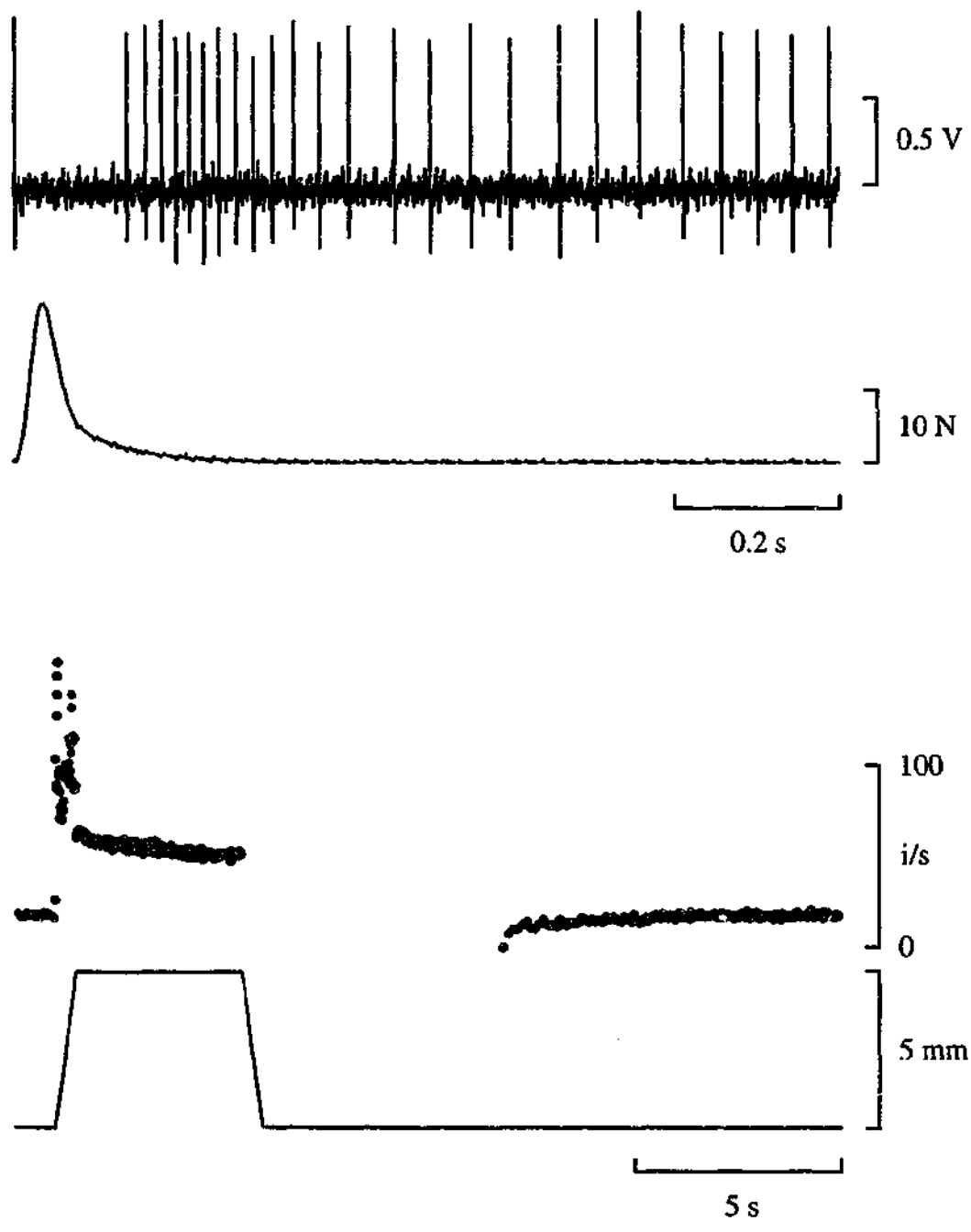
Figure 5.2   The silencing of the discharge from a muscle spindle primary ending during a muscle twitch typifies the 'in parallel' response of muscle spindles. The top panels show recorded action potentials and twitch tension. The response of a primary ending to a ramp-and-hold stretch is illustrated in the bottom panels as an instantaneous rate, together with muscle length. The response has a dynamic and static phase. The resting discharge is interrupted after the release, but returns approximately 5 s later. All measurements were taken at $L_{MAX} - 10$ mm.

the intrafusal muscle fibres (Hunt & Ottoson, 1976). The stable cross-bridges result in an increased stiffness of the polar regions of the muscle spindle. Most of the early part of the stretch is therefore transferred to the equatorial region of the muscle spindle where the primary ending is located. Once the elastic limit of the stable cross-bridges is passed they are forced to detach, reducing the stiffness of the polar regions of the muscle spindle. The decrease in stiffness results in the polar regions taking up relatively more of the imposed stretch than when there were stable cross-bridges present.

Further increases in length result in an increase in discharge that is influenced by both the change in length and the rate of change in length (Matthews, 1972). During the hold phase the discharge rate falls to a rate that is proportional to the maintained length. The dynamic index (Equation 3.3) is proportional to the velocity of lengthening but independent of the absolute length change (Matthews, 1963). During shortening the primary ending is typically silenced but recovers its maintained discharge within a few seconds, as illustrated in the bottom panels of Figure 5.2. Therefore, the muscle spindle primary afferent is proposed to signal changes in muscle length, due to its dynamic sensitivity, along with muscle length, as the maintained discharge is approximately proportional to muscle length.

The response of muscle spindle secondary endings is similar to that of the primary endings, except there is no 'initial burst' and the dynamic response is less distinct (Cooper, 1961). The secondary endings are less likely than primary endings to fall silent during shortening, in line with their proposed role of signalling absolute muscle length (Harvey & Matthews, 1961). Overall the static length sensitivities of both the primary and secondary endings are similar (Jansen & Matthews, 1962b). Therefore it may be possible to extract a velocity signal from the response of primary endings by subtracting the response of the secondary ending.

Sinusoidal Stretches

The response of muscle spindle primary endings to sinusoidal length changes is linear for movements of less than 100 μm peak-to-peak at 1 Hz (Matthews & Stein, 1969b); that is, the instantaneous rate of discharge exhibits a sinusoidal modulation, the amplitude of which is proportional to the sinusoidal stimulus amplitude. At high

frequencies the response of the muscle spindle primary ending leads the length by approximately 90°, as would be expected from a velocity sensitive receptor, which is due to the viscous properties of the intrafusal fibres. The muscle spindle secondary ending has a similar response but is linear over a wider range of amplitudes. Sinusoidal movements of as little as 5 μm peak-to-peak at 100-500 Hz (vibration) can 'drive' muscle spindle primary afferents to discharge one impulse for each cycle of the stimulus (Brown, Engberg & Matthews, 1967). The muscle spindle secondary endings are an order of magnitude less sensitive to stimuli in this frequency range.

Muscle History Effects

The response of muscle spindles is dependent on the previous history of the muscle as first reported by Kuffler et al. (1951). The thixotropic nature of muscle is related to the 'short range elastic component' of tension described by Hill (1968) and both are the result of the formation of stable cross-bridges within the relaxed muscle fibres. The stretch and contraction history of a muscle can affect the response of a muscle spindle to stretch by introducing slack into the intrafusal muscle fibres (Brown, Goodwin & Matthews, 1969; Proske, Morgan & Gregory, 1992).

'Hold Long' and 'Hold Short' Conditioning

It is possible to introduce slack, via stable cross-bridges, into the intrafusal muscle fibres by 'hold long' conditioning (Morgan, Prochazka & Proske, 1984). A series of rapid stretches or a brief period of fusimotor stimulation will detach any previously formed stable cross-bridges. After detachment of the stable cross-bridges, maintaining the muscle at a length greater than the test length, 'hold long' conditioning, allows the formation of stable cross-bridges at the longer length. On returning to the test length, the stable cross-bridges may cause the intrafusal fibres to fall slack, as the stable cross-bridges do not permit sarcomere shortening. Holding the muscle at the test length after the conditioning stretches, or fusimotor stimulation, results in the formation of stable cross-bridges at the test length, 'hold test' conditioning, with no slack in the intrafusal muscle fibre. The majority of stable cross-bridges form within three to six seconds but do not spontaneously detach for over half an hour. Therefore, conditioning the muscle

before test stretches is required to ensure the muscle spindle is in a known state (Proske, Morgan & Gregory, 1993).

Noise Conditioning

The effect on a 'hold long' conditioned muscle spindle of a movement consisting of small random length changes about a zero-mean length change (i.e. a noise-alone movement required for stochastic resonance studies) would be expected to be dependent on the amplitude of the noise. Noise-alone movements greater than $100\mu m$ would be expected to detach some stable cross-bridges that would then reform at the test length at the end of the noise-alone movements. Any detachment and subsequent reattachment at a slightly longer length will reduce the filament resting tension (Hill, 1968). This is because stable cross-bridges under the greatest strain, those formed at the shortest lengths, would be expected to yield first, and therefore a small 'hold long' conditioning will be produced as the stable cross-bridges reform at a longer length. The resulting 'hold long' condition, due to the noise-alone movement, would be expected to result in a lower maintained discharge, with larger noise amplitudes increasing the apparent 'hold long' effect of the noise-alone movement.

Maintained Discharge

It is possible to temporarily silence the maintained discharge from muscle spindle afferents by rapid shortening of the muscle (Gregory et al., 1991). At long muscle lengths the maintained discharge spontaneously resumes in all muscle spindles. At short muscle lengths the maintained discharge resumes in some but not others. It is proposed that the rapid shortening of the muscle introduces slack into the intrafusal muscle fibres that is taken up at long, but not short, muscle lengths (Gregory et al., 1991). Stimulation of the fusimotor fibres of muscle spindles that fall silent after a rapid shortening results in a return of the maintained discharge, which is proposed to be as a result of the removal of the slack from within the intrafusal muscle fibres, a 'hold test' conditioning. The spontaneous resumption of the maintained discharge in some muscle spindles after a rapid shortening is thought to be due to residual strain on the spiral endings by connective tissue attached to the muscle spindle capsule, and not the result of a 'leaky membrane' (Gregory et al., 1991).

Proprioception

It is generally accepted that although cutaneous and joint receptors are involved in kinaesthesia, the sense of position and movement of the extremities, the main afferent signal is from muscle spindles (McCloskey, 1978). The effects of muscle history on the detection threshold of movements of the elbow joint are consistent with the proposal that muscle spindles are a significant source of proprioceptive information (Wise, Gregory & Proske, 1996). Macefield et al. (1990a) stimulated various afferent fibres of the median and ulnar nerves at the wrist and found that while stimulation of cutaneous and joint afferents gave rise to distinct sensations, the stimulation of individual muscle spindle afferents was not perceived. Therefore, although muscle spindles appear to be an important source of proprioceptive information, it appears to require the response of a population of muscle spindles for their signals to reach consciousness.

In studies using microneurographic techniques it has been reported that approximately two thirds of muscle spindle primary afferents have a maintained discharge (Macefield et al., 1990). The actual proportion may be higher as muscle history effects may have left some intrafusal fibres slack. This is supported by the work of Wilson, Gandevia & Burke (1995) who found that weak voluntary contractions led to a sustained increase in maintained discharge, consistent with the removal of intrafusal muscle fibre slack. Also, Kakuda (2000) reported that all muscle spindle secondary endings had a maintained discharge. Proprioceptive thresholds for the detection of movements are lowest after voluntary contraction of the appropriate muscles (Wise, Gregory & Proske, 1998), which is consistent with the hypothesis that there is slack present in the intrafusal fibres of an unconditioned muscle.

Suitability for Stochastic Resonance

Muscle spindle primary and secondary endings have all the features required for stochastic resonance. The receptors are non-linear systems, with a threshold to small sinusoidal inputs. The stimulation of the receptor, via changes in muscle length, can be precisely controlled allowing for the application of near-threshold periodic and supra-threshold noise signals.

Cat Muscle Spindles

A total of eight cats *(Felis domesticus)* of both sexes were used for the experiments to seek evidence for stochastic resonance in muscle spindles in mammalian muscle. All experiments were performed with approval from the Monash University Physiology Animal Ethics Committee.

Materials and Methods

The anaesthesia, dissection methods and equipment used for experiments involving muscle spindles were the same as those involving Golgi tendon organs. For details refer to the Materials and Methods section of Chapter Four (p. 92).

Experimental Protocol

Afferent Identification

Functionally single afferents recorded in filaments of dorsal root were identified based on their conduction velocity and their response during a muscle twitch. A unit was identified as a muscle spindle if its discharge paused during the rising phase of muscle tension during a twitch (Figure 5.2, top panels). The division of muscle spindles into primary and secondary endings was based on the conduction velocity of the afferent fibres. Units were classified as primary endings of Ia afferents, if the conduction velocity was 75-120 m/s or as secondary endings of Group II afferents, if the conduction velocity was 36-70 m/s (Lloyd, 1943). Afferents with conduction velocities in the range of 70-75 m/s were excluded from the study to avoid ambiguity.

Effect of Conditioning

As the previous muscle history may affect the response of a muscle spindle (Proske et al., 1993), the effect of a noise-alone stimulus on the response of a muscle spindle was investigated. The effect of conditioning contractions at different muscle lengths on the maintained discharge of muscle spindle primary afferents was determined using the protocol illustrated in the top-left panel of Figure 5.3. Conditioning contractions were evoked by whole muscle nerve stimulation with a stimulus designed to recruit fusimotor
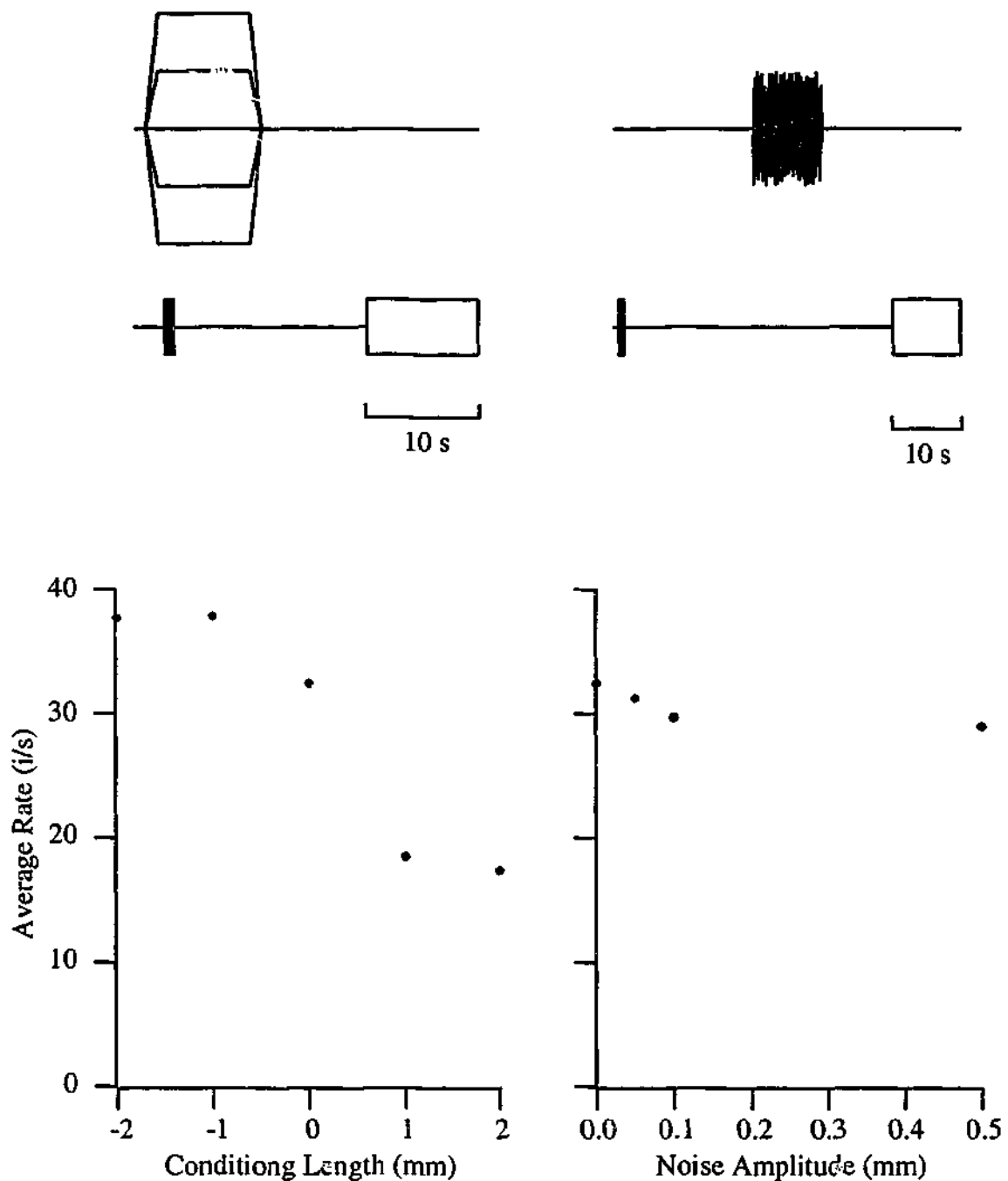
Figure 5.3 The protocol for conditioning the muscle at different lengths is illustrated in the top-left panel. The top trace is the muscle length and the bottom trace illustrates the timing of the 1 s of 50 pps stimulation (solid bar) and the 10 s recording period (open bar). The effect of conditioning at various lengths is illustrated ·in the bottom-left panel and it is clear that 'hold long' conditioning results in a reduction of the maintained discharge. The protocol for measuring the conditioning effects of a noise-alone movement is illustrated in the top-right panel. The top trace is the muscle length and the bottom trace illustrates the timing of the 1 s of 50 pps stimulation (solid bar) and the 10 s recording period (open bar). The maintained discharge is reduced after 'noise conditioning' (bottom-right panel) with larger noise amplitudes resulting in a greater reduction. All measurements were taken at a test length of $L_{MAX} - 10$ mm.

fibres. The stimulus strength was 150% of the stimulus strength required to achieve maximum isometric force, and the stimulus consisted of 1 s of 50 pps. The muscle was held at the conditioning length for a period of 5 s after the end of the contraction, before being returned to the test length. After a delay of 10 s the maintained discharge was recorded for a period of 10 s.

The effect of a noise-alone stimulus on the maintained discharge of a muscle spindle primary ending after 'hold test' conditioning was measured using the protocol illustrated in the top-right panel of Figure 5.3. After a 'hold test' conditioning, 10 s of a noise-alone mechanical stimulus was applied. After a further delay of 10 s the maintained discharge was recorded for a period of 10 s. The maintained discharge after the 'noise conditioning' was then compared to that after a 'hold test' conditioning.

Stochastic Resonance

The protocol used for the stochastic resonance experiments with muscle spindles was similar to that used for Golgi tendon organs in passive muscle, for details refer to the Experimental Protocol section of Chapter Four (p. 94). The only change to the protocol was that a 'hold test' conditioning contraction was used before each measurement to eliminate any conditioning effects of the previous noise stimulus. The 'hold test' conditioning consisted of 0.5 s of whole muscle nerve stimulation at 50 pps with a fusimotor strength stimulus, a stimulus strength that was 150% of that required to produced maximal isometric force.

Aperiodic Stimuli

Stochastic resonance is not the only mechanism whereby noise can enhance signal detection. To illustrate another constructive effect of noise on signal detection in muscle spindle primary endings a series of ramp-and-hold stretches was performed with various amplitudes of additional input noise. The stretches consisted of a 1 mm stretch at 10 mm/s from L_{MAX} – 6 mm. All stretches were done after 'hold test' conditioning and the amount of noise added to the test movement was varied in a pseudo-random order. The noise was added to the entire length signal, so it was present before and after the 1 mm stretch. The response of the muscle spindle to the stretch was quantified by calculating

the increase in the average discharge rate as a result of the stretch (Figure 5.11, top panel). For the primary ending shown the rate increased from 122 i/s to 153 i/s as a result of the stretch.

Results

Effect of Conditioning

Noise Conditioning

The effect of a noise-alone movement, 'noise conditioning', on the maintained discharge of a muscle spindle primary ending is illustrated in Figure 5.3 (bottom-right panel). The average rate of the maintained discharge decreased with increasing amplitudes of 'noise conditioning'. The largest noise-alone movement of 0.5 mm resulted in an average maintained discharge of 29 i/s, a reduction of 3.5 i/s compared to the average maintained discharge after 'hold test' conditioning of 32.5 i/s. The reduction in maintained discharge as a result of 'noise conditioning' was less than the 14 i/s reduction resulting from a 1 mm 'hold long' conditioning (Figure 5.3, bottom-left panel). This indicates that the condition of the muscle spindle after 'large' noise movements, the maximum noise amplitude used in the stochastic resonance investigations being 0.5 mm, is similar to that after a 'hold test' conditioning, but with a small amount of slack introduced. This is an important result as it means the sinusoidal stimulus-response curves that were measured after 'hold test' conditioning will not be dramatically altered as a result of the additional input noise used during the stochastic resonance experiments.

Maintained Discharge

After 'hold test' conditioning the majority of muscle spindles primary endings had a maintained discharge. An average of twenty muscle spindle primary endings were isolated from each animal; of these, typically fewer than five muscle spindle primary endings in each animal did not have a maintained discharge after the standard 'hold test' conditioning. This was true even when the 'hold test' conditioning was performed at the shortest muscle length at which the muscle was just taut, typically between $L_{MAX} - 16$ mm and $L_{MAX} - 20$ mm.

To test the hypothesis that the few silent spindles, the ones without a maintained discharge after 'hold test' conditioning, were silent as a result of being poorly perfused, whole muscle stimulation of 15 pps for 1 min, designed to increase blow flow to the muscle, was used (Folkow & Halicka, 1968). After the bout of Folkow stimulation the number of muscle spindle primary endings that did not have a maintained discharge after 'hold test' conditioning was reduced from approximately five in twenty to one in twenty.

Sinusoidal Threshold

Muscle spindle primary endings that had a maintained discharge did not have a threshold to small sinusoidal length changes within the reliable range of amplitudes available with the current equipment, that is, at amplitudes greater than 5 μm (Figure 5.4). A significant modulation of the afferent discharge, evident in the cycle histogram, to whole muscle sinusoidal length changes of less than 5 μm was observed for these primary endings. There was an approximately linear increase in SNR_{EXP} with increasing sinusoidal amplitude up to 50 μm after which the response increased less rapidly. It was therefore not possible to use these muscle spindles for stochastic resonance experiments, as a sub-threshold periodic stimulus is required.

Stochastic Resonance

Two muscle spindle primary endings and six muscle spindle secondary endings, chosen to have no maintained discharge after 'hold test' conditioning, were studied for stochastic resonance. All muscle spindles that were stimulated under the appropriate conditions, a sub-threshold periodic input and supra-threshold noise input, exhibited stochastic resonance.

The response of a muscle spindle primary ending to three different types of stimuli is illustrated in Figure 5.5. The instantaneous rate and resulting cycle histograms that were used to calculate SNR_{EXP} are shown for each response. A supra-threshold sinusoidal stimulus (Figure 5.5, left panel) resulted in a cycle histogram where the majority of action potentials occurred at about the same phase of the stimulus cycle and yielded a high SNR_{EXP} (3.36). A supra-threshold noise-alone stimulus (Figure 5.5, right panel)

111
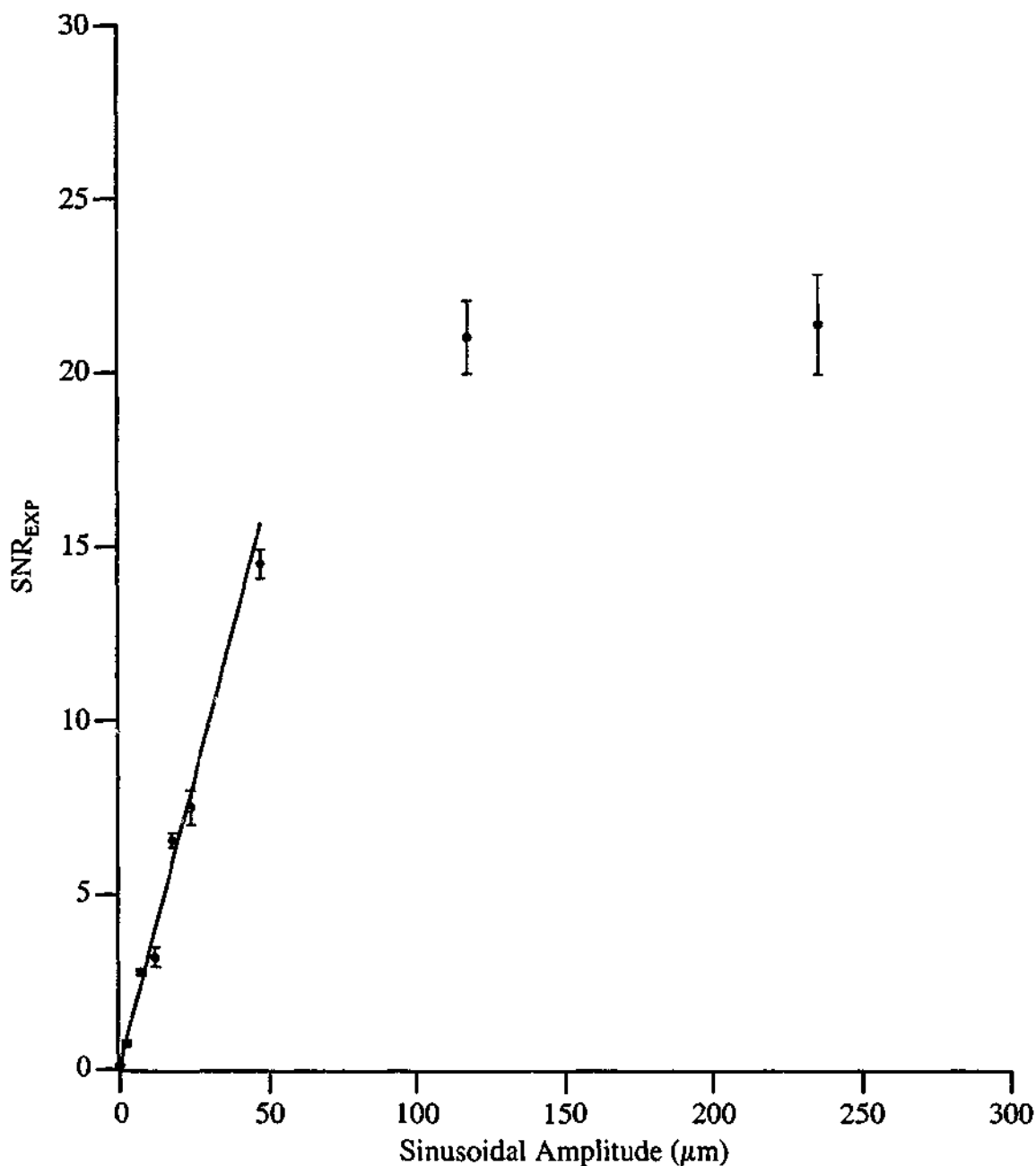
Figure 5.4   After 'hold test' conditioning the majority of muscle spindles have a resting discharge, and under these conditions the threshold to small sinusoidal length changes is below 5 μm (the limit of the equipment). Points are means ($\pm$ SEM) calculated from 10 repetitions of a 4.2 Hz sinusoidal length change to one muscle spindle. A straight line has been fitted to the response below 50 μm (r = 0.918). All measurements were taken at a test length of L_{MAX} − 10 mm.

resulted in a cycle histogram where the action potentials were evenly distributed across all phases of the stimulus and a low SNR_{EXP} (0.80). A sub-threshold sinusoidal stimulus and supra-threshold noise stimulus (Figure 5.5, middle panel) resulted in a cycle histogram with a significant modulation of the distribution of the action potentials across the different phases of the stimulus and a high SNR_{EXP} (5.23).

An example of the response of a muscle spindle primary ending that exhibited an optimal SNR_{EXP} with the addition of input noise is shown in Figure 5.6. The noise-alone response is shown in the bottom panel and is the average discharge rate during the 20 s of imposed noise-alone movement. The noise-alone threshold was approximately 100 μm, above which the average rate increased with increasing noise amplitude to reach a plateau of about 80 i/s (not shown). The noise-alone response was well fitted by the curve based on Kramers' rate, allowing for accurate predictions of D_{PRE}. For the three test frequencies used in the stochastic resonance protocol of 5.2, 9.6 and 26.1 Hz the predicted optimal noise amplitudes were 137, 172 and 297 μm respectively, indicated by the grey lines in the bottom panel of Figure 5.6.

There is a clear peak in SNR_{EXP} for each of the test frequencies used. Each point was calculated from 20 s of response. The responses are well fitted by logNormal curves and the optimal noise values were 55 ± 5 μm, 184 ± 6 μm and 456 ± 3 μm respectively ($D_{OPT} \pm$ SEM), indicated by the arrows in the upper panels of Figure 5.6. The increase of D_{OPT} with increasing sub-threshold periodic stimulus frequency is a key feature of stochastic resonance.

The response of a muscle spindle secondary ending to three different types of stimuli is illustrated in Figure 5.7. The instantaneous rate and resulting cycle histograms that were used to calculate SNR_{EXP} are shown for each response. A supra-threshold sinusoidal stimulus (Figure 5.7, left panel) resulted in a cycle histogram where the majority of action potentials occurred at about the same phase of the stimulus cycle and yielded a moderate SNR_{EXP} (1.45). A supra-threshold noise-alone stimulus (Figure 5.7, right panel) resulted in a cycle histogram where the action potentials were evenly distributed across all phases of the stimulus and a low SNR_{EXP} (1.23). A sub-threshold sinusoidal stimulus and supra-threshold noise stimulus (Figure 5.7, middle panel) resulted in a
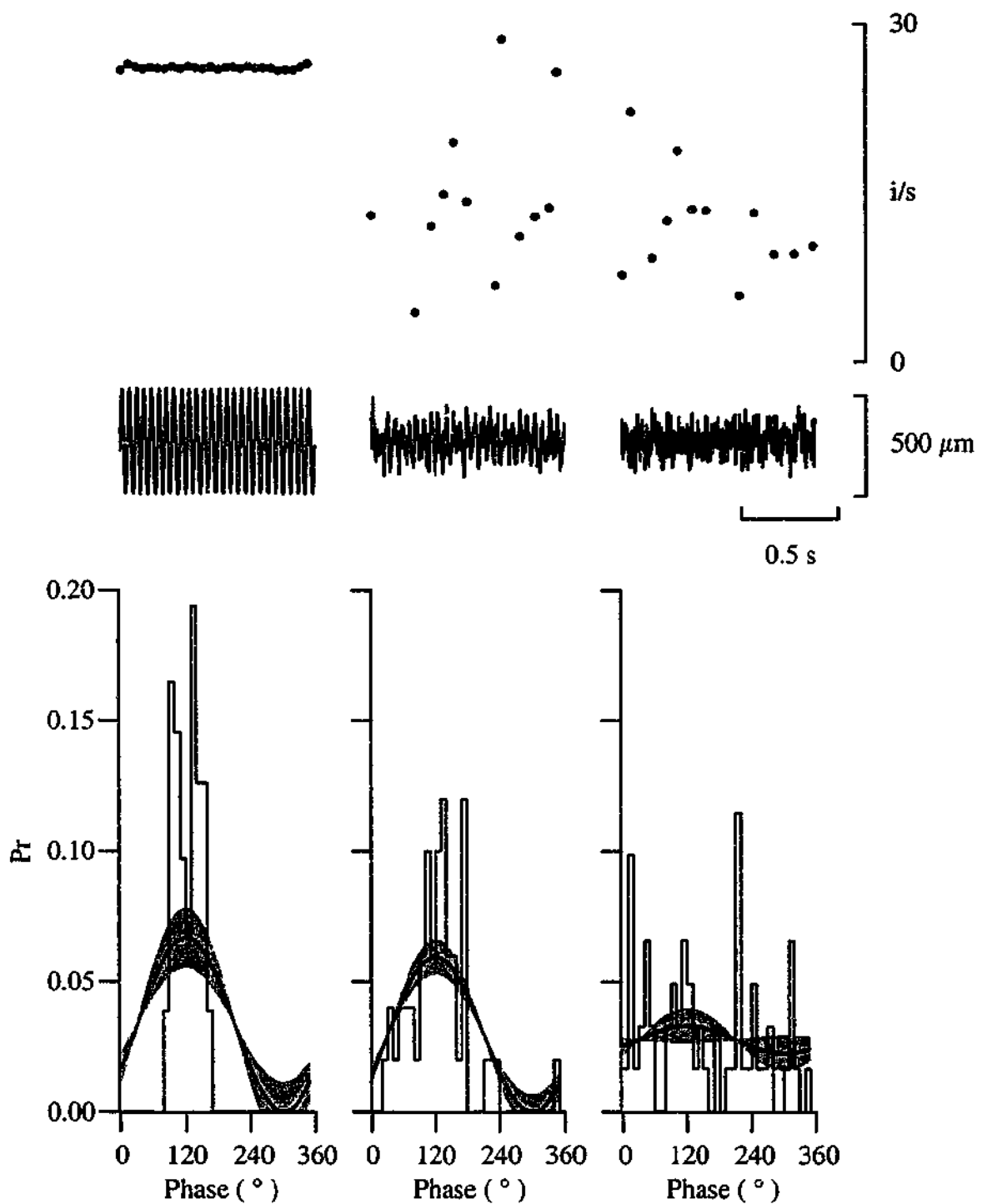
Figure 5.5 The response of a muscle spindle primary ending to a supra-threshold sinusoidal stimulus (260 μm at 26.1 Hz, left panel), a sub-threshold sinusoidal stimulus and supra-threshold noise stimulus (200 μm at 26.1 Hz with 200 μm of noise, middle panel), and to a noise-alone stimulus (200 μm of noise, right panel). In each panel the top trace is the instantaneous discharge rate of the receptor and the trace underneath is the imposed change in muscle length about a test length of L_{MAX} – 4.5 mm. The graph at the bottom of each panel is a cycle histogram that has been fitted with a sinusoid to determine SNR_{EXP}. The values of SNR_{EXP} for the three stimuli are 3.36 (supra-threshold sinusoidal stimulus), 5.23 (sub-threshold sinusoidal stimulus and supra-threshold noise stimulus) and 0.8 (noise-alone stimulus).
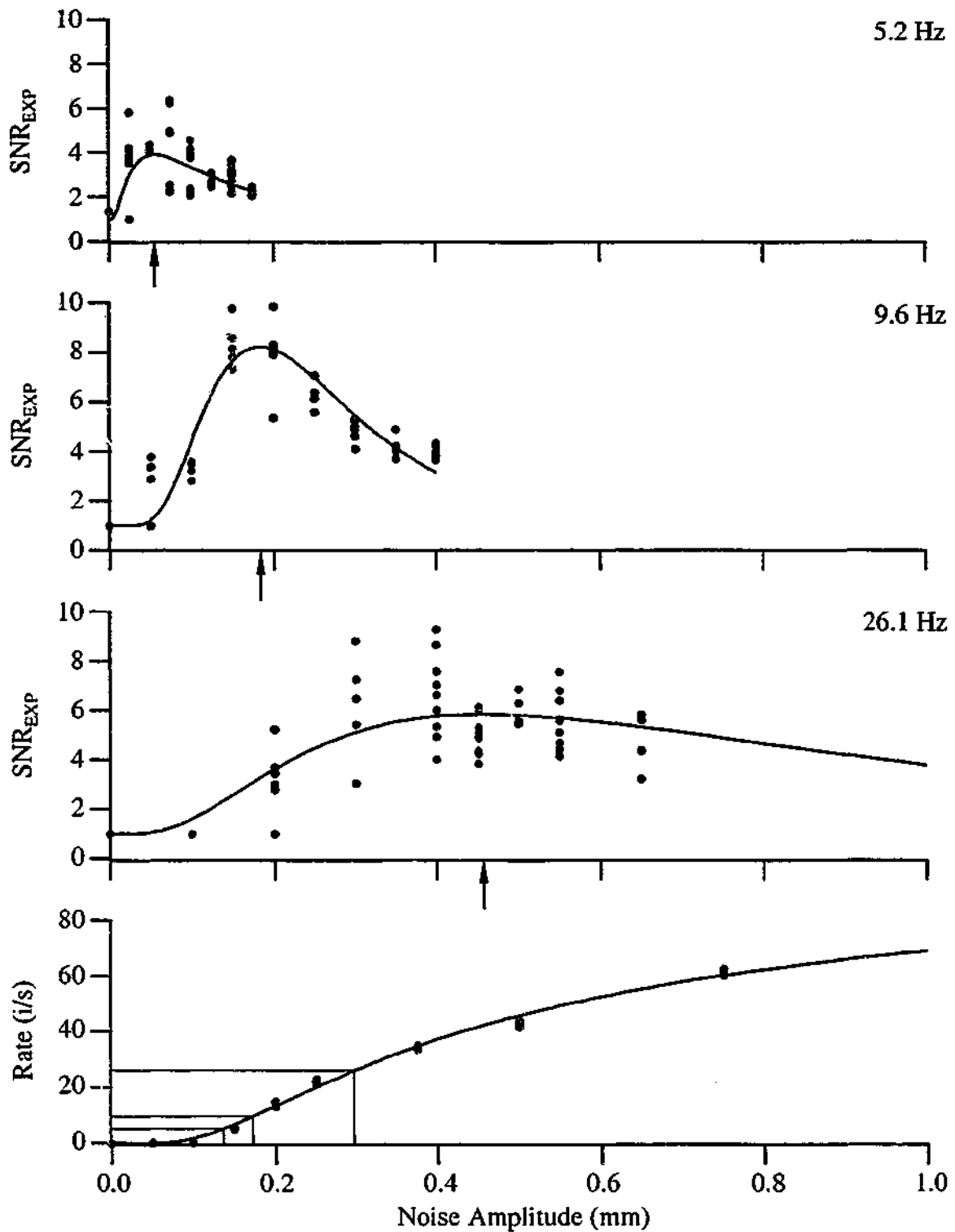
Figure 5.6 The response of a muscle spindle primary ending shows many of the characteristics of stochastic resonance. Each point is calculated from 20 s of response and the measurements were taken in a pseudo-random order. The blue symbol represents the data shown in Figure 5.5. The solid curves in the top three panels are logNormal curves that have been fitted to determine D_{OPT}, indicated by the arrows. The bottom panel is the noise-alone response, which has been fitted with a curve based on Kramers' Rate. They grey lines in the bottom panel indicate the predicted optimal noise value, D_{PRE}, for each test frequency.
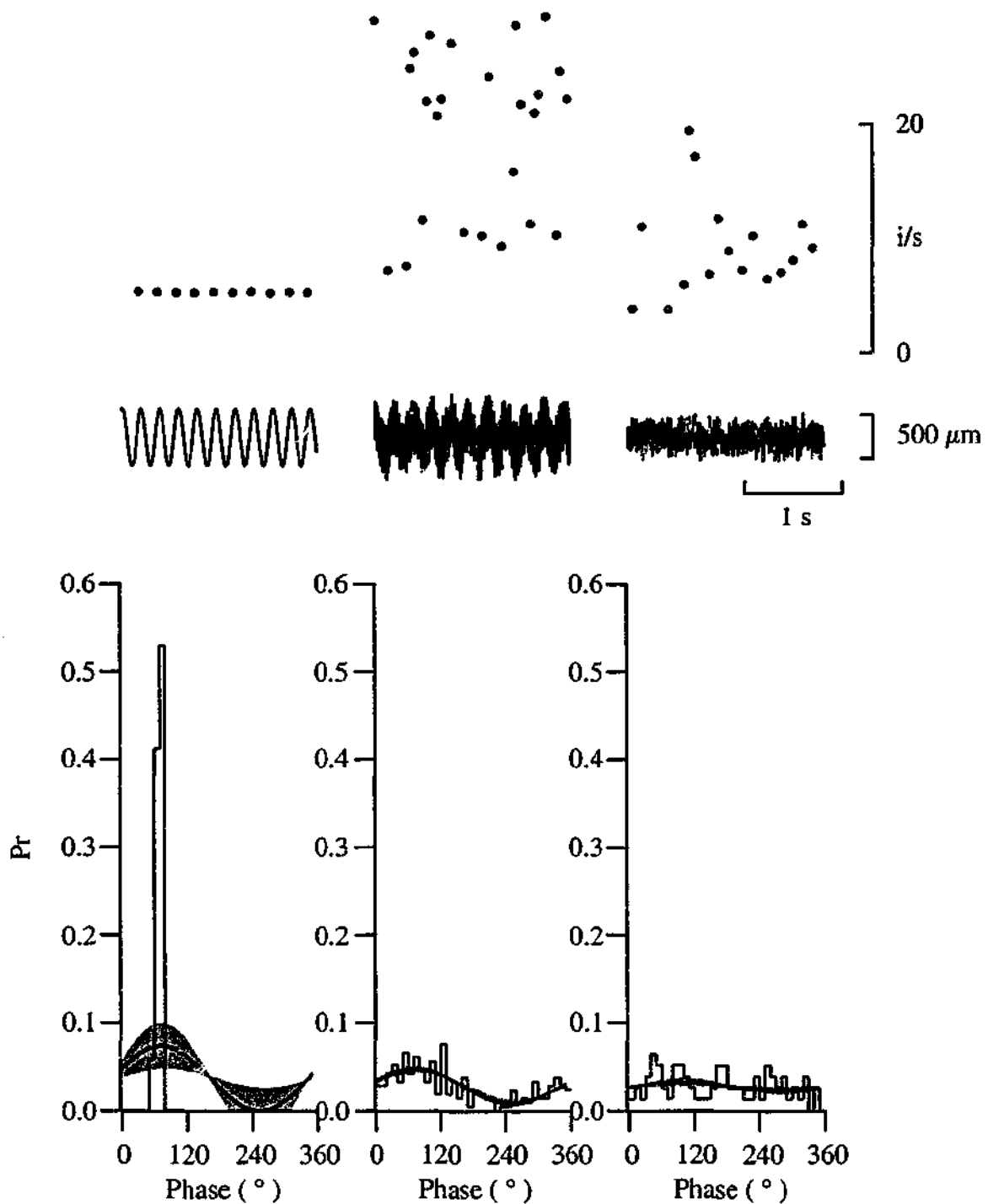
Figure 5.7   The response of a muscle spindle secondary ending to a supra-threshold sinusoidal stimulus (330 μm at 5.2 Hz, left panel), a sub-threshold sinusoidal stimulus and supra-threshold noise stimulus (165 μm at 5.2 Hz with 174 μm of noise, middle panel), and to a noise-alone stimulus (174 μm of noise, right panel). In each panel the top trace is the instantaneous discharge rate of the receptor and the trace underneath is the imposed change in muscle length about a test length of L_{MAX} − 1.5 mm. The graph at the bottom of each panel is a cycle histogram that has been fitted with sinusoids to determine SNR_{EXP}. The values of SNR_{EXP} for the three stimuli are 1.45 (supra-threshold sinusoidal stimulus), 6.50 (sub-threshold sinusoidal stimulus and supra-threshold noise stimulus) and 1.24 (noise-alone stimulus).

cycle histogram with a significant modulation of the distribution of the action potentials across the different phases of the stimulus and a high SNR_{EXP} (6.50).

Figure 5.8 is an example of the response of a muscle spindle secondary ending that exhibited an optimal SNR_{EXP} with the addition of input noise. The curves are similar to those for the muscle spindle primary ending, except the maximum noise-induced rate is approximately half that for the muscle spindle primary ending, as is the noise-alone threshold. For the two test frequencies of 1.04 and 5.2 Hz the predicted optimal noise levels were 53 and 87 μm respectively, indicated by the grey lines in the bottom panel of Figure 5.8. The corresponding values of D_{OPT} were 86 ± 2 μm and 126 ± 1 μm respectively (D_{OPT} ± SEM), indicated by the arrows in the upper panels of Figure 5.8. Again, the increase of D_{OPT} with increasing sub-threshold periodic stimulus frequency is a key feature of stochastic resonance.

The pooled results from all muscle spindles are presented in Figure 5.9. Each point is the measured optimal noise level (± SEM) plotted against the corresponding predicted optimal noise level. All the muscle spindle secondary endings and one of the muscle spindle primary endings were tested at two frequencies, while the remaining muscle spindle primary ending was tested at three frequencies, resulting in a total of 11 measurements. The data for each muscle spindle is joined to illustrate the correlation between D_{OPT} and D_{PRE} for each muscle spindle. The correlation between D_{OPT} and D_{PRE} for the pooled data was 0.699 (Pearson Product), indicating that there was a relationship between the predicted optimal noise and the measured optimal noise. The correlation between D_{OPT} and D_{PRE}, and therefore the dependence of D_{OPT} on the sub-threshold periodic stimulus frequency, is consistent with the hypothesis that the increase in SNR_{EXP} with additional noise is a result of stochastic resonance.

The low number of muscle spindles that exhibited stochastic resonance was a result of the low number of muscle spindles that, after 'hold test' conditioning, had a threshold for small sinusoidal length changes within the range of the equipment used. As with Golgi tendon organs (p. 98), muscle spindle primary and secondary endings with a maintained discharge, and therefore no clear threshold, did not exhibit stochastic resonance as illustrated by the example in Figure 5.10.
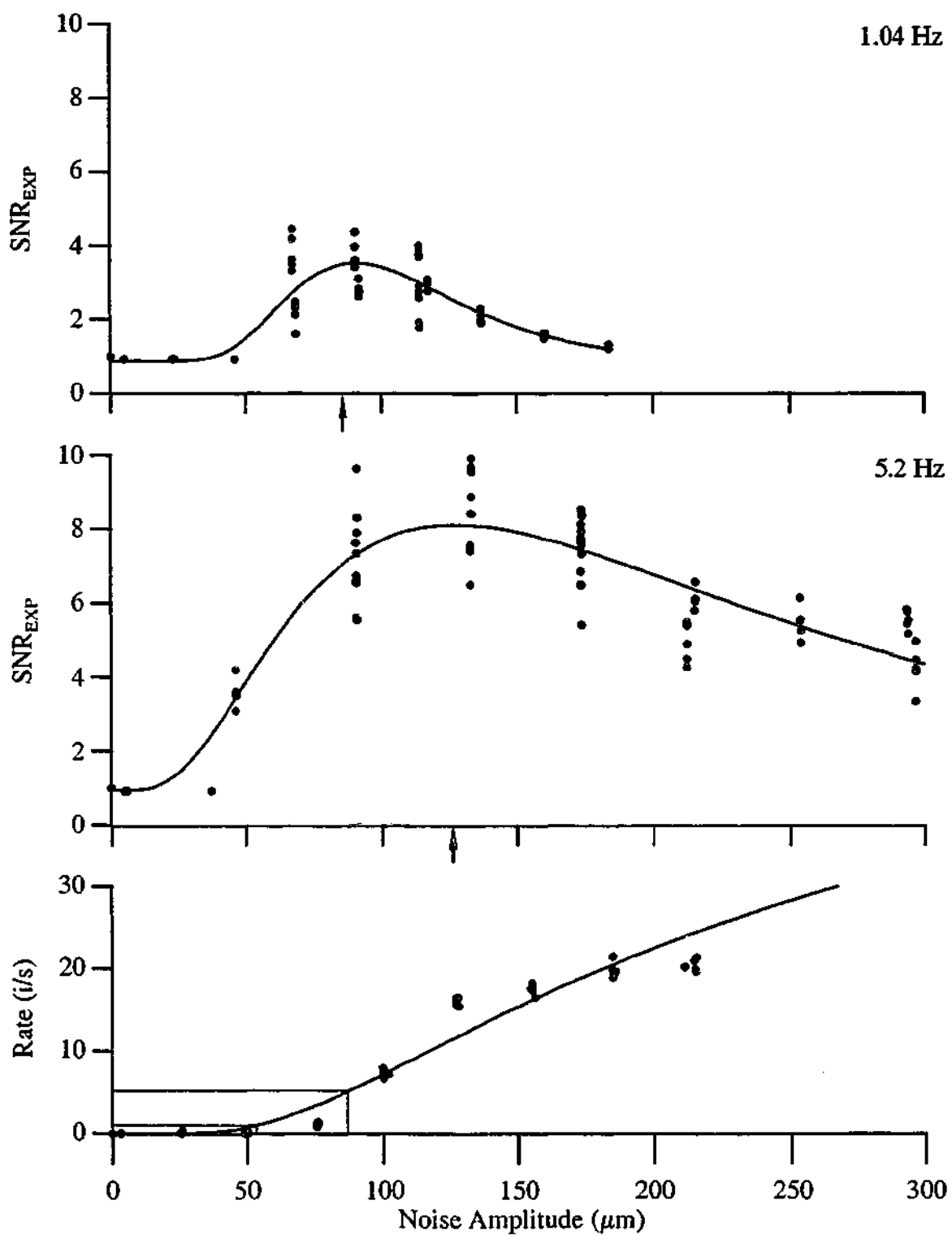
Figure 5.8 The response of a muscle spindle secondary ending shows many of the characteristics of stochastic resonance. Each point is calculated from 20 s of response and the measurements were taken in a pseudo-random order. The blue symbol represents the data shown in Figure 5.7. The solid curves in the top two panels are logNormal curves that have been fitted to determine D_{OPT}, indicated by the arrows. The bottom panel is the noise-alone response, which has been fitted with a curve based on Kramers' Rate. They grey lines in the bottom panel indicate the predicted optimal noise value, D_{PRE}, for each test frequency.
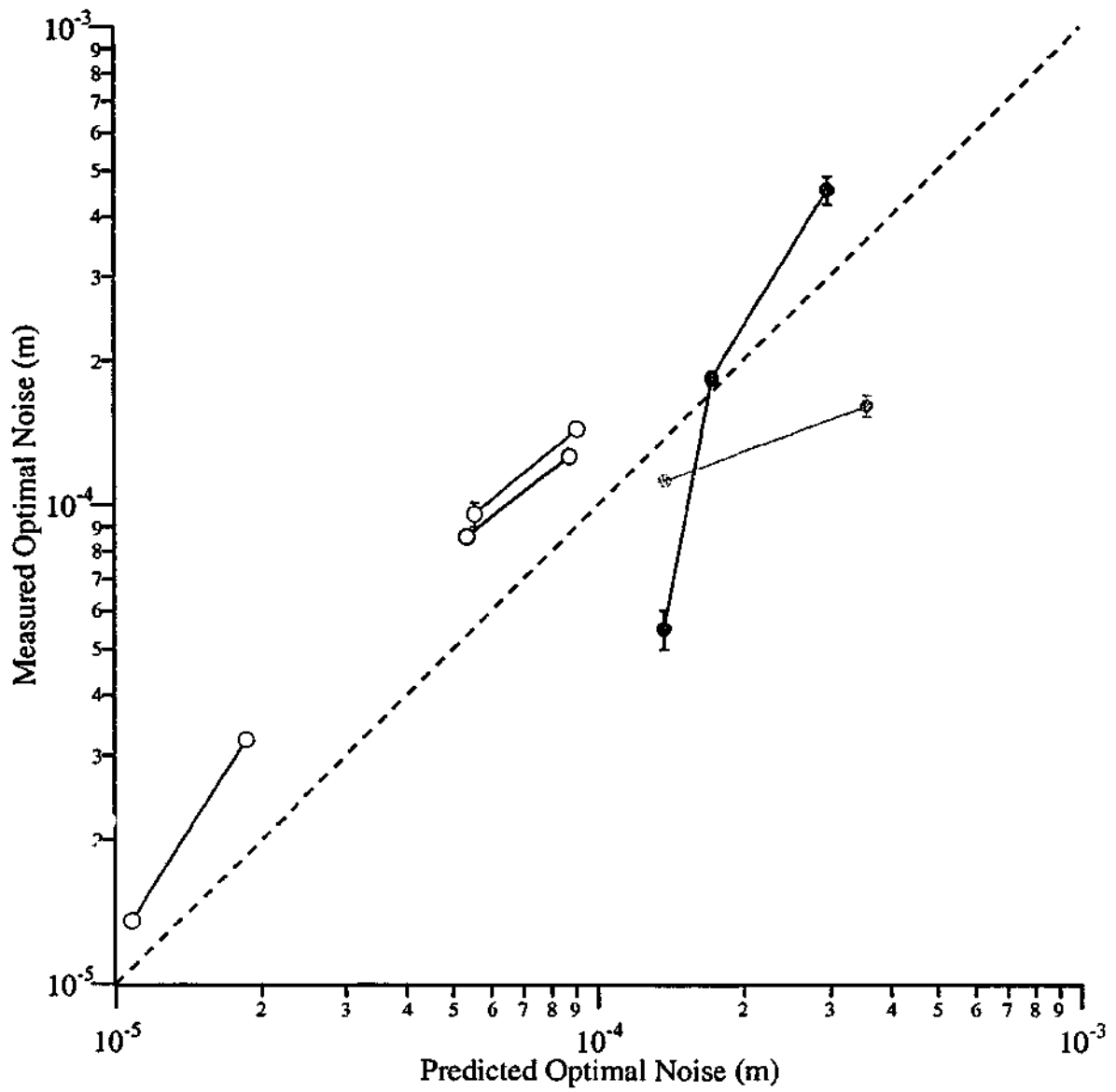
Figure 5.9   The pooled data from all muscle spindles that showed an optimal SRN_{EXP} with the addition of noise are scattered about the line of proportionality (dashed line) as predicted by stochastic resonance theory. Values shown are D_{OPT} and an estimate of the error in D_{OPT} plotted against D_{PRE}. The results for each muscle spindle are displayed in a different colour and joined to illustrate the correlation between D_{OPT} and D_{PRE} for each unit (filled symbols are Ias and open symbols are IIs). The muscle spindle primary ending illustrated in Figure 5.6 is shown in red and the muscle spindle secondary ending illustrated in Figure 5.8 is shown in blue.
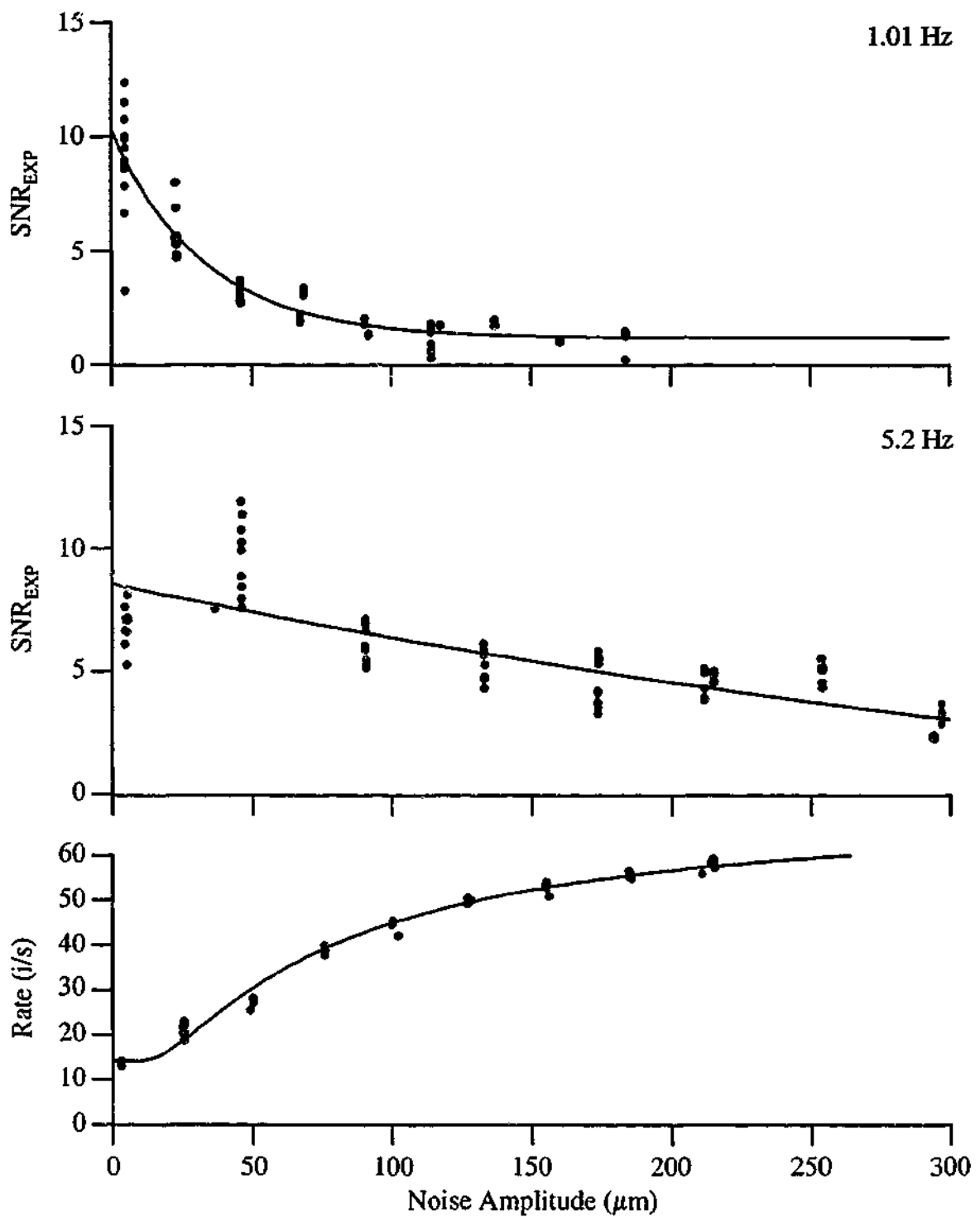
Figure 5.10   The response of a muscle spindle secondary ending with a resting discharge to a supra-threshold periodic input and noise shows none of the characteristics of stochastic resonance. The SNR_{EXP} is a monotonically decreasing function of the input noise. Each point is calculated from 20 s of response and the measurements were taken in a pseudo-random order. The solid curves in the top panels are exponential curves that have been fitted to the data. The bottom panel is the noise-alone response, which has been fitted with a curve based on Kramers' Rate.

Aperiodic Stimuli

The average discharge rate of a muscle spindle primary ending increases as a result of a 1 mm ramp-and-hold stretch (Figure 5.11, top panel). The increase in average rate, as a result of the ramp-and-hold stretch, passes through a maximum with the addition of noise to the movement signal (Figure 5.11, second panel). The increase in rate with various levels of input noise has a similar shape to the stochastic resonance plots shown in Figure 5.6 and Figure 5.8, and is well fitted by a logNormal curve. The effect, however, cannot be stochastic resonance, as the input signal, a ramp-and-hold stretch, is not periodic.

The effect is a result of the increase in dynamic sensitivity of the muscle spindle primary ending at longer muscle lengths. The noise-alone response of the primary ending is similar at both muscle lengths, $L_{MAX} - 6$ mm and $L_{MAX} - 5$ mm (Figure 5.11, bottom panel), with the average rate increasing with increasing noise amplitudes to a plateau at approximately 180 i/s. However, the response plateaus with a smaller amount of additional noise at the longer muscle length, as a result of the muscle spindle's increased dynamic sensitivity.

The third panel of Figure 5.11 illustrates the difference between the two noise-alone responses that are shown in the bottom panel of Figure 5.11. The shape of the difference between the noise-alone responses at $L_{MAX} - 6$ mm and $L_{MAX} - 5$ mm is similar to the response to a ramp-and-hold stretch. This is to be expected, as the difference between the noise-alone responses approximates the response to an infinitely slowly ramp-and-hold stretch. The differences between the curves in the second and third panels of Figure 5.11 are likely to be the result of transient changes in sensitivity that result in a further increase in dynamic sensitivity immediately after a ramp-and-hold stretch.

Psychophysical Experiments

A total of three adult human subjects of both genders were used for psychophysical experiments to seek evidence for stochastic resonance in elbow movement detection. All experiments were performed with approval from the Monash University Standing Committee on Ethics in Research on Humans.

400 i/s
0

1 mm

2 s

40
30
20
10
0

Increase in Rate (i/s)

50
40
30
20
10
0
-10

Rate Difference (i/s)

200
150
100
50
0

Average Rate (i/s)

0.0   0.1   0.2   0.3   0.4   0.5
Noise Amplitude (mm)
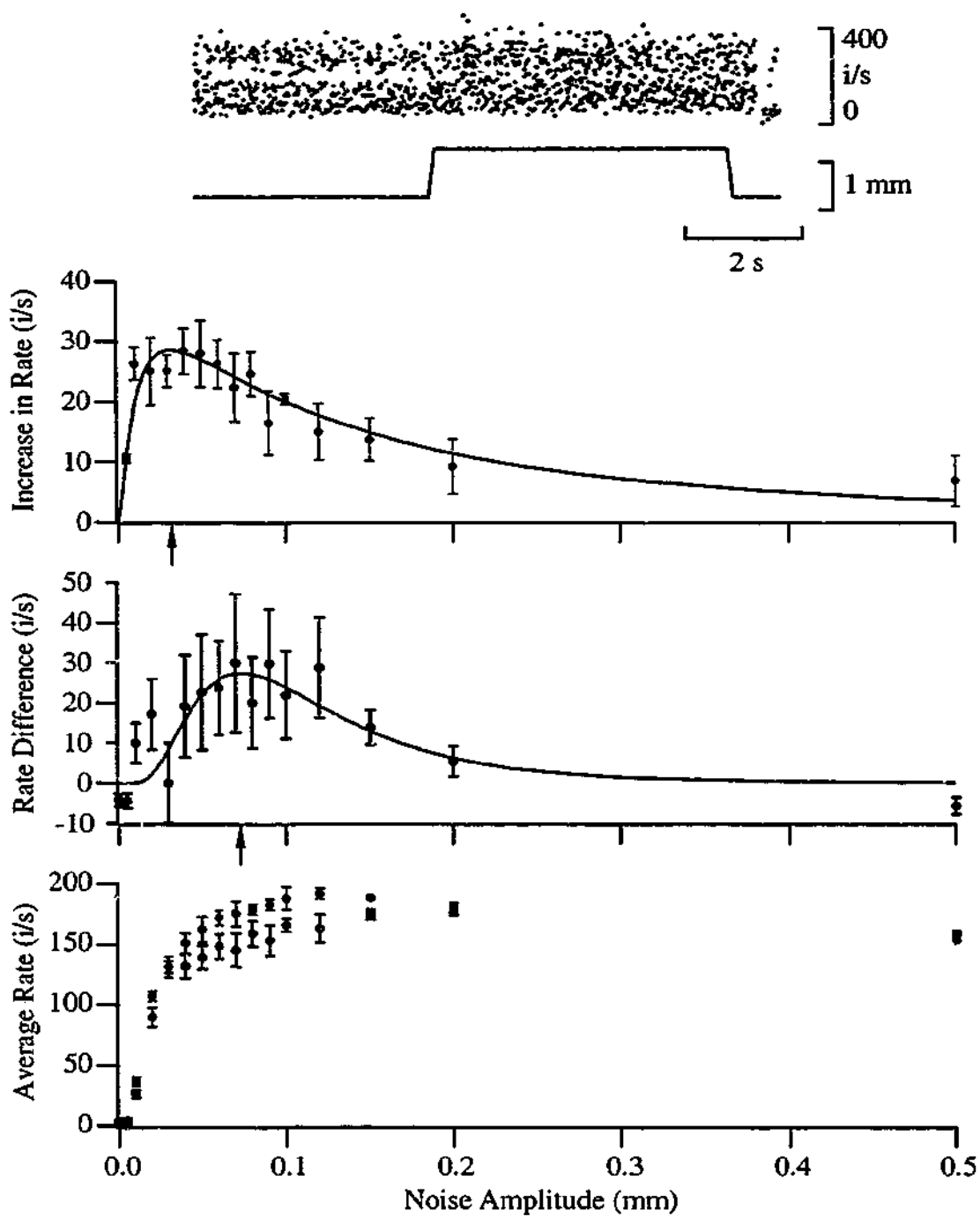
Figure 5.11   The response of a muscle spindle primary ending to ramp-and-hold stretches with various levels of additional input noise was examined using the protocol illustrated in the top panel. The response was measured as the increase in the average discharge rate during the last 2 s of the hold phase, over the average rate in the 2 s prior to the stretch. The increase in average rate as a result of the stretch was maximised by the addition of 30 μm of noise (second panel). Each point is the mean $\pm$ SEM for seven ramp and hold stretches with various levels of additional noise that were performed in a pseudo-random order. The noise-alone response (bottom panel) plateaus at approximately 180 i/s for the two test lengths of and $L_{MAX} - 6$ mm (●) and $L_{MAX} - 5$ mm (●), corresponding to the length before and after the stretch. The third panel from the top is a plot of the difference between the noise-alone responses at the two lengths. The solid curves in the middle two panels are logNormal curves that have been fitted to determine D_{OPT}, indicated by the arrows.

Materials and Methods

Subjects were blindfolded and seated comfortably with their right arm held in the horizontal plane in front of them. The forearm was held in a pronated position by an adjustable cuff, positioned just above the wrist, while the upper arm rested on a cushioned support. A horizontal lever attached to the cuff near the wrist was connected to an electro-magnetic position controller. This configuration limited movements to controlled rotation of the forearm about a vertical axis through the elbow joint.

Equipment

The electro-magnetic position controller was controlled by a data acquisition card (PCI-MIO-16E-4, National Instruments Corporation, Austin, Texas, U.S.A.) in a G3 desktop computer (Macintosh, Cupertino, California, U.S.A.) running Igor Pro (WaveMetrics, Lake Oswego, Oregon, U.S.A.). This combination of equipment is the same as that used for the multi-channel recorder used for the previous stochastic resonance experiments.

Experimental Protocol

All measurements were performed about the 90° mid-position and followed a co-contraction of both biceps and triceps, 'hold test' conditioning (Wise et al., 1998). The threshold of detection for small sinusoidal changes in elbow joint angle was measured using a modified staircase technique (Cornsweet, 1962). The staircase technique is illustrated in Figure 5.12 (bottom panel) and begins with the application of a sinusoidal test movement known to be readily detectable by the subject.

The sinusoidal test movement (Figure 5.12, top panel) consisted of 14 s of sinusoidal movements, which had been constructed to eliminate any sudden changes of velocity at the beginning or end of the movement. The smooth transition into the sinusoidal movement was required to eliminate the possibility that the subject was using the initial component of acceleration as a detection cue. An aural indication of the frequency of the sinusoidal movements was given to the subject during each test stimulus. The aural cue was a constant pitch tone the volume of which was modulated at the same frequency as the test movement. The aural cue was not phase-locked to the movement,
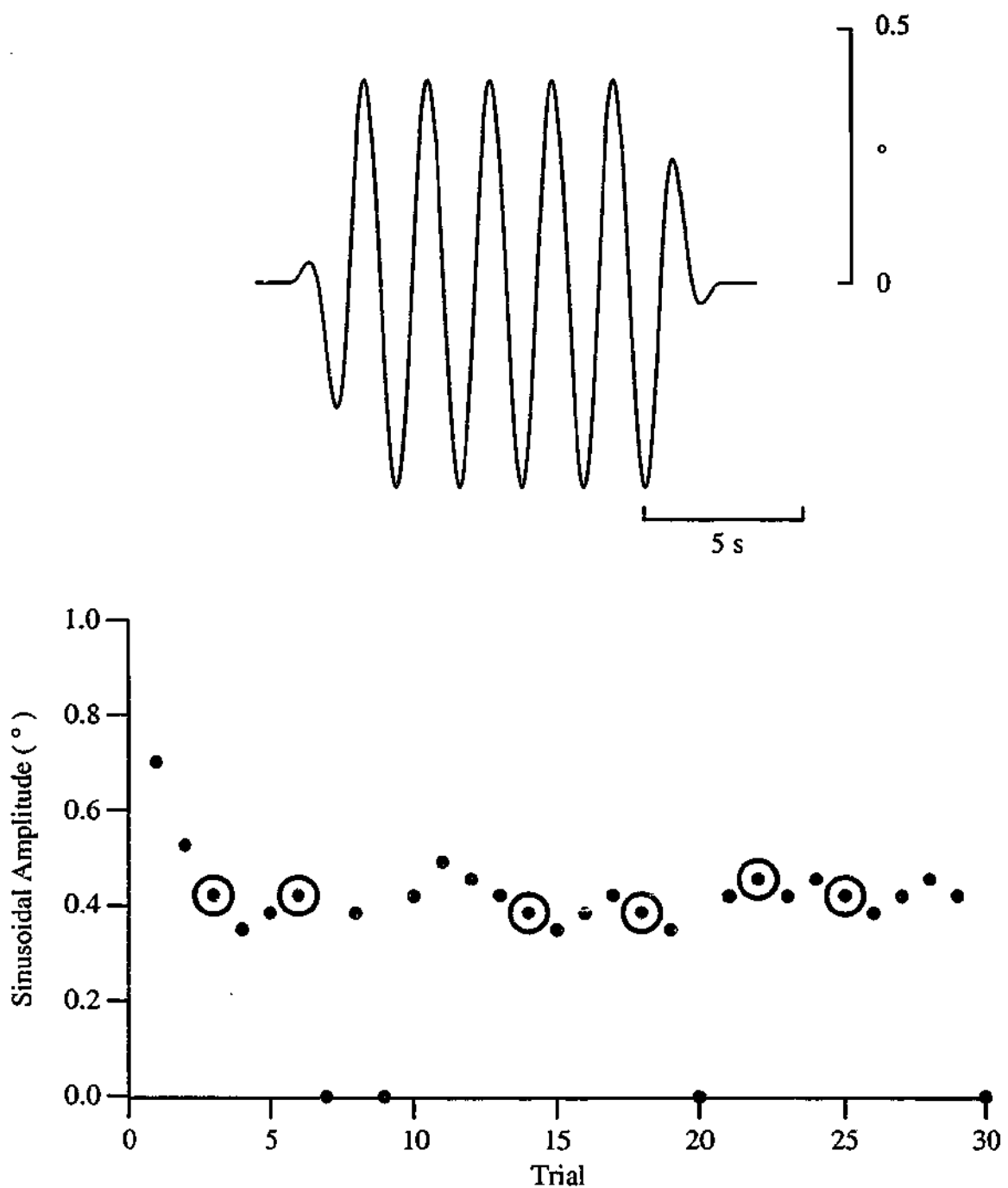
Figure 5.12 The test movement used during the psychophysical experiments on elbow movement detection consisted of 14 s of sinusoidal movement that had been shaped to remove any abrupt start and stop that may have served as a cue for the subject (top panel). The detection threshold was determined using the staircase technique (bottom panel). The amplitude of the sinusoidal stimulus was decreased following a correct detection (●), or increased if not detected (●). The series of amplitudes corresponding to a minimum correct detection (blue outlined circles) can then be used to determine the threshold, in this case 0.41 °. Trials 7, 9, 20 and 30 were presentations of a zero amplitude sinusoid.

although the relative phase of the cue to the movement was constant throughout an experimental session. The aural cue allowed the subject to distinguish between random movements (noise) and the sinusoidal movements that were synchronised to the aural cue.

The subjects were instructed to verbally report if they had felt a sinusoidal movement that was of the same frequency as the aural cue. If unsure of the presence of a sinusoidal movement the subjects were instructed to indicate that no sinusoidal movement had occurred. A supra-threshold noise-alone movement was present to familiarise the subjects with a noise-alone movement, that in future they should report as not containing any sinusoidal movement. The subjects were required to respond within 30 s of the end of the test movement, but often responded before the cessation of the test movement.

Null presentations, consisting of a zero amplitude sinusoid but with all other conditions the same, were used as a control measure. Any trial with more than 5 % of reports of the presence of a sinusoidal movement in response to a Null presentation, a false positive, were excluded from the analysis.

Starting with a test movement known to be readily detectable, in successive trials the amplitude of the sinusoidal movement was reduced until it was no longer detectable by the subject. The amplitude of the sinusoidal movement was then increased in successive trials until it was again detectable. The procedure was repeated several times to determine a series of minimum amplitude detection points, indicated by the blue outline circles in the bottom panel of Figure 5.12.

Threshold measurements were taken with various amplitudes of additional input noise. Noise trials were interleaved with no-noise trials. The threshold amplitude for sinusoidal movement was calculated by averaging the smallest sinusoidal amplitudes that resulted in a correct detection, indicated in Figure 5.12 (bottom panel) by the blue outline circles. Only the minimum correct detection points were used rather than turning points as used by Cornsweet (1962) because it was possible for lapses in concentration to result in the subject not detecting the movements. In such a case the turning points would become biased towards larger amplitude sinusoids, which were not a true

indication of the subjects detection threshold. In the experiments where the subjects did not show such behaviour (Figure 5.12, bottom panel), using the minimum correct detection points resulted in a similar threshold value to the value determined using the turning points. For the trial illustrated in Figure 5.12 (bottom panel) the resulting threshold measurement is $0.42 \pm 0.01°$ compared to 0.41 ± 0.01 using the turning points.

Results

Three healthy young subjects participated, two males and one female, aged 20-28 years, all free from any known neurological disorders. The addition of broad-spectrum noise increased the detection threshold for small sinusoidal changes in elbow joint angle for the subject illustrated in Figure 5.13 and for all of the subjects tested.

Discussion

Animal Experiments

Muscle spindle primary and secondary endings exhibit an optimal output SNR with the addition of input noise when stimulated under the appropriate conditions of a sub-threshold periodic signal and a supra-threshold noise signal. This effect is likely to be stochastic resonance as the optimal noise amplitude increases with increasing sub-threshold periodic stimulus frequency, which is a feature unique to stochastic resonance. As with the Golgi tendon organs, the measured optimal noise amplitudes were not precisely those predicted from the noise-alone response, but there was a correlation between the predicted and measured optimal noise amplitudes.

When stimulated under the appropriate conditions both muscle spindle primary and secondary endings may exhibit stochastic resonance, although the majority of muscle spindle primary endings did not exhibit stochastic resonance. The majority of muscle spindle primary endings in the soleus muscle have a maintained discharge after a fusimotor strength contraction at the test length, a 'hold test' conditioning. Under these conditions muscle spindle primary endings respond to sinusoidal length changes of less than 5 μm (the smallest reliable movement available using our equipment). Therefore, these muscle spindle primary endings were not capable of exhibiting stochastic
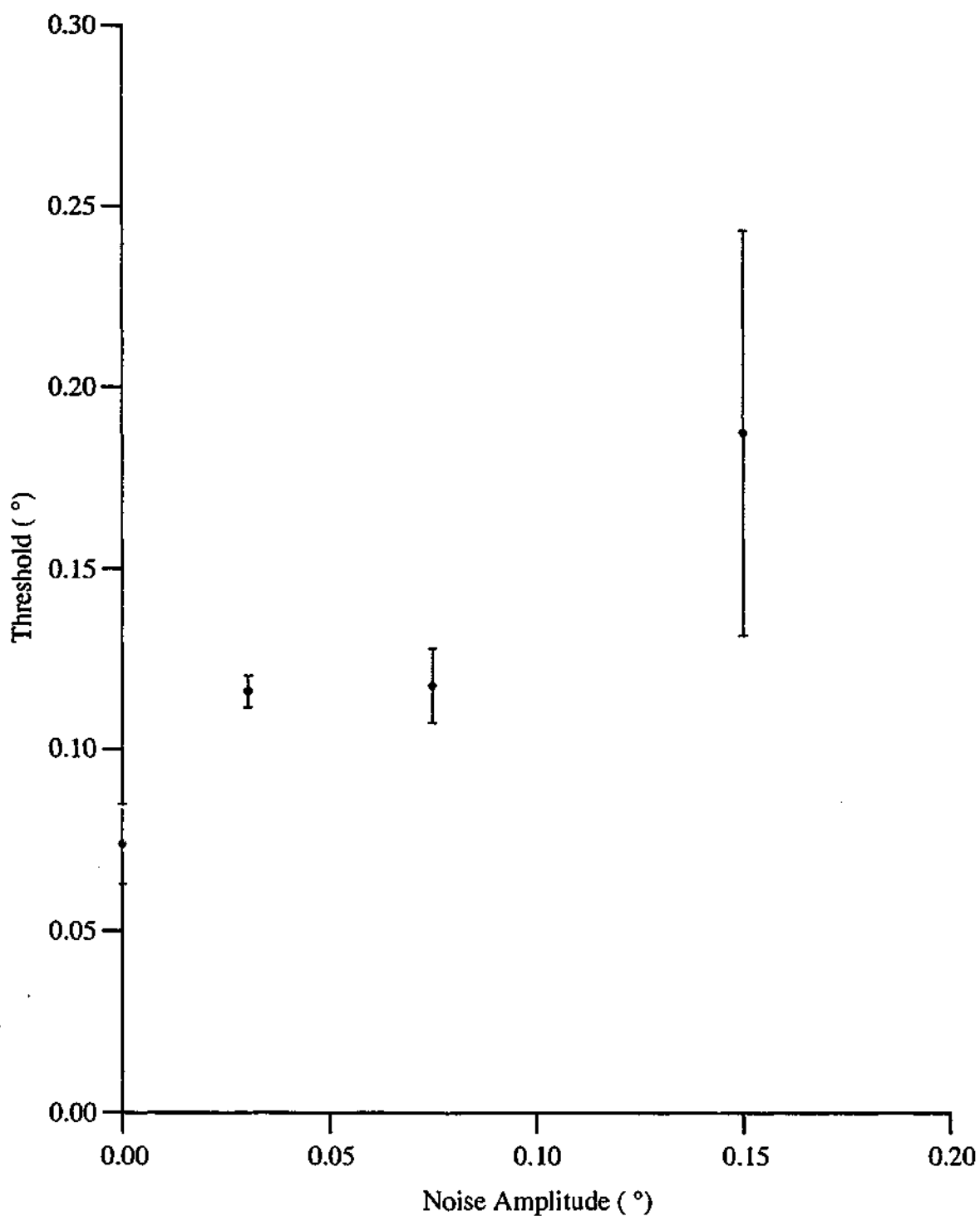
Figure 5.13 The minimum detection threshold for small sinusoidal changes in elbow joint angle occurs in the absence of additional input noise. For the subject shown the minimum detection threshold for the 0.5 Hz sinusoidal stimulus used was 0.07 °. Each point is the mean (± SEM) from a threshold measurement like the one illustrated in Figure 5.12.

resonance under the current experimental conditions. It is possible that with equipment capable of producing smaller sinusoidal length changes it may be possible to use a sub-threshold sinusoidal stimulus, and therefore most likely observe stochastic resonance.

'Hold long' conditioning would be expected to introduce a threshold for small sinusoidal length changes, and therefore it may be tempting to use 'hold long' conditioning for the stochastic resonance studies. The threshold produced by the 'hold long' conditioning would also be expected to produce an increased threshold for the noise-alone stimulus. As stochastic resonance requires the addition of supra-threshold noise to optimise the system's response, the noise levels required to observe stochastic resonance would result in a change of the conditioning of the intrafusal muscle fibres. The supra-threshold noise stimuli would 'undo' the 'hold long' conditioning, leaving the muscle spindle in an ill-defined condition. Therefore, it is not possible to use 'hold long' conditioning to introduce an artificial threshold in order to observe stochastic resonance.

The linear response of the muscle spindle primary endings to sinusoidal movements below 50 μm (Figure 5.4) is likely to have the same origins as the linear region reported by Matthews & Stein (1969). Although Matthews & Stein (1969) used a decerebrate preparation that had some level of 'spontaneous' fusimotor activity, it is likely that the main effect of the fusimotor activity would have been to maintain a 'hold test' conditioning. Therefore, the short linear region is likely to correspond to the region of elastic deformation of the stable cross-bridges.

Movements large enough to break the stable cross-bridges would be expected to result in a dramatic decrease in the stiffness of the polar regions of the intrafusal fibres, so that a smaller portion of the imposed length change would take place in the equatorial region. Therefore, noise-alone movements larger than the limit of elastic deformation of the stable cross-bridges would be expected to result in a decrease in SNR_{EXP} as a result of decreasing the stiffness of the polar regions of the intrafusal fibres. That the optimal noise levels were up to 400 μm indicates that stochastic resonance effects can overcome the reduction in sensitivity due to mechanical changes and even increase the sensitivity of the muscle spindle under these conditions.

Muscle spindle primary endings that did not have a maintained discharge after 'hold test' conditioning, and therefore exhibited a threshold, may have had depressed responses from an inadequate blood supply. After whole muscle stimulation designed to increase blood flow, 15 pps for 1 min (Folkow & Halicka, 1968), the majority of previously silent muscle spindles had a maintained discharge. This type of stimulation reduced the number of muscle spindle primary endings without a maintained discharge after 'hold test' conditioning from approximately five in twenty to less than one in twenty. Therefore, under the current experimental conditions the number of muscle spindles that would exhibit a threshold for sinusoidal movements, and hence possibly stochastic resonance, is very small, as few as one in twenty, or perhaps less.

The role of stochastic resonance in determining the response of muscle spindles is dependent on the condition of the muscle spindle. If the muscle spindle has a threshold for small periodic length changes, then it is possible that stochastic resonance could be used to detect an otherwise sub-threshold periodic signal. If, however, the muscle spindle has a maintained discharge, which was found to be the case for the majority of muscle spindles investigated, then it does not appear possible for stochastic resonance to occur and any additional input noise will result in a reduction in sensitivity. It appears therefore, that the muscle spindle receptors perform optimally under conditions of low external noise as a result of their maintained discharge.

Psychophysical Experiments

The detection threshold of small changes in angle of the elbow joint was increased with the addition of any amount of extra input noise. It is interesting that stochastic resonance does not appear to play a role in kinaesthesia at the elbow joint given that stochastic resonance can occur in individual muscle spindles of the cat. Cat muscle spindles are believed to be similar to human muscle spindles that are generally accepted as contributing to this sense (McCloskey, 1978).

There are several possibilities as to why stochastic resonance was not observed. It is possible that the noise levels used in these experiments were too large, which would be expected to result in an increase in threshold even if stochastic resonance did occur. However, the amplitudes of noise used were similar to the detection threshold, which

would be expected to be near optimal noise levels, as this was found to be the case for individual muscle spindles of the cat. It is therefore unlikely that stochastic resonance does occur in the detection of small changes in angle of the elbow joint but was simply not observed.

Individual muscle spindles with a maintained discharge did not exhibit stochastic resonance, as they responded to sinusoidal length changes of less that 5 μm, the limits of our equipment. After a voluntary conditioning co-contraction the majority of human muscle spindles would have a maintained discharge (Wilson et al., 1995). Under these conditions it may be that the majority of muscle spindles did not have a threshold to the movements available with our equipment (minimum amplitude movement of 0.003°). If this were the case then it would be expected that these muscle spindles would not exhibit stochastic resonance.

Interestingly, although individual muscle spindles may not have been stimulated with a sub-threshold periodic stimulus, it was still possible for the stimulus to be below the detection threshold for the subject. The detection threshold of the movement is likely to involve the response of a population of muscle spindles, as the stimulation of a single muscle spindle afferent is not consciously perceived (Macefield et al., 1990). Therefore, there must be some level of processing within the central nervous system to generate the population response, which includes the introduction of the threshold. Any individual muscle spindles that did exhibit stochastic resonance would be expected to be in the minority. Therefore, the increase in information available via the stochastic resonance effect in individual muscle spindles would be counteracted by the decrease in information from the other muscle spindles in the population that did not exhibit stochastic resonance.

It is also possible that the muscle spindles were capable of exhibiting stochastic resonance, but that the central nervous system did not process the afferent information in such a way that the extra information, available via the stochastic resonance effect, could be used in the detection task. The processing involved requires averaging the response from several cycles of the periodic stimulus. The averaging can either be done over several periods with a few muscle spindles or over a much shorter time with many

muscle spindles. It is possible that the central nervous system does not perform the type of analysis required to effectively average the afferent information and extract the periodic information. Although this is unlikely, as the central nervous system appears to create a population response, which would be sufficient to perform the averaging provided the population response was constructed from enough individual muscle spindles.

The threshold introduced by the processing required to create the population response may be a possible site where stochastic resonance could occur. As the modelling of a simple network of Hodgkin-Huxley neurones demonstrated, the combination of a periodic train of pulses with trains of random pulses can exhibit stochastic resonance (p. 58). It is possible that such a situation may have occurred with the elbow detection task, with some muscle spindles preferentially responding to the sinusoidal movement, while others preferentially responded to the noise movement. However, no such effect was observed. Again it is possible that the central nervous system simply does not perform the appropriate processing to extract the extra information available via stochastic resonance. Alternatively it may be that the intrinsic noise within the sensory system, including membrane and synaptic noise, may already have been optimal for the detection of the small sinusoidal changes in angle. If this were the case then any additional mechanical noise would result in an increase in detection threshold, as observed.

Although muscle spindles are capable of exhibiting stochastic resonance under limited conditions, it does not appear that stochastic resonance occurs during elbow movement detection tasks. Whether this is a result of the central nervous system not being capable of performing the necessary processing required to utilise the extra afferent information available via stochastic resonance is not clear. It may be that the muscle spindles were simply not stimulated under the appropriate conditions, and therefore could not exhibit stochastic resonance, or the task was too difficult for the subjects to perform.

Chapter Six

Cutaneous Mechanoreceptors

The afferent innervation of the skin varies from region to region, with rich innervation of some regions, such as the fingertips and the face, and poor innervation of other regions, such as the posterior aspect of the trunk (Catton, 1976). A variety of cutaneous mechanoreceptors are situated in the epidermis, dermis and through to the subcutaneous tissues. Each kind of mechanoreceptor selectively responds to a particular form of mechanical stimulation. The responses from these mechanoreceptors give the senses of touch, pressure and vibration.

The experiments in this chapter focus on the slowly adapting Type I (SAI) cutaneous mechanoreceptors of the cane toad and psychophysical experiments that were designed to preferentially stimulate the slowly adapting mechanoreceptors in hairy skin of the back of the hand. The slowly adapting receptors were chosen as the focus of the experiments to complement the earlier experimental results with the slowly adapting receptor in muscle, the muscle spindles and Golgi tendon organs.

Structure

Mammalian

Slowly adapting Type I cutaneous mechanoreceptors in the hair skin of mammals, including primates, are composed of an epidermal dome overlying several Merkel cells lying along the basement membrane. Each cell receives a branched terminal from the innervating myelinated axon (Figure 6.1). Merkel cells were first described in 1875 in the epidermis of the avian bill (Merkel, 1875). Since then similar receptors have been described in both glabrous and hairy skin of mammals (Iggo & Muir, 1969).

The slowly adapting Type I cutaneous mechanoreceptors in the hairy skin have a highly localised sensitivity that is restricted to the raised dome, although an individual afferents may innervate several receptors. The dermal core of the dome is composed of a dense mesh of fine collagen bundles, while the surrounding dermis is composed of a looser mesh of larger collagen bundles. The increased stiffness of the receptive dome, as a
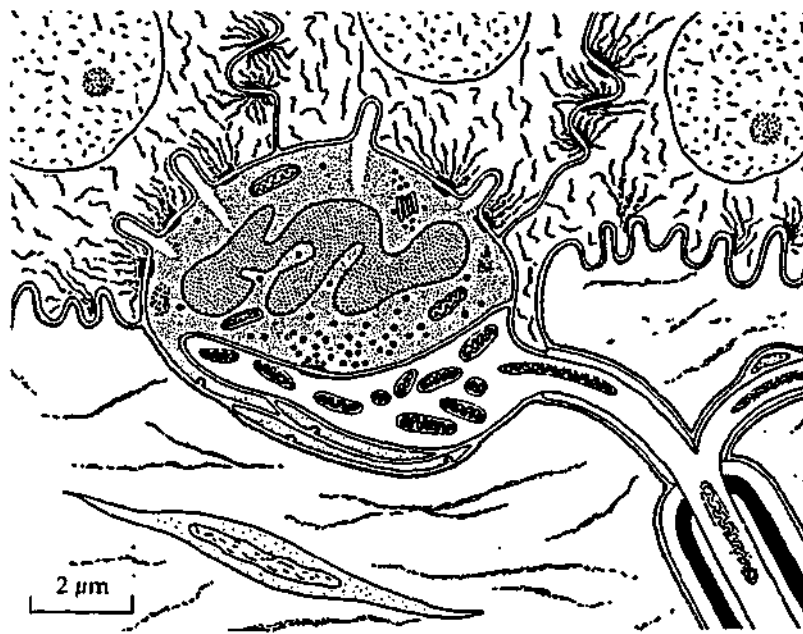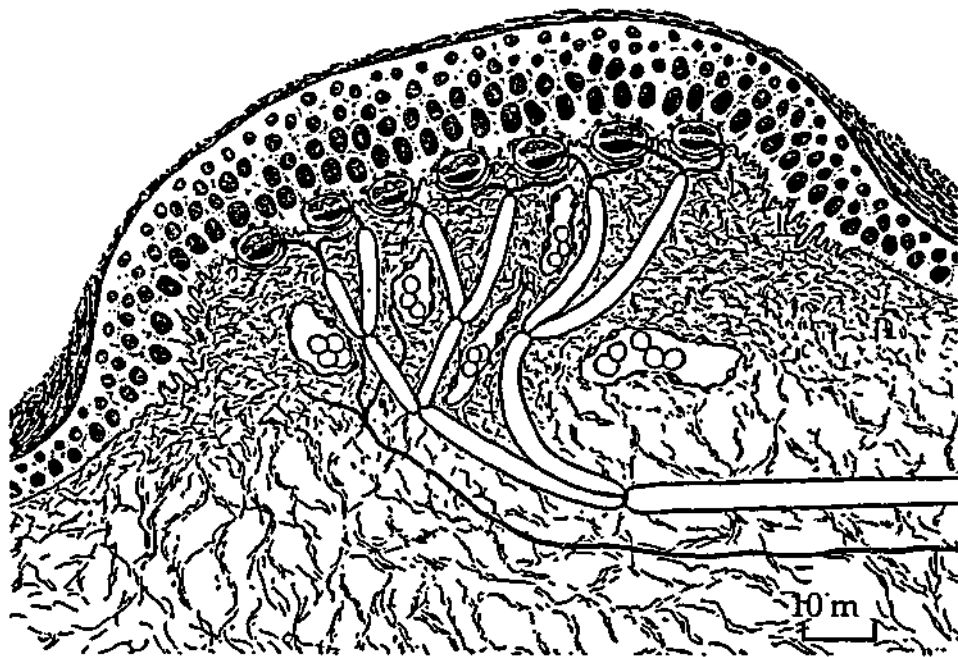
Figure 6.1 The slowly adapting Type I mechanoreceptors of the cat skin are composed of Merkel cells (speckled cell in bottom panel) that are in contact with terminal branches of the myelinated afferent (white, bottom panel). Each receptor is composed of several Merkel cells that are all innervated by a single myelinated afferent (top panel). The dermal core of the raised dome is composed of a dense mesh of fine collagen bundles that provide effective mechanical isolation of the receptor from surrounding tissue (adapted from Figure 1 of Iggo & Muir, 1969).

result of the denser mesh of collagen, results in effective mechanical isolation of the receptor from the surrounding dermis. The effective stimulus for the receptor is mechanical indentation of the raised dome, as stretching of the surrounding skin, even to the extent of causing displacement of the dome, fails to stimulate the receptor.

The Merkel cells are anchored within the dermis by rod-lie cylindrical cytoplasmic processes. A myelinated fibre enters the base of each dome and branches to supply individual Merkel cells, losing its myelination approximately 10 μm from the Merkel cells. The nerve endings enlarge to form expanded end plates that contact individual Merkel cells. Lamellae from individual Merkel cells extend around the edge of each end plate and overlap with lamellae from the Schwann cells surrounding the nerve fibre. The contact sites between the Merkel cell and nerve end plate are similar to those observed at synapses within the central nervous system. Action potential initiation is proposed to occur at individual Merkel cell – end plate complexes resulting in multiple impulse generators (Iggo, 1974).

Amphibian

All amphibian mechanoreceptors were originally thought to be free branching endings in the epidermis of axons that originated from either the superficial or deep plexus of myelinated fibres in the sub-epidermis (Catton, 1958). The different rates of adaptation were proposed to result from absorption of stimulus energy by the layers of tissue overlying the terminals, with the result being mechanical filtering of the stimulus. However, Nafstad & Baker (1973) observed Merkel cells in the skin of both the back and belly of the frog *(Rana pipiens)* which appeared to be 'morphologically identical to Merkel cells in mammals and birds.' This is in contrast to the initial observation of Merkel (1880) who observed the cells in the skin of the back only, but the wide distribution of Merkel cells has been confirmed by Fox & Whitear (1978). The existence of morphologically distinct mechanoreceptors in amphibian skin was confirmed by von Düring & Seiler (1974) who observed lamellated receptors in the skin from all areas of the frog *(Rana esculenta)*. Based on the similarity of amphibian and mammalian Merkel cells, and the similar responses of amphibian and mammalian SAI mechanoreceptors - specifically the irregular nature of the maintained discharge - it has

been proposed that Merkel cells in amphibians are the receptors innervated by SAI mechanoreceptor afferents (Yamashita, Ogawa & Taniguchi, 1986).

Response

Mammalian

A division of mammalian cutaneous mechanoreceptors into two main categories can be based on their response to ramp-and-hold indentations of their receptive fields. The 'on and off' response to a ramp-and-hold stimulus typifies rapidly adapting mechanoreceptors (Iggo, 1977). The receptor responds to the ramp phase of the stimulus with a brief burst of impulses, the 'on' response. The receptor is silent during the hold phase, and then responds with another brief burst of impulses to the release phase, the 'off' response.

The response of the slowly adapting mechanoreceptors to a ramp-and-hold stimulus (Figure 6.2, top panel) has a characteristic dynamic response during the ramp phase, which decays to a maintained response during the hold phase (Iggo & Muir, 1969). During a constant stimulus the maintained response of slowly adapting mechanoreceptors often completely adapts. Under these conditions the sensitivity of the slowly adapting mechanoreceptor to further skin indentations is near control levels (Horch & Burgess, 1975). However, the sensitivity to low frequency stimuli is slightly increased, while the sensitivity to high frequency stimuli remains unchanged.

Mammalian slowly adapting mechanoreceptors can be further sub-divided into two categories based on their receptive fields and responses to stimulation (Chambers & Iggo, 1967). The receptive fields of slowly adapting Type I (SAI) mechanoreceptors have several points of high sensitivity, while the receptive fields of slowly adapting Type II (SAII) mechanoreceptors have a single point of maximum sensitivity (Johansson, 1978).

Slow adapting Type I mechanoreceptors in mammalian hairy skin are silent in the absence of skin deformation and respond to steady indentations of the skin with a maintained discharge (Iggo & Muir, 1969). The intervals between impulses during the
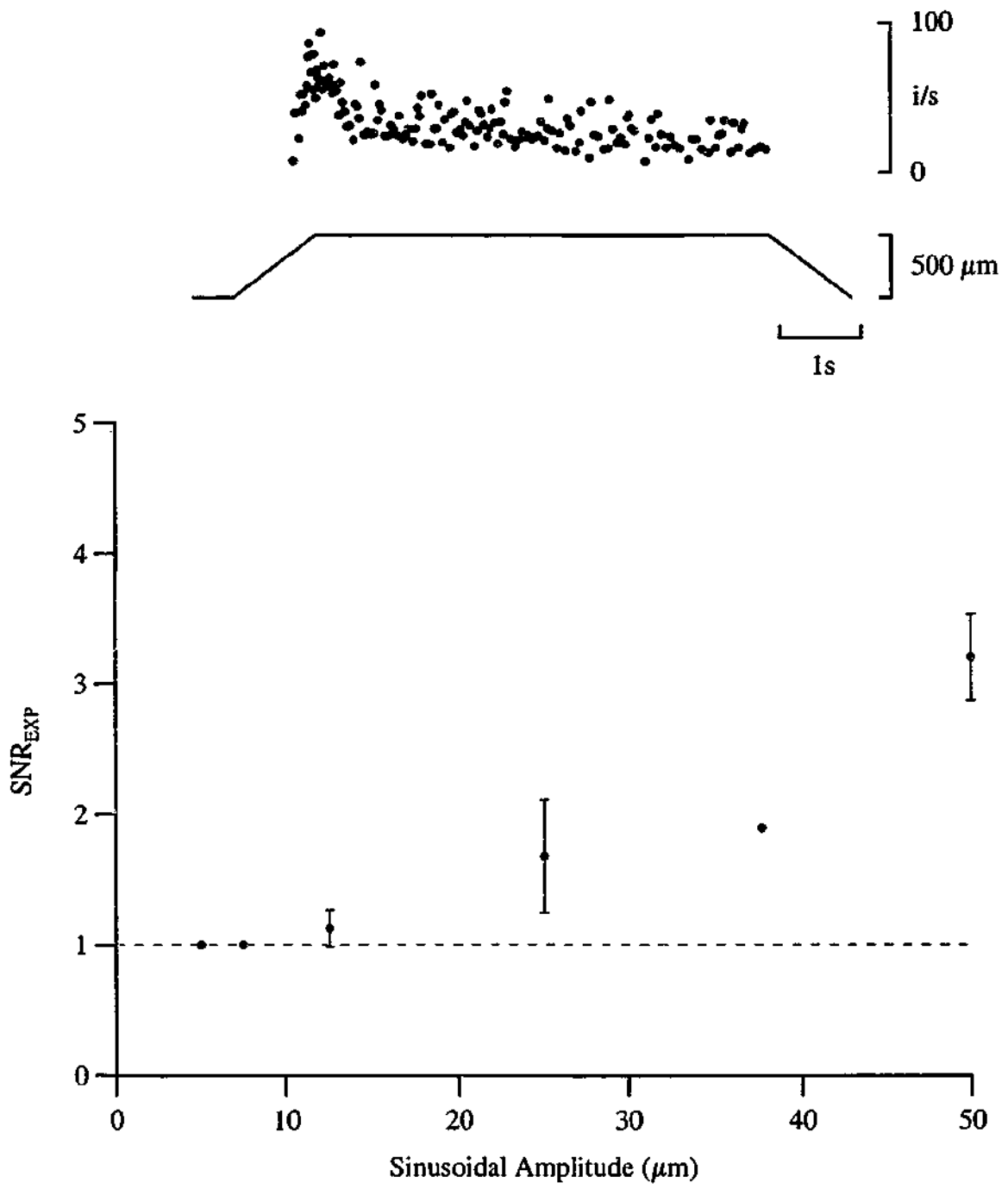
Figure 6.2   The ramp-and-hold response of a slowly adapting Type I cutaneous mechanoreceptor is characterised by a maintained discharge during the hold phase (top panel). The sinusoidal stimulus-response curve of a slowly adapting Type I cutaneous mechanoreceptor exhibits a threshold (bottom panel). The threshold for this particular receptor was approximately 10 μm for a 5 Hz sinusoid. Points in the stimulus response curve are mean $\pm$ SEM of three measurements, except for the measurement at 38 μm, which is a single measurement.

maintained discharge are randomly distributed, with a near Poisson distribution about the mean interval. The average rate of the maintained discharge is approximately proportional to the amplitude of the indentation. It has been proposed that the irregularity in the maintained discharge is a result of the interaction between multiple spike generators (Iggo, 1974). However, this is unlikely to be the case as re-setting of the spike generators by both antidromic and orthodromic impulses has been observed (Horch, Whitehorn & Burgess, 1974), which results in the domination of the response by the spike generator with the highest rate. The irregularity of the discharge is currently proposed to be the result of quantal fluctuations at the synapse that cause large fluctuations in the generator current (Horch et al., 1974).

The slowly adapting Type II mechanoreceptors also have a maintained discharge that increases proportionally with maintained indentations (Chambers, Andres, von Duering & Iggo, 1972). Unlike the random distribution of inter-spike intervals present in the maintained discharge from SAI mechanoreceptors, the maintained discharge from SAII mechanoreceptors is regular.

Human

The responses of cutaneous mechanoreceptors in glabrous skin of the hand in humans can be divided into four different types: rapidly adapting Type I (RAI) mechanoreceptors; rapidly adapting Type II (RAII) mechanoreceptors; and the two types of slowly adapting mechanoreceptors, SAI and SAII (Knibestöl & Vallbo, 1970). There are also four types of mechanoreceptors located in hairy skin. It has been proposed that the rapidly adapting mechanoreceptors are responsible for the sensation of 'flutter vibration' (Talbot, Darian-Smith, Kornhuber & Mountcastle, 1968). The slowly adapting Type I mechanoreceptors are thought to be responsible for the sensation of maintained pressure (Knibestöl & Vallbo, 1980), while electrical stimulation of the slowly adapting Type II mechanoreceptors does not lead to any conscious sensation (Torebjörk & Ochoa, 1980). In contrast to the afferents of muscle spindles and Golgi tendon organs, repeated electrical stimulation of single cutaneous afferents often gives rise to distinct sensations (Macefield et al., 1990).

The threshold for detection of triangular indentations of the glabrous skin of the human hand in psychophysical experiments is similar to the threshold for individual rapidly adapting mechanoreceptors recorded directly (Johansson & Vallbo, 1979). Harrington & Merzenich (1970) found that the response of SAII mechanoreceptors in hairy skin of the rhesus monkey *(Macaca mulatta)* to ramp-and-hold stimuli was similar to the subjective response from human subjects to similar stimuli and that therefore the SAII mechanoreceptors were responsible for the sensation of pressure. However, Knibestöl (1975) proposed that SAII mechanoreceptors may be used in proprioception, as SAII mechanoreceptors located near the base of the nail bed of fingernails of human subjects were able to signal joint angle, as a result of the stretch of the surrounding skin, with high fidelity. Knibestöl (1975) also proposed that SAI mechanoreceptors rather than SAII mechanoreceptors were responsible for the sensation of pressure.

The rapidly adapting mechanoreceptors, including Meissner's corpuscles in the glabrous skin and hair basket endings in the hairy skin, are most sensitive to sinusoidal frequencies in the range of 20 to 150 Hz and may respond to movements of 1 μm in this frequency range (Johansson et al., 1982). The Pacinian corpuscle is most sensitive to higher frequencies, greater than 200 Hz. The rapidly adapting mechanoreceptors are often also called vibration receptors or velocity detectors, due to their preferential sensitivity to rapidly changing stimuli. The slowly adapting mechanoreceptors are more sensitive to lower frequencies, in the range of 1 to 16 Hz, and respond to sinusoidal movements of less than 1 μm. The slowly adapting mechanoreceptors will respond to sinusoidal stimuli that are below the threshold of perception in both glabrous (Talbot et al., 1968) and hairy skin (Merzenich & Harrington, 1969). The amplitude of small low frequency skin indentations may be signalled by slowly adapting mechanoreceptors, as the rapidly adapting mechanoreceptor do not appear to have the ability to effectively encode stimulus amplitude (Konietzny & Hensel, 1977). The rapidly adapting mechanoreceptors typically exhibit one-to-one driving over a large range of stimulus amplitudes, which renders them incapable of signalling the stimulus amplitude.

Amphibian

It is possible to classify amphibian cutaneous mechanoreceptors into rapidly and slowly adapting types in a similar way to the classification of mammalian cutaneous mechanoreceptors (Adrian & Zotterman, 1926; Dun & Finley, 1938; Maruhashi, Mizuguchi & Tasaki, 1952). The initial classification was not clear as Lindblom (1962) classified the cutaneous mechanoreceptors of the toad *(Bufo bufo)* as either 'very rapidly adapting' or 'less rapidly adapting'. The two types appear to correspond to the rapidly and slowly adapting mechanoreceptors described in mammals, although the 'off' responses did not follow the same pattern (Höglund & Lindblom, 1961). Some of the trouble in the classification may have been a result of the changes in adaptation rate with temperature as later Ogawa, Morimoto & Yamashita (1981) were able to clearly demonstrate both rapidly and slowly adapting mechanoreceptors based on the absence of an 'off' response for the slowly adapting mechanoreceptors.

A separation of the slowly adapting mechanoreceptors into two types based on their receptive fields, corresponding to the SAI and SAII types in mammals, can also be made (Ogawa, Yamashita, Nomura & Taniguchi, 1984). The maintained discharge can be similarly distinguished on the basis of its irregularity, with SAII mechanoreceptors having a more regular maintained discharge (Yamashita et al., 1986). However, unlike the mammalian SAII mechanoreceptors, neither the SAI and SAII mechanoreceptors of the American bullfrog *(Rana catesbeiana)* have a maintained discharge (Ogawa & Yamashita, 1982).

The response of an amphibian SAI mechanoreceptor to a ramp-and-hold skin indentation (Figure 6.2, top panel) has both a dynamic and static phase (Loewenstein, 1956), . The dynamic component of the response is proportional to the logarithm of the rate of indentation (Lindblom, 1962), and decays with two time constants to a static level that is proportional to the amplitude of indentation (Ogawa et al., 1981). The response to a superimposed ramp-and-hold stimulus can be enhanced by a maintained indentation of the skin, as is the case for mammalian SAI mechanoreceptors. This form of conditioning does not have a similar affect on the sensitivity of the RA mechanoreceptors (Höglund & Lindblom, 1961).

Suitability for Stochastic Resonance

Slowly adapting cutaneous mechanoreceptors have all of the features required for stochastic resonance. The receptor is a non-linear system with a clear threshold to small indentations of the skin. Stimulation of the receptor, via indentations of the skin, can be precisely controlled allowing for the application of near-threshold periodic signals and superimposed noise signals.

Slowly Adapting Cutaneous Mechanoreceptors

A total of seven cane toads *(Bufo marinus)* of both sexes were used for experiments to seek evidence for stochastic resonance in slowly adapting Type I cutaneous mechanoreceptors of amphibian skin. All experiments were performed with approval from the Monash University Physiology Animal Ethics Committee.

Materials and Methods

Dissection

Animals were stunned and pithed, destroying the central nervous system. A skin flap extending from the ventral midline to the ilium and from the sternum to the pelvic girdle was removed. Spinal nerves 4, 5 and 6 were freed along their length and cut at their point of entry into the vertebrae.

Equipment

The skin flap was secured in an experimental chamber on a solid plate by four pins that held the skin flap taut. The preparation was perfused with amphibian Ringer solution (111 mM NaCl, 2.5 mM KCl, 0.1 mM K_2HPO_4, 11 mM Glucose, 2.4 mM $NaHCO_3$ and 2.38 mM $CaCl_2$) that was bubbled with carbogen (5% CO_2 in O_2) and was maintained at room temperature (20 – 25 °C). The spinal nerves were lifted into a paraffin oil-filled chamber used for recording. A small electro-magnetic actuator was used to mechanically stimulate the skin surface. The actuator had a rounded tip with a probe diameter of 1.2 mm. The multi-channel recorder as illustrated in Figure 3.1 and Figure

3.6 and described in Chapter Three was used to control the actuator and to record the afferent responses.

Experimental Protocol

Afferent Identification

Functionally single afferents were obtained by removing the sheath of connective tissue from a spinal nerve and then subdividing the nerve into smaller filaments. Afferents were identified based on their response to mechanical stimulation of the skin surface (Figure 6.2, top panel). An afferent was defined as a slowly adapting cutaneous mechanoreceptor if it maintained a discharge during the hold phase of a ramp-and-hold skin indentation (Maruhashi et al., 1952) and did not display an 'off' response, a burst of impulses during the release phase (Ogawa et al., 1981). The singularity of an afferent was determined by the consistent nature of the recorded action potential and the absence of extremely short inter-spike intervals that are characteristic of multi-unit recordings.

Stochastic Resonance

The protocol and analysis used for the stochastic resonance experiments with slowly adapting cutaneous mechanoreceptors was similar to that used for Golgi tendon organs in passive mammalian muscle (p. 94). Briefly, for each unit a noise-alone response curve was measured covering a wide range of noise amplitudes), for details of the applied noise see Appendix F. The average rate in response to the noise-alone stimulus exhibited a plateau, the start of which may be seen in the bottom panel of Figure 6.4. The maximum noise amplitude for the remainder of the experiment was chosen to fall below the amplitude required to reach the plateau rate. The noise-alone response curve was then fitted with a curve based on Kramers' rate (Equation 2.2).

A stimulus-response curve to small sinusoidal skin indentations was measured at each of two test frequencies to ensure that a clear threshold could be identified and a sub-threshold periodic stimulus could be employed for the remainder of the study. The test frequencies were chosen to lie within the approximately linear region of the noise-alone response, as this should allow for maximum separation of the predicted optimal noise levels, D_{PRE}. Stochastic resonance curves were then measured at each test frequency. A

logNormal curve (Equation 2.3) was then fitted to the results and was used to determine the optimal noise level, D_{OPT}.

The most significant difference between the protocol used for the Golgi tendon organs and the slowly adapting Type I cutaneous mechanoreceptors was that all test movements for the mechanoreceptors were superimposed on the plateau of a near-threshold ramp-and-hold movement (Figure 6.3). The near-threshold ramp-and-hold was used to reduce the contact time of the electro-magnetic actuator probe and the skin surface. Several hours were required to record a complete set of data; if the probe was left in contact with the surface for this length of time it led to permanent skin deformations. The skin deformation in turn resulted in a reduction in the sensitivity of the receptor. The effective noise amplitude was therefore reduced; resulting in a shifting optimal noise level as the sensitivity of the receptor changed over time. Using near-threshold ramp-and-hold movements the sensitivity of the receptors, as measured by the response to a noise-alone stimulus, did not decrease over the several hours required to record a complete set of data.

Results

Twelve slowly adapting Type I cutaneous mechanoreceptors were examined for stochastic resonance behaviour. All mechanoreceptors that were mechanically stimulated under the appropriate conditions, a sub-threshold periodic input and supra-threshold noise input, exhibited stochastic resonance.

Stimulus-Response Curve

A stimulus-response curve for small sinusoidal skin indentations is shown in Figure 6.2. For this mechanoreceptor there was a threshold of approximately 10 μm for sinusoidal skin indentations. Below this amplitude the receptor did not respond at all.

Stochastic Resonance

The response of a slowly adapting Type I cutaneous mechanoreceptor to three different types of stimuli is illustrated in Figure 6.3. The instantaneous rate and resulting cycle histograms that were used to calculate SNR_{EXP} are shown for each response. A supra-
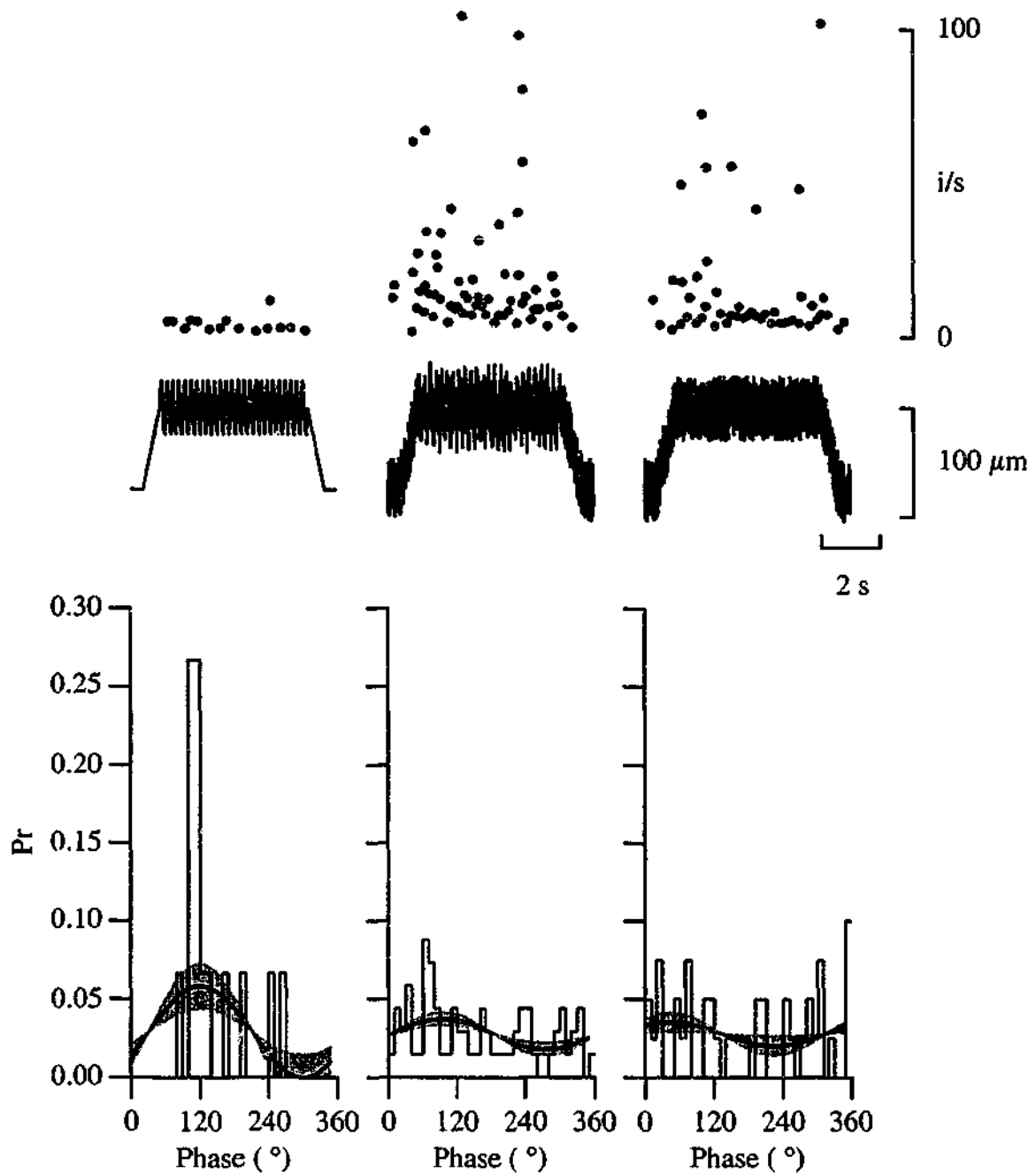
Figure 6.3 The response of a slowly adapting cutaneous mechanoreceptor to a supra-threshold periodic signal (25 μm at 5 Hz, left panel), a sub-threshold periodic signal and supra-threshold noise signal (12 μm at 5 Hz with 30 μm of noise, middle panel), and to a noise-alone signal (30 μm of noise, right panel). In each panel the top trace is the instantaneous discharge rate of the receptor and the trace underneath is the imposed movement. Note all movements have been superimposed on a sub-threshold ramp-and-hold movement of 75 μm. The graph at the bottom of each panel is cycle histogram that has been fitted with a sinusoid to determine SNR_{EXP}. The values of SNR_{EXP} for the three stimuli are 2.19 (supra-threshold periodic stimulus), 2.14 (sub-threshold periodic and supra-threshold noise stimulus) and 1.15 (noise-alone stimulus).

threshold sinusoidal stimulus (Figure 6.3, left panel) resulted in a cycle histogram where the majority of action potentials occurred at about the same phase of the stimulus cycle and yielded a high SNR_{EXP} (2.19). A supra-threshold noise-alone stimulus (Figure 6.3, right panel) resulted in a cycle histogram where the action potentials were evenly distributed across all phases of the stimulus and yielded a low SNR_{EXP} (1.15). A sub-threshold sinusoidal stimulus and supra-threshold noise stimulus (Figure 6.3, middle panel) resulted in a cycle histogram with a significant modulation of the distribution of the action potentials across the different phases of the stimulus and yielded a high SNR_{EXP} (2.14).

An example of the response of a mechanoreceptor that exhibited an optimal SNR_{EXP} with the addition of input noise is shown in Figure 6.4. The noise-alone response is shown in the bottom panel and is the average discharge rate during the 6 s of imposed noise-alone movement on the hold phase of the sub-threshold ramp-and-hold stimulus. The noise-alone threshold was approximately 50 μm, above which the average rate increased with increasing noise amplitude to reach a plateau of about 30 i/s. The noise-alone response was well fitted by the curve based on Kramers' rate, allowing for accurate predictions of D_{PRE}. For the two test frequencies used in the stochastic resonance protocol of 5 and 13 Hz the predicted optimal noise amplitudes were 87 and 135 μm respectively, indicated by the grey lines in the bottom panel of Figure 6.4.

There is a clear peak in SNR_{EXP} for both of the test frequencies used. Each point was calculated from 6 s of response during the hold phase of the sub-threshold ramp-and hold stimulus. The responses were well fitted by logNormal curves and the optimal noise values were 95 ± 1 μm and 143 ± 1 μm respectively (D_{OPT} ± SEM), indicated by the arrows in the upper panels of Figure 6.4. The increase in D_{OPT} with increasing sub-threshold periodic stimulus frequency is a key feature of stochastic resonance.

The pooled results from twelve slowly adapting Type I cutaneous mechanoreceptors are presented in Figure 6.5. The data is shown on log-log axes as it extends over several orders of magnitude. Also, the errors associated with each measure are approximately proportional to the measurement, and therefore are best displayed on a log-log plot. Each point is the measured optimal noise level (± SEM) plotted against the
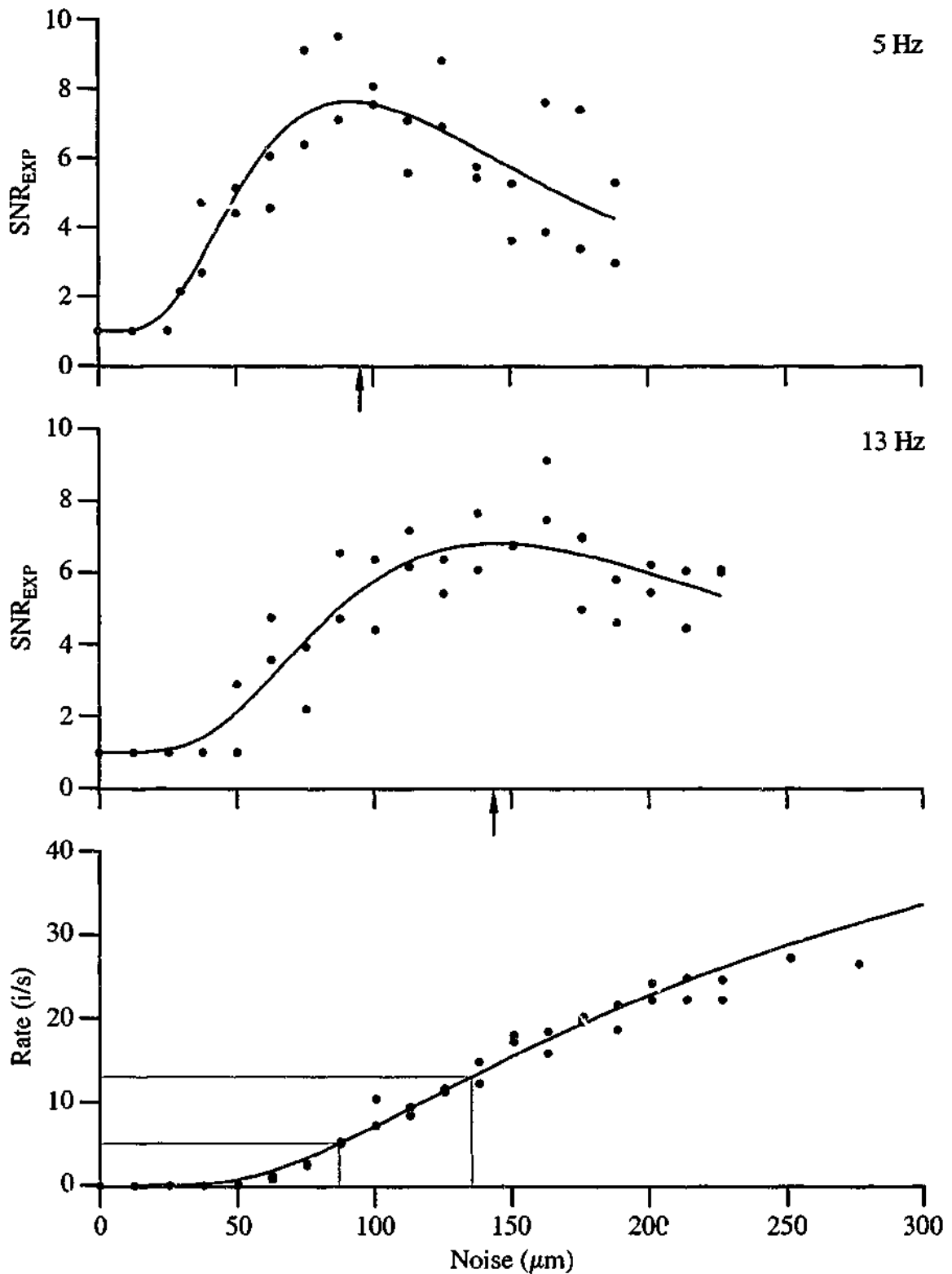
Figure 6.4   The response of a slowly adapting cutaneous mechanoreceptor shows many of the characteristics of stochastic resonance. Each point is calculated from 6 s of response and the measurements were taken in a pseudo-random order (the blue symbol represents the data shown in Figure 6.3). The fitted curves in the upper panels are logNormal curves used to estimate D_{OPT}, indicated by the arrows. The bottom panel is the noise-alone response, which has been fitted with a curve based on Kramers' rate. The grey lines in the bottom panel indicate the predicted optimal noise values, D_{PRE}, for each test frequency.
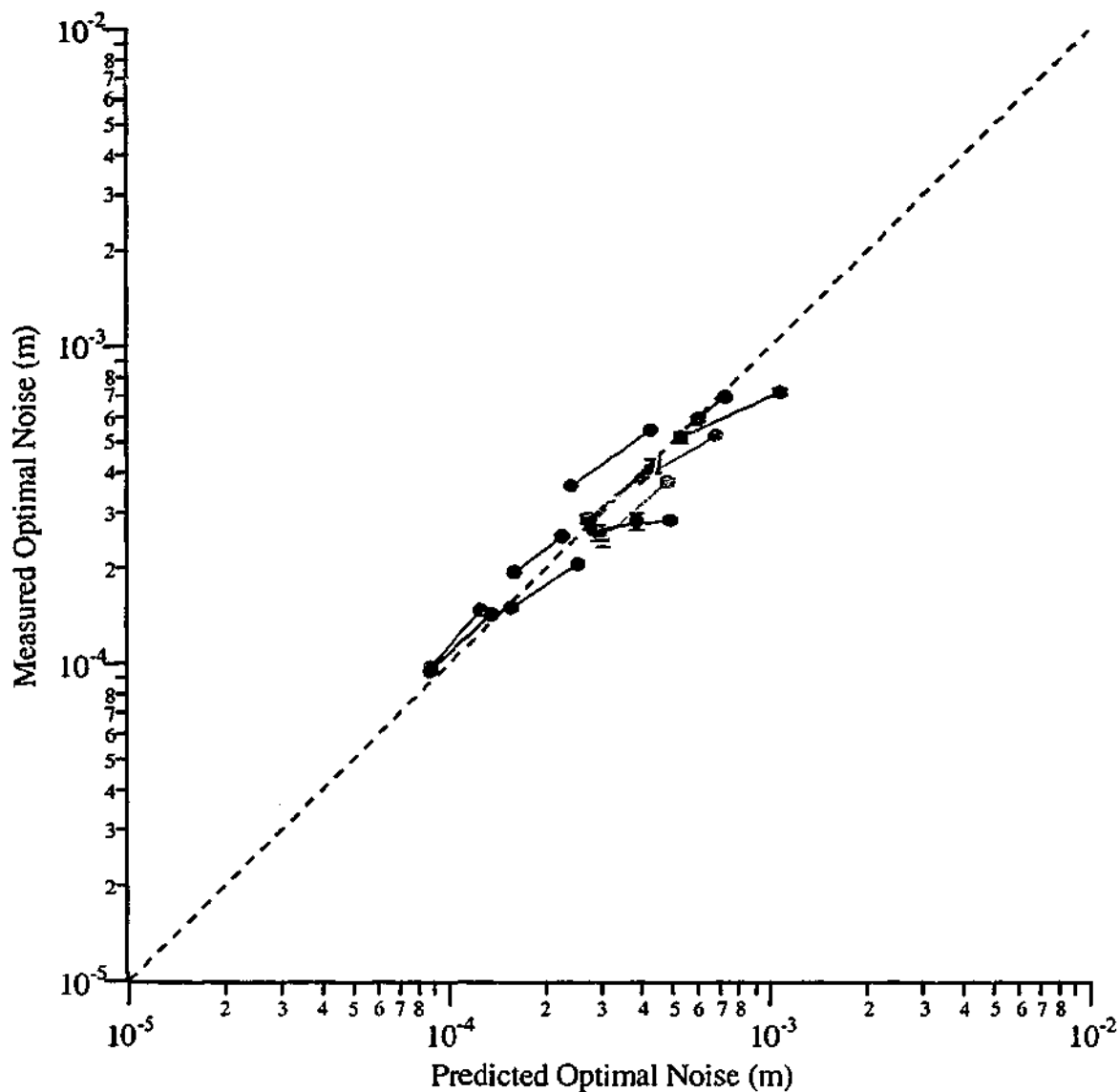
Figure 6.5   The pooled data from the twelve slowly adapting cutaneous mechanoreceptors that showed an optimal SNR_{EXP} with the addition of noise are scattered about the line of proportionality (dashed line), as predicted by stochastic resonance theory. Values shown are D_{OPT} and an estimate of the error in D_{OPT}, typically less than the size of the symbol, plotted against D_{PRE}. The results for each slowly adapting cutaneous mechanoreceptor are displayed in a different colour and joined to illustrate the correlation between D_{OPT} and D_{PRE} for each unit. The blue symbols represent the data from the slowly adapting cutaneous mechanoreceptor shown in Figure 6.4.

corresponding predicted optimal noise level. All mechanoreceptors were tested at two frequencies, resulting in a total of 24 measurements. The data for each mechanoreceptor are joined to illustrate the correlation between D_{OPT} and D_{PRE} for each unit. The correlation between D_{OPT} and D_{PRE} for the pooled data was 0.918 (Pearson Product). The correlation between D_{OPT} and D_{PRE} and therefore the sub-threshold periodic frequency dependence of the optimal noise level is consistent with the hypothesis that the increase in SNR_{EXP} with additional noise is a result of stochastic resonance.

Psychophysical Experiments

A total of six adult human subjects of both genders were used for the psychophysical experiments to seek evidence for stochastic resonance in cutaneous mechanoreceptors. All experiments were performed with approval from the Monash University Standing Committee on Ethics in Research on Humans.

Materials and Methods

Subjects were blindfolded and seated comfortably with their right-forearm resting on a horizontal cushioned support. Local indentations were applied to the hairy skin on the dorsal surface of hand, taking care to avoid superficial tendons and blood vessels.

Equipment

A small electro-magnetic actuator, the same one used for the experiments on cane toad skin, was used to mechanically stimulate the skin surface. The actuator was controlled by a data acquisition card (PCI-MIO-16E-4, National Instruments Corporation, Austin, Texas, U.S.A.) in a G3 desktop computer (Macintosh, Cupertino, California, U.S.A.) running Igor Pro (WaveMetrics, Lake Oswego, Oregon, U.S.A.). This combination of equipment is the same as that used for the multi-channel recorder and psychophysical experiments involving elbow movement used for the previous stochastic resonance experiments.

Experimental Protocol

The threshold for detection of small sinusoidal stimuli was measured using a modified staircase technique similar to that used for the psychophysical experiments on the elbow joint (p. 115). Each stimulus lasted for approximately 10 seconds and there was an inter-trial interval of at least 30 seconds to allow for full creep recovery of the skin (Pubols, 1982). Approximately four hours were required to acquire a complete set of data, in two sessions of approximately two hours each. If inter-trial intervals of less that 30 seconds were used then the detection threshold increased during the period of experimentation. With an inter-trial interval of 30 seconds the detection threshold for the no-noise condition did not significantly change during a session.

An example staircase measurement for the skin detection protocol is illustrated in Figure 6.6. For the trial illustrated the resulting threshold measurement is $230 \pm 40~\mu m$. Threshold measurements were taken with two different sinusoidal frequencies with various amplitudes of additional input noise. The sinusoidal test frequencies of 0.5 and 1 Hz were chosen to preferentially stimulate the slowly adapting mechanoreceptors, which are most responsive to sinusoidal stimuli of 1 to 16 Hz (Talbot et al., 1968; Merzenich & Harrington, 1969).

Threshold measurements for the different noise amplitudes were interleaved with no-noise threshold measurements and the thresholds were normalised to the no-noise threshold. The threshold curves were fitted with a logNormal curve (Equation 2.3, with $Z=1$) that was used to determine the noise level that resulted in the smallest detection threshold, D_{OPT}. The fitting procedure also produced an estimate of the error in D_{OPT}. The measured values of D_{OPT} for the different test frequencies were then compared, using an analysis of variance (ANOVA).

Results

Six healthy young subjects participated, four male and two female, aged 20-31, all free from any known neurological disorder. Subjects reported a low frequency modulation in pressure as a result of the periodic stimuli. All subjects had a reduction in sinusoidal detection thresholds with the addition of optimal amplitudes of broad-spectrum noise as
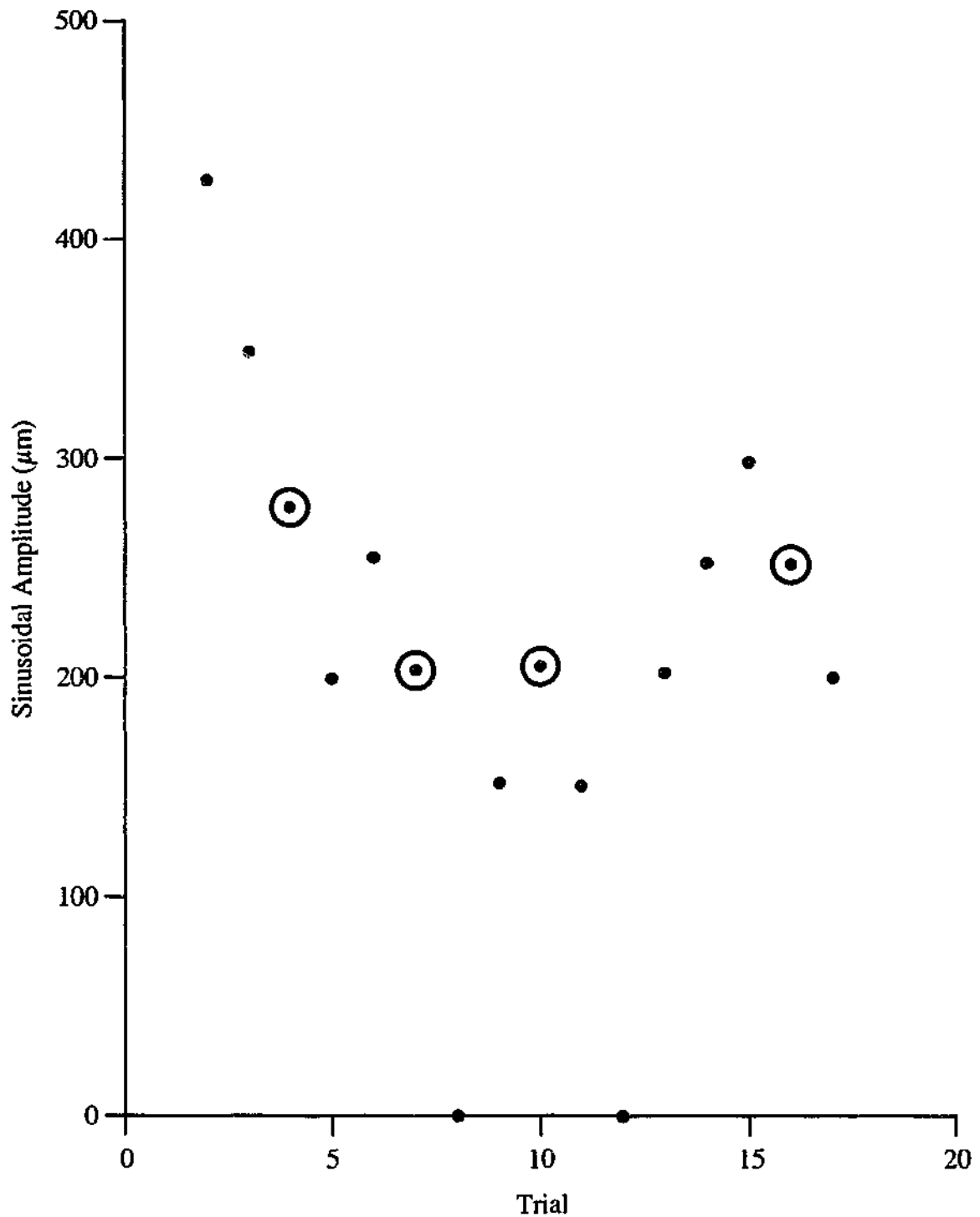
Figure 6.6 The sinusoidal detection threshold for skin indentations of the back of the hand was determined using the staircase technique. The amplitude of the sinusoidal stimulus was decreased following a correct detection (●), or increased if not detected (●). The series of amplitudes corresponding to a minimum correct detection (blue outlined circles) were then averaged to determine the threshold. Trials 8 and 12 were Null presentations of a zero amplitude sinusoid, which were correctly reported as "no movement".

illustrated in Figure 6.7 (top panel). With a sinusoidal stimulus frequency of 1 Hz, the detection threshold was reduced from 390 ± 80 μm to 230 ± 40 μm with the addition of 1.2 mm of input noise for this subject. For the two test frequencies of 0.5 and 1 Hz, the normalised optimal noise levels, D_{OPT}, for this subject were 2.0 ± 0.1 and 0.8 ± 0.5 (Figure 6.7, bottom panel).

Each threshold measurement took approximately 30 minutes to collect; therefore it was generally only possible to collect four threshold values for each subject. The lack of data below the estimated optimal noise level for the 0.5 Hz sinusoid threshold measurement (Figure 6.7, bottom panel) results in a large error in the estimated optimal noise, D_{OPT}. It is clear however, that the optimal noise value for a 0.5 Hz sinusoidal stimuli is lower than that for a 1 Hz sinusoidal stimuli, which is a key feature of stochastic resonance.

The pooled results from all subjects are shown in Figure 6.8, in which values of D_{OPT} for the 1 Hz sinusoidal stimulus have been plotted against values of D_{OPT} for the 0.5 Hz sinusoidal stimulus. The points all lie above the line of proportionality, indicating that larger noise amplitudes are required to minimise the threshold for the 1 Hz sinusoidal stimulus than for the 0.5 Hz sinusoidal stimulus. The values of D_{OPT} for the 1 Hz sinusoidal stimulus are significantly larger than the values of D_{OPT} for the 0.5 Hz sinusoidal stimulus ($p < 0.05$, ANOVA), indicating that D_{OPT} is frequency dependent. The frequency dependence of D_{OPT} is consistent with the hypothesis that the reduction in detection threshold for sinusoidal stimuli is the result of stochastic resonance.

Discussion

Animal Experiments

All the key features of stochastic resonance are present in the response of slowly adapting cutaneous mechanoreceptors in the cane toad. All the mechanoreceptors exhibited an increase in D_{OPT} with an increase in stimulus frequency. This unique feature of stochastic resonance was present under all conditions when a sub-threshold periodic input and supra-threshold noise input were used. However, the measured optimal noise amplitudes were not precisely those predicted from the noise-alone
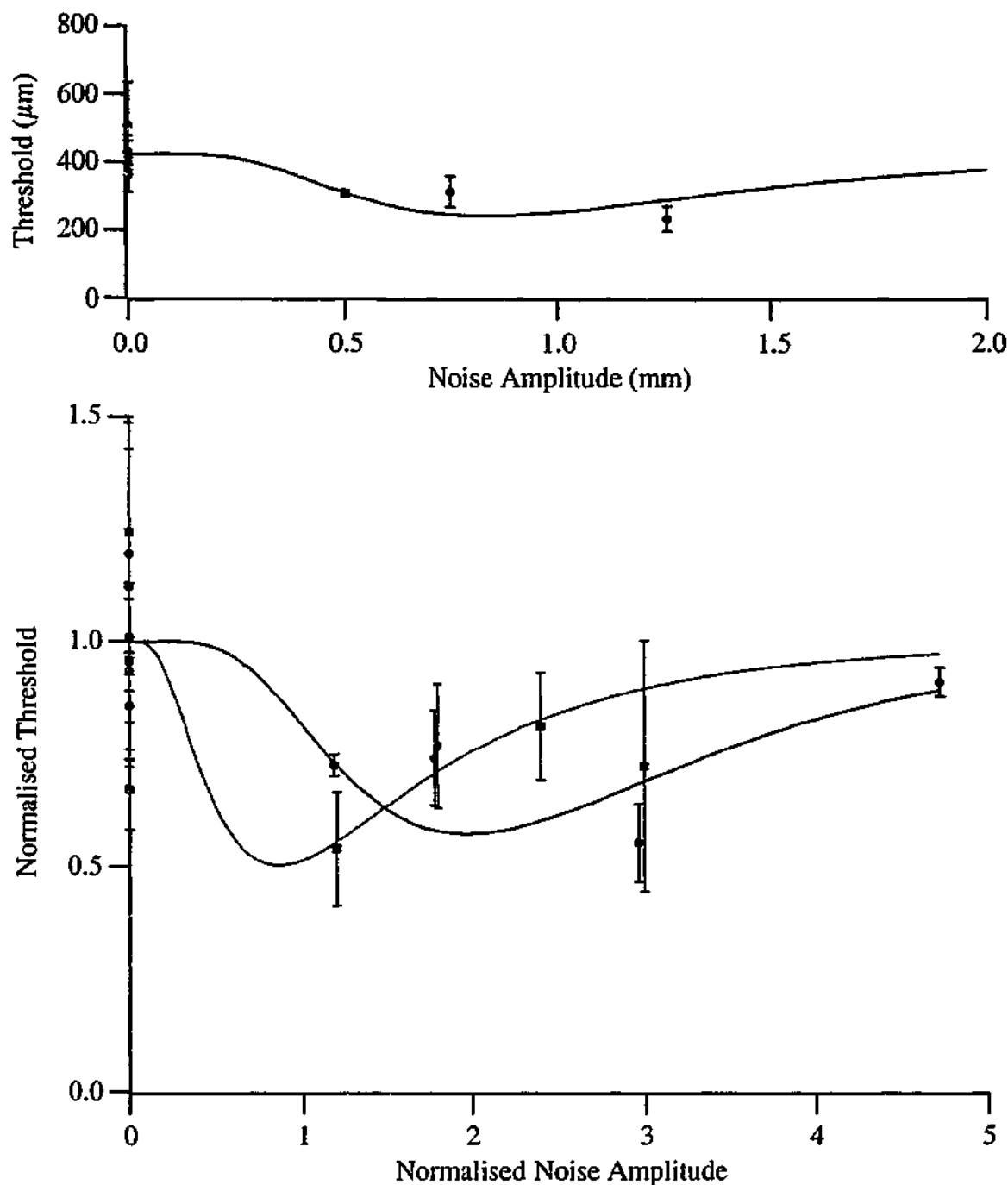
Figure 6.7   The detection threshold for a 1 Hz sinusoidal indentation of the skin on the back of the hand can be reduced by the addition of noise (top panel). The level of noise that produces the greatest decrease in detection threshold is lower for a 0.5 Hz sinusoid (bottom panel, red line) than for a 1.0 Hz sinusoid (bottom panel, blue line, same data as the top panel). The values shown are threshold ± SEM, calculated using the staircase method (Figure 6.6). The fitted curves are logNormal curves, Equation 2.3 with Z set to the no-noise threshold.
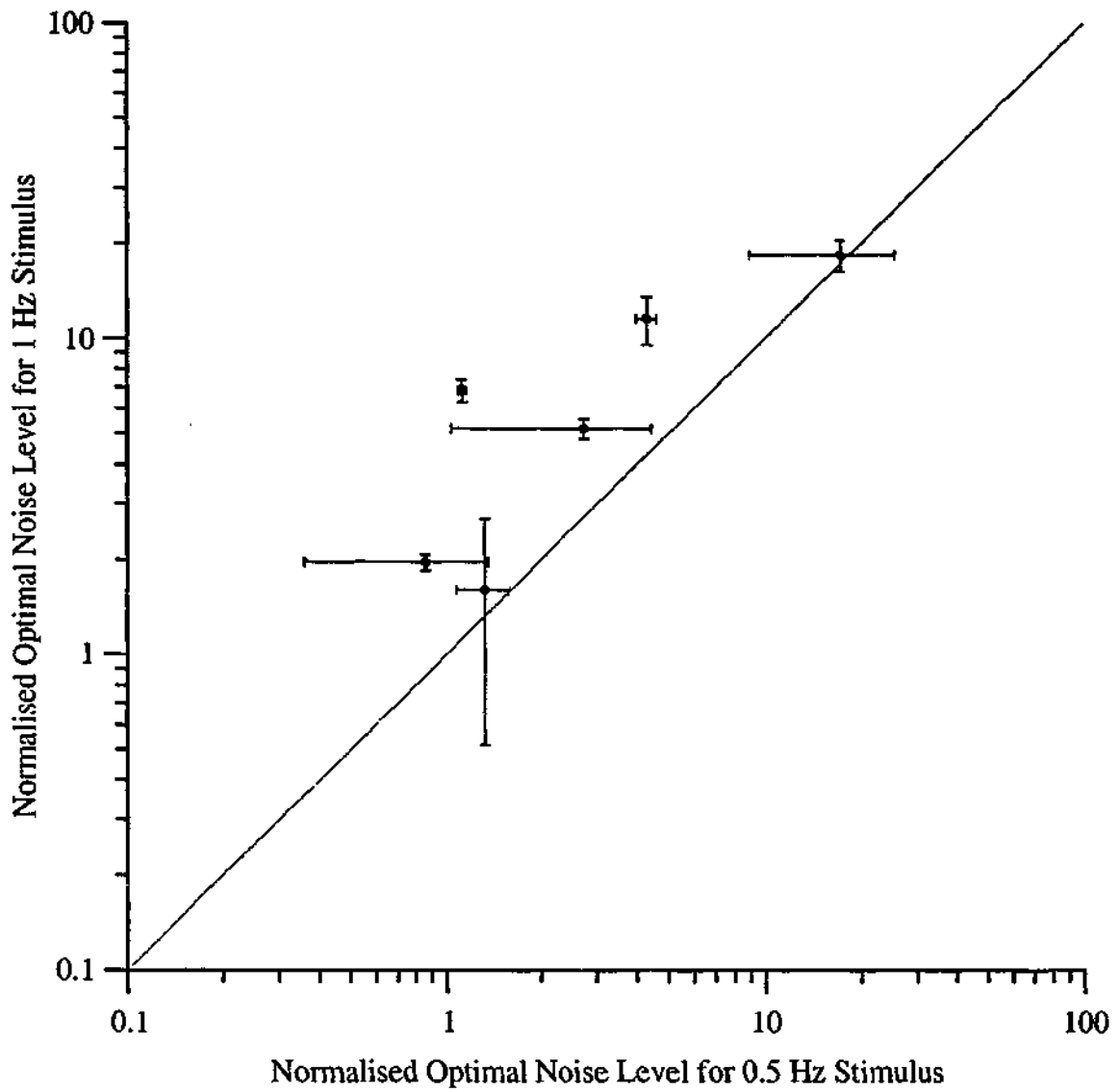
Figure 6.8   Results from all subjects lie above the line of proportionality (grey line), indicating that the optimal noise level for 1 Hz sinusoidal stimuli is larger than the optimal noise level for 0.5 Hz sinusoidal stimuli. This is consistent with the hypothesis that the reduction in the detection threshold is the result of stochastic resonance. The results from each subject are shown in a different colour, with the results from the subject illustrated in Figure 6.7 in blue.

response curve. As previously mentioned in Chapter Two (p. 57), the predicted optimal noise levels are only valid for near-threshold periodic stimulation, and therefore the small discrepancy is not surprising.

There is some variation in SNR_{EXP} between trials (Figure 6.4) due to the random nature of the noise stimulus. Increasing the period of recording would have reduced the variation, but the recording period was kept to a minimum to reduce the effects of adaptation. As the receptor adapts to the stimuli, the sensitivity of the receptor to the noise decreases, effectively decreasing the noise input. A reduction in the effective noise input would be expected to shift both the measured optimal noise, D_{OPT}, and the predicted optimal noise, D_{PRE}, to larger noise amplitudes. A change in the effective noise input during the experiment may obscure any stochastic resonance effect. Multiple measurements for each noise amplitude were therefore taken and the curve fitting procedure effectively averaged the results.

Psychophysical Experiments

Reductions in detection thresholds during psychophysical experiments with the addition of noise have previously been reported (Collins et al., 1996b; Collins et al., 1997; Ivey et al., 1998; Richardson et al., 1998), but the frequency dependence of the optimal noise level has not been clearly observed before. For the first time, a statistically significant frequency dependence of the optimal level of additional noise required to reduce detection thresholds for sinusoidal indentations of the skin has been shown. Therefore, the reduction in detection thresholds can be attributed to a stochastic resonance effect rather than dithering or some other noise-induced effect, which would not be expected to exhibit a frequency dependence of the optimal noise amplitude.

The receptor or receptors utilised by the subjects in the psychophysical experiments are not known. However, they are likely to be the slowly adapting Type I mechanoreceptors because of the low sinusoidal test frequencies used. It is impossible to determine if the observed reductions in detection thresholds were a result of stochastic resonance occurring in a specific receptor, for example the SAI mechanoreceptor as occurred with the cane toad slowly adapting mechanoreceptor, or resulted from processes deeper within the central nervous system.

It is possible that the stochastic resonance effect occurred within the central nervous system and was the result of combining afferent information from many receptors, as supported by the modelling of a neural network that was capable of exhibiting stochastic resonance (p. 61). It is likely that more than one type of mechanoreceptor was activated by the stimulus that was used in the psychophysical experiments, due to the overlap of the thresholds of the various mechanoreceptors in human skin (Johansson et al., 1982). It is possible that the periodically modulated signal from the SAI mechanoreceptors (known to have a threshold below the threshold of perception (Talbot et al., 1968; Merzenich & Harrington, 1969)), was combined with the response from the RAI mechanoreceptors (likely to be random spike trains evoked by the noise stimulus) at some level within the central nervous system. Therefore, the stochastic resonance effect may have occurred within the central nervous system. The ability of the central nervous system to utilise the stochastic resonance effect, evident as a reduction in the detection threshold, is the key result of the psychophysical experiments.

Although the sinusoidal frequencies used were lower than the optimal range of frequencies for SAI mechanoreceptors in the glabrous skin of humans (Talbot et al., 1968; Johansson et al., 1982; Vallbo & Johansson, 1984), the stochastic resonance effect is still predicted to occur at higher frequencies. The low test frequencies were chosen to limit the amplitude of noise required. Higher sinusoidal test frequencies would be expected to require larger noise amplitudes to produce an optimal reduction in detection threshold. The maximum range of movement available with the electro-magnetic actuator was limited to 5 mm. A 5 mm noise-alone movement caused discomfort for the subject, and because of this the maximum amplitude noise used in the psychophysical experiments was 3 mm. Larger noise amplitudes may also result in more rapid desensitisation of the test area, resulting in longer inter-trial intervals being required.

Chapter Seven

General Discussion

Although stochastic resonance was first proposed in 1981 by Benzi et al., it was not until 1993 that Douglass et al. reported the first experimental evidence for stochastic resonance in a biological system. It was several more years before experimental evidence from other biological systems was reported. There have been claims that many biological systems exhibit stochastic resonance. Using the definition of stochastic resonance given in Chapter One, very few of the biological systems have been proved to do so. Some of the systems discussed in Chapter One clearly do not exhibit stochastic resonance, but many others were simply not tested sufficiently to be able to distinguish the stochastic resonance effect from other noise effects such as dithering (see Table 1.2). Therefore it is worth reiterating the features that are unique to stochastic resonance, which are summarised in Table 1.1.

Unique Features of Stochastic Resonance

For a system to exhibit stochastic resonance it must be non-linear, and typically the non-linearity takes the form of a threshold. Therefore, all biological receptors may be capable of exhibiting stochastic resonance, as all biological receptors have a threshold below which a change in the input does not result in a change in the output.

The input to the non-linear system must consist of a sub-threshold periodic signal together with a supra-threshold noise signal. Although the periodic input signal is typically a sinusoid, it is possible to use a periodic input consisting of a periodic train of impulses, as shown in Figure 2.17. An aperiodic signal, such as a ramp-and-hold stimulus, cannot, by definition, be used to observe stochastic resonance. It is not possible to observe a matching of time-scales (or resonance) that is unique to stochastic resonance if an aperiodic signal is used. Therefore, 'aperiodic stochastic resonance' as described by Collins et al. (1995a) is not stochastic resonance. The effect observed with such inputs is likely to be dithering or system linearisation (Gammaitoni, 1995; Chialvo et al., 1997).

A system exhibits stochastic resonance if the output meets two criteria. Firstly, the output SNR must be optimised with the addition of a supra-threshold level of noise, D_{OPT}. That is, the optimal output SNR occurs with an input SNR of less than one. Secondly, and most importantly in distinguishing stochastic resonance from other noise effects, the optimal noise level must be dependent on the frequency of the sub-threshold periodic stimulus. Either D_{OPT} must increase with increasing periodic stimulus frequency or D_{OPT} must match D_{PRE}, the predicted optimal noise level. Testing of the system with several different periodic input frequencies should show a frequency dependence of D_{OPT}, while measurement of the noise-alone response curve should show a matching of D_{OPT} and D_{PRE}. Many noise effects may result in an optimal output SNR with the addition of input noise, however, only a system exhibiting stochastic resonance will result in a frequency dependent D_{OPT}.

As illustrated in Chapter Two, it is possible for a system to exhibit stochastic resonance (Figure 2.10) and also exhibit other noise effects (Figure 2.22). Therefore, it is vital to observe the frequency dependence of the optimal noise level to distinguish the stochastic resonance effect from other constructive noise effects. This is the important feature that has not been thoroughly shown for many of the biological systems that have been proposed to exhibit stochastic resonance. Whether the increase in output SNR is a result of stochastic resonance, or other noise effects, is of more than academic interest. If the increase in output SNR is a result of stochastic resonance, then the effect will only occur under limited conditions (sub-threshold periodic signal and supra-threshold noise signal) while a different set of conditions is required if the effect is dithering (sub-threshold periodic signal and near-threshold noise signal). Therefore, the method by which the output SNR is optimised affects the functional significance of any such improvement.

Biological Systems Exhibiting Stochastic Resonance

Bearing the above criteria in mind, of all the published examples of systems that have been proposed to exhibit stochastic resonance, only three examples fulfil both criteria.

These are the crayfish multi-modal interneurones (Pei et al., 1996b); psychophysical experiments involving tactile detection tasks, although here the evidence is weak (Ivey et al., 1998); and psychophysical experiments involving visual perception tasks (Chialvo & Apkarian, 1993). To this meagre list can now be added: Golgi tendon organs and muscle spindle primary and secondary endings (under limited conditions) in the cat; and slowly adapting Type I cutaneous mechanoreceptors in the toad. Further evidence has also been gathered to strengthen the case for psychophysical experiments involving tactile detection tasks. A significant reduction in detection threshold with the addition of noise has now been measured, with the optimal noise level being frequency dependent.

A new output SNR measure based on the cycle histogram, SNR_{EXP} (p. 56), was used to quantify the stochastic resonance effect experimentally, while recording from a variety of biological receptors. Unlike the SNR_{RES} and SNR_{ISIH} measurements (p. 54) based on the inter-spike interval histogram, which have been extensively used in the past, the SNR_{EXP} measurement is unlikely to result in a false positive indication of stochastic resonance. However, the tendency for the optimal noise level, D_{OPT}, to be less than the predicted optimal noise level, D_{PRE}, can mask some of the frequency dependence of D_{OPT} if extremely small periodic stimuli are used. The evidence for stochastic resonance occurring in Golgi tendon organs, muscle spindles, and slowly adapting Type I mechanoreceptors using the SNR_{EXP} measure is therefore stronger than previous evidence of stochastic resonance in biological systems.

The evidence that the increase in output SNR is the result of stochastic resonance is also strengthened by the measurement of several periodic stimulus frequencies and the noise-alone response curve. The frequency dependence of D_{OPT} can be observed from the multiple periodic stimulus frequency measurements. As expected from stochastic resonance theory, the level of noise required to optimise the output SNR for all the receptors studied increased with an increase in frequency of the sub-threshold periodic stimulus. This alone would be enough evidence to support the hypothesis that the increase in output SNR is a result of stochastic resonance. The matching of the predicted optimal noise values, D_{PRE}, and measured optimal noise values, D_{OPT}, provides further evidence that the increase in the output SNR is a result of stochastic resonance.

Dithering

Many of the systems that have been proposed to exhibit stochastic resonance may in fact be exhibiting dithering. A key component of the dithering effect is that the output must be averaged over time. The rapid variations resulting from the addition of the noise can be averaged to zero, while the slower input can be recovered, with higher fidelity, from the averaged output. Another way to consider dithering is to imagine a sub-threshold input to a system with a threshold. Alone, the sub-threshold signal will never cause a change in the output, but with the addition of noise, the combined input will occasionally be above threshold, and result in a change in the output. The key to dithering is that the combined input will, on average, cross the threshold a number of times that is proportional to the otherwise sub-threshold input. The additive noise acts as a pedestal for the signal, allowing an otherwise sub-threshold signal to be detected.

An interesting feature of dithering is that the effect can be achieved with the addition of different signals, not just noise signals, to the sub-threshold input. The optimal signal to add is evenly distributed noise, which can completely reduce the error introduced by a simple quantising system (Wannamaker et al., 2000). However, any signal that has a zero-mean and evolves rapidly, compared to the input signal of interest, can be used as the pedestal signal. An example of such an effect occurring with muscle spindle primary endings has been described by Matthews & Watson (1981a) who used a high-frequency sinusoidal signal as the pedestal.

Dithering is optimised by addition of near-threshold levels of the pedestal signal. This is in contrast to stochastic resonance, for which the output SNR is optimised with the addition of supra-threshold levels of noise that are dependent on the noise-alone response of the system. It is therefore possible to distinguish effects such as those described by Matthews & Watson (1981a) and stochastic resonance, as a single amplitude of pedestal sinusoid was optimal for all frequencies of periodic signal. If the effect was related to stochastic resonance, then it would be expected that different amplitudes of pedestal sinusoid would be required to optimise the response for different frequencies of the periodic signal.

A key difference between dithering and stochastic resonance is that stochastic resonance will not occur if a non-random signal is added to the sub-threshold periodic signal. If for example a sinusoid were used rather than a random noise signal, the sinusoid would need to be adjusted to produce an average transition rate of the output that was equal to the sub-threshold periodic signal. The only sinusoid that could produce such a transition rate would be a supra-threshold sinusoid at the same frequency as the sub-threshold periodic signal. The addition of such a signal would simply result in the detection of the additional sinusoid, and not the sub-threshold signal. Therefore, although the dithering effect can occur with the addition of non-random signals, stochastic resonance requires a random 'noise' signal.

Other Effects of Noise

An increase in output SNR can be a result of effects not related to stochastic resonance or dithering, as illustrated by the effect of noise on the ramp-and-hold response of muscle spindle primary endings (Figure 5.11). The addition of an appropriate level of noise led to an increase in the response of the muscle spindle primary endings to a ramp-and-hold stretch. The increase in the average rate of discharge during the plateau compared to the average rate before the stretch was optimised with the addition of near-threshold levels of noise. The increase was a consequence of the greater dynamic sensitivity of the muscle spindle primary endings at longer muscle lengths and not the result of effects like stochastic resonance or dithering. This is similar to the effect observed by Querfurth & Gruser (1986) using frog muscle spindles and supra-threshold sinusoidal stimuli.

The addition of noise during the ramp-and-hold stimulus, while resulting in an increase in the average rate as a result of the stretch, is likely to have resulted in a decreased sensitivity to the initial stretch. Muscle spindle primary endings will typically respond to a ramp stretch with an initial burst at the beginning of the ramp that is thought to be due to stable cross-bridges (Hunt & Ottoson, 1976). The addition of supra-threshold levels of noise will result in the breaking of some of the stable cross-bridges, reducing the initial burst. The effective size of the initial burst, when compared to the discharge before the ramp stimulus, will also be reduced. Without the addition of noise, the

variability of the maintained discharge from a muscle spindle primary ending in a passive muscle is low (Stein & Matthews, 1965), so any increase in rate as a result of the initial burst would be quite prominent. The addition of noise would increase the variability of the discharge, reducing the effective size of the initial burst. Therefore, the increased sensitivity to the size of the ramp-and-hold stretch, via the addition of noise, comes at the cost of a reduced sensitivity to the initiation of the movement, via a decrease in the size of the initial burst. This is a factor in considering the functional role of stochastic resonance or any other effect requiring the addition of supra-threshold levels of noise.

Functional Role of Stochastic Resonance

The usefulness of stochastic resonance, by increasing the output SNR or allowing the detection of an otherwise sub-threshold signal, is obvious. There is a growing body of experimental evidence that stochastic resonance can occur in a variety of receptors and theoretical evidence that it may occur within neutral networks. Given that all biological receptors have a threshold, and therefore are potential candidates for stochastic resonance, it is interesting to ponder the role of stochastic resonance as a method of signal analysis that might be employed by the central nervous system.

Controlling the Noise

The external environment is full of signals that are of interest to the central nervous system and can be detected by a variety of receptors. There is also a large amount of information detected by the various receptors that is not of interest, and therefore may be considered as noise. However, the sources of noise are not confined to the external environment, as there are many possible sources of intrinsic noise within the receptive systems. It may be possible to reduce the noise from intrinsic sources, but it is not possible to control or eliminate external sources of noise. However, it may be possible to utilise the noise, via stochastic resonance or other effects such as dithering, to actually aid in the detection of weak signals.

The response of the receptive system can be optimised by the addition of the appropriate level of noise, D_{OPT}. As it is not possible to control the external noise

sources if the central nervous system is to utilise the external noise, via stochastic resonance or dithering, it must control it own intrinsic level of noise. There are several areas within each sensory system where it may be possible to add a controlled amount of noise, and these include the generator potential, the impulse generator (pacemaker), and some locations within the neutral network responsible for processing the afferent information.

Increased Sensitivity

Stochastic resonance can result in the detection of an otherwise sub-threshold periodic signal, as emphasised by the reduction in the detection threshold for small sinusoidal skin indentations in Chapter Six. The threshold of detection was often halved with the addition of the appropriate amount of input noise (Figure 6.7) although smaller reductions were also observed. It is worth noting however, that the stochastic resonance effect will only occur with a sub-threshold periodic stimulus. That is, the increase in sensitivity with the addition of noise will only occur if the periodic stimulus is otherwise undetectable. This point was illustrated by the experiments with receptors that were stimulated with a supra-threshold periodic stimulus (Figure 4.7 and Figure 5.10). The addition of noise to a supra-threshold periodic stimulus resulted in a reduction of SNR_{EXP}, as expected. The addition of noise will not always increase the sensitivity of the system, and only with a sub-threshold periodic signal is it possible for stochastic resonance to occur.

The effective reduction in threshold also has the advantage that a less sensitive receptor can be used to detect an equivalent-sized signal. A less sensitive receptor should reduce the effective level of external noise to which the receptor is subjected, resulting in greater control of the total noise level by the central nervous system. As already mentioned, there is a trade-off between the addition of noise to a signal, to improve detection via stochastic resonance, and the loss of sensitivity to other aspects of the signal, such as the initial burst in the response of muscle spindle primary endings to ramp stretches. Therefore, a lowering of the effective external noise may result in an increased sensitivity to other aspects of the signal.

Range of Frequencies

Although only two or three different frequencies of sub-threshold periodic signals were tested for each receptor that exhibited stochastic resonance, the stochastic resonance effect would be expected to occur over a wide range of frequencies. As a matching of the noise-alone induced rate and the periodic stimulus frequency is the essence of stochastic resonance, the range of frequencies over which it would be expected to occur is limited by the maximum noise-alone induced frequency. Therefore, it would be expected that different receptors could exhibit stochastic resonance over a different range of frequencies. This is illustrated by the fact that periodic signal frequencies up to approximately 100 Hz could be optimised for Golgi tendon organs and muscle spindle primary endings in the cat. This is contrasted by the muscle spindle secondary endings in the cat and slowly adapting Type I cutaneous mechanoreceptors in the toad, for which the frequency range would be limited to below 40 Hz.

Filtering

As the optimal noise level is dependent on the noise-alone response of the system, it is possible to use stochastic resonance as a type of filtering system. If the input noise to the system is held constant, then only a narrow range of periodic input frequencies will be optimised, and therefore only these frequencies will be passed by the 'stochastic resonance filter'. The input noise level could be adjusted to control the particular frequency the 'stochastic resonance filter' is most sensitive to, by adjusting the noise level such that a noise-alone signal resulted in an average discharge rate at the specified frequency.

Stochastic Resonance vs Dithering

Stochastic resonance is not the only mechanism whereby the addition of noise can improve signal detection. In fact, the dithering effect may be a better method of increasing the sensitivity of a system by the addition of noise. Dithering has the advantage that a signal noise level (near-threshold) is optimal for all signals, including aperiodic signals. Therefore, if a system were to utilise dithering rather than stochastic

resonance, there would be no need to adjust the noise signal to detect different frequencies of sub-threshold periodic stimuli.

Another advantage of dithering over stochastic resonance is that the optimal noise level required is lower for dithering than for stochastic resonance. In a situation where the input signal is supra-threshold, rather than sub-threshold, the addition of the optimal noise level would degrade the output SNR less for dithering than for stochastic resonance.

Dithering is likely to have a greater functional significance than stochastic resonance in biological systems. The ability to optimise a system's response with a single noise level, and for the response to be optimised for all sub-threshold stimuli, means that dithering is likely to be of more practical benefit than stochastic resonance. The one advantage of stochastic resonance is that the system can be preferentially tuned to respond to a narrow range of frequencies.

Stochastic Resonance Example

The best way to illustrate how stochastic resonance may be utilised by the central nervous system is with the aid of an example. Muscle spindle primary endings will respond to changes in muscle length, as a result of the lengthening of the equatorial regions of the intrafusal fibres, with the passive stretch response being predominantly from nuclear bag_2 intrafusal fibres (Proske et al., 1992). Contractions of the polar segments of the intrafusal fibres, via the γ motoneurones, can also result in lengthening of the equatorial regions (Bessou & Pagés, 1975). A single pacemaker is proposed to sum the generator current from the endings on the nuclear bag_2 fibre and nuclear chain fibres (Carr & Proske, 1996). This generator is then subject to pacemaker switching, with a small amount of summation, with the pacemaker associated with the endings on the nuclear bag_1 fibre (Fallon, Carr, Gregory & Proske, 2001). Given that the length changes are signalled by the afferent endings on the nuclear bag_2 fibre, and that there are ending of the same afferent on other intrafusal fibres, it may be possible for the central nervous system to optimise the response of the muscle spindle primary ending to a particular frequency range via stochastic resonance.

Activation of the nuclear chain fibres, via the γ_s motoneurones, may produce a noise input for the muscle spindle primary endings. The nuclear chain fibres have a higher contraction velocity than the nuclear bag fibres, and therefore would be most suited to providing a rapidly changing, pseudo-random signal to be used as a source of noise. In decerebrate cats the spontaneous activity in fusimotor fibres innervating the medial gastrocnemius muscle is essentially a white noise source (Matthews & Stein, 1969a; Blesic, Milosevic, Stratimirovic & Ljubisavljevic, 1999). Provided the random activity in the fusimotor fibres is converted into a random signal which can be summed at the site of action potential generation within the muscle spindle, the spontaneous fusimotor activity would provide a noise source for stochastic resonance within the muscle spindle system (Stratimirovic, Milosevic, Blesic & Ljubisavljevic, 2001).

A situation in which a periodic movement with a narrow frequency spectrum is of interest is in the detection of muscle tremor, during which the movements are typically around 10 Hz (Joyce & Rack, 1974). The level of contraction of the nuclear chain fibres could be adjusted to produce an averaged maintained discharge of approximately 10 i/s, which would optimise the response of the muscle spindle primary endings to preferentially detect the tremor. This would enable the central nervous system to react to the generation of smaller amplitudes of tremor, resulting in smaller corrections to the motor stimulation pattern being required.

However, the muscle spindle primary endings are proposed to have a role in the development of the tremor (Matthews & Watson, 1981b), with an increase in their discharge, in response to vibration, resulting in an increase in tremor (Joyce, Rack & Ross, 1974). Therefore, using contraction of the nuclear chain fibres to control the maintained level of discharge may not be feasible, as this may in itself result in an increase in the tremor.

Signals from individual muscle spindles do not result in a conscious sensation (Macefield et al., 1990), but are thought to be pooled with signals from other muscle spindles to produce a conscious sensation. Therefore, a signal that is supra-threshold for a particular muscle spindle may be sub-threshold for the population of muscle spindles involved in the production of a conscious sensation. Stochastic resonance may therefore

occur within the network involved in the production of the conscious sensation. That stochastic resonance can occur in such a network was suggested by the results presented in Figure 2.17 and by the work of Mato (1999), who also showed that a suitable noise source could be generated by a simple neural network. Therefore it is possible that stochastic resonance might play a role at some level within the central nervous system itself.

Interestingly, the experimental results from Chapter Five indicate that stochastic resonance can occur in individual muscle spindles, bu: failed to show stochastic resonance during a proprioceptive task that was designed to utilise the response from muscle spindles. Individual muscle spindle primary and secondary endings were able to exhibit stochastic resonance when stimulated under the appropriate conditions: sub-threshold periodic stimulus plus a supra-threshold noise stimulus. A corresponding reduction in the detection threshold for small sinusoidal movements of the elbow during psychophysical experiments was not observed. It may be that there were already optimal conditions for detecting the small sinusoidal movements of the elbow. The addition of extra external noise would then be expected to result in increases of detection threshold, as observed.

Summary

It is worth reiterating that the stochastic resonance effect can result in an increase in the output SNR of a system, or a corresponding reduction in detection threshold, with the appropriate level of additional input noise. Although stochastic resonance can improve the performance of a fixed system, if it is possible to adjust the system by altering the criteria on which the output of a system is based, then the stochastic resonance effect will, at best, give the same performance as an optimal choice of the decision criteria (Tougaard, 2000). That is, stochastic resonance cannot improve the performance of an optimally designed system. However, for fixed systems, such as many biological systems, the addition of appropriate levels of input noise, via stochastic resonance, can result in the detection of otherwise sub-threshold periodic signals.

The appropriate level of additional noise needed to optimise a system's response can be determined from the noise-alone response of the system, and is unique for each frequency of periodic stimulus. This is the key feature of stochastic resonance that separates it from other noise effects, such as dithering. However, stochastic resonance will only occur with a periodic stimulus that is sub-threshold in the absence of any additional input. Therefore, there are a limited number of circumstances where the stochastic resonance effect will be of biological significance.

An interesting feature of the stochastic resonance modelling was that none of the models that were able to produce a physiological level of maintained discharge, were also able to exhibit stochastic resonance. The ability of a model to exhibit stochastic resonance can now be added to the range of criteria that must be met if it is to be a good model of a biological system that can exhibit stochastic resonance. The role of apparently random discharges within a neutral network may also need to be reinterpreted as a possible indication of stochastic resonance, rather than a limiting influence on the sensitivity of the system.

As the ability of biological systems to exhibit stochastic resonance has been confirmed, any discussions of the fidelity of sensory systems will now have to take stochastic resonance into account. Given the ubiquity of background noise in the environment and within the central nervous system itself, there are many opportunities for stochastic resonance to occur. Therefore, the finding that a system can perform better than expected in the presence of inescapable sources of noise may need to be reinterpreted, taking stochastic resonance into account.

Appendix A

Appendix A is an index for the CD that has been included inside the back cover of this thesis. The CD includes the IGOR Pro (WaveMetrics, Lake Oswego, Oregon, U.S.A.) procedure files and the 'C' code for the XOPs required for implementation of the multi-channel recorder program. The 'C' code for the XOPs that were written to perform the simulations discussed in Chapter Two are also included. A QuickTime® movie that illustrates the double-well model and the resulting output SNR with different levels of input noise is included. An electronic copy of this thesis has also been included and can be viewed using Adobe Acrobat Reader.

Appendix B

Hodgkin-Huxley Membrane Model Equations

$$I = C_M \frac{dV}{dt} - g_K n^4 (V - V_K) - g_{Na} m^3 h (V - V_{Na}) - g_l (V - V_l)$$

$$\frac{dn}{dt} = \alpha_n (1 - n) - \beta_n n$$

$$\alpha_n = \frac{0.01(V + 10)}{e^{\left(\frac{V+10}{10}\right)} - 1}$$

$$\beta_n = 0.125 \, e^{\frac{V}{80}}$$

$$\frac{dm}{dt} = \alpha_m (1 - m) - \beta_m m$$

$$\alpha_m = \frac{0.1(V + 25)}{\exp^{\left(\frac{V+25}{10}\right)} - 1}$$

$$\beta_m = 4 \, e^{\frac{V}{18}}$$

$$\frac{dh}{dt} = \alpha_h (1 - h) - \beta_h h$$

$$\alpha_h = 0.07 \, e^{\frac{V}{20}}$$

$$\beta_h = \frac{1}{e^{\left(\frac{V+30}{10}\right)} + 1}$$

Constant	Value
C_M ($\mu F / cm^2$)	1.0
V_{Na} (mV)	-115
V_K (mV)	12
V_l (mV)	-10.613
g_{Na} (mS / cm^2)	120
g_K (mS / cm^2)	36
g_l (mS / cm^2)	0.3

Appendix C

Otten Model Equations

$$I = C_M \frac{dV}{dt} + I_{Na} + I_K + I_P + I_{Ks} + I_l$$

$$I_K = P_K n^2 \frac{VF^2}{RT} \left([K]_o - \frac{[K]_i e^{\frac{VF}{RT}}}{1 - e^{\frac{VF}{RT}}} \right)$$

$$\frac{dn}{dt} = \alpha_n (1-n) - \beta_n n$$

$$\alpha_n = \frac{0.02(V+35)}{1 - \exp\left(\frac{105-V}{10}\right)}$$

$$\beta_n = \frac{0.05(80-V)}{1 - e^{\frac{V+60}{10}}}$$

$$I_{Ks} = P_{Ks} q^2 \frac{VF^2}{RT} \left([K]_o - \frac{[K]_i e^{\frac{VF}{RT}}}{1 - e^{\frac{VF}{RT}}} \right)$$

$$\frac{dq}{dt} = \alpha_q (1-q) - \beta_q q$$

$$\alpha_q = \frac{0.0005(V+55)}{1 - \exp\left(\frac{85-V}{5}\right)}$$

$$\beta_q = \frac{0.0005(85-V)}{1 - e^{\frac{V+55}{5}}}$$

$$I_P = P_P p^2 \frac{VF^2}{RT} \left([Na]_o - \frac{[Na]_i e^{\frac{VF}{RT}}}{1 - e^{\frac{VF}{RT}}} \right)$$

$$\frac{dp}{dt} = \alpha_p (1-p) - \beta_p p$$

$$\alpha_p = \frac{0.006 + 30}{1 - \exp\left(\frac{110-V}{10}\right)}$$

$$\beta_p = \frac{0.09(-95-V)}{1 - e^{\frac{V+95}{20}}}$$

$$I_l = g_L(V - V_L)$$

$$I_{Na} = P_{Na} m^2 h \frac{VF^2}{RT} \left([Na]_o - \frac{[Na]_i e^{\frac{VF}{RT}}}{1 - e^{\frac{VF}{RT}}} \right)$$

$$\frac{dm}{dt} = \alpha_m (1-m) - \beta_m m$$

$$\alpha_m = \frac{0.36(V+48)}{1 - \exp\left(\frac{92-V}{3}\right)}$$

$$\beta_m = \frac{0.4(83-V)}{1 - e^{\frac{V+57}{20}}}$$

$$\frac{dh}{dt} = \alpha_h (1-h) - \beta_h h$$

$$\alpha_h = \frac{0.1(-80-V)}{1 - e^{\frac{V+80}{6}}}$$

$$\beta_h = \frac{4.5}{e^{\left(\frac{-25-V}{10}\right)} + 1}$$

Constant	Value
C_M ($\mu F / cm^2$)	2.0
P_{Na} (cm / sec)	0.010
P_K (cm / sec)	0.0005
P_{Ks} (cm / sec)	0.00005
P_P (cm / sec)	0.00061
g_l (mS / cm^2)	0.0083
V_L (mV)	0.026
$[Na]_o$ (mM)	114.5
$[Na]_i$ (mM)	13.74
$[K]_o$ (mM)	2.5
$[K]_i$ (mM)	120
F (K)	96487
R (K / mol)	8314.32

Appendix D
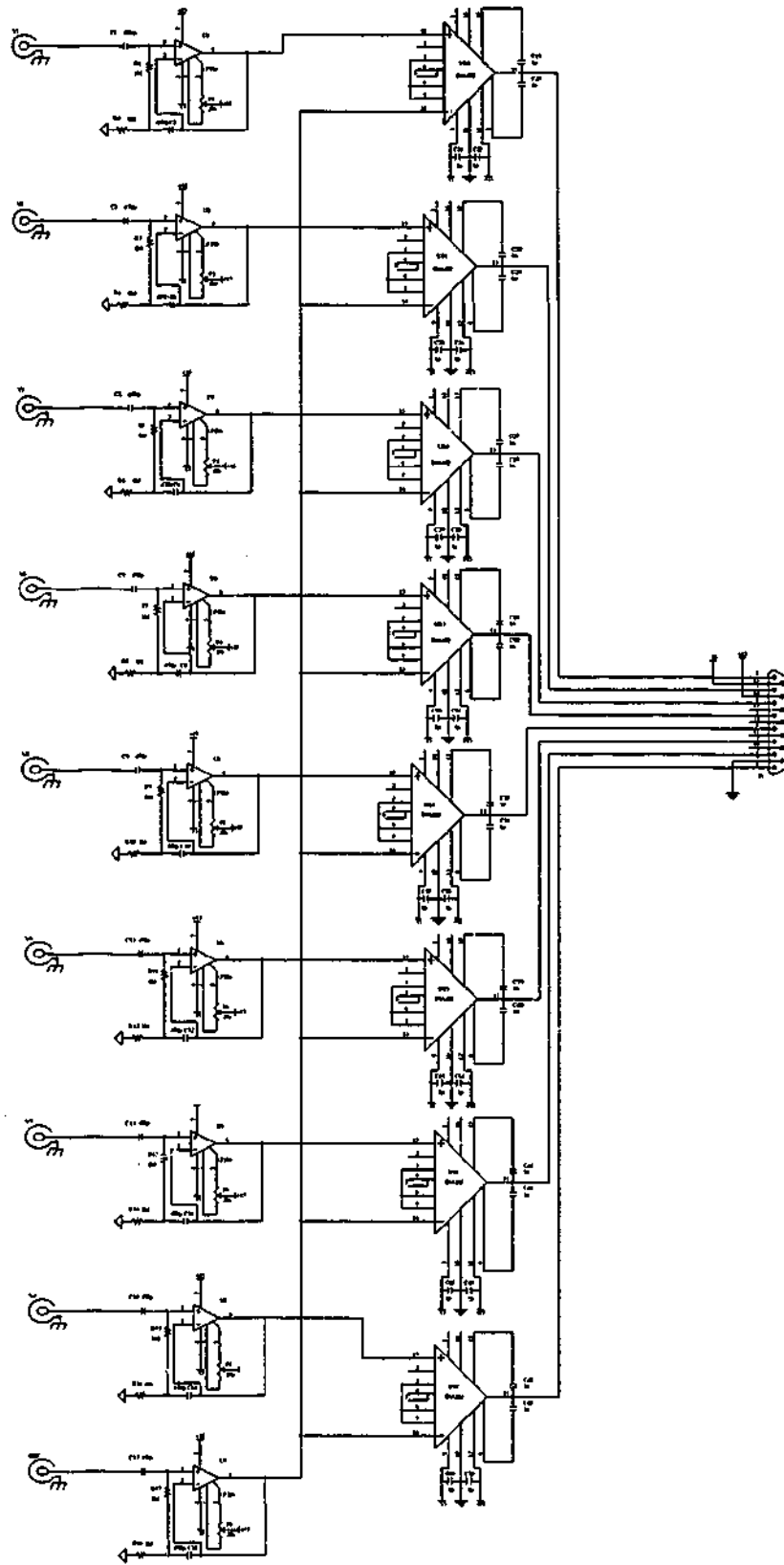
Schematic of the amplifiers used in the header stage of the multi-channel recording system.

Appendix E
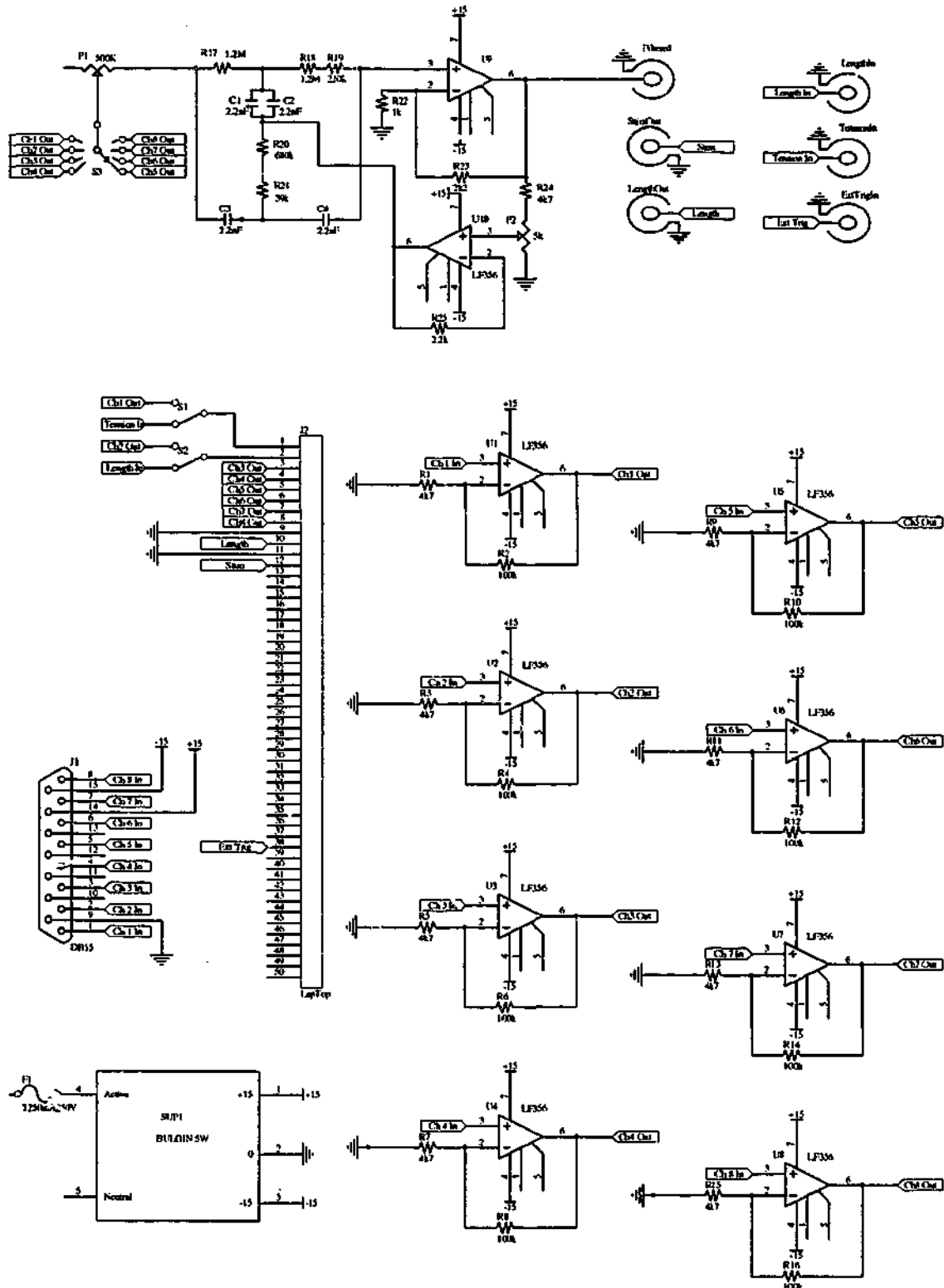
Schematic of the second stage of the multi-channel recording system.

153

Appendix F

Noise Signal Characteristics

The clock-interval for up-dating all computer controlled analogue signals was 1 ms, although all length control signals were digitally filtered by a single low-pass Butterworth filter with a corner frequency of 500 Hz. The normalized power spectrum of a noise-alone movement produced with the electro-magnetic position controller is illustrated in Figure F.1. The spectrum was computing from output length signal from the electro-magnetic position controller. The spectrum is flat below 200 Hz, after which it rapidly rolls off due to the combined effects of the digital filter, the signal up-date rate and the response properties of the electro-magnetic position controller. As the maximum sinusoidal test frequencies investigated were below 50 Hz, the noise signal was considered to represent an effective broad-band noise signal.

The background noise level of the electro-magnetic position controller with feedback, used for the experiments with soleus muscle of the cat and the psychophysical experiments with the elbow, was approximately 3 μm. Compressed air was used to provide an effective 'air bearing' system for the controller. The 'air bearing' was used to reduce any possible stiction of the controller, which was confirmed via observations of the recorded length signals.

The response properties of the electro-magnetic actuator, used for the experiments with slowly adapting cutaneous mechanoreceptors of the toad and the psychophysical experiments with skin, were similar to those of the electro-magnetic position controller with feedback. However, as can be seen in the normalized power spectrum of a noise-alone movement (Figure F.2), the response begins to decrease above 20 Hz. As the electro-magnetic actuator did not have feedback control and had no output length signal, to record the actuator's response to the command signal the actuator tip was connected to a high compliance strain gauge (Grass FT03C, Quincy, Massachusetts, U.S.A.) and the resulting force signal interpreted as length. The maximum sinusoidal test frequency investigated with the electro-magnetic actuator was 15 Hz, so again the noise was considered to represent an effective broad-band noise signal. Any reduction in noise content at the higher frequencies, due to the response properties of the actuator, would be consistent for both the noise-alone and noise plus sub-threshold sinusoidal signal conditions. Therefore, the coloured noise would not be expected to result in a qualitative change in the results.
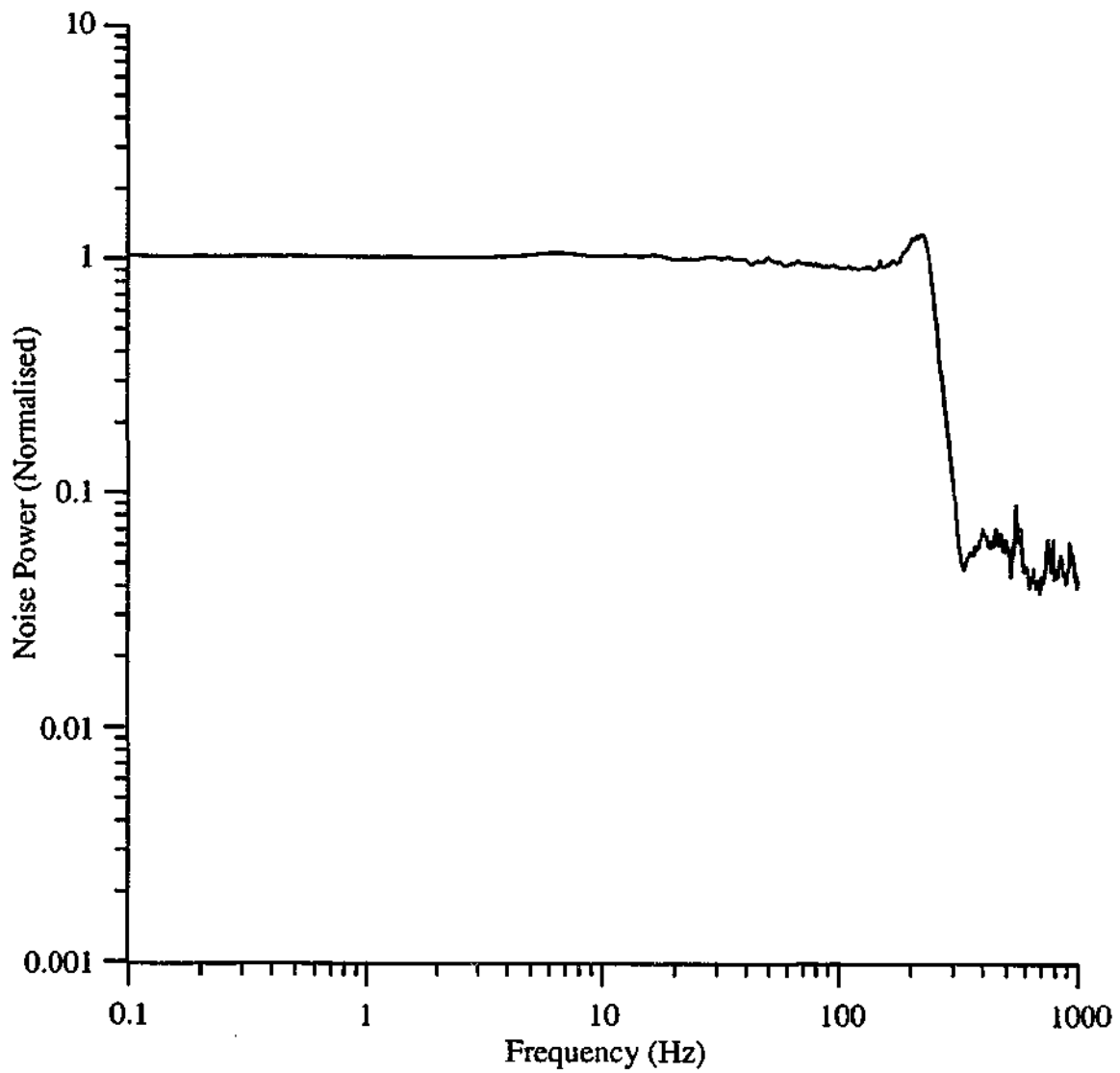
Figure F.1 The normalised power spectrum of a 100 μm noise-alone movement generated by the electro-magnetic position controller with feedback used for the experiments with soleus muscle of the cat is flat up to approximately 200 Hz.
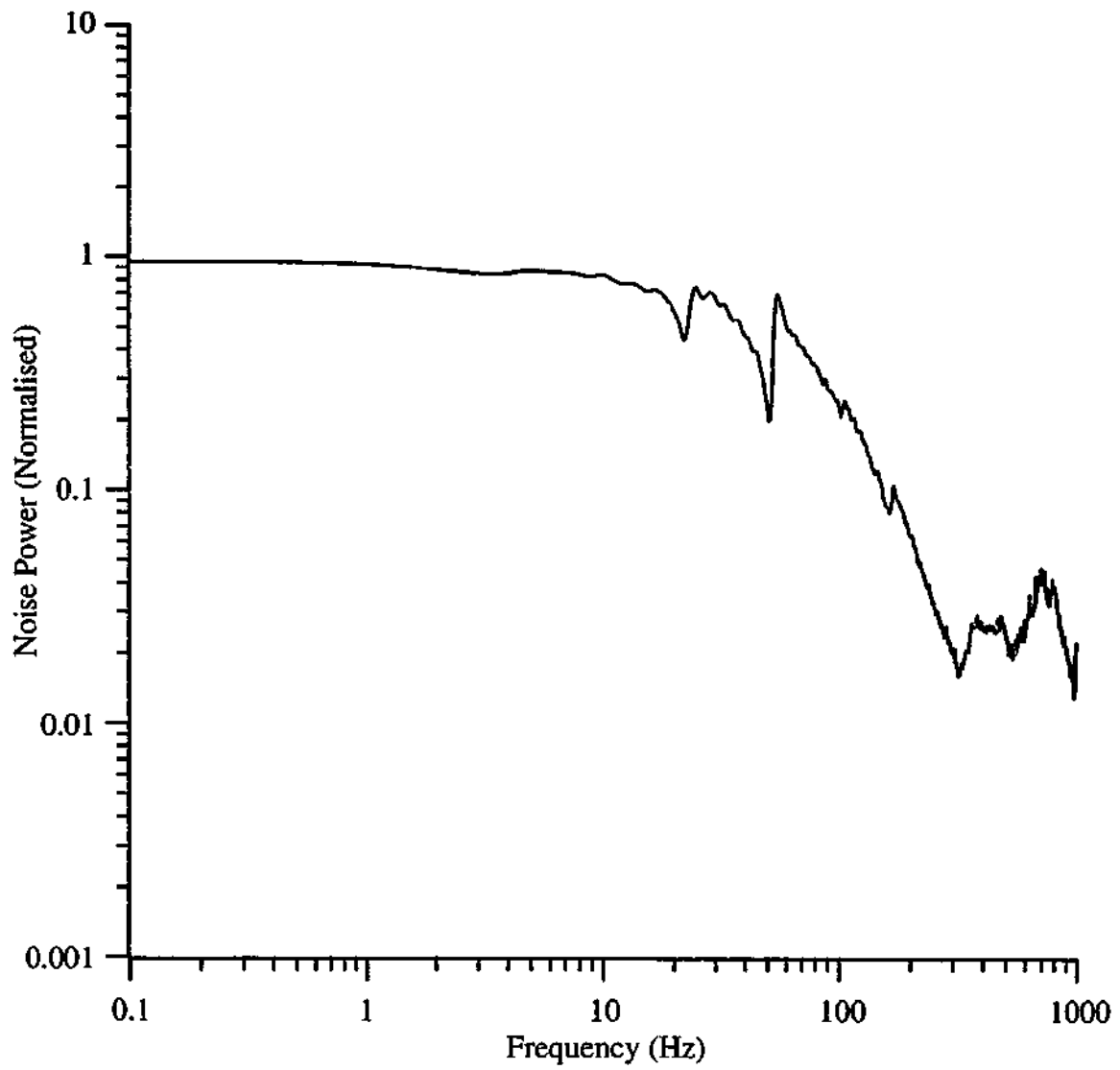
**Figure F.2** The normalised power spectrum of a 50 μm noise-alone movement generated by the electro-magnetic actuator used for the experiments with slowly adapting cutaneous mechanoreceptors of the toad is flat up to approximately 20 Hz.

Bibliography

Adrian, E. D. (1926) The impulses produced by sensory nerve endings. Part 1. *Journal of Physiology*, **61**, 49-72.

Adrian, E. D. & Zotterman, Y. (1926) The impulses produced by sensory nerve endings. Part 3. Impulses set up by touch and pressure. *Journal of Physiology*, **61**, 465-483.

Alnes, E. (1967) Static and dynamic properties of Golgi tendon organs in the anterior tibial and soleus muscles of the cat. *Acta physiologica Scandinavica*, **70**, 176-187.

Anderson, J. H. (1974) Dynamic characteristics of Golgi tendon organs. *Brain Research*, **67**, 531-537.

Anderson, J. S., Lampl, I., Gillespie, D. C. & Ferster, D. (2000) The contribution of noise to contrast invariance of orientation tuning in cat visual cortex. *Science*, **290**, 1968-1972.

Andresen, M. C. & Kunze, D. L. (1994) Nucleus tractus solitarius - gateway to neural lcirculatory control. *Annual Review of Physiology*, **56**, 93-116.

Balazsi, G., Kiss, L. B. & Moss, F. E. (1999) Spatiotemporal stochastic resonance and its consequences in a neural system. *Unsolved Problems of Noise and Fluctuations*, **1**, 159-168.

Banks, R. W. (1981) A histological study of the motor innervation of the cat's muscle spindle. *Journal of Anatomy*, **133**, 571-591.

Banks, R. W., Barker, D. & Stacey, M. J. (1977) Intrafusal branching and distribution of primary and secondary afferents. *Journal of Physiology*, **272**, 66P-67P.

Banks, R. W., Barker, D. & Stacey, M. J. (1982) Form and distribution of sensory terminals in cat hindlimb muscle spindles. *Philosophical Transactions of the Royal Society of London. Series B, Biological Sciences*, **299**, 329-364.

Barbi, M., Chillemi, S. & Di Garbo, A. (2000) The leaky integrate-and-fire with noise: A useful tool to investigate SR. *Chaos Solitons & Fractals*, **11**, 1849-1853.

Barker, D. (1948) The innervation of the muscle-spindle. *Quarterly Journal of Microscopical Science*, **98**, 177-199.

Barker, D. (1962) The sturcture and distribution of muscle receptors. In *Symposium on muscle recpetors*, ed. Barker, D., 227-240. Hong Kong: Hong Kong University Press.

Barker, D. (1974) The morphology of muscle receptors. In *Muscle receptors*, ed. Hunt, C. C., 1-190. Berlin: Spinger-Verlag.

Benzi, R., Parisi, G., Sutera, A. & Vulpiani, A. (1982) Stochastic resonance in climatic change. *Tellus*, **34**, 10-16.

Benzi, R., Sutera, A. & Vulpiani, A. (1981) The mechanism of stochastic resonance. *Journal of Physics A Mathematical & General*, **14**, L453-L457.

Bessou, P. & Laporte, Y. (1962) Responses from primary and secondary endings of the same neuromuscular spindle of the tenuissimus muscle of the cat. In *Symposium on muscle receptors*, ed. Barker, D., 105-119. Hong Kong: Hong Kong University Press.

Bessou, P. & Pagés, B. (1975) Cinematographic analysis of contractile events produced in intrafusal muscle fibres by stimulation of static and dynamic fusimotor axons. *Journal of Physiology*, **252**, 397-427.

Bezrukov, S. M. & Vodyanoy, I. (1995) Noise-induced enhancement of signal transduction across voltage-dependent ion channels. *Nature*, **378**, 362-364.

Bezrukov, S. M. & Vodyanoy, I. (1997) Signal transduction across alamethicin ion channels in the presence of noise. *Biophysical Journal*, **73**, 2456-2464.

Bezrukov, S. M. & Vodyanoy, I. (1998) Stochastic resonance in thermally activated reactions: Application to biological ion channels. *Chaos*, **8**, 557-566.

Blesic, S., Milosevic, S., Stratimirovic, D. & Ljubisavljevic, M. (1999) Detrended fluctuation analysis of time series of a firing fusimotor neuron. *Physica A*, **268**, 275-282.

Boyd, I. A. (1962) The structure and innervation of the nuclear bag muscle fibre system and the nuclear chain muscle fibre system in mammalian muscle spindles.

Philosophical Transactions of the Royal Society of London. Series B, Biological Sciences, **245**, 81-136.

Boyd, I. A. & Ward, J. (1975) Motor control of nuclear bag and nuclear chain intrafusal fibres in isolated living muscle spindles from the cat. *Journal of Physiology*, **244**, 83-112.

Bridgeman, C. F. (1968) The structure of tendon organs in the cat: A proposed mechanism for responding to muscle tension. *Anatomical Record*, **162**, 209-220.

Bronzino, J. D. (1995) *The biomedical engineering handbook*. Boca Raton, Florida: CRC Press.

Brown, M. C., Engberg, I. & Matthews, P. B. C. (1967) The relative sensitivity to vibration of muscle receptors of the cat. *Journal of Physiology*, **192**, 773-800.

Brown, M. C., Goodwin, G. M. & Matthews, P. B. C. (1969) After-effects of fusimotor stimulation on the response of muscle spindle primary afferent endings. *Journal of Physiology*, **205**, 677-694.

Brown, T. I. H., Huang, Y., Morgan, D. L., Proske, U. & Wise, A. (1999) A new strategy for controlling the level of activation in artificially stimulated muscle. *IEEE Transactions on Rehabilitation Engineering*, **7**, 167-173.

Bulsara, A., Jacobs, E. W., Zhou, T., Moss, F. & Kiss, L. (1991) Stochastic resonance in a single neuron model: Theory and analog simulation. *Journal of Theoretical Biology*, **152**, 531-555.

Carr, R. W. (1999) Impulse initiation in sensory receptors of skin and muscle. PhD thesis from Monash University.

Carr, R. W. & Proske, U. (1996) Multiple sites of impulse initiation in the mammalian muscle spindle. *Primary Sensory Neuron*, **1**, 327-339.

Catton, W. T. (1958) Some properties of frog skin mechanoreceptors. *Journal of Physiology*, **141**, 305-322.

Catton, W. T. (1976) Cutaneous mechanoreceptors. In *Frog neurobiology*, ed. Llinás, R. & Precht, W., 629-642. Berlin: Springer-Verlag.

Chambers, M. R., Andres, K. H., von Duering, M. & Iggo, A. (1972) The structure and function of the slowly adapting Type II mechanoreceptor in hairy skin. *Quarterly Journal of Experimental Physiology & Cognate Medical Sciences*, **57**, 417-445.

Chambers, M. R. & Iggo, A. (1967) Slowly-adapting cutaneous mechanoreceptors. *Journal of Physiology*, **192**, 26P-27P.

Chapeau-Blondeau, F. & Godivier, X. (1997) Theory of stochastic resonance in signal transmission by static nonlinear systems. *Physical Review E. Statistical Physics, Plasmas, Fluids, & Related Interdisciplinary Topics*, **55**, 1478-1495.

Chialvo, D. R. & Apkarian, A. V. (1993) Modulated noisy biological dynamics: Three examples. *Journal of Statistical Physics*, **70**, 375-391.

Chialvo, D. R., Longtin, A. & Muller-Gerking, J. (1997) Stochastic resonance in models of neuronal ensembles. *Physical Review E. Statistical Physics, Plasmas, Fluids, & Related Interdisciplinary Topics*, **55**, 1798-1808.

Chiou-Tan, F. Y., Magee, K. N., Robinson, L. R., Nelson, M. R., Tuel, S. S., Krouskop, T. A. & Moss, F. (1996) Enhancement of subthreshold sensory nerve action potentials during muscle tension mediated noise. *International Journal of Bifurcation & Chaos in Applied Sciences & Engineering*, **6**, 1389-1396.

Chow, C. C., Imhoff, T. T. & Collins, J. J. (1998) Enhancing aperiodic stochastic resonance through noise modulation. *Chaos*, **8**, 616-620.

Collins, J. J., Chow, C. C. & Imhoff, T. T. (1995a) Aperiodic stochastic resonance in excitable systems. *Physical Review E. Statistical Physics, Plasmas, Fluids, & Related Interdisciplinary Topics*, **52**, R3321-R3324.

Collins, J. J., Chow, C. C. & Imhoff, T. T. (1995b) Stochastic resonance without tuning. *Nature*, **376**, 236-238.

Collins, J. J., Imhoff, T. T. & Grigg, P. (1996a) Noise-enhanced information transmission in rat SA1 cutaneous mechanoreceptors via aperiodic stochastic resonance. *Journal of Neurophysiology*, **76**, 642-645.

Collins, J. J., Imhoff, T. T. & Grigg, P. (1996b) Noise-enhanced tactile sensation. *Nature*, **383**, 770.

Collins, J. J., Imhoff, T. T. & Grigg, P. (1997) Noise-mediated enhancements and decrements in human tactile sensation. *Physical Review E. Statistical Physics, Plasmas, Fluids, & Related Interdisciplinary Topics*, **56**, 923-926.

Connor, J. A. & Stevens, C. F. (1971) Prediction of repetitive firing behaviour from voltage clamp data on an isolated neurone soma. *Journal of Physiology*, **213**, 31-53.

Cooper, S. (1961) The responses of the primary and secondary endings of muscle spindles with intact motor innervation during applied stretch. *Quarterly Journal of Experimental Physiology*, **46**, 389-398.

Cordo, P., Inglis, J. T., Verschueren, S., Collins, J. J., Merfeld, D. M., Rosenblum, S., Buckley, S. & Moss, F. (1996) Noise in human muscle spindles. *Nature*, **383**, 769-770.

Cornsweet, T. N. (1962) The staircase method in psychophysics. *American Journal of Psychology*, **75**, 485-495.

Crowe, A. & Matthews, P. B. C. (1964) The effects of stimulation of the static and dynamic fusimotor fibre on the response to stretching of the primary endings of muscle spindles. *Journal of Physiology*, **174**, 109-131.

Ditzinger, T., Stadler, M., Struber, D. & Kelso, J. A. S. (2000) Noise improves three-dimensional perception: Stochastic resonance and other impacts of noise to the perception of autostereograms. *Physical Review E. Statistical Physics, Plasmas, Fluids, & Related Interdisciplinary Topics*, **62**, 2566-2575.

Djupsjobacka, M., Johansson, H., Bergenheim, M. & Sandstrom, U. (1994) A multichannel hook electrode for simultaneous recording of up to 12 nerve filaments. *Journal of Neuroscience Methods*, **52**, 69-72.

Douglass, J. K., Wilkens, L., Pantazelou, E. & Moss, F. (1993) Noise enchancement of information transfer in crayfish mechanoreceptors by stochastic resonance. *Nature*, **365**, 337-340.

Dun, F.-T. & Finley, C. B. (1938) The rate of adaptation of cutaneous nerve endings in the frog. *Journal of Physiology*, **94**, 170-176.

Emonet-Denand, F., Laporte, Y., Matthews, P. B. C. & Petit, J. (1977) On the subdivision of static and dynamic fusimotor actions on the primary ending of the cat muscle spindle. *Journal of Physiology*, **268**, 827-861.

Fallon, J. B., Carr, R. W., Gregory, J. E. & Proske, U. (2001) Summing responses of cat soleus muscle spindles to combined static and dynamic fusimotor stimulation. *Brain Research*, **888**, 348-355.

Fankenhaeuser, B. & Huxley, A. F. (1964) The action potential in the myelinated nerve fibre of *Xenopus laevis* as computed on the basis of voltage clamp data. *Journal of Physiology*, **171**, 302-315.

Fauve, S. & Heslot, F. (1983) Stochastic resonance in a bistable system. *Physics Letters A*, **97**, 5-7.

Finkel, A. S. & Redman, S. J. (1983) The synaptic current evoked in cat spinal motoneurones by impulses in single Group 1a axons. *Journal of Physiology*, **342**, 615-632.

Fitzhugh, R. A. (1961) Impulses and physiological states in theoretical models of nerve membrane. *Biophysical Journal*, **1**, 445.

Folkow, B. & Halicka, H. D. (1968) A comparison between 'red' and 'white' muscle with respect to blood supply, capillary surface area and oxygen uptake during rest and exercise. *Microvascular Research*, **1**, 1-14.

Fox, H. & Whitear, M. (1978) Observation of Merkel cells in amphibians. *Biologie cellulaire*, **32**, 223-232.

Fox, R. F. (1989) Stochastic resonance in a double well. *Physical Review A. General Physics*, **39**, 4148-4153.

Fukami, Y. & Wilkinson, R. S. (1977) Responses of isolated Golgi tendon organs of the cat. *Journal of Physiology*, **265**, 673-689.

Fulton, J. F. & Pi-Suñer, J. (1928) A note concerning the probable function of various afferent end-organs in skeletal muscle. *American Journal of Physiology*, **83**, 554-562.

Gammaitoni, L. (1995) Stochastic resonance and the dithering effect in threshold physical systems. *Physical Review E. Statistical Physics, Plasmas, Fluids, & Related Interdisciplinary Topics*, **52**, 4691-4698.

Gammaitoni, L., Hanggi, P., Jung, P. & Marchesoni, F. (1998) Stochastic resonance. *Reviews of Modern Physics*, **70**, 223-287.

Gammaitoni, L., Marchesoni, F. & Santucci, S. (1995) Stochastic resonance as a bona fide resonance. *Physical Review Letters*, **74**, 1052-1055.

Gebeshuber, I. C. (2000) The influence of stochastic behavior on the human threshold of hearing. *Chaos Solitons & Fractals*, **11**, 1855-1868.

Giacomelli, G., Marin, F. & Rabbiosi, I. (1999) Stochastic and bona fide resonance: An experimental investigation. *Physical Review Letters*, **82**, 675-678.

Gluckman, B. J., Netoff, T. I., Neel, E. J., Ditto, W. L., Spano, M. L. & Schiff, S. J. (1996) Stochastic resonance in a neuronal network from mammalian brain. *Physical Review Letters*, **77**, 4098-4101.

Gluckman, B. J., So, P., Netoff, T. I., Spano, M. L. & Schiff, S. J. (1998) Stochastic resonance in mammalian neuronal networks. *Chaos*, **8**, 588-598.

Godivier, X. & Chapeau-Blondeau, F. (1996) Noise-enhanced transmission of spike trains in the neuron. *Europhysics Letters*, **35**, 473-477.

Goychuk, I. & Hanggi, P. (2000) Stochastic resonance in ion channels characterized by information theory. *Physical Review E. Statistical Physics, Plasmas, Fluids, & Related Interdisciplinary Topics*, **61**, 4272-4280.

Greenwood, P. E., Ward, L. M., Russell, D. F., Neiman, A. & Moss, F. (2000) Stochastic resonance enhances the electrosensory information available to paddlefish for prey capture. *Physical Review Letters*, **84**, 4773-4776.

Gregory, J. E., Harvey, R. J. & Proske, U. (1977) A 'late supernormal period' in the recovery of excitability following an action potential in muscle spindle and tendon organ receptors. *Journal of Physiology*, **271**, 449-472.

Gregory, J. E., Morgan, D. L. & Proske, U. (1985) The discharge of cat tendon organs during unloading contractions. *Experimental Brain Research*, **61**, 222-226.

Gregory, J. E., Morgan, D. L. & Proske, U. (1991) Two kinds of resting discharge in cat muscle spindles. *Journal of Neurophysiology*, **66**, 602-612.

Harrington, T. & Merzenich, M. M. (1970) Neural coding in the sense of touch: Human sensations of skin indentation compared with the responses of slowly adapting mechanoreceptive afferents innervating the hairy skin of monkeys. *Experimental Brain Research*, **10**, 251-264.

Harvey, R. J. & Matthews, P. B. C. (1961) The response of de-efferented muscle spindle endings in the cat's soleus to slow extension of the muscle. *Journal of Physiology*, **157**, 370-392.

Henry, K. R. (1999) Noise improves transfer of near-threshold, phase-locked activity of the cochlear nerve: Evidence for stochastic resonance? *Journal of Comparative Physiology A. Sensory Neural & Behavioral Physiology*, **184**, 577-584.

Hidaka, I., Nozaki, D. & Yamamoto, Y. (2000) Functional stochastic resonance in the human brain: Noise induced sensitization of baroreflex system. *Physical Review Letters*, **85**, 3740-3743.

Hill, D. K. (1968) Tension due to interaction between the sliding filaments in resting striated muscle. The effect of stimulation. *Journal of Physiology*, **199**, 637-684.

Hille, B. (1992) *Ionic channels of excitable membranes.* Sunderland, Mass.: Sinauer Associates.

Hodgkin, A. L. & Huxley, A. F. (1952) A quantitative description of membrane current and its application to conduction and excitation in nerve. *Journal of Physiology*, **117**, 500-544.

Höglund, G. & Lindblom, U. F. (1961) The discharge in single touch receptors elicited by defined mechanical stimuli. *Acta physiologica Scandinavica*, **52**, 108-119.

Horch, K. W. & Burgess, P. R. (1975) Effect of activation and adaptation on the sensitivity of slowly adapting cutaneous mechanoreceptors. *Brain Research*, **98**, 109-118.

Horch, K. W., Whitehorn, D. & Burgess, P. R. (1974) Impulse generation in Type I cutaneous mechanoreceptors. *Journal of Neurophysiology*, **37**, 267-281.

Houk, J. & Henneman, E. (1967) Responses of Golgi tendon organs to active contractions of the soleus muscle of the cat. *Journal of Neurophysiology*, **30**, 466-481.

Hunt, C. C. (1951) The reflex activity of mammalian small-nerve fibres. *Journal of Physiology*, **115**, 456-469.

Hunt, C. C. (1954) Relation of function to diameter in afferent fibers of muscle nerves. *Journal of General Physiology*, **38**, 117-131.

Hunt, C. C. & Kuffler, S. W. (1951) Further study of efferent small-nerve fibres to mammalian muscle spindles. Multiple spindle innervation and activity during contraction. *Journal of Physiology*, **113**, 283-297.

Hunt, C. C. & Ottoson, D. (1976) Initial burst of primary endings of isolated mammalian muscle spindles. *Journal of Neurophysiology*, **39**, 324-330.

Iggo, A. (1974) Cutaneous receptors. In *The peripheral nervous system*, ed. Hubbard, J. I., 347-404. New York: Plenum Press.

Iggo, A. (1977) Cutaneous and subcutaneous sense organs. *British Medical Bulletin*, **33**, 97-102.

Iggo, A. & Muir, A. R. (1969) The structure and function of a slowly adapting touch corpuscle in hairy skin. *Journal of Physiology*, **200**, 763-796.

Ivey, C., Apkarian, A. V. & Chialvo, D. R. (1998) Noise-induced tuning curve changes in mechanoreceptors. *Journal of Neurophysiology*, **79**, 1879-1890.

Jami, L. (1992) Golgi tendon organs in mammalian skeletal muscle: Functional properties and central actions. *Physiological Reviews*, **72**, 623-666.

Jansen, J. K. S. & Matthews, P. B. C. (1962a) The central control of the dynamic response of muscle spindle receptors. *Journal of Physiology*, **161**, 357-378.

Jansen, J. K. S. & Matthews, P. B. C. (1962b) The effects of fusimotor activity on the static responsiveness of primary and secondary endings of muscle spindles in the decerebrate cat. *Acta physiologica Scandinavica*, **55**, 376-386.

Jansen, J. K. S. & Rudjord, T. (1964) On the silent period and Golgi tendon organs of the soleus muscle of the cat. *Acta physiologica Scandinavica*, **62**, 364-379.

Jaramillo, F. & Wiesenfeld, K. (1998) Mechanoelectrical transduction assisted by brownian motion - a role for noise in the auditory system. *Nature Neuroscience*, **1**, 384-388.

Jaramillo, F. & Wiesenfeld, K. (2000) Physiological noise level enhances mechanoelectrical transduction in hair cells. *Chaos Solitons & Fractals*, **11**, 1869-1874.

Johansson, H., Bergenheim, M., Djupsjobacka, M. & Sjolander, P. (1995) A method for analysis of encoding of stimulus separation in ensembles of afferents. *Journal of Neuroscience Methods*, **63**, 67-74.

Johansson, R. S. (1978) Tactile sensibility in the human hand: Receptive field characteristics of mechanoreceptive units in the glabrous skin area. *Journal of Physiology*, **281**, 101-125.

Johansson, R. S., Landstrom, U. & Lundstrom, R. (1982) Responses of mechanoreceptive afferent units in the glabrous skin of the human hand to sinusoidal skin displacements. *Brain Research*, **244**, 17-25.

Johansson, R. S. & Vallbo, Å. B. (1979) Detection of tactile stimuli. Thresholds of afferent units related to psychophysical thresholds in the human hand. *Journal of Physiology*, **297**, 405-422.

Joyce, G. C. & Rack, P. M. (1974) The effects of load and force on tremor at the normal human elbow joint. *Journal of Physiology*, **240**, 375-396.

Joyce, G. C., Rack, P. M. & Ross, H. F. (1974) The forces generated at the human elbow joint in response to imposed sinusoidal movements of the forearm. *Journal of Physiology*, **240**, 351-374.

Kakuda, N. (2000) Response of human muscle spindle afferents to sinusoidal stretching with a wide range of amplitudes. *Journal of Physiology*, **527**, 397-404.

Kanamaru, T., Horita, T. & Okabe, Y. (1998) Stochastic resonance in the Hodgkin-Huxley network. *Journal of the Physical Society of Japan*, **67**, 4058-4063.

Kashimori, Y., Hoshino, O. & Kambara, T. (2000) A positive role of noises in accurate detection of time difference by electrosensory system of weakly electric fish. *Neurocomputing*, **32**, 855-862.

Kember, G. C., Fenton, G. A., Collier, K. & Armour, J. A. (2000) Aperiodic stochastic resonance in a hysteretic population of cardiac neurons. *Physical Review E. Statistical Physics, Plasmas, Fluids, & Related Interdisciplinary Topics*, **61**, 1816-1824.

Knibestöl, M. (1975) Stimulus-response functions of slowly adapting mechanoreceptors in the human glabrous skin area. *Journal of Physiology*, **245**, 63-80.

Knibestöl, M. & Vallbo, Å. B. (1970) Single unit analysis of mechanoreceptor activity from the human glabrous skin. *Acta physiologica Scandinavica*, **80**, 178-195.

Knibestöl, M. & Vallbo, Å. B. (1980) Intensity of sensation related to activity of slowly adapting mechanoreceptive units in the human hand. *Journal of Physiology*, **300**, 251-267.

Konietzny, F. & Hensel, H. (1977) Response of rapidly and slowly adapting mechanoreceptors and vibratory sensitivity in human hairy skin. *Plügers Archives. European Journal of Physiology*, **368**, 39-44.

Kramers, H. A. (1940) Brownian motion in a field of force and the diffusion model of chemical reactions. *Physica*, **7**, 284-304.

Kuffler, S. W., Hunt, C. C. & Quilliam, J. P. (1951) Function of medullated small-nerve fibers in mammalian ventral roots: Efferent muscle spindle innervation. *Journal of Neurophysiology*, **14**, 29-54.

Lee, S. G. & Kim, S. (1999) Parameter dependence of stochastic resonance in the stochastic Hodgkin-Huxley neuron. *Physical Review E. Statistical Physics, Plasmas, Fluids, & Related Interdisciplinary Topics*, **60**, 826-830.

Levin, J. E. & Miller, J. P. (1996) Broadband neural encoding in the cricket cercal sensory system enhanced by stochastic resonance. *Nature*, **380**, 165-168.

Lindblom, U. F. (1962) The relation between stimulus and discharge in a rapidly adapting touch receptor. *Acta physiologica Scandinavica*, **56**, 349-361.

Lloyd, D. P. C. (1943) Neuron patterns controlling transmission of ipsilateral hind limb reflexes in cat. *Journal of Neurophysiology*, **6**, 293-315.

Loewenstein, W. R. (1956) Excitation and changes in adaptation by stretch of mechanoreceptors. *Journal of Physiology*, **133**, 588-602.

Longtin, A. (1993) Stochastic resonance in neuron models. *Journal of Statistical Physics*, **70**, 309-327.

Longtin, A., Bulsara, A. & Moss, F. (1991) Time-interval sequences in bistable systems and the noise-induced transmission of information by sensory neurons. *Physical Review Letters*, **67**, 656-659.

Longtin, A., Bulsara, A., Pierson, D. & Moss, F. (1994) Bistability and the dynamics of periodically forced sensory neurons. *Biological Cybernetics*, **70**, 569-578.

Macefield, G., Gandevia, S. C. & Burke, D. (1990) Perceptual responses to microstimulation of single afferents innervating joints, muscles and skin of the human hand. *Journal of Physiology*, **429**, 113-129.

Marchesoni, F., Gammaitoni, L., Apostolico, F. & Santucci, S. (2000) Numerical verification of bona fide stochastic resonance. *Physical Review E. Statistical Physics, Plasmas, Fluids, & Related Interdisciplinary Topics*, **62**, 146-149.

Maruhashi, J., Mizuguchi, K. & Tasaki, I. (1952) Action currents in single afferent nerve fibres elicited by stimulation of the skin of the toad and the cat. *Journal of Physiology*, **117**, 129-151.

Massanes, S. R. & Vicente, C. J. P. (1999) Classical-like resonance induced by noise in a Fitzhugh-Nagumo neuron model. *International Journal of Bifurcation & Chaos in Applied Sciences & Engineering*, **9**, 2295-2303.

Mato, G. (1999) Stochastic resonance using noise generated by a neural network. *Physical Review E. Statistical Physics, Plasmas, Fluids, & Related Interdisciplinary Topics*, **59**, 3339-3343.

Matthews, B. H. C. (1933) Nerve endings in mammalian muscle. *Journal of Physiology*, **78**, 1-53.

Matthews, P. B. C. (1962) The differentiation of two types of fusimotor fibre by their effects on the dynamic response of muscle spindle primary endings. *Quarterly Journal of Experimental Physiology*, **47**, 324-333.

Matthews, P. B. C. (1963) The response of de-efferented muscle spindle receptors to stretching at different velocities. *Journal of Physiology*, **168**, 660-678.

Matthews, P. B. C. (1972) *Mammalian muscle receptors and their central actions.* London: Edward Arnold Ltd.

Matthews, P. B. C. & Stein, R. B. (1969a) The regularity of primary and secondary muscle spindle afferent discharges. *Journal of Physiology,* 202, 59-82.

Matthews, P. B. C. & Stein, R. B. (1969b) The sensitivity of muscle spindle afferents to small sinusoidal changes of length. *Journal of Physiology,* 200, 723-743.

Matthews, P. B. C. & Watson, J. D. (1981a) Action of vibration on the response of cat muscle spindle Ia afferents to low frequency sinusoidal stretching. *Journal of Physiology,* 317, 365-381.

Matthews, P. B. C. & Watson, J. D. (1981b) Effect of vibrating agonist or antagonist muscle on the reflex response to sinusoidal displacement of the human forearm. *Journal of Physiology,* 321, 297-316.

McCloskey, D. I. (1978) Kinesthetic sensibility. *Physiological Reviews,* 58, 763-820.

McNamara, B., Wiesenfeld, K. & Roy, R. (1988) Observation of stochastic resonance in a ring laser. *Physical Review Letters,* 60, 2626-2629.

Merkel, F. (1875) Tastzellen und taskörperchen bei den hausthieren und beim menschen. *Archiv für Mikrospische Anatomie,* 11, 636-652.

Merkel, F. (1880) Über die endigungen der sensiblen nerven in der haut der wirbeltiere.

Merzenich, M. M. & Harrington, T. H. (1969) The sense of flutter-vibration evoked by stimulation of the hairy skin of primates: Comparison of human sensory capacity with the responses of mechanoreceptive afferents innervating the hairy skin of monkeys. *Experimental Brain Research,* 9, 236-260.

Mitzdorf, U. (1987) Properties of the evoked potential generators: Current source-density analysis of visually evoked potentials in the cat cortex. *International Journal of Neuroscience,* 33, 33-59.

Morgan, D. L., Prochazka, A. & Proske, U. (1984) The after-effects of stretch and fusimotor stimulation on the responses of primary endings of cat muscle spindles. *Journal of Physiology,* 356, 465-477.

167

Morse, R. P. & Meyer, G. F. (2000) The practical use of noise to improve speech coding by analogue cochlear implants. *Chaos Solitons & Fractals*, **11**, 1885-1894.

Moss, F., Pierson, D. & O'Gorman, D. (1994) Stochastic resonance: Tutorial and update. *International Journal of Bifurcation & Chaos in Applied Sciences & Engineering*, **4**, 1383-1397.

Nafstad, P. H. & Baker, R. E. (1973) Comparative ultrastructural study of normal and grafted skin in the frog, *Rana pipiens*, with special reference to neuroepithelial connections. *Zeitschrift Fur Zellforschung Und Mikroskopische Anatomie*, **139**, 451-462.

Nozaki, D., Mar, D. J., Grigg, P. & Collins, J. J. (1999) Effects of colored noise on stochastic resonance in sensory neurons. *Physical Review Letters*, **82**, 2402-2405.

Ogawa, H., Morimoto, K. & Yamashita, Y. (1981) Physiological characteristics of low threshold mechanoreceptor afferent units innervating frog skin. *Quarterly Journal of Experimental Phsyiology*, **66**, 105-116.

Ogawa, H. & Yamashita, Y. (1982) Patterns of impulses discharged by slowly adapting cutaneous mechanorecptive units in the wary skin of frogs in response to prolonged displacements. *Japanese Journal of Physiology*, **32**, 945-958.

Ogawa, H., Yamashita, Y., Nomura, T. & Taniguchi, K. (1984) Discharge patterns of the slowly adapting mechanoreceptor afferent units innervating the non-warty skin of the frog. *Japanese Journal of Physiology*, **34**, 255-267.

Otten, E., Hulliger, M. & Scheepstra, K. A. (1995) A model study on the influence of a slowly activating potassium conductance on repetitive firing patterns of muscle spindle primary endings. *Journal of Theoretical Biology*, **173**, 67-78.

Ovalle, W. K. & Smith, R. S. (1972) Histochemical identification of three types of intrafusal muscle fibers in the cat and monkey based on the myosin atpase reaction. *Canadian Journal of Physiology and Pharmacology*, **50**, 195-202.

Owens, A. L., Denison, T. J., Versnel, H., Rebbert, M., Peckerar, M. & Shamma, S. A. (1995) Multi-electrode array for measuring evoked potentials from surface of ferret primary auditory cortex. *Journal of Neuroscience Methods*, **58**, 209-220.

Pantazelou, E., Dames, C., Moss, F., Douglass, J. & Wilkens, L. (1995) Temperature dependence and the role of internal noise in signal transduction efficiency of crayfish mechanoreceptors. *International Journal of Bifurcation & Chaos in Applied Sciences & Engineering*, **5**, 101-108.

Pei, X., Wilkens, L. & Moss, F. (1996a) Noise-mediated spike timing precision from aperiodic stimuli in an array of Hodgkin-Huxley-type neurons. *Physical Review Letters*, **77**, 4679-4682.

Pei, X., Wilkens, L. A. & Moss, F. (1996b) Light enhances hydrodynamic signaling in the multimodal caudal photoreceptor interneurons of the crayfish. *Journal of Neurophysiology*, **76**, 3002-3011.

Petracchi, D. (2000) What is the role of stochastic resonance? *Chaos Solitons & Fractals*, **11**, 1827-1834.

Piana, M., Canfora, M. & Riani, M. (2000) Role of noise in image processing by the human perceptive system. *Physical Review E. Statistical Physics, Plasmas, Fluids, & Related Interdisciplinary Topics*, **62**, 1104-1109.

Plesser, H. E. & Geisel, T. (1999) Markov analysis of stochastic resonance in a periodically driven integrate-and-fire neuron. *Physical Review E. Statistical Physics, Plasmas, Fluids, & Related Interdisciplinary Topics*, **59**, 7008-7017.

Plesser, H. E. & Tanaka, S. (1997) Stochastic resonance in a model neuron with reset. *Physics Letters A*, **225**, 4-6.

Proske, U. (1997) The mammalian muscle spindle. *News in physiological sciences*, **12**, 37-42.

Proske, U., Morgan, D. L. & Gregory, J. E. (1992) Muscle history dependence of responses to stretch of primary and secondary endings of cat soleus muscle spindles. *Journal of Physiology*, **445**, 81-95.

Proske, U., Morgan, D. L. & Gregory, J. E. (1993) Thixotropy in skeletal muscle and in muscle spindles: A review. *Progress in Neurobiology*, **41**, 705-721.

Pubols, B. H. (1982) Factors affecting cutaneous mechanoreceptor response. Ii. Changes in mechanical properties of skin with repeated stimulation. *Journal of Neurophysiology*, **47**, 530-542.

Querfurth, H. & Gruser, O. J. (1986) Facilitation effect of auxiliary noise stimuli on response of isolated frog muscle spindle to sinusoidal movements. *Journal of Neurophysiology*, 1, 23-33.

Richardson, K. A., Imhoff, T. T., Grigg, P. & Collins, J. J. (1998) Using electrical noise to enhance the ability of humans to detect subthreshold mechanical cutaneous stimuli. *Chaos*, 8, 599-603.

Richmond, F. J. & Abrahams, V. C. (1975) Morphology and distribution of muscle spindles in dorsal muscles of the cat neck. *Journal of Neurophysiology*, 38, 1322-1339.

Rouse, R., Siyuan, H. & Lukens, J. E. (1995) Flux amplification using stochastic superconducting quantum interference devices. *Applied Physics Letters*, 66, 108-110.

Ruffini, A. (1898) On the minute anatomy of the neuromuscular spindles of the cat, and on their physiological significance. *Journal of Physiology*, 23, 190-208.

Russell, D. F., Wilkens, L. A. & Moss, F. (1999) Use of behavioural stochastic resonance by paddle fish for feeding. *Nature*, 402, 291-294.

Schaafsma, A., Otten, E. & van Willigen, J. D. (1991) A muscle spindle model for primary afferent firing based on a simulation of intrafusal mechanical events. *Journal of Neurophysiology*, 65, 1297-1312.

Shannon, C. E. (1949) The mathematical theory of communication. In *The mathematical theory of commication*, ed. Shannon, C. E. & Weaver, W., 29-125. Urbana: The University of Illinois Press.

Sherrington, C. S. (1894) On the anatomical constitution of nerves of skeletal muscles; with remarks on recurrent fibres in the ventral spinal nerve-root. *Journal of Physiology*, 17, 211-258.

Shimokawa, T., Pakdaman, K. & Sato, S. (1999a) Time-scale matching in the response of a leaky integrate-and-fire neuron model to periodic stimulus with additive noise. *Physical Review E. Statistical Physics, Plasmas, Fluids, & Related Interdisciplinary Topics*, 59, 3427-3443.

Shimokawa, T., Rogel, A., Pakdaman, K. & Sato, S. (1999b) Stochastic resonance and spike-timing precision in an ensemble of leaky integrate and fire neuron models.

Physical Review E. Statistical Physics, Plasmas, Fluids, & Related Interdisciplinary Topics, **59**, 3461-3470.

Simonotto, E., Riani, M., Seife, C., Roberts, M., Twitty, J. & Moss, F. (1997) Visual perception of stochastic resonance. *Physical Review Letters*, **78**, 1186-1189.

Spano, M. L., Wun-Fogle, M. & Ditto, W. L. (1992) Experimental observation of stochastic resonance in a magnetoelastic ribbon. *Physical Review E. Statistical Physics, Plasmas, Fluids, & Related Interdisciplinary Topics*, **46**, 5253-5256.

Srebro, R. & Malladi, P. (1999) Stochastic resonance of the visually evoked potential. *Physical Review E. Statistical Physics, Plasmas, Fluids, & Related Interdisciplinary Topics*, **59**, 2566-2570.

Stacey, W. C. & Durand, D. M. (2000) Stochastic resonance improves signal detection in hippocampal CA1 neurons. *Journal of Neurophysiology*, **83**, 1394-1402.

Stein, R. B. (1967) The frequency of nerve action potentials generated by applied currents. *Proceedings of the Royal Society of London - Series B: Biological Sciences*, **167**, 64-86.

Stein, R. B. & Matthews, P. B. C. (1965) Differences in variability of discharge frequency between primary and secondary muscle spindle afferent endings of the cat. *Nature*, **208**, 1217-1218.

Stemmler, M., Usher, M. & Niebur, E. (1995) Lateral interactions in primary visual cortex: A model bridging physiology and psychophysics. *Science*, **269**, 1877-1880.

Stratimirovic, D., Milosevic, S., Blesic, S. & Ljubisavljevic, M. (2001) Wavelet analysis of discharge dynamics of fusimotor neurons. *Physica A*, **291**, 13-23.

Stufflebeam, S. M., Poeppel, D. & Roberts, T. P. L. (2000) Temporal encoding in auditory evoked neuromagnetic fields: Stochastic resonance. *Neuroreport*, **11**, 4081-4085.

Talbot, W. H., Darian-Smith, I., Kornhuber, H. H. & Mountcastle, V. B. (1968) The sense of flutter-vibration: Comparison of the human capacity with response patterns of mechanoreceptive afferents from the monkey hand. *Journal of Neurophysiology*, **31**, 301-334.

Torebjörk, H. E. & Ochoa, J. L. (1980) Specific sensations evoked by activity in single identified sensory units in man. *Acta physiologica Scandinavica*, **110**, 445-447.

Tougaard, J. (2000) Stochastic resonance and signal detection in an energy detector - implications for biological receptor systems. *Biological Cybernetics*, **83**, 471-480.

Usher, M. & Feingold, M. (2000) Stochastic resonance in the speed of memory retrieval. *Biological Cybernetics*, **83**, L11-L16.

Vallbo, Å. B. & Johansson, R. S. (1984) Properties of cutaneous mechanoreceptors in the human hand related to touch sensation. *Human Neurobiology*, **3**, 3-14.

von Düring, M. & Seiler, W. (1974) The fine structure of lamellated receptors in the skin of *Rana esculenta*. *Zeitschrift fur Anatomie und Entwicklungsgeschichte*, **144**, 165-172.

Wannamaker, R. A., Lipshitz, S. P. & Vanderkooy, J. (2000) Stochastic resonance as dithering. *Physical Review E. Statistical Physics, Plasmas, Fluids, & Related Interdisciplinary Topics*, **61**, 233-236.

Wiesenfeld, K. & Jaramillo, F. (1998) Minireview of stochastic resonance. *Chaos*, **8**, 539-548.

Wilson, L. R., Gandevia, S. C. & Burke, D. (1995) Increased resting discharge of human spindle afferents following voluntary contractions. *Journal of Physiology*, **488**, 833-840.

Winterer, G., Ziller, M., Dorn, H., Frick, K., Mulert, C., Dahhan, N., Herrmann, W. M. & Coppola, R. (1999) Cortical activation, signal-to-noise ratio and stochastic resonance during information processing in man. *Clinical Neurophysiology*, **110**, 1193-1203.

Wise, A. K., Gregory, J. E. & Proske, U. (1996) The effects of muscle conditioning on movement detection thresholds at the human forearm. *Brain Research*, **735**, 125-130.

Wise, A. K., Gregory, J. E. & Proske, U. (1998) Detection of movements of the human forearm during and after co-contractions of muscle acting at the elbow joint. *Journal of Physiology*, **508**, 325-330.

Yamashita, Y., Ogawa, H. & Taniguchi, K. (1986) Differential effects of manganese and magnesium on two types of slowly adapting cutaneous mechanoreceptor afferent units in frogs. *Plügers Archives. European Journal of Physiology*, **406**, 218-224.

Zeng, F. G., Fu, Q. J. & Morse, R. (2000) Human hearing enhanced by noise. *Brain Research*, **869**, 251-255.

Zhong, S. & Xin, H. W. (2000) Noise-induced oscillations and internal stochastic resonance in a model of excitable biomembrane. *Chemical Physics Letters*, **321**, 309-314.